Development of Neural Tissue Engineering Scaffolds for Guided Neurite Extension within the Central Nervous System

A thesis for the Degree of Doctor of Philosophy:

by

David R Nisbet
BEng (Hons. I)

Conducted primarily within the
Department of Materials Engineering
and the Division of Biological Engineering
Monash University
Victoria, Australia 3800

Dedicated to my sister Elizabeth,

as when I was in high school I told her I would….

Table of Contents

Preface

This thesis reports on the development of two unique neural tissue engineering scaffolds for cellular support and guided neurite extension within the central nervous system (CNS). For this reason this work is presented in 3 Parts to allow for a thorough understanding to be obtained, in regard to the development and characterisation of each unique neural tissue engineering scaffold; Part I focuses on the development of nanoscale polymer fibres produced using electrospinning; Part II is concerned with the examination of smart xyloglucan hydrogels, which are injected into the body as a liquid and then assemble forming a hydrogel scaffold when the temperature is raised to 37 ºC. Part III contains the final chapter and links the preceding Parts so that ultimately the benefits of each can be incorporated into a 'composite' scaffold. Such a scaffold may generate individual cellular niche environments that are more permissible for cell differentiation and maintenance or for directed axonal regeneration through mimicking some of the neurochemical and neuroanatomical architecture of physiological tissue.

Abstract

Currently, there are no definitive treatments for nerve damage within the central nervous system and the consequences for the patient are devastating and permanent. This thesis reports on the development and modification of nanostructured scaffolds for neural tissue engineering to grow and guide neurites within the central nervous system. The aim of the thesis is to examine the suitability of electrospun fibrous scaffolds and xyloglucan hydrogel scaffolds to be used in the treatment of disease and injuries within the CNS, such as Parkinson's Disease and spinal cord injuries.

Part I

Electrospinning is a process that has been utilised in tissue engineering to fabricate scaffolds that mimic some of the features of the native extracellular matrix. The technique generates a scaffold with a nanofibrous morphology, where the fibres have similar diameters to those within the native basement membrane. The technique is versatile and can be used with a variety of different polymers. This work focuses on the use of poly(α-hydroxy esters), as their surfaces are easily modified, they are biodegradable and they already have the Therapeutic Goods Administration (Australia's equivalent of the Food and Drug Administration (FDA)) approval for use in the body.

The first investigatory stage involved a biocompatibility study of 2D surfaces of poly($_L$-lactic acid) (P_LLA) and poly(lactic-co-glycolic acid) (PLGA) with cortical neurones to assess their potential to fabricate 3D neural tissue engineering scaffolds. These surfaces were modified with potassium hydroxide to investigate the influence of changes to the surface energy on the cellular response. It was found that the materials were biocompatible with cortical neurones with the PLGA surface responding better than the P_LLA. On surfaces with lower contact angles for both materials the cells spread evenly and their morphology, distribution and neurite extensions look similar to that of the poly-$_D$-lysine (PDL) positive control. However, while this was the case it was discovered that there was better cellular survival and longer neurites obtained on hydrophobic surfaces where the cells existed as colonies.

The second stage was to electrospin 3D scaffolds from these materials and subject them to the same surface treatments as in the case of the 2D surfaces. The scaffolds were biocompatible with cortical neurones, with the neurones taking on morphologies similar to physiological neurones. Hydrophilicity did not influence the number of primary and secondary neurite branches, however it did significantly influence neurite lengths, with longer neurite's attained on hydrophobic surfaces. Such a discovery resulted in poly(ε-caprolactone) (PCL) being used in additional studies as this poly(α-hydroxy ester) is inherently more hydrophobic than P_LLA and PLGA, hence did not require modification. This study showed that contact guidance was not a "dominant cue" in directing CNS neurites in randomly orientated nanofibres, as it was discovered that neurites draped themselves across the electrospun fibres using them as a "springboard" to jump to neighbouring fibres.

The third phase of this work was to evaluate how stem cells interacted with the electrospun PCL scaffolds, as it was recognised that delivery of stem cells seeded on such scaffolds into the body would be an important step in regenerating neurites within the CNS. The surfaces were aminolysed in preparation for growth factor immobilisation. In the first study with rat brain derived stem cells it was found that aminolysation allowed the stem cells to penetrate throughout the entirety of the scaffolds, instead of re-forming large neurospheres on the surface. It was also discovered that aminolysation did not influence differentiation, but that the scaffolds did differentiate stem cells primarily towards the oligodendrocytes phenotype, which are a critical cell type of the remyelination of damaged CNS neurites to restore their appropriate function.

However, while the neurone affinity with the scaffold has been explored extensively, this is not a full description of the materials biocompatibility. For this reason in the last stage the scaffolds were implanted into the brains of rats and the inflammation assessed. It was found that the scaffolds did not cause severe inflammation and were not encapsulated by a scar after 60 days. Furthermore, endogenous neurites actually extended throughout the

scaffolds that had random fibre alignment. When the fibres where aligned, CNS neurites extended at a perpendicular orientation to the fibre alignment.

Part II

This work focused on xyloglucan hydrogel scaffolds, which exist as a solution at room temperature, but upon heating to physiological temperature, assemble to form a 3D macroporous scaffold. This property makes it useful in tissue engineering as the material can be injected into the body in a minimally invasive manner. Furthermore, due to its structure, xyloglucan can be easily modified to incorporate growth factors and bio-chemical cues in desired concentrations. The aim of this work was to examine the suitability of xyloglucan for use as a neural tissue engineering scaffold, considering its biocompatibility as well as its capacity to bio-chemically and physically support neural cells.

Examination began through extensive characterisation of these gels. It was discovered that the gelation of xyloglucan occurred over a broad temperature range and occurred in two distinct stages. The first stage of gelation resulted in the formation of large membrane structures in the pre-gel. The second stage was characterised by the joining of these membranes into a strong 3D network. The formation of such membrane structures was accelerated by the presence of ions in the phosphate buffered saline solution (PBS). Post gelation, the elastic modulus of the gel was similar to that of spinal cord tissue.

The next step was to test the biocompatibility of xyloglucan with cortical neurones and neural stem cells (NSCs) *in vitro*. The xyloglucan was modified by the immobilisation of poly-$_D$-lysine (PDL), and this molecule was presented at different concentrations to the cells. The material supported the maintenance and differentiation of cortical neurones under 2 and 3D culture conditions. The addition of PDL also provided a means of controlling and optimising cellular function including cell diameter, number, migration and axonal density. NSCs behaved in a similar way on the scaffolds, surviving and differentiating into neurones. They also sent out long neurites, indicating the trophic

effect of the scaffolds were not cell specific. These results show great potential for the use of modified xyloglucan in neural tissue engineering, as the scaffold may be capable of providing neurotrophic milieu.

While it was discovered that neurones and neural stem cells were maintained and supported *in vitro* on xyloglucan scaffolds, this was not a full description of the materials biocompatibility. As a result, the last stage of experimentation involved *in vivo* testing of the materials where they were implanted into the brains of rats and the level of inflammation assessed. Both the unmodified xyloglucan and the xyloglucan with different concentrations of polylysine immobilised, did not cause severe inflammation and were not encapsulated by astrocytes after 60 days. Furthermore, endogenous neurites also extended throughout all scaffolds that had polylysine immobilised within its structure. By changing the amount of immobilised polylysine it was possible to control the inflammation (amount of microglia and astrocytes present around the implantation), and also to control the manner in which endogenous neurites interacted with the scaffolds. Xyloglucan scaffolds have great potential in neural tissue engineering, and through the incorporation of different growth factors and cell adhesion molecules, or combinations of immobilised molecules, the outlook for regeneration within the CNS can be viewed in a more positive light.

Refereed Publications

1. **D.R. Nisbet,** D. Moses, T.R. Gengenbach, J.S. Forsythe, M.K. Horne, D.I. Finkelstein, “Interaction of embryonic cortical neurones and neurospheres on thermoreversible xyloglucan hydrogel: For neural tissue engineering”, *J. Biomed. Mat. Res.*, accepted 2/1/2008.

2. **D.R. Nisbet**, W. Shen, D.I. Finkelstein, M.K. Horne, J.S. Forsythe, “Electrospinning for tissue engineering applications”, *J. Biomat. App.*, accepted, Sep. 2008.

3. **D.R. Nisbet**, A. Rodda, D. I. Finkelstein, M. K. Horne, J. S. Forsythe, W. Shen, “Characterisation of electrospun scaffolds – problems and improvements”, *J. Colloid Int. Sci.,* submitted October. 2008.

4. **D.R. Nisbet,** J.S. Forsythe, “New stem cell stragies for nerve regeneration”, Aus. Sci., 25, pp 23-25, 2008.

5. **D.R. Nisbet,** J.S. Forsythe, “Firm Foundations”, The Chemical Engineer, Accepted, 2008.

6. **D.R. Nisbet**, L.M.Y. Yu, T. Zahir, J.S. Forsythe, M.S. Shoichet, “Characterisation of neural stem cells on electrospun poly(ε-caprolactone) submicron scaffolds: evaluating their potential in neural tissue engineering”, Invited Publication, *J. Biomat. Sci. – Poly. Ed.*, 19, pp 623-634, 2008.

7. G.A. Thouas, K. Contreras, C.C.A. Bernard, Q. Sun, K.M.C. Tsang, K. Zhou, **D.R. Nisbet**, J.S. Forsythe, "Biomaterials for spinal-cord regeneration: polycaprolactone scaffolds with layer-by-layer surface modifications influences the outgrowth of stem cell-derived neurites", IEEE EMBS, 414, 2008

8. **D.R. Nisbet,** J.S. Forsythe, “Feature Article – Monash researchers pioneers nano scaffolds to rebuild nerve damage”, *Aust. Bio. Tech.*, 18, pp56-57, 2008.

9. **D.R. Nisbet**, A. Rodda, M. K. Horne, J. S. Forsythe, D. I. Finkelstein, “Functionalized thermoreversible xyloglucan hydrogel response upon injection into the brain”, *Biomaterials.*, manuscript in draft format, October 2008.

10. **D.R. Nisbet**, A. Rodda, M. K. Horne, J. S. Forsythe, D. I. Finkelstein, “Neurite inflitration and inflammatory response of electrospun polycaprolactone scaffolds implantated into the brain”, *Acta Biomaterialia.*, manuscript in draft format, October 2008.

11. **D.R. Nisbet,** C.L. Parish, D.I. Finkelstein, J.S. Forsythe, M.K. Horne, “Interaction of neural stem cells derived from the cortex with electrospun poly(ε-caprolactone) scaffolds: a differentiation study”, *Stem Cells,* manuscript in draft format, October 2008.

12. **D.R. Nisbet**, K.E. Crompton, M.K. Horne, D.I. Finkelstein, J.S. Forsythe, “Neural tissue engineering of the CNS using hydrogels – A Review”, *J. Biomed. Mat. Res.* 87, pp 251-263, 2008.

13. **D.R. Nisbet**, S. Pattanawong, N. E. Ritchie, W. Shen, D. I. Finkelstein, M. K. Horne, J. S. Forsythe, “Interaction of embryonic cortical neurones on nanofibrous scaffolds for neural tissue engineering”, *J. Neural Eng.*, 4, pp 35-41, 2007.

14. **D.R. Nisbet,** S. Pattanawong, J. Nunan, W. Shen, M.K. Horne, D.I. Finkelstein, J.S. Forsythe, “The effect of surface hydrophilicity on the behaviour of embryonic cortical neurones”, *J. Colloid Int. Sci*. 299, pp 647-655, 2006.

15. **D.R. Nisbet,** K.E. Crompton, S.D. Hamilton, S. Shiwakawa, R.J. Prankerd, D.I. Finkelstein, M.H. Horne, J.S. Forsythe, “Thermosensitive xyloglucan hydrogels: morphology and gelation, *Biophys. Chem*. 121, pp 14-20 2005.

Conference Papers

1. **D.R. Nisbet**, J.S. Forsythe, M.K. Horne, D.I. Finkelstein, "Neurite infiltration and inflammatory response to functionalised xyloglucan hydrogel scaffolds within the brain", Australian Polymer Symposium, Melbourne, Accepted 19/9/08

2. J. Pettikiriarachchi, J.S. Forsythe, A. Javadi, **D.R. Nisbet**, G. Thouas, K.G. Contreras, G. Simon, K. Suzuki, "Super paramagnetic nanofibre scaffolds for mechanically stimulating cells", Australian Polymer Symposium, Melbourne, Accepted 19/9/08

3. **D.R. Nisbet**, J.S. Forsythe, M.K. Horne, D.I. Finkelstein, "Implantation of electrospun PCL scaffolds into the brain", World Biomaterials Congress, Amsterdam, 2008.

4. A. Javadil, **D.R. Nisbet**, J.S. Forsythe, G. Simon, "Fabrication of Polycaprolactone magnetic composite nanofibres by electrospinning, Polymer Processing Society, Italy, 2008.

5. **D.R. Nisbet**, J.S. Forsythe, "Obtaining longer neurite extensions from neural stem cells using thermoreversible hydrogels", Australian Society of Biomaterials and Tissue Engineering Annual meeting, Canberra 2008.

6. **D.R. Nisbet**, J.S. Forsythe, "New stem cell strategies for nerve regeneration", Invited presentation for CRC conference, Sydney, 2008.

7. **D.R. Nisbet**, J.S. Forsythe, M.S. Shoichet, "Characterisation of neural stem cells on electrospun nanofibrous scaffolds: their potential in neural tissue engineering", Polymers in Medicine, USA, 2007.

8. D. Fon, M.K. Horne, D.I. Finkelstein, **D.R. Nisbet**, J.S. Forsythe, "Electrospun poly(ε-caprolactone) scaffolds for nerve tissue engineering applications", Polymers in Medicine, USA, 2007.

9. **D.R. Nisbet**, J.S. Forsythe, "Enhance neurite outgrowth of neurospheres using a thermoreversible hydrogel", Regenerate Conference, Canada, 2007.

10. **D.R. Nisbet**, J.S. Forsythe, M.S. Shoichet, "The evaluation of neural stem cells cultured on electrospun submicron fibres", 17th Australian Society of Biomaterials Conference, AUS, 2007.

11. **D.R. Nisbet**, W. Shen, D. I. Finkelstein, M. K. Horne, J. S. Forsythe, "The interaction of cortical neurones on electrospun PLGA and PLLA nanofibrous scaffolds", 29 Australian Polymer Symposium, AUS, 2007.

12. **D.R. Nisbet,** J.S. Forsythe "Scaffolds for Brain Regeneration", Invited lecture, CRC Annual Dinner, AUS, 2007.

13. **D.R. Nisbet**, W. Shen, D. I. Finkelstein, M. K. Horne, J. S. Forsythe, " Interaction of embryonic cortical neurones on nanofibrous scaffolds for neural tissue engineering", Gordon Conference (signal transduction by engineered extracellular matrices), USA, 2006.

14. **D.R. Nisbet**, J.S.Forsythe, “Neural tissue engineering scaffolds for guided neurite extensions”, Invited Lecture - Research Week, AUS, 2006.
15. **D.R. Nisbet**, D.I. Finkelstein, M.K. Horne, J.S. Forsythe, “Morphology and gelation characteristics of thermosensitive xyloglucan”, Australasian Society for Biomaterial, NZ 2005.

Media Coverage

1. ABC national news TV feature
2. ABC international broadcasting half hour interview (innovation)
3. Radio Australia news feature
4. ABC talk back radio (Red Symons)
5. Australian Science Magazine
6. Australasian Biotechnology Magazine
7. Local Leader newspapers (March and July editions)
8. Monash Magazine (June)
9. Monash Memo (March)
10. Over 100 international and national web blogs, features and forums

Invited Presentations

1. Keynote speaker at ***Nanotech India***, August 2009 - http://www.nanotechindia.in/
2. Showcasing CRCs Annual Conference 2008 – Prize for best student speaker
3. Mental Health Research Institute of Victoria 2008.
4. Monash Research Week 2007.
5. Monash Seminar, Neural Tissue Engineering 2006

Acknowledgments

I would like to express my gratitude and thanks to my supervisors Dr John Forsythe, Prof. Mal Horne and Prof. David Finkelstein, as well as my international supervisor Prof. Molly Shoichet. I am very grateful for their encouragement, patience and support through out my entire candidature, and they have achieved this whilst also providing a fun and interesting working environment.

I would like also to recognise the training that I received from Dr Janelle Nunan, Dr David Moses, Dr Richard Donovan and Soraya Pattanwong. Their knowledge has been critical in my project and will continue to be throughout my career.

I would like to also acknowledge the undergraduate and honors students that I have supervised throughout my PhD, Shaun Hamilton (2005), Niki Ritchie (2005), Deniece Fon (2006), Andrew Rodda (2007), Kelly Tsang (2007), Xavier Chapman (2008), Jerani Pettikiriarachchi (2008) and Kun Zhou (2008). I also express my thanks to all the past and current students within the neural tissue engineering group for many great memories and the friendly working atmosphere within the office.

Finally, I would like to thank my family and friends for their support right throughout my education and my life, they have been constantly interested in my research and developments throughout my PhD. In particular, Peta who is probably sick of proof reading draft papers and this thesis. She also provides a relaxing and entertaining environment for me to un-wind in.

I have also appreciated the scholarship funding from the Australian Postgraduate Award and the Cooperative Research Center for Polymers (CRC-P) throughout the entirety of my PhD candidature. I also wish to acknowledge the combined financial support of the Australian Society of Biomaterials and Tissue Engineering, Monash Research Graduate School and the CRC-P, which has allowed me to attend several conferences (nationally and internationally) and also partly funded a 6month international visit in Canada.

I would again like to finish by thanking my main supervisor Dr John Forsythe, who has mentored me from an undergraduate in second year to the present. I have been very fortunate to have a supervisor who would always go out of his way for me, at times seeming more concerned with the development of my career than his own. This is exemplified by him funding the major component of the laboratory visit to Canada, as he maintained that it is a critical requirement when pursuing a career in academia.

PART A: General Declaration

Monash University

Monash Research Graduate School

Declaration for thesis based or partially based on conjointly published or unpublished work

General Declaration

In accordance with Monash University Doctorate Regulation 17/ Doctor of Philosophy and Master of Philosophy (MPhil) regulations the following declarations are made:

I hereby declare that this thesis contains no material which has been accepted for the award of any other degree or diploma at any university or equivalent institution and that, to the best of my knowledge and belief, this thesis contains no material previously published or written by another person, except where due reference is made in the text of the thesis.

This thesis includes a total of 10 publications; 6 original papers published in peer reviewed journals 2 submitted publications and 2 draft publications. The core theme of the thesis is the development of neural tissue engineering scaffolds to achieve guided neurite extension within the central nervous system. The ideas, development and writing of all the papers in the thesis were the principal responsibility of myself, the candidate, working within the tissue engineering group based in the Department of Materials Engineering and Division of Biological Engineering under the primary supervision of Dr John Forsythe.

The inclusion of co-authors reflects the fact that the work came from active collaboration between researchers and acknowledges input into team-based research.

In the case of chapters 2 through to 7 my contribution to the work involved the following:

Part	Chapter	Publication title	Status	Contribution
I	2	Electrospinning for tissue engineering applications	Accepted	Planning, researching and writing.
	2	Characterisation of electrospun scaffolds – A review	Submitted	Experimental design and conduct, writing.
	3	The effect of surface hydrophilicity on the behaviour of embryonic cortical neurones	Published	Experimental design and conduct, writing.
	3	Interaction of embryonic cortical neurones on nanofibrous scaffolds for neural tissue engineering	Published	Experimental design and conduct, writing.
	3	Characterisation of neural stem cells on electrospun poly(ε-caprolactone) submicron scaffolds: evaluating their potential in neural tissue engineering	Published	Experimental design and conduct, writing.
	4	Neurite inflitration and inflammatory response of functionalised electrospun polycaprolactone scaffolds implantated into the brain	Draft	Experimental design and conduct, writing.
II	5	Neural tissue engineering of the CNS using hydrogels – A Review	Published	Experimental design and conduct, writing.
	6	Thermosensitive xyloglucan hydrogels: Morphology and gelation	Published	Experimental design and conduct, writing.
	6	Interaction of embryonic cortical neurones and neurospheres on thermoreversible xyloglucan hydrogel: For neural tissue engineering	Published	Experimental design and conduct, writing.
	7	Functionalized thermoreversible xyloglucan hydrogel response upon injection into the brain	Draft	Experimental design and conduct, writing.

I have / have not renumbered sections of submitted or published papers in order to generate a consistent presentation within the thesis.

Signed: ……

Date: ……

List of Abbreviations

ALP	Alkaline phosphate
AFM	Atomic force microscopy
ATR	Attenuated total reflection
ANOVA	Statistical analysis of variance
BDNF	Brain derived neurotrophic factor
BMP	Bone morphogenetic protein
βIII	Beta III tublin
CBQCA	3-(4-carboxybenzoyl)-quinoline-2-carboxaldehyde
CNPase	2', 3'-cyclic nucleotide 3'-phosphodiesterase
CNS	Central nervous system
CMs	Cardiomyocytes
CP	Cell pellet
ddH_2O	Double distilled deionised water
DRG	Dorsal root ganglia
DSC	Differential scanning calorimetry
DSμC	Differential scanning microcalorimetry
E14	Embryo 14 days
ECM	Extracellular Matrix
ECs	Endothelial cells
ED	Ethylenediamine
EDAC	*N*-(3-Dimethylaminopropyl)-*N'*-ethylacarbodiimide hydrochloride
EGF	Epidermal growth factor
ESCA	Electron spectrometry for chemical analysis
ESC	Embroynic stem cell
FDA	Food and drug administration
FBS	Fetal bovine serum
FTIR	Fourier transform infrared

FGF	Fibroblast growth factor
GAG	Glycosamino glycan
GDNF	Glial-derived neurotrophic factor
GFAP	Glial fibrillary acidic protein
HA	Hydroxyapatite
HCAECs	Human coronary artery endothelial cells
KOH	Potassium hydroxide
LCST	Lower critical solution temperature
LSCM	Laser scanning confocal microscope
MEM	Modified eagles medium
MG63	measured by production of bone derived growth fator
MSCs	Mesenchymal stem cells
MW	Molecular weight
MPa	Mega pascal
NBM	Neural basal medium
NGF	Nerve growth factor
NF	Neurofilament
NFS	Electrospun nanofibres
NGS	Normal goat serum
NIH	National institute of health
NSCs	Neural stem cells
Ox-42	Monoclonal cell surface antigen antibody
PBS	Phosphate-buffered saline
PCL	Polycaprolactone
PD	Parkinson's Disease
PDL	Poly-$_{D}$-lysine
PEG	Poly(ethylene glycol)
PET	Pelyethylene terephalate
PEO	Poly(ethylene oxide)
PFA	Paraformaledhyde
PGA	Poly(glycolic acid)

PLCL	Poly(lactide-co-caprolactone)
PLL	Poly-$_L$-lysine
PLGA	Poly(lactic-co-glycolic acid)
P_LLA	Poly-L-(lactic acid)
PNS	Peripheral nervous system
PU	Polyurethane
RPM	Revolutions per minute
RMS	Root mean square
SANS	Small angle neutron scattering
SAXS	Small angle X-ray scattering
SCI	Spinal cord injury
SEM	Scanning electron microscopy
SMCs	Smooth muscle cells
TCP	Tissue culture plastic
TEA	Triethanolamine
TIPS	Thermally induced phase separation
TEM	Transmission electron microscopy
TGF	Transforming growth factor
ToF-SIMS	Time of flight secondary ion mass spectroscopy
UV	Ultraviolet
Wnts	Signaling Pathway

List of Symbols

A_o	Projected area
A_r	Actual area
A	Area
γ	Strain
δ	Phase angle
G'	Elastic modulus
G''	Viscous modulus
G*	Complex modulus
η	Viscosity
$[\eta]$	Intrinsic viscosity
λ	Wavelength
n	Number of samples
ω	Angular frequency
σ	Stress
ε	Strain
$^\circ$	Degrees
T	Temperature
T_g	Glass transition temperature
ΔT	Change in temperature
ρ	Density
μm	Micrometer
nm	Nanometer
V	Volume
θ_o	Contact angle on smooth surfaces
θ_r	Contact angle on rough surfaces

Chapter 1

Introduction

Chapter 1 provides a general introduction and background to the thesis. The concept of tissue engineering is introduced prior to a description of neural tissue engineering with particular focus on Parkinson's disease and spinal cord injury, the main focus of this work. A discussion about tissue engineering materials and scaffold design is also provided before the two different types of materials investigated in this thesis, poly(α-hydroxy esters) and xyloglucan hydrogel, are briefly introduced. In addition the research objectives and aim are outlined.

Table of Contents

1.0 Introduction

1.1 Overview of Tissue Engineering

Tissue engineering can be described as the application of the principles and methods from engineering and life sciences to gain an understanding and assist in the development of biological substitutes for human tissue regeneration.[1] The design of bioresorbable scaffolds that act as artificial extracellular matrices (ECM) is critical to tissue engineering, as the ECM should provide the correct microenvironmental and biological cues to the cells at appropriate times.[2] In time, the scaffold ideally should be excreted from the body, leaving the cells to exist within their natural ECM, forming fully functional tissue.[3]

A common tissue engineering approach is to initially "seed" cells of a specific phenotype onto a scaffold *in vitro* for future *in vivo* implantation. Most cells used in tissue engineering will only proliferate and carry out normal cellular processes when they adhere to a substrate, i.e. they are anchorage dependant. Therefore it is critical to gain an understanding of cellular adhesion, and the interaction of cells with the nano-interface of the scaffold. Potentially, this will also allow for the optimisation of cell proliferation rates and increase the biocompatibility of tissue engineering scaffolds. The selection of cell types to be used in tissue engineering studies is crucial, as there are a variety of different cells types and their selection is specifically defined by the end application.

For the purpose of this research into the development of scaffolds that can guide neurite extension within the central nervous system (CNS), only neurones and neural stem cells that have been derived from the CNS were investigated.

1.2 Nerve Regeneration within the CNS

The central nervous system is the core control system of the body, and consists of the brain and spinal cord. It provides a pathway for motor and sensory information to be passed, so that physiological responses requested by the brain can be carried out. Messages are carried in the form of electrical signals through axons, which are fibres extending from the neuronal cell bodies. Anatomically, nerves are bundles of axons from different neurones that conduct electrical signals in the same direction. The axons/nerves conduct the electrical signals long distances from the cell body to the axon terminal where the signal is transmitted to other cell by specialised neurochemical transmitters. Therefore, when nerves are damaged the electrical signals from the brain are interrupted; this results in an inability for neurones to convey physiological requests such as muscle movement.

Within the CNS the majority of cells are not neurones, but are different types of glial cells responsible for supporting neurones metabolically and physically. While axonal extension is required to achieve the regeneration of neural pathways, the neural support cells, in particular oligodendrocytes and astrocytes, can inhibit extension.[4] Injury to the CNS also results in extensive inflammation, which is an important process that results in the removal of tissue debris and is required to maintain tissue integrity. However, this process also results in astrocyte proliferation, which can produce a scar that acts as a physical barrier preventing axonal re-growth.[5] Axons are not only impeded physically but also by molecules excreted by cells such as oligodendrocytes. The main reason that the CNS inhibits regeneration is to provide a cellular environment that only allows neurones to extend to the appropriate locations and at specific times (generally during early development). Once an axon has reached its target, the outgrowth is shut down by inhibiting molecules, ultimately anchoring it to that location. This provides the highly complex CNS with limited ability to reorganise itself ensuring that it fulfils and maintains its appropriate function. However, on the flip side, this also provides it with limited ability to regenerate once injured.

Therefore, despite extensive research there are currently no definitive treatments for nerve damage within the CNS. Consequently, injury to the brain or spinal cord results in the death of neurones, which causes an associated loss of neural tracks and therefore connectivity with other parts of the brain/body.

The aim of this current work is to engineer smart scaffolds that instruct stem cells and direct nerve regeneration in the brain and spinal cord to specific locations. While this thesis is broadly concerned with nerve regeneration within the CNS, it does have particular focus on regenerating and directing nerve regeneration for the treatment of Parkinson's Disease (PD) and Spinal Cord Injury (SCI). For this reason it is appropriate to provide a brief overview of these conditions at this point.

1.2.1 Parkinson's Disease

Parkinson's disease (PD) is a neurodegenerative disorder that impairs a patient's motor skills, speech and a variety of other functions.[6] PD is a complex series of symptoms that results from the death of dopaminergic neurones within the *pars compacta* region of the substantia nigra, hence leading to alterations of the neural circuitry within the brain which regulates movement. It is only once a patient has lost approximately 50 - 75% of dopaminergic neurones that they begin to show symptoms of the illness. Fundamentally, symptoms result from the loss of substantia nigra cells and the inability to release dopamine within the caudate putamen (shown in Figure 1). Diagnosis of PD generally results from the analysis of medical history and from neurological examinations, as currently there are no blood or laboratory tests available to diagnose the illness accurately.[7-9]

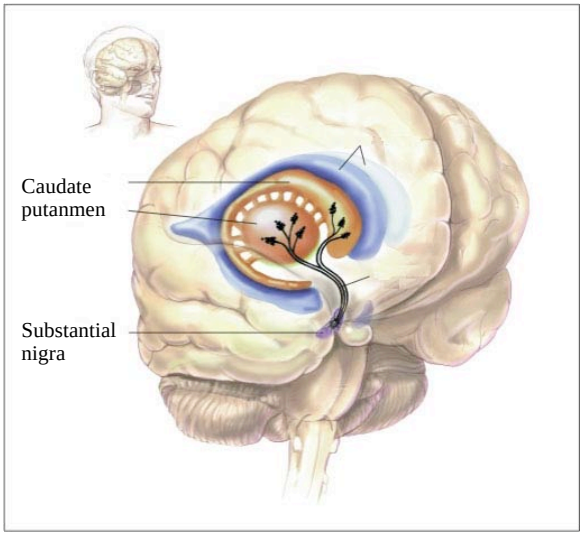

Figure 1 - Highlights the axonal pathway between the substantial nigra (cell body) to the caudate putamen (axon terminals) that degenerate as a consequence of Parkinson's Disease. Reproduced with permission © 2001 Terese Winslow.

It is estimated that within Australia approximately 2 in 1000 people have PD, and that value increases to 1 in 100 after the age of 60.[10] Currently there is a total of approximately 40,000 people within Australia living with PD. In 2005, PD accounted for around $527.8 million expenditure for the Australian National Health Budget with that value expected to increase by 15% over the next 5 years due to the aging demographic.[10] These are real economical costs, however in addition to these is the traumatic suffering and shortening of life on the affected individual. PD is a chronic disorder that has severe consequences for the patient, resulting in a dramatic loss in their quality of life.

Currently there is no cure for PD however the options of medication and surgery can help to relieve some of the symptoms, but these do not work for every patient.[11] Furthermore, the main problem with such treatments is that they do not prevent the further loss of dopaminergic neurones, hence eventually treatment will fail and the patient will lose their independence as the disease takes hold.

1.2.2 Spinal Cord Injury

The spinal cord provides a pathway for motor and sensory information to pass between the brain and body. This information is conducted in the form of electrical signals through long tubular membranes known as axons which connect nerve cells to each other. Therefore, when the spinal cord is damaged by injury or disease, electrical signals from the brain are interrupted, resulting in an inability for neurones to convey physiological requests such as muscle movement. For this reason spinal cord injury (SCI) results in paralysis and depending where the injury occurs this may be confined to the legs, or in the most serious of cases, of all four extremities. SCIs can also strike down an individual irrespective of age, with the majority of cases occurring before the age of 30.[12]

In Australia alone, there are 12,000 people with SCIs with 400 new cases reported each year. This is a global epidemic with over 2.5 million people afflicted.[13] While SCIs caused by trauma are well known, damage caused by tumours, vascular disease, bone degeneration and vertebral disk disease collectively cause far more spinal cord damage. Because people can live for many years after spinal cord damage, the financial and social burdens are immense because of their dependence on a third party for maintained livelihood. People with SCIs undergo variable loss of function to limbs, bowel, bladder and sexual function and struggle to maintain their independence. SCIs cost the Australian public $1.2 billion per annum, and account for 2% of the Australian health expenditure, compared with 5.8% for all cancers.[12, 14] In the USA, the estimated lifetime cost for a 25-year old with paralysis of all four extremities is US$2.9 million.[15]

1.3 Tissue engineering scaffolds

Tissue engineering scaffolds are artificial structures that allow for the implantation or seeding of cells, whilst also providing appropriate support to allow them to undergo normal cellular functions such as differentiation.[2] Such materials have a variety of different design features that must be considered, as ultimately they must be implanted into the human body and support 3D tissue formation.[2] Generally, tissue engineering scaffolds must simulate some of the features of the native extracellular matrix to allow

cells to influence and interact within an environment that replicates some of the features of the native cellular microenvironments. Fundamentally, these scaffolds are designed to mimic the *in vivo* milieu. A perfect scaffold would exactly describe the native ECM allowing for cell attachment and migration, controlling cellular function by delivering biochemical factors, provide appropriate avenues for the diffusion of nutrients and waste in and out of the scaffold and influence the behaviour of cells through specific mechanical and biological cues.[16] However, it is currently not possible to fabricate scaffolds that capture all of the structural and chemical complexities of the native ECM. Typically scaffolds are designed to present the minimum level of biological signals to control cell function, i.e. biocompatibility, biodegradation, angiogenesis, cellular function, compliance matching of mechanical properties, ease of implantation and interconnection of porosity.

The term biocompatibility when referring to tissue engineering scaffolds can often be ambiguous unless defined by the author, as there are several opposing uses of the same term. For the purpose of this thesis, biocompatibility can be considered to be materials that can be used to support living cells without being toxic or having a negative influence on their natural function. Furthermore, a biocompatible material will not elicit an immune reaction upon implantation and should encourage cellular adhesion and proliferation both *in vivo* and *in vitro*. In the case of neural tissue engineering, the focus of this thesis, a biocompatible scaffold should promote neurite extension or differentiation of the cells, which for this application is more critical than the proliferation of neurones.

Biodegradability is also an important design criteria as it is preferable that the scaffold should be absorbed by the surrounding tissue over a specific time period to avoid the need for surgical removal.[17] This is due to the fact that tissue engineering scaffolds are *only* designed to assist in the regeneration of damaged tissue; hence they must degrade and do so at a rate, which is supportive to 3D tissue formation and cellular function. A further consideration is that the degradation products must also be biocompatible, and in many instances the materials should degrade over long duration to avoid locally high

concentrations of the degradation products, which may have adverse effect on surrounding cells.[17]

Scaffolds must be able to withstand the environmental stresses within the body and maintain their structural integrity. For instance many scaffolds may be used in load bearing application such as tendons and bone, hence when designing a scaffold for such purposes it is important to compliance match it to the surrounding tissue.[18] This is not only desirable to mimic the load bearing and strain capabilities of the surrounding tissue, but also so they can be fully integrated within the body. If scaffolds that are implanted into the brain have moduli much greater than the surrounding tissue, sudden movements to the head can result in tearing of the tissue at the interface between the implant and endogenous tissue. Therefore for each different application the modulus and mechanical properties must be optimized.

A desirable property of a scaffold is the ease of implantation into the body to avoid major surgery, which can result in complications such as infection, scarring and perhaps an unnecessary risk.[19] This is why many researchers are opting for injectable biomaterials, which can be easily and accurately introduced to a specific location in the body to encourage local regeneration of tissue within that region.[19]

When cells are incorporated within a scaffold it is also crucial that metabolites and nutrients can be readily transported into the scaffold and that waste can be transported out.[20] This is generally achieved by producing scaffolds with high porosity, the size of such pores must be optimised to not only allow for the transportation of nutrients, but also to facilitate cellular seeding and diffusion throughout the entire structure.[20] A scaffold with the correct level of interconnected porosity will allow for the contact and communication of cells as well as their proliferation, growth and migration, so that ultimately the cells are able to influence their own microenvironments.

Many different types of materials, both natural and synthetic have been investigated for tissue engineering applications. Many of these are materials that are known to be biocompatible and biodegradable, with some already having the Food and Drug

Administration (FDA) approval for use in the body. However, new biomaterials are also continually being synthesized and engineered so that their function and properties can be customised for desired applications.

In this thesis commonly used poly(α-hydroxy esters) in the form of nanofibrous scaffolds as well as, a thermally responsive polysaccharide hydrogel xyloglucan, were investigated specifically for neural tissue engineering applications.

1.4 Poly(α-hydroxy esters)

Poly(α-hydroxy esters) have received considerable attention as bioresorbable polymers used for the fabrication of tissue engineering scaffolds. These polymers break down and can be metabolised by the body. Furthermore, the degradation rates can be easily adjusted by ultilising hydrophilic co-polymers and varying the ratio of the more hydrophilic constituent of the co-polymer. The degradation mechanism occurs via hydrolysis of the ester bonds, hence the polymer is degraded by random chain scission events along the polyester chain. Partial hydrolysis is often exploited to manipulate the surface hydrophilicity of the polyester surface.[21, 22] This is commonly achieved by exposing the polyester to acid or base solutions which catalyse the hydrolysis reaction, yielding acid and alcohol moieties at the surface and increasing the surface hydrophilicity.

Poly(α-hydroxy esters) have other advantages because they have good mechanical properties, low immunogenicity and toxicity and excellent biocompatibility. There are also many techniques, such as gas foaming, electrospinning and solvent casting that can be used with these materials to produced scaffolds with a variety of different morphologies. Such requirements are critical to the successful fabrication of a tissue engineering scaffold.

The three main poly(α-hydroxy acids) that were investigated in this thesis were poly(L-lactide), poly(D,L-lactic-co-glycolic) acid and polycaprolactone:

1.4.1 Poly($_L$-lactide) (P_LLA)

P_LLA has a glass transition temperature (T_g) of *ca.* 54°C and high hydrophobicity compared to other poly(α-hydroxy acids). This is responsible for the material having a slow biodegradation time, and depending on the thickness may last for more than 24 months in the body. P_LLA consists of only the L-isomer and is semicrystalline because of its sterioregularity. It has also been extensively investigated for its ability to support cell regeneration. [23, 24]

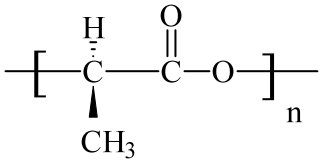

Figure 1 Chemical structure of P_LLA

1.4.2 Poly($_{D,L}$-lactic-*co*-glycolic) acid (PLGA)

PLGA is one of the most widely used synthetic degradable polymers in medicine. It is a random copolymer of lactic acid and glycolic acid and is amorphous due to non-sterioregularity. PLGA has a greater rate of hydrolysis than P_LLA, which is due to the glycolic acid content and its amorphous nature, giving it a resorption time of approximately 1-2 months. PLGA is a widely used polymer within the tissue engineering field and has demonstrated a proven biocompatibility with neurons as well as stem cells.[25, 26]

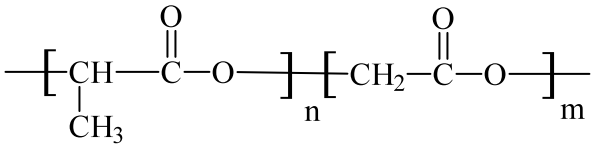

Figure 2 Chemical structure of PLGA

1.4.3 Polycaprolactone (PCL)

PCL is a thermoplastic material that has a melting temperature of *ca.* 60°C and T_g of *ca.* -60°C and a so it is rubbery at room temperature. PCL is easy to manufacture, and has a relatively slow degradation time, greater than approximately 12 months within the body.[27] PCL has been shown to support different cell types in tissue engineering, especially from *in vitro* cultures.[28]

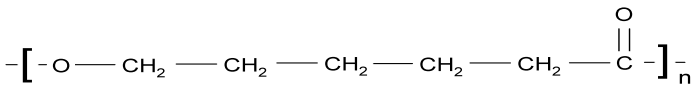

Figure 3 Chemical structure of PCL

1.5 Xyloglucan hydrogels

Another common type of material currently being investigated as alternatives to preformed scaffolds for tissue engineering are *in situ*-forming hydrogels.[29] One class of these "smart" materials are thermally responsive hydrogels which respond to small changes in temperature, often producing dramatic changes in their physical state and properties as the material forms physical cross-links.[30] The macroporous nature of some physical hydrogels and the volume of water phase present ensures cellular viability, permits cell migration and increases transportation of nutrients, oxygen and metabolites.

Thermally responsive xyloglucan is a polysaccharide formed using fungal β-galactosidase to remove more than 35% of the galactose side chains.[31] Xyloglucan is extracted from the tamarind seed and is a major component of higher plant cell walls. It is composed of a β-1,4 linked D-glucan backbone where the O-6 positions of the glucopyranosyl moieties are partially substituted with α-D-xylopyranose. Figure 4 shows

the structures of the four saccharide units of xyloglucan representing galactopyranose (Gal), glucopyranose (Glu) and xylopyranose (Xyl).

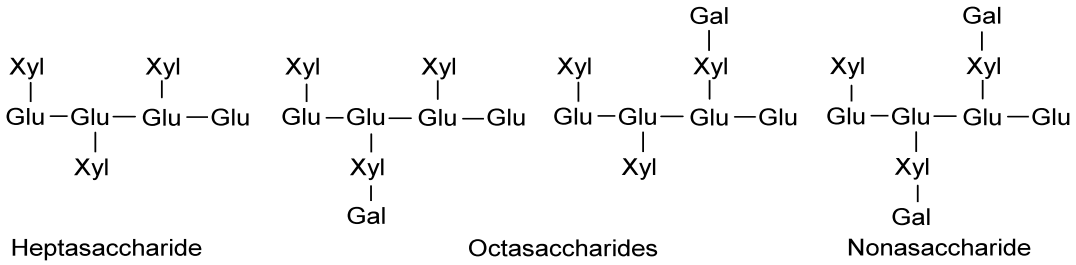

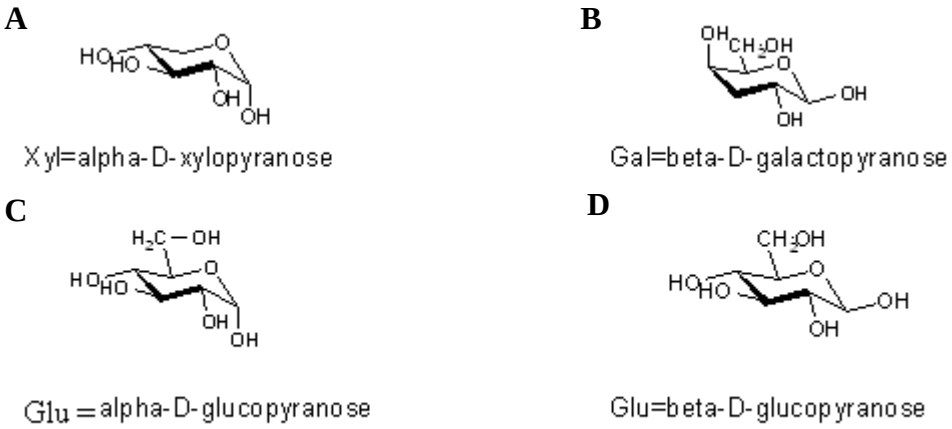

Figure 4 Oligiosaccharide structures found in xyloglucan A) hepata-saccharide B & C) octa-saccharide and D) nona-saccharide. Structures of the individual sugar units that exist in the three oligomer structures are also shown.

1.6 Research objectives and aims

The central hypothesis of this thesis was that electrospun nanofibrous scaffolds and hydrogels are suitable materials for neural tissue engineering within the CNS. Nanofibrous scaffold have an ability to support nerve infiltration and provide a means of directing it via contact guidance, whilst hydrogel scaffolds are capable of providing supportive microenvironments for neuronal support.

The aim of this project is focused on injectable/implantable scaffolds for the treatment of nerve damage within the CNS, in particular Parkinson's disease and spinal cord injury.

When regenerating damaged neural pathways, the logical location for the new cells is in the original position where they can receive the appropriate afferent signals. The problem with this approach is that the axons must be guided across the injury site in the case of spinal cord injuries (SCI), or from the substantia nigra (SNpc) to cells in the caudate putamen (CPu) in the case of Parkinson's disease, where they can make synaptic contact. In order to achieve this, an artificial microenvironment between such regions that allows axons to traverse this distance (approximately 5cm in humans for PD and variable for SCI) must be fabricated. Ideally this scaffold must also be resorbed to ultimately allow regenerated cells to exist within their natural niche microenvironments within their native extracellular matrix.

Therefore, manufacturing suitable scaffolds for this purpose is paramount to the successful regeneration of neural pathways within the CNS. Two different types of candidate scaffolds have been investigated for this application, electrospun nanofibres and thermally sensitive xyloglucan (an injectable hydrogel). The work presented in this thesis addresses three main research aims that are listed below.

Research Aims:

AIM 1: Manufacture novel nanofibrous and hydrogel scaffolds and evaluate their capacity to maintain and promote the differentiation of cortical neurones and NSCs *in vitro*.

AIM 2: Engineer these scaffolds to attempt to encourage directional guidance of neurites, through the immobilising of PDL in the case of the xyloglucan hydrogel, and through changing the chemistry, surface tension, fibre alignment and architecture in the case of the electrospun scaffolds.

AIM 3: Assess the effect of these modifications of both the electrospun and hydrogel scaffolds *in vivo*, attempting to optimise the scaffolds from AIM 1 & 2 to promote axonal guidance and reducing inflammation.

Electrospun fibres were investigated to provide contact guidance to neural processes. The design criteria when fabricating electrospun scaffolds was to generate a synthetic ECM to support neurones, whilst also providing a ***contact guidance conduit***. Furthermore, such scaffolds are inherently highly porous, nutrients and waste could be easily passed in and out of the scaffold and cell-cell interactions could be facilitated.

Xyloglucan scaffolds offer another alternative to the electrospun materials and the pros and cons of each are investigated in the thesis. The reason that xyloglucan hydrogels were selected was to complement the nanofibrillar scaffolds (that provide contact guidance) and provide a favourable and protective niche environment for neural stem cells and their progeny. This material is a "smart" thermoreversible hydrogel allowing it to be injected to a specific site within the body eg. a neural tract, and the gelation temperature is easily manipulated through the glactose removal ratio. The hydrogel can be compliance matched to tissue within the spinal cord by changes in the concentration.

Future work that lies outside the scope of this thesis will see both the electrospun fibrous scaffold and the hydrogel system combined into a ‘composite’ scaffold so that the advantages of each material for neural regeneration can be utilized to achieve the best outcomes; this will be addressed in Part III Chapter 8.

1.7 Thesis Outline

This thesis reports on the development of two unique neural tissue engineering scaffolds for cellular support and guided neurite extension within the CNS. For this reason this work is presented in three individual Parts.

Part I containing Chapters 2-4 focuses on the investigation of electrospun scaffolds;
Part II containing Chapters 5-7 is concerned with the examination of xyloglucan hydrogel.
Part III contains Chapter 8 linking the preceding two Parts so that ultimately the benefits of each scaffold can be easily recognised and incorporated into a 'composite' scaffold.

This thesis is submitted by publication. Within Part I a total of two publications are included in Chapter 2, three publications are included within Chapter 3 and one publication is included within Chapter 4. Part II consists of one publication included within Chapter 5, two publications included within Chapter 6 and one publication included within Chapter 7. As this thesis is submitted by publication the referencing styles, format and language used in each publication is specific to that of each journal.

1.7.1 Part I - Electrospinning

Chapter 2 is a literature review of electrospinning used for tissue engineering applications, including neural, bone, cartilage and cardiac tissue engineering. Also included is a literature review of the variety of characterisation methods used to investigate electrospun scaffolds, many of which have been used extensively within this thesis.

Chapter 3 contains *in vitro* studies that were conduced on electrospun scaffolds. It addresses how changes to the surface hydrophilicity of 2D films and 3D electrospun biomaterial scaffolds influence the behaviour of primary cortical neurones. The

differentiation of adult brain derived stem cells and their migration throughout electrospun PCL scaffolds is also explored.

Chapter 4 contains *in vivo* studies that were conducted using electrospun scaffolds produced from PCL. It investigates the inflammatory response that arises from introducing the scaffold within rat brains. Here we also explore the endogenous neurite infiltration into the scaffold at different time points.

1.7.2 Part II - Xyloglucan hydrogel

Chapter 5 is a literature review regarding the use of hydrogels specifically in neural tissue engineering within the central nervous system. The use of both naturally derived and synthetic hydrogels are explored.

Chapter 6 is a detailed investigation into the properties of xyloglucan hydrogels to ascertain how effective they could be as a neural tissue engineering scaffold. This investigation has particular focus on the morphology and gelation properties of the material. The interaction of embryonic cortical neurones and neural stem cells with xyloglucan scaffolds is also investigated in 2D and 3D culture.

Chapter 7 involves the *in vivo* implantation of xyloglucan hydrogels into the brain of adult rats. This hydrogel was also modified with polylysine and the inflammatory response of these materials along with the endogenous neurite infiltration into the scaffolds were investigated.

1.7.3 Part III - Conclusion and Future Work

Chapter 8 is the final chapter and contains the conclusion to this thesis. It also makes mention of future work that will be conducted. This chapter effectively links the preceding two parts of this thesis so that ultimately the benefits of each scaffold can be easily recognised and incorporated into "composite" scaffolds to generate a novel type of

neural tissue engineering construct that may have the potential to rapidly advance the field.

1.8 References

[1] R. Langer, J.P. Vacanti, Tissue Engineering, Science, 260 (1993) 920-926.

[2] L.G. Griffith, M.A. Swartz, Capturing Complex 3d Tissue Physiology *In Vitro*, Nature Reviews: Molecular cell biology, 7 (2006) 211-224.

[3] G.P. Dillon, Z. Yu, A. Sridharan, J.P. Ranieri, R.V. Bellamkonda, The Influence of Physical Structure and Charge on Neurite Extension in a 3d Hydrogel Scaffold, J Biomaterials Sci Polymer Ed, 9 (1998) 1049-1069.

[4] A.D. Buchli, M.E. Schwab, Inhibition of Nogo: A Key Strategy to Increase Regeneration, Plasticity and Functional Recovery of the Lesioned Central Nervous System, Annals of Medicine 37 (2005) 556-557.

[5] S. Worely, Resorative Surgery of the Central Nervous System by Means of Tissue Engineering Using Neurogel Implants, Neurosurgical Review, 23 (2000) 125-136.

[6] J. Jankovic, Parkinson's Disease: Clinical Features and Diagnosis, J Neurol Neurosurg Psychiatr, 79 (2008) 368-376.

[7] D. Gelb, E. Oliver, S. Gilman, Diagnostic Criteria for Parkinson Disease, Arch Neurol, 56 (1999) 33-39.

[8] K.A. Follet, The Surgical Treatment of Parkinson's Disease, Annu Rev Med, 51 (2000) 135-147.

[9] H.I. Hurtig, Problems with Current Pharmacological Treatment of Parkinson's Disease, Exp Neurol, 144 (1997) 10-16.

[10] Parkinson's Disease Foundation Inc. About Parkinson's. http://wwwpdforg/ 2005.

[11] Parkinson's Australia Inc. About Parkinson's Disease. http://wwwparkinsonsorgau/ .2004.

[12] R.A. Cripps, Spinal Cord Injury, Australia, 2004 – 2005, Research and Statistics Series, 29 (2006) Adelaide: AIHW

[13] M. Adams, J.F.R. Cavanagh, Campaign for Cures of Spinal Cord Injury Paralysis (Iccp): Another Step Forward for Spinal Cord Injury Research, Spinal Cord, 42 (2004) 273-280.

[14] Breast Cancer in Australia: An Overview. Camberra; 2006.

[15] Spinal Cord Injury Facts and Figures at a Glance. Alabama, Birmingham; 2006.

[16] D.R. Nisbet, K.E. Crompton, M.K. Horne, D.I. Finkelstein, J.S. Forsythe, Neural Tissue Engineering of the CNS Using Hydrogels-a Review., Journal of Biomedical Materials Research, 87 (2008) 251-263.

[17] C.M. Agrawal, K.A. Athanasiou, Technique to Control Ph in Vicinity of Biodegrading PLA-PGA Implants, J Biomed Mater Res, 38 (1997) 105-114.

[18] X. Yu, R.V. Bellamkonda, Dorsal Root Ganglia Neurite Extension Is Inhibited by Mechanical and Chondroitin Sulfate-Rich Interfaces., J Neurosci Res, 66 (2001) 303-310.

[19] K.E. Crompton, D. Tomas, D.I. Finkelstein, M. Marr, J.S. Forsythe, M. Horne, Inflammatory Response on Injection of Chitosan/GP to the Brain, J Mater Sci - Mater Med, 17 (2005) 633-639.

[20] P. Aebischer, P.A. Tresco, S.R. Winn, L.A. Greene, C.B. Jaeger, Long-Term Cross-Species Brain Transplantation of a Polymer-Encapsulated Dopamine-Secreting Cell Line, Exp Neurol, 111 (1991) 269-275.

[21] H.B. Lee, J.H. Lee, Biocompatibility of Solid Substrates Based on Surface Wettability Marcel Dekker, New York, 1995.

[22] S.J. Lee, G. Khang, Y.M. Lee, H.B. Lee, The Effect of Surface Wettability on Induction and Growth of Neurites from the PC-12 Cell on a Polymer Surface, Journal of Colloid and Interface Science, 259 (2003) 228-235.

[23] J. Harrision, S. Pattanawong, J.S. Forsythe, K.A. Gross, D.R. Nisbet, H. Beh, T.F. Scott, A.O. Trounson, R. Mollard, Colonization and Maintenance of Murine Embryonic Stem Cells on Poly(α-Hydroxy Esters), Biomaterials, 25 (2004) 4963.

[24] F. Yang, R. Murugan, C. Wang, S. Ramakrishna, Electrospinning of Nano/Micro Scale Poly(L-Lactic Acid) Aligned Fibers and Their Potential in Neural Tissue Engineering, Biomaterials, 26 (2005) 2603-2610.

[25] K. Ma, C.K. Chan, S. Liao, W.Y. Hwang, Q. Feng, S. Ramakrishna, Electrospun Nanofiber Scaffolds for Rapid and Rich Capture of Bone Marrow-Derived Hematopoietic Stem Cells., Biomaterials, 29 (2008) 2096-2103.

[26] K.D. Newman, M.W. McBurney, Poly(D,L Lactic-Co-Glycolic Acid) Microspheres as Biodegradable Microcarriers for Pluripotent Stem Cells, Biomaterials, 25 (2004) 5763–5771.

[27] C.X. Lam, D.W. Hutmacher, J.T. Schantz, M.A. Woodruff, S.H. Teoh, Evaluation of Polycaprolactone Scaffold Degradation for 6 Months *In Vitro* and *In Vivo*., Journal of Biomedical Materials Research, (2008) 10.1002/jbm.a.32052.

[28] L. Ghasemi-Mobarakeh, M.P. Prabhakaran, M. Morshed, M.H. Nasr-Esfahani, S. Ramakrishna, Electrospun Poly(ε-Caprolactone)/Gelatin Nanofibrous Scaffolds for Nerve Tissue Engineering., Biomaterials, 29 (2008) 4532-4539.

[29] S. Woerly, Restorative Surgery of the Central Nervous System by Means of Tissue Engineering Using Neurogel Implants, Neurosurg Rev, 23 (2000) 59-77.

[30] R. Bellamkonda, J.P. Ranieri, N. Bouche, P. Aebischer, Hydrogel-Based Three-Dimensional Matrix for Neural Cells, J Biomed Mater Res, 29 (1995) 663-671.

[31] M. Shirakawa, K. Yamatoya, K. Nishinari, Tailoring of Xyloglucan Properties Using an Enzyme, Food Hydrocolloids, 12 (1998) 25-28.

Part I
Electrospinning

Chapter 2

Part I - Electrospinning

Literature Review

Contents

Declaration

Two publications have been inserted into Chapter 2. Below the reference information and publication status for these publications is provided.

Chapter 2.1

D.R. Nisbet, W. Shen, D.I. Finkelstein, M.K. Horne, J.S. Forsythe, "Electrospinning for tissue engineering applications", *J. Biomat. App.*, accepted, Sep. 2008.

Chapter 2.2

D.R. Nisbet, A. Rodda, D. I. Finkelstein, M. K. Horne, J. S. Forsythe, W. Shen, "Characterisation of electrospun scaffolds : problems and improvements", *Colloids and Surfaces B.*, submitted October 2008.

Declaration for Thesis Chapter 2.1

Monash University

Declaration by candidate

In the case of Chapter 2.1 the nature and extent of my contribution to the work was the following:

Nature of contribution	Extent of contribution (%)
Planning, research and article writing.	85

The following co-authors contributed to the work. Co-authors who are students at Monash University must also indicate the extent of their contribution in percentage terms:

Name	Nature of contribution	Extent of contribution (%) for students
W. Shen	Assisted in planning & corrected manuscript	N/A
D.I. Finkelstein	Assisted in planning & corrected manuscript	N/A
M.K. Horne	Assisted in planning & corrected manuscript	N/A
J.S. Forsythe	Assisted in planning & corrected manuscript	N/A

Candidate's Signature	[redacted]	**Date** 14/10/2008

Declaration by co-authors

The undersigned hereby certify that:

(1) the above declaration correctly reflects the nature and extent of the candidate's contribution to this work, and the nature of the contribution of each of the co-authors.
(2) they meet the criteria for authorship in that they have participated in the conception, execution, or interpretation, of at least that part of the publication in their field of expertise;
(3) they take public responsibility for their part of the publication, except for the responsible author who accepts overall responsibility for the publication;
(4) there are no other authors of the publication according to these criteria;

(5) potential conflicts of interest have been disclosed to (a) granting bodies, (b) the editor or publisher of journals or other publications, and (c) the head of the responsible academic unit; and
(6) the original data are stored at the following location(s) and will be held for at least five years from the date indicated below:

Name	Location
W. Shen *	Monash University - Australian Pulp and Paper Institute
D.I. Finkelstein	The Mental Health Research Institute of Victoria
M.K. Horne	Melbourne University - Howard Florey Institute
J.S. Forsythe	Monash University - Department of Materials Engineering

Name	Signature	Date
W. Shen *		14/10/2008
D.I. Finkelstein		14/10/2008
M.K. Horne		14/10/2008
J.S. Forsythe		14/10/2008

Declaration for Thesis Chapter 2.2

Monash University

Declaration by candidate

In the case of Chapter 2.2 the nature and extent of my contribution to the work was the following:

Nature of contribution	Extent of contribution (%)
Planning, research and article writing.	80

The following co-authors contributed to the work. Co-authors who are students at Monash University must also indicate the extent of their contribution in percentage terms:

Name	Nature of contribution	Extent of contribution (%) for students
A.E. Rodda	Assisted in research, writing & corrected manuscript	10
D.I. Finkelstein	Assisted in planning & corrected manuscript	N/A
M.K. Horne	Assisted in planning & corrected manuscript	N/A
J.S. Forsythe	Assisted in planning & corrected manuscript	N/A
W. Shen *	Assisted in planning & corrected manuscript	N/A

Candidate's Signature	[redacted]	**Date** 14/10/2008

Declaration by co-authors

The undersigned hereby certify that:

(7) the above declaration correctly reflects the nature and extent of the candidate's contribution to this work, and the nature of the contribution of each of the co-authors.
(8) they meet the criteria for authorship in that they have participated in the conception, execution, or interpretation, of at least that part of the publication in their field of expertise;
(9) they take public responsibility for their part of the publication, except for the responsible author who accepts overall responsibility for the publication;
(10) there are no other authors of the publication according to these criteria;

(11) potential conflicts of interest have been disclosed to (a) granting bodies, (b) the editor or publisher of journals or other publications, and (c) the head of the responsible academic unit; and
(12) the original data are stored at the following location(s) and will be held for at least five years from the date indicated below:

Name	Location
A.E. Rodda	Monash University - Department of Materials Engineering
D.I. Finkelstein	The Mental Health Research Institute of Victoria
M.K. Horne	Melbourne University - Howard Florey Institute
J.S. Forsythe	Monash University - Department of Materials Engineering
W. Shen *	Monash University - Australian Pulp and Paper Institute

Name	Signature	Date
A.E. Rodda		14/10/2008
D.I. Finkelstein	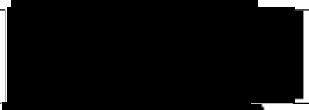	14/10/2008
M.K. Horne		14/10/2008
J.S. Forsythe	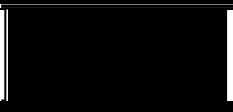	14/10/2008
W. Shen *		14/10/2008

2.0 Literature Review

2.1 Electrospinning for tissue engineering applications

Electrospinning is a method that has been increasingly used in tissue engineering to fabricate 3D scaffolds, from either natural or synthetic polymers, as it is possible to simulate some of the features of the natural cellular microenvironment. While in this thesis electrospinning has been employed to produce scaffolds specifically for neural tissue engineering, this method is also ultilised to fabricate scaffolds for a variety of other tissue engineering applications. The following publication provides a literature review of different tissue engineering applications where electrospinning has been employed to fabricate a scaffold. These application are, neural (the focus of this thesis), bone, cartilage and vascular tissue engineering.

A review of the cellular response on electrospun nanofibers for tissue engineering

D.R. Nisbet[1,2], W. Shen[3], D.I. Finkelstein[4], M.K. Horne[5], J.S. Forsythe[1,2]*

1. Department of Materials Engineering, Monash University, Victoria, Australia

2. CRC for Polymers, 32 Business Park Drive, Notting Hill, VIC, Australia.

3. Australian Pulp and Paper Institut, Monash University, VIC, Australia

4. The Mental Health Research Institute of Victoria Parkville, VIC, Australia

5. Howard Florey Institute, The University of Melbourne, VIC, Australia

2.1.1 ABSTRACT

Electrospinning has been employed extensively in tissue engineering to generate nanofibrous scaffolds from either natural or synthetic biodegradable polymers to simulate the cellular microenvironment. Electrospinning rapidly produces fibers of the nano length scale and the process offers many opportunities to tailor the physical, chemical and biological properties of a material for specific applications and cellular environments. There is growing evidence that nanofibers amplify certain biological responses such as contact guidance and differentiation however this has not been fully exploited in tissue engineering. This review addresses the *cellular interactions* with electrospun scaffolds, with particular focus on neural, bone, cartilage and vascular tissue regeneration. Some aspects of scaffold design, including architectural properties, surface functionalization and materials selection are also addressed.

2.1.2 KEY WORDS

Electrospinning; Neural tissue engineering; Bone; Cartliage; Heart; Cardiac; Stem Cell; Polymer.

2.1.3 INTRODUCTION

An increasingly growing trend in tissue engineering is the production and deliberate manipulation of nano-scale 3D architectures to control cell function[1]. Nano-fibrous scaffolds are ideal for this purpose because their dimensions are similar to components in the extracellular matrix (ECM) and mimic its fibrillar structure, providing essential cues for cellular organisation, survival and function[2]. Electrospinning provides a versatile and rapid method to fabricate nanofibrous scaffolds. While these nanofiber assemblies do not yet fully mimic the native ECM, electrospinning does allow for the engineering of fibers at the nano length scale.

Electrospun scaffolds, often incorporating biological polymers, composites or even ceramic precursors can provide bioactive cues[3]. Nanofibrous scaffolds have inherently high porosities and surface-area-to-volume ratios[4], whilst also offering a wide variety of topographical features to encourage cellular adhesion and proliferation[5]. Furthermore, different scaffold architectures may have varying influence on cell function. Generally, electrospinning produces a 3D mesh of non-woven nano/micro fibers. However, the orientation of the fibers can be easily changed using different collection devices such as dual rings[6], rapidly rotating drums[7], or a gap method of alignment[8]. In these cases directional scaffolds can be produced where the fibers are highly aligned, which may be useful to replicate the ECM for specific tissue such as tendons, where the fibrils are also aligned.

2.1.3.1 Electrospun Nanofibres: 2D or 3D Scaffolds?

One of the major outcomes of tissue engineering has been the realisation of the potent effect that 3D environmental signalling plays on cellular behaviour. Cells behave differently when cultured in 3D compared to traditional 2D cultures and often adopt more *in vivo* like morphologies[5]. Culturing cells in 3D radically alters the mechanical signalling from those provided in 2D, thus affecting cell-receptor ligation, intercellular

signalling and cellular migration[9, 10]. The 3D environment also influences the diffusion and adhesion of proteins, growth factors and enzymes, which ensures cell viability and can influence function[10].

Cells cultured on electrospun scaffold often adhere to the surface of the scaffold with minimum penetration. This may be due to a combination of small interfiber distances, fiber diameters, size of the cells and the chemical and interfacial properties of the fibers. While in these instances the cells don't migrate into the scaffold, it is still uniquely different from a 2D planar surface, as the cells receive nutrients and growth cues 3-dimensionally. This concept has recently been exploited with the commercialisation of electrospun nanofibrous culture inserts to replace or augment the traditional 2D tissue culture surfaces.[11, 12]

However in some instances cells can be encouraged to migrate and spread throughout electrospun nanofibrous scaffolds and are truly in a 3D environment[13]. Dissociated neural stem cells (NSCs) plated onto electrospun PCL nanofibers exist on the surface of the scaffold and form large spheres, however when the PCL nanofibers were aminolysed the cells penetrated and populated the entirety of the scaffold[13].

2.1.3.2 The Extracellular Matrix (ECM)

Methods of influencing cellular function using electrospun scaffolds remains a challenge, as the scaffold must mimic some of the components that make up the natural ECM, whilst providing the appropriate biochemical and mechanical inputs for the cellular microenvironment[10, 14]. The ECM is defined as any material that is known broadly as tissue, but which is not part of a cell. The main components that make up the ECM are glycoproteins (the most abundant being collagens), proteoglycans and hyaluronic acid[15]. However, the physical structure and composition of ECM is often unique to specific tissues, and in some instances little is known of the components and 3D arrangements. The ECM often contains other molecules depending on the specific tissue, such as fibrin, elastin, fibronectins, laminins, hydroxylapatite and even fluids such as

serum and bound adhesive motifs. Local physiological events may deliver proteases and growth factors into the ECM[16], providing chemical cues through which the ECM can influence cellular behaviour[17]. The ECM can also influence cellular function by the physical arrangement of the network of molecules that constitute it[18, 19]. As fibril arrangements are tissue specific, it has proven difficult to replicate the physical features of the ECM for regenerative medicine[2]. However a comprehensive knowledge of the microenvironmental niche of cells is an essential starting point for the successful manipulation of cells in 3D scaffolds.

This article reviews the *cellular interactions* on electrospun scaffolds with particular reference to their use in neural, bone, cartilage and vascular regeneration. Some of the challenges in scaffold design for these particular applications are discussed, including scaffold architecture, surface functionalisation and material selections.

2.1.4 CELLULAR INTERACTIONS ON ELECTROSPUN SCAFFOLDS FOR NEURAL TISSUE ENGINEERING

The growth cone at the tip of the axon transduces guidance cues into intracellular signals for neurite extension and orientation. Growth cones cyclically extend into the ECM, searching for cues and retract when inhibitory molecules are encountered or if no positive cues are found[20]. Guidance cues may be diffusible chemicals or surface contact chemicals inherent in the physical structure of the surface. Cues appropriate to the axon must be built into scaffolds if they are to provide positive enhancement of neural regeneration. Conventional macroporous hydrogel scaffolds are isotropic, providing no directional cues and thus depend entirely on exogenously delivered neurotrophic factors for directional axon growth[21, 22]. Polymer nanofibers on the other hand can interact intimately with the growth cone providing contact guidance cues allowing for directed neurite outgrowth[5, 23].

By optimising the nano-scale dimensions of 3D polymer nanofibrous scaffolds, neuronal morphologies more closely resemble neurons *in vivo*, than for those cultured on flat 2D substrates composed of the same material[5]. Electrospun scaffolds may provide superior cues for the differentiation of neurons and neurite outgrowth because of the large surface area, hence the higher concentrations of adsorbed serum proteins[13].

Neurons grown on surfaces with parallel nanoscale ridges extend neurites that are aligned with the ridges[24, 25]. Similarly, the direction of neuronal growth from neural stem cells (NSC) depends on fiber alignment[23]. Neurites extending from neonatal mouse cerebellum C17.2 NSCs run parallel to the aligned electrospun P_LLA nanofibers (Figure 1). Axons of up to 100 μm formed on aligned fibers and were attributed to enhanced contact guidance[23]. However, the highly aligned nature of the scaffold (and therefore low interfiber distance) may limit penetration of the cells into the scaffold and cause the scaffold to be perceived as a 2D surface with groves instead of a porous 3D scaffold.

Dorsal root ganglia (DRG) explants cultured on aligned electrospun P_LLA grew neurites radially outwards before they turned to follow electrospun fibers upon contact[26]. This provides a further example of neurite outgrowth being enhanced by contact guidance from the substrate. However, when cortical neurons were cultured on random, non-woven electrospun PLGA and P_LLA scaffolds there was little evidence of contact guidance with the axons extending in random directions on non-aligned scaffolds[5]. Specific neuronal cell types may respond in different ways to guidance cues. For cortical neurons, the density of electrospun fibers had a stronger influence on neurite outgrowth than contact guidance. When the interfiber distance of the scaffold was greater than 15μm, neurites followed the fibers[5]. Alternatively, neurites avoided regions of greater fiber density when neighbouring fibers were less than 2μm apart, and at intermediate densities, axons traversed perpendicularly to the scaffold fibers. Although these investigations are preliminary, the findings are similar to human umbilical vein endothelial cells which attached to many fibers when they were close together[27], but attached principally to one fiber when the interfiber distance was large. The axons of cortical neurons cultured on random electrospun scaffolds make marked directional

changes which can not be explained by topological cues that they traverse, a contrasting result to what has been observed with NSCs and DRG explants[5, 23, 26]. However analysis of axonal directions on random weave may be difficult to interpret and a systematic comparison of fiber direction and other surface characteristics will be necessary to fully explore the relative importance of fiber density, fiber alignment and surface characteristics in guiding neurites. Other factors, for example chemical cues from adjacent neurons, will also need to be investigated.

Fiber diameter appears to play an important role on the differentiation of NSC into neurons with more cells differentiated on aligned nanofibers than on aligned microfibers, (Figure 1)[23]. While fiber diameter may influence NSC differentiation, surface chemistry is also important. NSCs attach more readily to electrospun scaffolds when collagen was immobilised on the surface of the polymer fibers[28]. Aminolysation of the surface of PCL electrospun fibers with ethylene diamine (ED) improved the adhesion and migration into the scaffold of adult rat brain derived NSCs[13]. Adhesion to the polymer fibers may be due to the type and amount of adsorbed proteins on the modified surfaces or the optimal conformation of adsorbed proteins. When NSCs were seeded onto the scaffolds in the presence of either 10% fetal bovine serum or mitogens, they differentiated primarily towards oligodendrocytes[13]. The preferential differentiation of NSCs towards oligodendrocytes may be due to the 3-dimensitonal nature of the microenvironment and has potential to be employed to achieve the remyelination of damaged axons for spinal cord injuries, as it is the oligodendrogytes are responsible for the myelination of axons. Biomaterials that enhance proliferation of both neurones and supporting cells may support better reinnervation than those that focus exclusively on the neuron.

Neuronal adhesion and neurite outgrowth from cerebellar granule, cerebral cortical, hippocampal, motor and dorsal root ganglion neurons were similar on electrospun polyamide nanofibrous membranes and planar surfaces (poly-L-lysine coated glass coverslips)[29]. However, for the cell types tested the number of neurites increased on the electrospun membranes. The interactions of neurones with electrospun polyamide

nanofibrous scaffolds has also been further enhanced by covalently attaching neuroactive peptides derived from human tenascin-C to the surface (the peptides were the D5 peptide and an extended version known as the D5' peptide). The peptide modification enhanced neuron adhesion, the number of neurites and neurite extension[29].

Electrospun conduits have been used for the culture of explants as preliminary studies for *in vivo* experiments[30]. Aligned nanofibers fabricated from PCL and PCL blended with collagen (25:75), were designed as scaffolds to encourage nerve guidance[30]. Both the PCL and blended samples supported oriented axonal growth and Schwann cell migration from dorsal root ganglia explants[30]. Schwann cells serve a similar purpose to oligodendrocytes, but they myelinate peripheral nerves and may be critical in regenerating axons. The response of Schwann cells to various types of electrospun scaffolds has been investigated *in vitro*[31]. The next step will be to incorporate electrospun scaffolds that support cell proliferation, axonal outgrowth and migration from DRG explants into the intact brain or explants. While electrospun scaffolds have not been deployed *in vivo*, fibrous tubular conduits produced by microbraiding have been investigated[32]. The conduits were placed between the two ends of a transacted rat sciatic nerve and no inflammatory response or nerve body colonization resulted. Furthermore, neurites grew into and through the conduit over 1 month[32]. Although this conduit was produced using microbraiding, it points to the potential of electrospun fibers which may provide enhanced contact guidance. Chitosan tubes have been prepared by electrospinning with the particular application of nerve-regenerating guidance tubes in mind[33].

Electrospun scaffolds are usually fabricated prior to sterilisation and are subsequently seeded with cells, or implanted into the body. However, coaxial electrospinning technology can be used to produce composites of living brain cells and poly(dimethylsiloxane)[34]. A bio-suspension of astrocytoma cell line in medium was formed and encapsulated within the poly(dimethysiloxane) microthread shell[35]. The cells that were collected and cultured post electrospinning remained viable and showed no evidence of damage during the process. This technique demonstrates the possibility of

depositing living cells as composite microthreads into brain tissue and opens the door for many modifications, such as replacing the poly(dimethysiloxane) fibers with biodegradable polymers of superior structural integrity and compliance matching of the scaffold to the surrounding tissue. This technology is a significant advance in the electrospinning process with a variety of applications, not only for tissue engineering, but also to address fundamental cellular and biological questions.

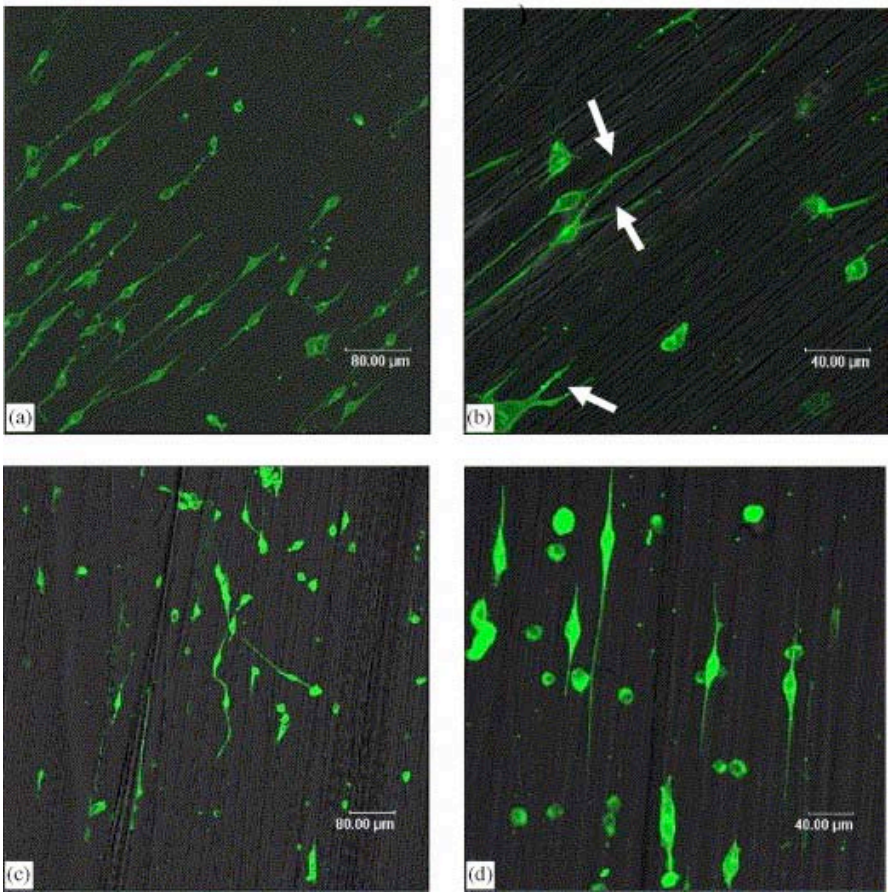

Figure 1: Laser scanning confocal microscopy (LSCM) of neonatal mouse cerebellum C17.2 stem cells (NSC) after 2 days of culture on aligned nano fibers; A) low magnification images (×200); B) high magnification image (×400); and aligned micro fibers; C) low magnification images (×200); D) high magnification image (×400). Reproduced by permission from Elsevier[23].

2.1.5 CELLULAR INTERACTIONS ON ELECTROSPUN SCAFFOLDS FOR BONE TISSUE ENGINEERING

Bone is a composite material made from an organic phase of collagen, gylcoproteins, and glycosaminoglycans (GAGs) and an inorganic phase primarily consisting of hydroxyapaptite (HA) $Ca_{10}(PO_4)_6(OH)_2$ [36]. Bone serves several critical functions including muscular support, production of blood cells and immune cells and as a mineral reservoir to maintain electrolyte balance in the body. Bone may be lost after trauma, cancer, fractures, periodontitis, osteoporosis and infectious disease and presently there is no definitive method for regeneration[37]. Bone grafts are increasingly used, however they are plagued by high failure rates of between 16% to 50%[38]. Autographs also present problems associated with a secondary surgery site as well as a limited supply and morbidity of the donor site[39]. Similarly metal implants have a high failure rate and often require a second surgical procedure[40]. Tissue engineering approaches are therefore presently being investigated as a method of regenerating bone in defects. Scaffolds engineered by electrospinning are increasing being utilised although they currently lack the mechanical integrity for major load bearing applications.

Mesenchymal stem cells (MSCs) are precursor cells for bone and are central to the process of bone and connective tissue repair. When seeded onto PCL nanofibers, they differentiate into osteoblasts, migrate into the scaffold and produce collagen[41]. The scaffold constructs were dimensionally stable and became noticeably harder over 4 weeks, presumably due to mineralisation. MSCs cultured on PCL nanofibrous scaffolds have been implanted into the omenta of rats, where they were dimensionally stable with evidence of mineralization and type I collagen within the graft[41].

When HA is incorporated into polymer nanofibers it creates more biomimetic constructs and improves the mechanical properties. Employing a stepwise process, nanocrystals of HA were incorporated into electrospun gelatin fibers by initially mineralising HA in the gelatin and then forming electrospun non woven membranes which were subsequently

crosslinked[42]. Up to 40% HA could be successfully incorporated using this technique: above this the electrospinning process became unstable and the fibers beaded. More bone was produced (measured by production of bone-derived cell factor [MG63] and alkaline phosphate [ALP] activity) on the 20 & 40% HA nanofibers compared to the gelatin control.

HA and bone morphogenetic protein (BMP) were incorporated in electrospun nanofibers of silk fibroin and promoted differentiation of human MSCs towards an osteogenic fate[43]. When HA and BMP were used in combination they acted synergistically to enhance mineralisation. The aqueous electrospinning process prevented denaturing of the BMP and it is envisaged that this process could be used for the delivery of other labile proteins. Nanofibers of starch/PCL blends (30:70), produced by electrospinning were incorporated between microfibers (produced via a fiber bonding process) of the same material forming “nano-bridges” (average diameter of fibers was 400nm)[44]. The larger microfibers were incorporated to increase the pore size and therefore improve cell migration. Interestingly, human osteoblast-like osteosarcoma and rat bone marrow stromal cells bridged the microfibers using the nanofibers. The nanofiber bridges also increased metabolic activity, growth rates and ALP activity.

Badami *et al.* recently addressed the issue of nanofiber scaffold morphology on bone tissue behaviour[45]. Higher densities of osteoprogenitor cells (MC3T3-E1) were obtained when cultured on randomly orientated meshes with 2.1 μm fiber diameter compared to smaller fiber diameters of 0.14 μm[45]. There was no increase in ALP activity, suggesting that there was no greater propensity to form bone like structures. Cell morphology was not influenced by the fiber diameters, but was smaller than the cells cultured on the 2D controls. The aspect ratio of the cells cultured on the larger fibers was significantly higher and attributed to increased contact guidance. Focal adhesion contacts occurred predominantly as clusters along the polymer fibers and the actin stress fibers extended perpendicularly across the polymer fibers and were parallel to each other. (Figure 2)

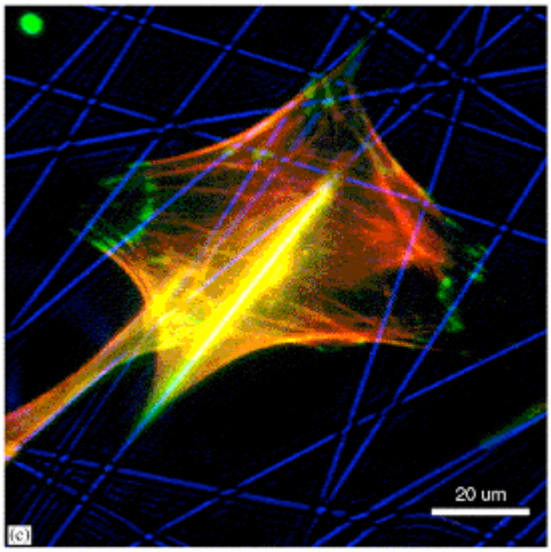

Figure 2: Immunofluorescent staining of adherent MC3T3-E1 cells has been superimposed onto a phase contrast image of PDLLA fibers (red). The green corresponds to vinculin and the blue is the actin. Reproduced by permission from Elsevier[45].

2.1.6 CELLULAR INTERACTIONS ON ELECTROSPUN SCAFFOLDS FOR ARTICULAR CARTILAGE TISSUE ENGINEERING

The articular cartilage of joints provides a smooth, near frictionless surface, whilst also mediating load transfer between the joint and the underlying subchondral bone[46-48]. The architecture of the scaffold is critical, and should promote cellular adhesion, proliferation, differentiation and migration, whilst also providing resistance to tensile, compressive and shear stresses. Electrospinning can produce structures that mimic some of the features of the ECM of articular cartilage[49]. However, while electrospinning can produce similar fiber diameters, composition and alignment, the native ECM of cartilage is much more complex than the nanofibrous scaffolds developed thus far. The native cartilage consists of a complex arrangement of fibers that are both parallel and perpendicular to the surface of a joint. The exact structural arrangements of nanofibrous

scaffolds to achieve the best tissue engineering outcomes for articular cartilage is currently not well understood. It seems that mimicking some of the features of the native ECM may be good enough for tissue engineering applications until the cells develop their own ECM. For instance it has been shown that submicron fibers support chondrogenesis, which is relevant to the quantity of cartilage that can be produced and the subsequent integration into host tissue[50].

Nanofibrous scaffolds for cartilage tissue have been electrospun from chitosan [50, 51], chitosan/PEO (90:10)[49], PLGA[52], PLA-PEG[52], PCL[8, 53], collagen type II[47] and hyaluronic acid[4]. All of these materials support chondrogenesis and can be seeded with either chondrocytes or MSCs and generally the cellular attachment and proliferation on electrospun nanofibers is improved when compared to 2D surfaces[54]. MSCs cultured on randomly orientated PCL electrospun nanofibers underwent chondrogenesis to a significantly greater extent compared to the benchmark high density cell pellet (CP) protocol[53]. The presence of transforming growth factor β (TGF) is necessary for chondrogenesis and similar cell morphologies are obtained in both culture systems (Figure 3).

Crossslinked electrospun collagen type II scaffolds provide suitable environments for chondrocyte growth and infiltration *in vitro*.[47] Chitosan/PEO blends (90:10) have been electrospun to produce aligned 3 μm parent fibres which were interestingly bridged by much smaller nanofibres which formed possibly by a charge dissipation process[51]. Chrondrocyte proliferation on the electrospun scaffolds were similar to flat cast films of the same material after 3 and 7 days culture but were significantly higher after 10 days. The elastic modulus of these scaffolds were significantly greater than cast films (2.25 MPa compared to 1.19 MPa), demonstrating that electrospun chitosan scaffolds are able to be used for some load bearing applications.

So far, the assessment of scaffold materials for cartilage tissue engineering has been related to biocompatibility and promotion of cellular proliferation and infiltration. Whilst there are many positive outcomes resulting from this research, there are still some major

limitations that must be understood and overcome. In general an electrospun scaffold for this type of application would be utilized to support regeneration and not be a permanent implant. However to successfully achieve this, the major challenge of satisfactorily withstanding compressive stresses *in vivo* must be addressed. More research will be required to address the integration of the scaffold within the boundary between the implant and surrounding tissue, as well as attaching the implant, or tissue once the scaffold has degraded to the bone. This may require the development of advanced 'composite' scaffolds; for instance the incorporation of hydrogels with electrospun materials to support compressive stresses, bioceramic nanocomposites for strengthening and macro sized elements to fulfil the load bearing requirements.

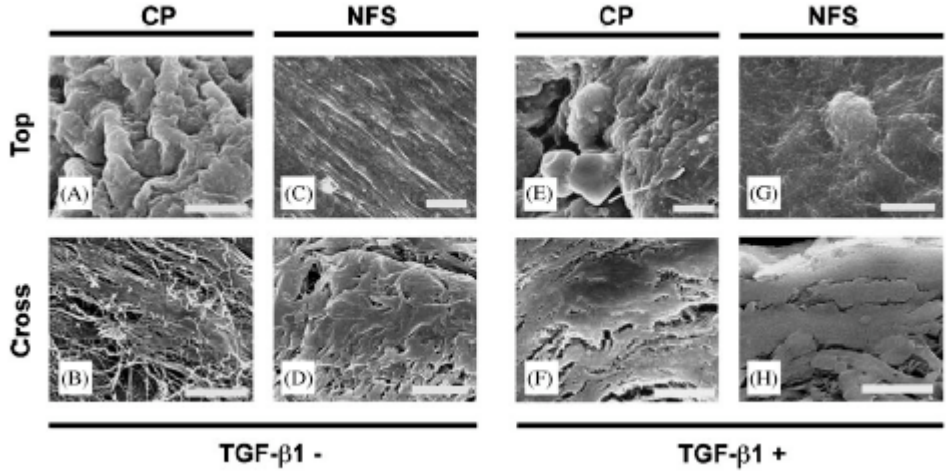

Figure 3: Morphology of MSCs after 21 days cultures on random 700 nm PCL electrospun fibers (NFS) and the cell pellet protocol control (CP). Figures A-D represent cultures maintained without TGF-β1 and E-H were cultures with TGF-β1 treatment. The image shows a top view (Top) and cross-sectional (Cross) view of the MSC cells. Reproduced by permission from Elsevier[53].

2.1.7 CELLULAR INTERACTIONS ON ELECTROSPUN SCAFFOLDS FOR VASCULAR TISSUE ENGINEERING

2.1.7.1 Vascular Grafts

The challenge for producing vascular grafts is to engineer vascular replacements that can withstand pulsation (i.e. have adequate shape recovery), and are able to withstand the high pressure and flow rate of the blood stream. Compliance matching also presents a major challenge and has been addressed by modifying the materials, structure and fabrication of the graft[55, 56], without compromising the capacity for cells to form strong attachments and a complete monolayer covering of the graft to reduce thrombus[57, 58]. A further complication with compliance matching arises when biodegradable materials are used, as their properties change over time. Decisions on compliance matching a scaffold to tissue needs to be made during scaffold design to determine whether it is required to initially match the properties exactly or allow for the matching to occur over time (degradation). A major reason that grafts fail is because the graft surface is incompletely covered by endothelial cells and as a consequence myointimal hyperplasia occurs[59]. To address this problem, scaffold materials have been coated with proteins such as fibronectin, vitronectin and lamin[60]. However, such surface proteins also provide good substrates for platelet adhesion resulting in thrombus[61]. Seeding of autologous endothelial cells (ECs) onto the vascular grafts prior to surgery has been attempted to avoid platelet adhesion and the formation of thrombus[62].

Electrospinning offers the potential for greater control over composition, mechanical properties and structure of a graft[62-64] making it easier to match the compliance of the synthetic scaffold to that of the native artery. This technique is used to fabricate vascular grafts and heart tissue constructs[63, 65-67]. Topographically aligned submicron fibers have similar circumferential orientations to the cells and fibrils found in the medial layer of the native artery[68]. Because of these similarities cell viability is often superior on electrospun scaffolds than on other substrates. Electrospun vascular grafts have been

produced from collagen and elastin[69], PLGA[64], poly($_L$-lactide-co-ε-caprolactone) (PLCL)[65, 68], polyethylene terephhalate (PET)[62], and polyurethane (PU)[63].

Many *in vitro* studies have focused on optimizing growth, development and adhesion of cells on electrospun scaffolds produced for vascular grafts. Human coronary artery smooth muscle cells (SMCs) have been investigated for their ability to form a complete monolayer of cells over aligned electrospun PLCL (75:25) nanofibers of approximately 500 nm in diameter[68]. The SMCs adhered and migrated in the direction of fiber alignment, and the phenotype was spindle-like contractile, as shown in Figure 4. The distribution of the smooth muscle cytoskeleton proteins within the cells was in the direction of alignment and the cell adhesion and proliferation were superior on the electrospun scaffold than the film controls. Electrospun PLCL is also mechanoactive and can be designed to pulsate synchronously by changing the electrospun wall thickness[65].

Human coronary artery endothelial cells (HCAECs) have been cultured on electrospun scaffolds produced from PLLA-CL that were either coated[70] or blended with collagen [71]. In both instances the nanofibrous scaffolds enhanced the viability, spreading and attachment of the HCAECs. HCAECs cultured on aligned collagen coated nanofibers produced from the same materials grew along the direction of fiber alignment and had elongated morphologies that were similar to native endothelial cells under blood flow[72].

In some instances 3D electrospun scaffolds have been “outperformed” by 2D surfaces in terms of cell proliferation rates and adhesion. Human vascular endothelial cells have enhanced adhesion and proliferation rates when cultured on 2D surfaces compared to 3D electrospun scaffolds of PLLA[73]. However this provides opportunities for the development of composite scaffolds for vascular tissue engineering and indeed all tissue engineering applications. Different cells respond uniquely to interfacial properties, some interacting more favourably on smooth 2D surfaces e.g. endothelial cells, and others more favourably on rough 3D scaffolds e.g. smooth muscle cells. One can therefore envisage an advanced composite 3D scaffold that incorporates nanofibers and 2D surfaces for the

growth and control of different cell types required for the successful development of vascular grafts by tissue engineering.

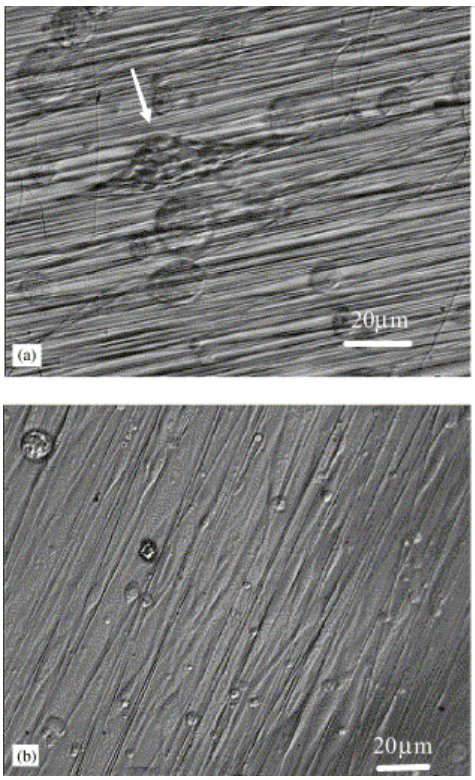

Figure 4: Image of SMCs that have adhered to aligned PLCL and migrated along the scaffolds in the direction of fiber alignment. A) represents an image taken 1 hour after the SMCs were seeded and B) is taken 5 hours after seeding. Reproduced by permission from Elsevier[68].

2.1.7.2 Cardiac Grafts

The requirements involved in fabricating cardiac grafts are similar to those faced in producing vascular grafts as the scaffolds must withstand pulsation and the high pressure and flow rate of the blood stream. It also follows that the scaffold must promote strong cellular attachment whilst also being compliance matched to the surrounding tissue. Currently in cardiac grafts cellular survival is a critical issue, as generally the cells are dense in the outer regions of the graft meaning that the transportation of nutrients and waste in and out of the scaffold is restricted[74, 75]. This results in significantly less

cells in the inner regions of the scaffold producing an undesired core effect[75]. Therefore an important design criterion is to promote the rapid vascularisation of the scaffold.

Electrospinning offers the potential to fabricate highly porous scaffolds to promote the transportation of nutrients and waste and encourage blood vessel formation. This technique has been investigated as a potential method of fabricating cardiac grafts. Primary cardiomyocytes (CMs) cultured on electrospun P_LLA and PLGA scaffolds make use of external cues for isotropic and anisotropic growth. Figure 5 shows the architecture of the nanofibers designed to allow cells to embed and encourage better adhesion[66]. These studies suggest that a desirable scaffold for cardiac grafts should consist of aligned fibers in order to provide contact guidance cues, but have 'adequate' porosity to allow the cells to respond to external cues and allow for the transportation of nutrients and waste in and out of the scaffold.

Random non-woven meshes of PCL were electrospun onto wire rings, before being coated with type I collagen to improve the cellular attachment[75]. On such scaffolds, rat cardiomyocytes formed tight arrangements and intercellular contacts throughout the entire mesh. The scaffolds were thin and soft enough to ensure that the contractions of the cardiomyocytes could occur at their normal frequency.

Electrical stimulation increases the adsorption of serum proteins on electrically conducting polymers for more favourable cellular interactions[2]. Blends of polyaniline and gelatin have been electrospun to determine if the electrical conductivity of the fibers affected the cellular response of rat cardiac myoblasts to the scaffold[76]. It was possible to fabricate a conducting scaffold that was biocompatible and supported the attachment, migration and proliferation of rat cardiac myoblasts. This demonstrated that electrospun polyaniline blended gelatin scaffolds offers greater potential for cardiac tissue engineering, by utilizing their conducting properties and biocompatibility. However further research is required to develop the next generation conducting polymers which are biodegradable.

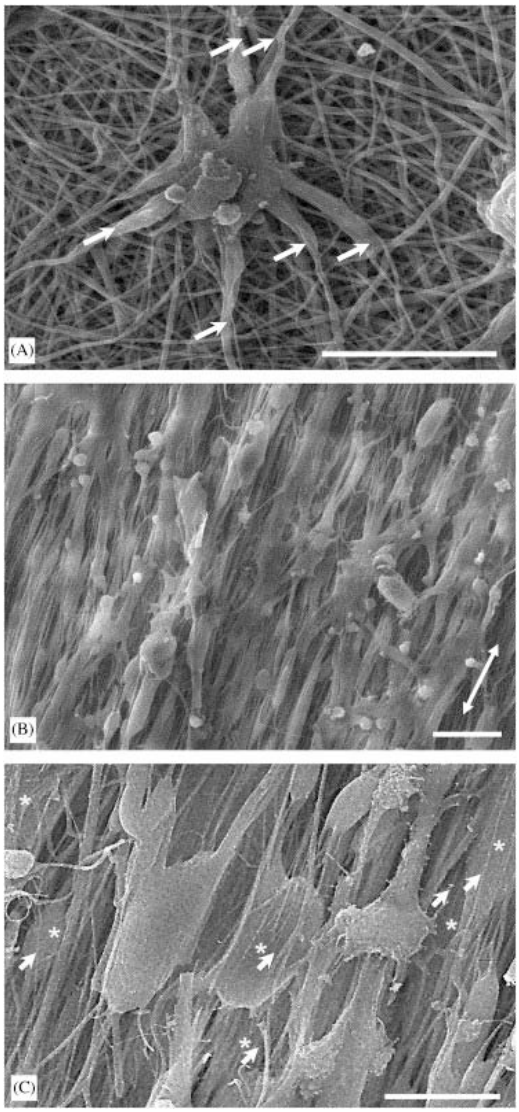

Figure 5: Cardiac myocytes that have been embedded on the electrospun scaffold. They were cultured on uniaxially stretched and aligned P_LLA, with A, B, and C representing different magnifications. The arrows in image A) point in the direction of the fiber guided extensions and in B) indicate the matrix fiber direction. The stars in C) highlight fine fibers running along the top. The scale bars in these images are 40 μm. Reproduced by permission from Elsevier[66].

2.1.8 CONCLUDING REMARKS

Electrospinning offers a rapid and convenient way of producing scaffolds with nanoscale elements and has been utilised across a broad range of polymer systems and tissue engineering endeavours. Electrospinning allows the tissue engineer to specifically tailor materials to each specific application and cellular environment. However it remains largely unkown what the best fiber diameter or interfiber distance is to optimise cell function. This is confounded by the fact that 3D electrospun nanofibrous environments are quite complex, and by changing a dimension such as fibre diameter or alignment, you automatically change the interfiber distance which can influence cell migration.

It is clearly evident from this review article that many cells respond differently when subject to 3D nano-scale fibers compared with 2D smooth surfaces. This response, as often quoted in the literature, has simply been attributed to similarities with the natural ECM environment. Whether this is entirely true or not, it is known that cells exist in a 3D niche and interact with ECM components at the nano-length scale. The underlying mechanisms for enhanced cellular response to nanostructures are only now beginning to be realized by using highly regular and reproducible nanostructured surfaces e.g. using microimprinting[77]. However transferring lessons learned from these model systems over to highly complex 3D electrospun scaffolds is the next step for the advancement of the electrospinning technique for tissue engineering.

The need to improve the biomechanical properties of electrospun scaffolds is paramount and is a major obstacle currently facing tissue engineers. This has led researchers to investigate polymer-ceramic composite fibres and thermal treatments to enhance fibre bonding[78]. It may be required to develop 3D scaffolds that incorporate layered structures e.g. random and aligned fibre layers that could provide cell niches as well as regions for contact guidance. As fibre diameter[23] and surface functionalisation[79] have been shown to effect stem cell differentiation, gradient fibre scaffolds (through the

depth of the scaffold) could readily be produced using electrospinning to regenerate more complex tissue structures. However to move forward from our current position, there is a clear need for further research into the effects of 3D nanofiber architecture, functionalisation and interfacial properties on cell behaviour.

2.1.9 ACKNOWLEDGEMENTS

We are grateful to the Australian postgraduate award and the Cooperative Research Centre (CRC) for Polymers for funding David Nisbet. We also acknowledge the ARC Discovery (DP0663573) for funding and Amanda Melville with assistance with certain sections of this review.

2.1.10 REFERENCES

[1] Stevens, M.M. and George, J.H. (2005). Exploring and Engineering the Cell Surface Interface, *Science*, **310**: 1135-1138.

[2] Teo, W.E., He, W. and Ramakrishna, S. (2006). Electrospun Scaffold Tailored for Tissue Specific Extracellular Matrix, *Biotechnology Journal*, **1**: 918-929.

[3] Ma, Z., Kotaki, M., Inai, R. and Ramakrishna, S. (2005). Potential of Nanofiber Matrix as Tissue-Engineering Scaffolds, *Tissue Engineering*, **11**: 101-109.

[4] Chiu, J.B., Luu, Y.K., Fang, D., Hsiao, B., Chu, B. and Hadjiargyrou, M. (2005). Electrospun Nanofibrous Scaffolds for Biomedical Applications, *Journal of Biomedical Nanotechnology*, **1**: 115-132.

[5] Nisbet, D.R., Pattanawong, S., Ritchie, N.E., Shen, W., Finkelstein, D.I., Horne, M.K. and Forsythe, J.S. (2007). Interaction of Embryonic Cortical Neurones on Nanofibrous Scaffolds for Neural Tissue Engineering, *Journal of Neural Engineering*, **4**: 35-41.

[6] Dalton, P.D., Klee, D. and Möller, M. (2005). Electrospinning with Dual Collection Rings, *Polymer*, **46**: 611-614.

[7] Huang, Z.-M., Zhang, Y.-Z., Kotaki, M. and Ramakrishna, S. (2003). A Review on Polymer Nanofibers by Electrospinning and Their Applications in Nanocomposites, *Composites Science and Technology*, **63**: 2223-2253.

[8] Li, D., Wang, Y. and Xia, Y. (2003). Electrospinning of Polymeric and Ceramic Nanofibers as Uniaxially Aligned Arrays, *Nano Letters*, **3**: 1167-1171.

[9] Knight, B., Laukaitis, C., Akhtar, N., Hotchin, N.A., Edlund, M. and Horwitz, A.R. (2000). Visualizing Muscle Cell Migration *In Situ*, *Current Biology*, **10**: 576-585.

[10] Griffith, L.G. and Swartz, M.A. (2006). Capturing Complex 3D Tissue Physiology *In Vitro*, *Nature Reviews: Molecular Cell Biology*, **7**: 211-224.

[11] Nur-E-Kamala, A., Ahmeda, L., Kamala, J., Schindlerb, M. and Meinersa, S. (2006). Three-Dimensional Nanofibrillar Surfaces Promote Self-Renewal in Mouse Embryonic Stem Cells, *Stem Cells*, **24**: 426-433.

[12] Schindler, M., Ahmed, I., Kamal, J., Nur-E-Kamal, A., Grafe, T.K., Chung, H.Y. and Meiners, S. (2005). A Synthetic Nanofibriallar Matrix Promotes *In Vivo*-Like Organization and Morphogenesis for Cells in Culture, *Biomaterials*, **26**: 5624-5631.

[13] Nisbet, D.R., Yu, L.M.Y., Zahir, T., Forsythe, J.S. and Shoichet, M.S. (2008). Characterization of Brain-Derived Stem Cells on Electrospun Poly(ε-Caprolactone) Submicron Scaffolds: Evaluating Their Potential in Neural Tissue Engineering, *Journal of Biomaterials Science Polymer Edition*: **19**: 623-634..

[14] Yang, S.T. and Ng, R. (2007). A New Dimension to Biomaterials, *Materials Today*, **10**, (5): 64.

[15] Han, D. and Gouma, P.I. (2006). Electrospun Bioscaffolds That Mimic the Topology of Extracellular Matrix, *Nanomedicine*, **2**: 37-41.

[16] Borg, T.K. (2004). It's the Matrix!, *The American Journal of Pathology*, **164**: 1141-1142.

[17] Hoshiba, T., Wakejima, M., Cho, C.S., Shiota, G. and Akaike, T. (2007). Different Regulation of Hepatocyte Behaviors between Natural Extracellular Matrices and Synthetic Extracellular Matrices by Hepatocyte Growth Factor, *Journal of Biomedical Materials Research Part A*, **85**: 228-235.

[18] Murugan, R. and Ramakrishna, S. (2007). Design Strategies of Tissue Engineering Scaffolds with Controlled Fiber Orientation, *Tissue Engineering*, **13**: 1845-1866.

[19] Berthiaume, F., Moghe, P.V., Toner, M. and Yarmush, M.L. (1996). Effect of Extracellular Matrix Topology on Cell Structure, Function, and Physiological Responsiveness: Hepatocytes Cultured in a Sandwich Configuration, *The FASEB Journal*, **10**: 1471-1484.

[20] Zhong, Y., Yu, X., Gilbert, R. and Bellamkonda, R.V. (2001). Stabilizing Electrode-Host Interfaces: A Tissue Engineering Approach, *Journal of Rehabilitation Research and Development* **38**: 627-632.

[21] Nisbet, D.R., Crompton, K.E., Horne, M.K., Finkelstein, D.I. and Forsythe, J.S. (2007). Neural Tissue Engineering of the CNS Using Hydrogels, *Journal of Biomedical Materials Research: Part B*, **87**: 251-263.

[22] Nisbet, D.R., Crompton, K.E., Hamilton, S.D., Shirwakawa, S., Prankerd, R.J., Finkelstein, D.I., Horne, M.K. and Forsythe, J.S. (2005). Morphology and Gelation of Thermosensitive Xyloglucan Hydrogels, *Biophysical Chemistry*, **121**: 14-20.

[23] Yang, F., Murugan, R., Wang, C. and Ramakrishna, S. (2005). Electrospinning of Nano/Micro Scale Poly(L-Lactic Acid) Aligned Fibers and Their Potential in Neural Tissue Engineering, *Biomaterials*, **26**: 2603-2610.

[24] Johansson, A., Carlbergb, C., Danielsenc, N., Monteliusb, L. and Kanjea, M. (2006). Axonal Outgrowth in Nano-Imprinted Patterns, *Biomaterials*, **27**: 1251-1258.

[25] Foley, J., Grunwald, E., Nealey, P. and Murphy, C. (2005). Cooperative Modulation of Neuritogenesis by PC12 Cells by Topography and Nerve Growth Factor, *Biomaterials*, **26**: 3639-3644.

[26] Corey, J.M., Lin, D.Y., Mycek, K.B., Chen, Q., Samuel, S., Feldman, E.L. and Martin, D.C. (2007). Alighned Electrospun Nanofibers Specify the Direction of Dorsal Root Ganglia Neurite Growth, *Journal of Biomedical Materials Research Part A*, **83**: 636-645.

[27] Kwon, I., Kidoaki, S. and Matsuda, T. (2005). Electrospun Nano- to Microfiber Fabrics Made of Biodegradable Copolyesters: Structural Characteristics, Mechanical Properties and Cell Adhesion Potential, *Biomaterials*, **26**: 3929- 3939.

[28] Li, W., Guo, Y., Wang, H., Shi, D., Liang, C., Ye, Z., Qing, F. and Gong, J. (2007). Electrospun Nanofibers Immobilized with Collagen for Neural Stem Cell Culture, *Journal of Materials Science: Materials in Medicine*, **19**: 847-854.

[29] Ahmed, I., Liu, H.Y., Mamiya, P.C., Ponery, A.S., Babu, A.N., Weik, T., Schindler, M. and Meiners, S. (2006). Three-Dimensional Nanofibrillar Surfaces Covalently Modified with Tenascin-C-Derived Peptides Enhance Neuronal Growth *In Vitro*, *Journal of Biomedical Materials Research*, **76**: 851-860.

[30] Schnell, E., Klinkhammer, K., Balzer, S., Brook, G., Klee, D., Dalton, P.D. and Mey, J. (2007). Guidance of Glial Cell Migration and Axonal Growth on Electrospun Nanofibers of Poly-ε-Caprolactone and a Collagen/Poly-ε-Caprolatone Blend, *Biomaterials*, **28**: 3012-3025.

[31] Sangsanoh, P., Waleetorncheepsawat, S., Suwantong, O., Wutticharoenmongkol, P., Weeranantanapan, O., Chuenjitbuntaworn, B., Cheepsunthorn, P., Pavasant, P. and

Supapho., P. (2007). *In Vitro* Biocompatibility of Schwann Cells on Surfaces of Biocompatible Polymeric Electrospun Fibrous and Solution-Cast Film Scaffold, *Biomacromolecules*, **8**: 1587-1594.

[32] Bini, T.B., Gao, S., Tan, T.C., Wang, S., Lim, A., Hai, L.B. and Ramakrishna, S. (2004). Electrospun Poly(L-Lactide-Co-Glycolide) Biodegradable Polymer Nanofibre Tubes for Peripheral Nerve Regeneration, *Nanotechnology*, **15**: 1459-1464.

[33] Matsuda, T., Kagata, G., Kino, R. and Tanaka, J. (2007). Preparation of Chitosan Nanofiber Tube by Electrospinning, *Journal of Nanoscience and Nanotechnology*, **7**: 852-855.

[34] Townsend-Nicholson, A. and Jayasinghe, S.N. (2006). Cell Electrospinning: A Unique Biotechnique for Encapsulating Living Organisms for Generating Active Biological Microthreads/Scaffolds, *Biomacromolecules*, **7**: 3364-3369.

[35] Jayasinghe, S.N. and Townsend-Nicholson, A. (2006). Stable Electric-Field Driven Cone-Jetting of Concentrated Biosuspensions, *Lab on a Chip*, **6**: 1086-1090.

[36] Rhoades, R. and Pflanzer, R. Human Physiology, 3rd Ed. Orlando: Saunders College Publishing, 1996.

[37] Kimakhe, S., Bohic, S., Larrose, C., Reynaud, A., Pilet, P., Giumell, B., Heymann, D. and Daculsi, G. (1999). Biological Activities of Sustained Polymyxin B Release from Calcium Phosphate Biomaterial Prepared by Dynamic Compaction: An *In Vitro* Study, *Journal of Biomedical Materials Research*, **47**: 18-27.

[38] Stevenson, S., Emery, S.E. and Goldberg, V.M. (1996). Factors Affecting Bone Graft Incorporation, *Clinical Orthopaedics and Related Research*, **324**: 66-74.

[39] Goldberg, V.M. and Stevenson, S. (1994). Bone graft options: fact and fancy, *Orthopedics*, **17**: 809-810,821.

[40] Graves, S.E., Davidson, D., Ingerson, L., P., R., Griffith, E.C., McDermott, B.F., McElroy, H.J. and Pratt, N.L. (2004). The Australian Orthopaedic Association National Joint Replacement Registry, *The Medical Journal of Australia*, **180**: S31-34.

[41] Shin, M., Yoshimoto, H. and Vacanti, J.P. (2004). *In Vivo* Bone Tissue Engineering Using Mesenchymal Stem Cells on a Novel Electrospun Nanofibrous Scaffold, *Tissue Engineering*, **10**: 33-41.

[42] Kim, H.W., Song, J.H. and Kim, H.E. (2005). Nanofiber Generation of Felatin-Hydroxyapatite Biomimetics for Guided Tissue Regeneration, *Advanced Functional Materials*, **15**: 1988-1994.

[43] Li, C., Vepari, C., Jin, H.J., Kim, H.J. and Kaplan, D.L. (2006). Electrospun Silk-BMP-2 Scaffolds for Bone Tissue Engineering, *Biomaterials*, **27**: 3115-3124.

[44] Tuslakoglu, K., Bolgen, N., Salgado, A.J., Gomes, M.E., Piskin, K. and Reis, R.L. (2005). Nano and Micro Fiber Combined Scaffolds: A New Architecture for Bone Tissue Engineering, *Journal of Materials Science: Materials in Medicine*, **16**: 1099-1104.

[45] Badami, A.S., Kreke, M.R., Thompson, M.S., Riffle, J.S. and Goldstein, A.S. (2006). Effect of Fiber Diameter on Spreading, Proliferation, and Differentiation of Osteoblastic Cells on Electrospun Poly(Lactic Acid) Substrates, *Biomaterials*, **27**: 596-606.

[46] Woodfield, T.B.F., Malda, J., de Wijin, J., Peters, F., Riesle, J. and van Blitterswijk, C.A. (2004). Design of Porous Scaffolds for Cartilage Tissue Engineering Usings a Three-Dimensional Fiberdeposition Technique, *Biomaterials*, **25**: 4149-4161.

[47] Shields, K.J., Beckman, M.J., Bowlin, G.L. and Wayne, J.S. (2001). Mechanical Properties of Cellular Proliferation of Electrospun Collagen Type II, *Tissue Engineering*, **10**: 1510-1517.

[48] Riesle, J., Hollander, A.P., Langer, R., Freed, L.E. and Vunjak-Novakovic, G. (1998). Collagen in Tissue-Engineered Cartilage: Types, Structure, and Crosslinks, *Journal of Cellular Biochemistry*, **71**: 313.

[49] Bhattarai, N., Edmondson, D., Veiseh, O., Matsen, F.A. and Zhang, M. (2005). Electrospun Chitosan-Based Nanofibers and Their Cellular Compatibility, *Biomaterials*, **26**: 6176-6184.

[50] Subramanian, A., Lin, H.Y., Vu, D. and Larsen, G. (2004). Synthesis and Evaluation of Scaffolds Prepared from Chitosan Fibers for Potential Use in Cartilage Tissue Engineering, *Biomedical Sciences Instrumentation*, **40**: 117-122.

[51] Subramanian, A., Vu, D., Larsen, G. and Lin, H.Y. (2005). Preparation and Evaluation of the Electrospun Chitosan/PEO Fibers for Potential Applications in Cartilage Tissue Engineering, *Journal of Biomaterials Science Polymer Edition*, **16**: 861-873.

[52] Luu, Y.K., Kim, K., Hsiao, B., Chu, B. and Hadjiargyrou, M. (2003). Development of a Nanosturcture DNA Delivery Scaffold Via Electrospinning of PLGA and PLA-PEG Block Copolymers, *Biomaterials*, **89**: 341-353.

[53] Li, W., Tuli, R., Okafor, C., Derfoul, A., Danielson, K.G., Hall, D.J. and Tuan, R.S. (2005). A Three-Dimensional Nanofibrous Scaffold for Cartilage Tissue Engineering Using Human Mesenchymal Stem Cells, *Biomaterials*, **26**: 599-609.

[54] Zhang, Y.-Z., Lim, T.C., Ramakrishna, S. and Huang, Z.-M. (2005). Recent Development of Polymer Nanofibers for Biomedical and Biotechnological Applications, *Journal of Materials Science: Materials in Medicine*, **16**: 933-946.

[55] Van der Lei, B., Nieuwenhuis, P., Molenaar, I. and Wildevuur, C.R.H. (1987). Long-Term Iologic Fate of Neoarteries Regenerated in Microporous, Compliant, Biodegradable, Small-Caliber Vascular Grafts in Rats, *Surgery*, **101**: 459-467.

[56] Sonoda, H., Takamizawa, K., Nakayama, Y., Yasui, H. and Matsuda, T. (2001). Small-Diameter Compliant Arterial Graft Prosthesis: Design Concept of Coaxial Double Tubular Graft and Its Fabrication, *Journal of Biomedical Materials Research*, **55**: 266-276.

[57] Tiwari, A., Salacinski, H.J., Samilton, G. and Sefalian, A.M. (2001). Tissue Engineering of Vascular Bypass Grafts: Role of Endotherlial Cells Extraction, *European Journal of Vascular and Endovascular Surgery*, **21**: 193-201.

[58] Seifalian, A.M., Tiwari, A., Hamilton, G. and Salacinski, H.J. (2002). Improving the Clinical Patency of Prosthetic Vascular and Coronary Bypass Grafts: The Role of Seeding and Tissue Engineering, *Artificial Organs*, **26**: 301-320.

[59] Lian, X. and Greisler, H.P. (2003). Biomaterials in the Development and Future of Vascular Grafts, *Journal of Vascular Surgery*, **37**: 472-480.

[60] Kumar, T.R.S. and Krishnan, L.K. (2001). Endothelial Cell Growth Factor (ECGF) Enmeshed with Fibrin Matrix Enhances Proliferation of EC *In Vitro*, *Biomaterials*, **22**: 2769-2776.

[61] Rothlein, R., Dustin, M.L., Marlin, S.D. and Springer, T.A. (1986). A Human Intracellular Adhesion Molecule (ICAM-1) Distinct from LFA-1, *Journal of Immunology*, **137**: 1270-1274.

[62] Ma, Z., Kotaki, M., Yong, T., He, W. and Ramakrishna, S. (2005). Surface Engineering of Electrospun Polyethylene Terephthalate (PET) Nanofibers Towards Development of a New Material for Blood Vessel Engineering, *Biomaterials*, **26**: 2527-2536.

[63] Williamson, M.R., Black, R. and Kielty, C. (2006). PCL-PU Composite Vascular Scaffold Production for Vascular Tissue Engineering: Attachment, Proliferation and Bioactivity of Human Vascular Endothelial Cells, *Biomaterials*, **27**: 3608-3616.

[64] Stitzel, J., Liu, J., Lee, S.J., Komura, M., Berry, J., Soker, S., Lim, G., Dyke, M.V., Czerw, R., Yoo, J.J. and Atala, A. (2006). Controlled Fabrication of a Biological Vascular Substitute, *Biomaterials*, **27**: 1088-1094.

[65] Inoguchi, H., Kwon, I., Inoue, E., Takamizawa, K., Maehara, Y. and Matsuda, T. (2006). Mechanical Responses of a Compliant Electrospun Poly(L-Lactide-Co-ε-Caprolactone) Small-Diameter Vascular Graft, *Biomaterials*, **27**: 1470-1478.

[66] Zong, X., Bien, H., Chung, C., Yin, L., Fang, D., Hsiao, B., Chu, B. and Entcheva, E. (2005). Electrospun Fine-Textured Scaffolds for Heart Tissue Constructs, *Biomaterials*, **26**: 5330-5338.

[67] Zong, X., Bien, H., Chung, C., Yin, L., Kim, K.F., D, Chu, B., Hsiao, B. and Entcheva, E. (2003). Electrospun Non-Woven Membranes as Scaffolds for Heart Tissue Constructs, *Polymer Preprints*, **44**: 96-97.

[68] Xu, C.Y., Inai, R., Kotaki, M. and Ramakrishna, S. (2004). Aligned Biodegradable Nanofibrous Structure: A Potential Scaffold for Blood Vessel Engineering, *Biomaterials*, **25**: 877-886.

[69] Boland, E.D., Matthews, J.A., Pawlowski, K.J., Simpson, D.G., Wnek, G.E. and Bowlin, G.L. (2004). Electrospinning Collagen and Elastin: Preliminary Vascular Tissue Engineering, *Frontiers in Bioscience* **9**: 1422-1432.

[70] He, W., Ma, Y., Yong, T., Teo, W.E. and Ramakrishna, S. (2005). Fabrication of Collagen-Coated Biodegradable Polymer Nanofiber Mesh and Its Potential for Endothelial Cell Growth, *Biomaterials*, **26**: 7606-7615.

[71] He, W., Yong, T., Teo, W.E., Ma, Z. and Ramakrishna, S. (2005). Fabrication and Endothelialization of Collagen-Blended Biodegradable Polymer Nanofibers: Potential Vascular Graft for Blood Vessel Tissue Engineering, *Tissue Engineering*, **11**: 1574-1588.

[72] He, W., Yong, T., Ma, Z.W., Inai, R., Teo, W.E. and Ramakrishna, S. (2006). Biodegradable Polymer Nanofiber Mesh to Maintain Functions of Endothelial Cells, *Tissue Engineering*, **12**: 2457-2466.

[73] Xu, C.Y., Yang, F., Wang, S. and Ramakrishna, S. (2004). *In Vitro* Study of Human Vascular Endothelial Cell Function on Materials with Various Surface Roughness, *Journal of Biomedical Materials Research*, **71**: 154-161.

[74] Li, R.K., Yau, T.M., Weisel, R.D., Mickle, D.A., Sakai, T., Choi, A. and Jia, Z.Q. (2000). Construction of a Bioengineered Cardiac Graft, *Journal of Thoracic and Cardiovascular Surgery*, **119**: 368-375.

[75] Shin, M., Ishii, O., Sueda, T. and Vacanti, J.P. (2004). Contractile Cardiac Grafts Using a Novel Nanofibrous Mesh, *Biomaterials*, **25**: 3717-3723.

[76] Li, M., Guo, Y., Wei, Y., MacDiarmid, A.G. and Lelkes, P.I. (2006). Electrospinning Polyaniline-Contained Gelatin Nanofibers for Tissue Engineering Applications, *Biomaterials*, **27**: 2705-2715.

[77] Yim, E., K. and Leong, K.W. (2005). Significance of Synthetic Nanostructures in Dictating Cellular Response, *Nanomedicine*, **1**: 10-21.

[78] Lee, S.J., Oh, S.H., Liu, J., Soker, S., Atala, A. and Yoo, J.J. (2007). The Use of Thermal Treatments to Enhance the Mechanical Properties of Electrospun Poly(Caprolactone) Scaffolds, *Biomaterials*, **29**: 1422-1430.

[79] Choi, J.S., Leong, K.W. and Yoo, H.S. (2008). *In Vivo* Wound Healing of Diabetic Ulcers Using Electrospun Nanofibers Immobilized with Human Epidermal Growth Factor (EGF), *Biomaterials*, **29**: 587-596.

2.2 Characterisation of electrospun membranes

Due to the variety of different applications where electrospun fibres are being used and the specialist and interdisciplinary nature of some fields, often the characterisation aspects are overlooked (tissue engineering is no exception). The composition, surface, morphology and architecture all play critical roles that dictate the performance of the electrospun construct for its particular application. The following review article was targeted to address the scarcity of relevant information surrounding the effective characterisation of electrospun membranes and provides a description of the characterisation methods as well as recommendations on how the technique and/or interpretations can be improved.

Characterisation of electrospun membranes: problems and improvements.

D.R. Nisbet[1,2], A.E. Rodda[1], D.I. Finkelstein[4], M.K. Horne[5], J.S. Forsythe[1,2], W. Shen[3]*

1. Department of Materials Engineering, Division of Biological Engineering , Monash University, PO Box 69M, Victoria 3800, Australia

2. CRC for Polymers, 32 Business Park Drive, Notting Hill, VIC 3168, Australia.

3. Australian Pulp and Paper Institute, Department of Chemical Engineering, Monash University, PO Box 69M, Victoria 3800, Australia

4. The Mental Health Research Institute of Victoria 155 Oak Street, Parkville, Victoria 3052, Australia

5. Howard Florey Institute, Gate 11, Royal Parade, The University of Melbourne, VIC 3010, Australia

2.2.1 Abstract

Electrospun membranes are used in a variety of applications, including filtration systems and sensors for chemical detection and have attracted increased interest in the field of tissue engineering and regenerative medicine. Successful integration of these materials into a specific technology will require understanding of the fibres surface, bulk and architectural properties. Detailed characterisations of these properties are frequently overlooked, particularly in specialised interdisciplinary fields such as tissue engineering. In this article we have reviewed the current status of characterising electrospun scaffolds with a special focus on surface characterisation and recommend improvements in using these techniques to better understand these very interesting nanostructured materials.

2.2.2 Key words

Electrospinning, nanofibre, characterisation, scaffold, fibre mechanical properties

2.2.3 Introduction

As advanced materials are synthesised and fabricated their characterisation by surface science becomes relevant.[80] Characterisation by surface science is paramount to understanding and generating advanced, functional and "smart" materials in modern technologies, such as metallurgy, microelectronics, nanotechnology, corrosion and tissue engineering. This review focuses on the surface characterisation of non-woven polymer membranes that are produced by electrospinning; although the same principles would be relevant to any fibrous membranes fabricated using other processes. We have also addressed the characterisation of modulus and architectural properties of such membranes.

The surface properties of polymeric materials strongly influence their interactions with other materials and interfaces within their surrounding environment and determine the polymer material's suitability for particular engineering applications. The main surface properties of polymeric materials are (a) geometric and topographic and (b) surface chemical properties. Geometric and topographic properties include the roughness of two dimensional polymer surfaces [73, 81, 82] as well as the porosity,[62, 66] pore size,[5, 81, 83, 84] pore size distribution [83, 85] and specific surface area for porous and non-woven polymer membranes, and intra fibre surface roughness.[86] Surface chemical properties include the chemical composition (which can be different from that of the bulk),[87] which in some instances can be altered by surface modification.[62, 88] This can affect water wettability/hydrophilicity,[62, 66, 82, 89] and surface energetics.[90, 91] In this review, commonly used surface characterisation methods are examined.

2.2.3.1 Current state of surface characterisation in nanofibrous membranes

Although the technology for fabricating electrospun nanofibres was first reported in 1934 [92] , there has been renewed interest in electrospinning because of the growing demand

for nanostructured materials and their unique properties obtained at this length scale, particularly for tissue engineering and regenerative medical technologies. This includes nanostructured drug delivery vessels, cellular microenvironments and conduits for cell regeneration after injury or disease. Successful integration of these materials into a specific technology will require understanding of the fibre surface, bulk and architectural properties.

Biologists will frequently overlook the effect that material surfaces will have on the biological questions they are asking[93] whereas, materials and surface scientists may see biological questions as too complex for the analytical tools at their disposal. This gap between the understandings of interdisciplinary fields can be bridged by assembling interdisciplinary teams, and through the emergence of "new" scientists whose expertise crosses the traditional fields of materials, surface science, engineering and biology. This review is a contribution to bridging this gap and addresses the current status of characterising electrospun scaffolds for use in tissue engineering, highlighting the advantages and disadvantages of analytical techniques in different applications. Where possible, we have recommended improvements in the characterisation of polymer membranes in anticipation of providing a more informed choice of characterisation methods.

2.2.4 Surface characterisation of porous and fibrous polymer materials.

2.2.4.1 Porosity Characterisation

Electrospun scaffolds are highly porous (Fig. 1) and therefore have very large volume to surface ratios, a property central to their use in technologies such as filtration,[94, 95] chemical sensors [96] and tissue engineering.[5, 13, 82] Consequently accurate characterisation of the porosity of these membranes is required for optimal deployment. One simple method for determining porosity of electrospun membranes is by measuring

their apparent weight to volume ratio with the knowledge of bulk polymer density.[95] This results in very basic descriptions of porosity. Other techniques, including mercury porosimetry, capillary flow porosimetry and BET gas adsorption allow for far more detailed characterisation.

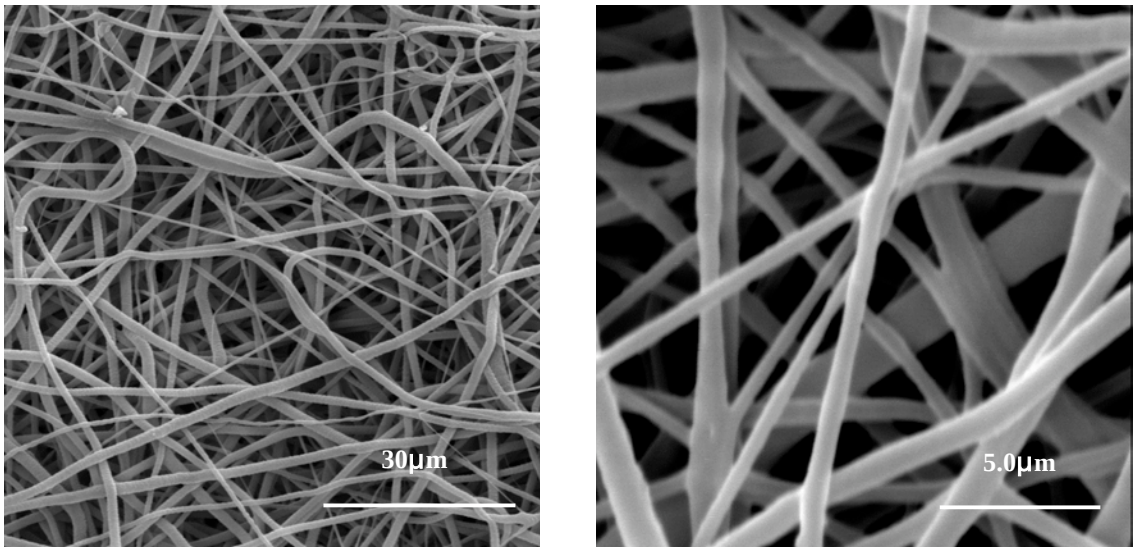

Figure 1 – Polycaprolactone (PCL) scaffolds of highly porous morphology produced by electrospinning. Reproduced with permission from BRILL.[13]

2.2.4.2 Mercury Porosimetry

Mercury porosimetry is a traditional method for characterising porosity and pore size distribution.[85, 91] It is a liquid intrusion method which relies on the principle of the Laplace equation. Mercury has a high surface tension (485.5 dyne/cm at 25˚C) [97] and therefore forms large contact angles with most other materials (≅130˚)[98]. Based on the Laplace equation,[97] mercury does not spontaneously penetrate pores by capillary action. An external pressure must be applied to force mercury into the pores. By assuming that the pores in a porous materials are cylindrical in shape, the pore diameters intruded by mercury can be correlated with the applied pressure according to the following equation (1): [98]

$$D = \frac{-4\gamma \cos\theta}{p} \quad (1)$$

where D is the diameter of the pore, γ is the surface tension of mercury, θ is the contact angle between mercury and the solid and p is the applied pressure. The direct data acquired is the accumulated volume of mercury entering the porous system. A pore size distribution curve is obtained by relating the log differential intrusion volume to log pore diameter, i.e., dV/d(logD). A description of this procedure can be found in reference.[97]

Assuming pores are cylindrical, the pore surface area can also be calculated from the accumulated mercury intrusion volume and the pore diameter data. Since the surface area of a cylindrical pore is πDL and the volume of the pore is $\pi D^2L/4$ (where D and L are the diameter and the length of the cylindrical pore), the wall area of the pore thus equals to:

$$A = \frac{4V}{D} \quad (2)$$

Ryu *et al.* [99] found that mercury porosimetry could detect changes in pore sizes of electrospun nylon-6 membranes of different fibre diameters. Instead of relying on the pore size data obtained directly from the log differential intrusion curve, they calculated the average pore diameters using Eq. 2 with the intrusion volume and pore surface area data obtained by BET measurements. Their pore diameter results ranged from 2.737 – 0.167 μm.[99] Direct volumes of mercury intrusion also provided data on the fraction of voids within the membrane, which ranged from 25 – 80 %.[99] However, assuming that pores are cylindrical is often an over-simplification. The use of Eq. (2) may not provide an accurate surface area measurement, due to a well-known problem associated with the so-called “bottle neck” effect where large cavities behind narrow necks are considered to be pores having the diameter of the neck.[97] Furthermore, high pressure applied to polymer membranes has been reported to cause irreversible structural compression.[100] Thus mercury intrusion method can provide useful representations of porosity and surface

area of polymer nanofibre membranes[86, 97, 99] providing the above caveats are considered.

2.2.4.3 Capillary Flow Porometry

Capillary flow porometry is a liquid extrusion method for measuring pore size.[101] It requires that all pores must first be completely filled with a wetting liquid which is then forced out of the pores by a non-reacting gas. The work done by the gas in forcing liquid out of the pores is assumed to be equal to the surface free energy when the sample-liquid interface is replaced by the sample gas interface.

$$p\,dV = \left(\gamma_{s/g} - \gamma_{s/l}\right) dS \qquad (3)$$

where p is the pressure applied; dV is the displaced volume of liquid by gas; $\gamma_{s/g}$ and $\gamma_{s/l}$ are the surface free energies of solid-gas and solid-liquid; dS is the increase of solid-gas surface area. Jena and Gupta [101] proposed that, by combining Eq. (3) with the Young's equation (Eq. 4), and by replacing the pore cross section area with the equal area circle, a working equation (Eq.5) could be derived:

$$\left(\gamma_{s/g} - \gamma_{s/l}\right) = \gamma_{l/g}\cos\theta \qquad (4)$$

$$p = \frac{4\gamma_{l/g}\cos\theta}{D} \qquad (5)$$

where $\gamma_{l/g}$ is the liquid gas interfacial tension or liquid surface tension; D is the diameter of the equivalent circular area of the pore cross section.[101]

Capillary flow porometry has been used to study the pore size distribution of electrospun fibre membranes.[84, 102] Since capillary flow porometry is a liquid extrusion method, it is more appropriate to use the receding contact angle, which is usually small and leads $\cos\theta$ in Eq. (5) equalling unity. Capillary flow porometry is suitable for measuring

"through pores" that connect one side of the material to the other side, but is not suitable for closed (isolated pores in the matrix) or blind-end pores (connected to the external surface via a single channel or orifice).[102] Like mercury porosimetry, capillary flow porometry is also sensitive to the "bottle neck effect", [102] but unlike mercury porosimetry can not measure blind-end pores.

2.2.4.4 Brunauer-Emmett-Teller (BET) Gas Adsorption

BET gas adsorption method is a well established method for characterising surface area and pore structure of porous materials. The fundamental consideration is the quantity of a single molecular adsorption layer of a known gas. By assuming the Langmuir adsorption model and incorporating the concept of multimolecular layer adsorption, as well as knowing the area occupied by single adsorbed molecule, the surface area of the substrate can be calculated.[97] Gregg and Sing [103] have presented theoretical details of the method. The BET equation is usually written in the following form to allow the determination of values of V_m and C by graphical means:[103]

$$\frac{P}{V_a(P_0 - P)} = \frac{1}{V_m C} + \frac{C-1}{V_m C}\left(\frac{P}{P_0}\right) \qquad (6)$$

Where P and P_0 are the gas pressure and the saturated gas pressure at the temperature of experiment, V_a and V_m are the quantity of gas adsorbed under pressure P and the quantity of gas required for a monolayer adsorption on the sample surface, respectively. C is a constant related to the heat of adsorption of the first molecular layer of gas. By plotting $P/V_a(P_0\text{-}P)$ against (P/P_0). C and V_m can be calculated from the intercept and the slope of the straight line.[103] Since there is no assumption on cylindrical pore geometry, the specific surface area determined by the BET method is more reliable than capillary flow and mercury porsimetry.

Ryu *et al*. [99] used an image analyser to measure the diameters of electrospun fibres (which were controlled by the concentration of polymer solutions and ranged between 90

to 480 nm), and found using BET that the total pore area of nanofibrous membranes to range between 9–51 m^2/g, with the porosity size decreasing within increasing fibre diameter.[99] Based on their specific surface area and porosity data, the authors assumed that pores within the non-woven nanofibrous membranes were fully interconnected when using this method. Although the experimental specific surface area data of nanofibre membrane was smaller, it did not differ greatly from the value calculated using Eq. (2). (by dividing 4 x the volume of the fibres {i.e. membrane mass over polymer density} and the experimental average fibre diameter). The small diameter of the fibres, rather than fibre surface morphology, contributed most to the large specific surface areas found in this study. [99]

2.2.5 Surface and Bulk Morphology: Characterisation and Imaging

2.2.5.1 Scanning Electron Microscopy

Surface morphology is a critical surface parameter that can not only affect the responses of secondary surfaces (such as cells in tissue engineering),[5, 13] but can also affect the characterisation of the material surface.[82] SEM is a method that provides qualitative assessment of fibre diameter distribution, surface roughness and architecture of electrospun polymer membranes.[82, 86, 89, 104] Because this method is very well understood and already extensively used a detailed discussion of this method will not be provided here. However, care must be taken to ensure that fibre diameters and interfibre spacings measured using SEM, are taken on the image plane to ensure that the scale is correct for post analysis. More quantitative evaluation of surface roughness may be obtained using atomic force microscopy (for nano-scale roughness) and a range of contact and non-contact (optical) profilometers (for larger scale roughnesses).[105]

2.2.5.2` Transmission Electron Microscopy

Transmission electron microscopy (TEM) is a characterisation method where the beam of electrons is transmitted through a thin sample and the interaction of the electrons and the sample are used to generate an image. This method has been used on electrospun scaffolds to image core shell structures, shown in Fig. 2 [106], electrospun fibres with incorporated composite particles [107] and carbon nanotubes [108] and the like. Like SEM, this method is well understood and is extensively used to image electrospun scaffolds, so a detailed discussion of the method is not warranted. TEM is a good method to use to image the inclusion of nano-domains within electrospun fibers. One problem with this method is the size of the samples that can be imaged, as they must to ultra thin (less than 1 μm) to allow the focus beam to pass through the sample (generally not an issue for electrospun membranes) and they must be able to withstand high vacuum.

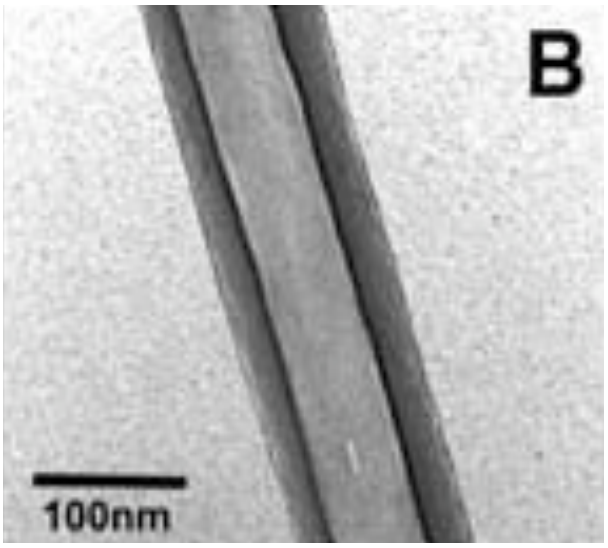

Figure 2 – TEM image of a hollow or core shell electrospun polymer fiber produced from poly(vinylpyrrolidone). Reproduced with permission from Springer-Verlag.[106]

2.2.5.3 Atomic Force Microscopy

Atomic Force Microscopy (AFM) was originally developed to probe the topography of surfaces, and has been used for this purpose on polymer samples, including electrospun

membranes, for many years. However several innovations have allowed the study of other surface properties such as the distribution of a chemical of interest in blended mixtures and the distribution of crystalline and amorphous areas on a surface. The hardness and elastic modulus (through nanoindentation) can also be determined using this technique, and this will be examined in the "Mechanical Properties" section of this review. Thus AFM is very useful for characterising electrospun membranes and indeed any nanoscale surface.

Contact mode is the most conceptually simple form of AFM imaging and is analogous to feeling a surface's texture by running fingers over its surface. However this technique is generally unsuitable for electrospun polymers, as even soft cantilevers have stiffness's comparable or even higher than the stiffness of the bonds in many polymers. Attempts at imaging will therefore cause damage to the sample, due to lateral (frictional) forces.[109] Contact mode has been used[110] to investigate adhesion force on electrospun PET synthetic fibres after the surfaces were modified by plasma treatment. The interested reader is referred to the following excellent review for a more detailed discussion of contact mode AFM imaging.[111]

The AFM mode most often used for polymer imaging and indeed the characterisation of electrospun scaffolds is amplitude modulation, intermittent contact or "tapping" mode. The tip is driven at a fixed frequency, allowing both the amplitude and phase change of the oscillation to be monitored. As the name "tapping" suggests, the tip only briefly enters the contact zone during measurement. Tapping mode copes with large height variations better than the non-contact modes, and also requires smaller forces than contact modes, an important factor when imaging electrospun polymers. Vertical forces are reduced because the tip barely taps the surface, while lateral forces are minimised as the tip is not in constant contact with the surface during scanning. This dramatically reduces surface damage to polymer samples[112]. It is also possible to perform AFM in a liquid surrounding, further reducing requisite forces[109, 112], although the tip response can be more difficult to analyse in such an environment. These advantages of tapping mode (with phase imaging discussed below) have made it the standard for imaging polymers

and characterising electrospun scaffolds.

While amplitude of response is related to surface topography, phase change in the oscillation is loosely related to energy dissipation, although it is not easy to determine the exact contributions from different losses[109]. The phase and topographic image can be conveniently taken and analysed simultaneously. This is advantageous because the fine details on the rough surfaces of fibrous polymers have large height variations[109] **,** and would otherwise remain undetected. The other application for phase imaging is to detect the distribution of composition variation on the surface, even when topography does not change[110, 113]. This could be useful when the distribution of the components of blended electrospun scaffolds, or even electrospun core shell structures are investigated. Some studies have been able to discern differences between crystalline and amorphous areas of a sample based on the phase image, which may also be useful for characterising electrospun scaffolds[109].

It should be noted that phase imaging cannot directly test the chemical makeup of the sample; all of the above techniques rely on changes in mechanical response between the different chemical moities or phases. Thus limited contrast between properties of materials, for example hardness, limits their detection by phase imaging. Attempts at sensing both the physical and chemical makeup of a nano-scale sample have been made by combining AFM with both IR[114] and soft X-ray[115] spectroscopy.

Notwithstanding the power of AFM in surface analysis, users must be aware of its limitations in analysing images of electrospun membranes. AFM images do suffer from small amounts of distortion, in both horizontal and vertical directions. Horizontal images tend to be broadened when a non-ideal tip interacts with the surface. For example, AFM most likely overestimates the diameters of individual electrospun fibres because of the AFM tip geometry,[116] and while the correct choice of tip and a filtering algorithm may reduce this phenomena, it can never be eradicated. While vertical images tend to be compressed by the downward forces exerted on the surface, with appropriate choice of

operating conditions the distortion is usually quite small (0.1 nm) and is unlikely to be a major problem for most polymer-based applications.

Surface roughness measured by AFM can be expressed in many ways, but is most commonly expressed in terms of area average roughness (R_a) and area root-mean-square roughness (R_{ms}).

$$R_a = \frac{1}{N}\sum_{i=1}^{N}\left|Z_i - \overline{Z}\right| \qquad (7)$$

$$R_{ms} = \sqrt{\frac{1}{N}\sum_{i=1}^{N}\left\langle Z_i - \overline{Z}\right\rangle^2} \qquad (8)$$

where N is the total number of data acquired, ($Z_i - \overline{Z}$) is the height (z-value) difference between each data point and the average z-value of all data points. Most AFM software also calculates actual scan area A_{actual} as a ratio of the projected scan area A_{proj},[82] which is a useful index of roughness when calculating the surface energy of the substrate (discussed later in this review).

Providing these limitations of AFM are understood and acknowledged, it is a very useful technique when coupled with SEM, for accurately imaging surface roughness and architecture.

2.2.6 Surface chemical analysis

Techniques for chemical investigation of porous polymeric surfaces include X-ray photoelectron spectroscopy (XPS, also known as electron spectrometry for chemical analysis or ESCA), Fourier Transform Infrared Spectroscopy (FTIR) and Time of Flight Secondary Ion Mass Spectrometry (ToF-SIMS). When using these techniques, their

application to electrospun membranes is similar to a 2D film, which is widely understood, and only a brief description of their use for the surface chemical characterisation of electrospun membranes is warranted.

2.2.6.1 X-ray Photoelectron Spectroscopy

The most commonly used surface chemical analysis technique for polymers and biomedical materials, including electrospun membranes, is X-ray photoelectron spectrum (XPS).[62, 87-89, 104, 117] XPS has been extensively reviewed as an experimental tool for biomaterial research and is a very sensitive surface technique.[118] The main reason for this is that the average mean-free-path of photoelectrons of the relevant kinetic energy range is small; meaning that the sampling depth is therefore localized to around 10 nm below the surface.[117] It has been reported that XPS is capable of a detection limit for protein adsorption of as low as 10 ng/cm^2 at the near surface,[119] highlighting its great potential in the characterisation of electrospun scaffolds.

XPS uses soft X-ray sources, i.e., Mg Kα or Al Kα lines to eject photoelectrons from sample surfaces. It relies on binding energy shifts of photoelectrons ejected from the inner shells of atoms to identify their chemical difference and bonding environment.[120] As spectral resolution is most affected by the energy width of the incident X-ray, it can be improved by use of monochromators.[120] The binding energy shifts of C1s, O1s and N1s have been widely used to derive information of functional groups on surfaces of biomaterials.[119-121] XPS has also been used to investigate whether full encasement has occurred in studies of electrospun polymer membranes with a core shell structure[122, 123] and other similar coatings.[124] However, the binding energy shifts can sometimes be too small to allow full characterisation of the surface; curve fittings must be used to de-convolute XP spectra. Modern XP spectrometers provide computer software for curve fitting using multivariable analysis methods.

Synchrotron radiation sources enable photoelectron surface analysis of greater resolution. However, synchrotron radiation sources are still not widespread and are usually expensive and more complicated than XPS.[125]

2.2.6.2 Attenuated Total Reflection Fourier Transform Infrared Spectroscopy

Fourier Transform Infrared Spectroscopy (FTIR) is a vibrational spectroscopic technique in which infrared radiation interacts with molecules by exciting their bond vibration modes. Attenuated Total Reflection (ATR) FTIR is powerful technique suitable for studying surface properties and surface adsorption.[126] When linearly polarized FTIR light travels through an ATR crystal against the sample surface, it is reflected from the crystal/sample interface, creating an evanescent electric field at each reflection. The depth of penetration of the evanescent field can be determined using the following formula:[126]

$$d_p = \frac{\lambda}{2\pi n_1 \sqrt{\sin^2\theta - (n_2/n_1)^2}} \quad (9)$$

Where λ is the wavelength of the light, n_1 and n_2 are the refractive index of the ATR crystal and the rare medium, θ is the angle of incidence. For germanium n_1 is 4.0. If the angle of incident is 45°, assuming the refractive index of the rare medium being n_2 =1.5 at 1550 cm^{-1} (a typical refractive index for proteins), the depth of penetration is 0.428 μm.[127]

ATR-FTIR has been widely used for surface characterisation of biomedical materials and protein adsorption,[127, 128] and more recently for electrospun membranes surface characterisation to confirm the extent of cross linking in chitosan fibres[129]. It can also be used to investigate the degradation[130] and surface conditions of polymer and co-polymer nanofibrous membranes,[96] antigen immobilisation,[131] layer-by-layer deposition of coatings of different functionalities on the surface of electrospun polymer membranes.

Due to its large penetration depth (approximately 2μm), ATR-FTIR is less surface sensitive than XPS or ToFSIMS. However, if these techniques are used complimentarily, they can provide a good range of detailed surface chemistry information.[95]

Recently polarised FTIR has been used to measure the bulk properties of electrospun polymer fibres. The electrical fields and mechanical forces that are a result of the electrospinning process during the macroscopic nanofibre alignment, also align the polymer chains parallel to the direction of fibre alignment.[132] The degree of alignment of the polymer chains can easily be determined through the analysis of polarised FTIR spectra.[133] While the utilisation of this method for the determination of the molecular orientation within electrospun polymer fibre is recent, polarised FTIR is an established and accurate method that has been extensively used to determine the molecular orientation within polymers. However, generally to determine the degree of polymer molecular alignment, polarised FTIR is coupled with other methods including: polarised Raman spectroscopy and wide angle X-ray diffraction.[132]

2.2.6.3 Secondary Ion Mass Spectrometry (SIMS)

SIMS is a technique with even higher surface sensitivity than XPS with sampling depth of only the top few atomic layers, typically 1 – 2 nm[118, 119] and has an detection limit of 0.1 ng/cm^2.[119] ToFSIMS can also be used to create a spatial distribution, or a map, of the location of different chemical components.[85, 87, 88] Although some advanced XPS and FTIR instruments also have surface mapping functions, these mappings are based on fixed binding energy or fixed wavenumber. SIMS uses a beam of energetic (primary) ions, usually argon or gallium to bombard the surface. As these ions hit the surface, atoms and molecules are removed from the materials surface. A small fraction of the removed atoms and molecules will then be ionized to produce secondary ions, which can be accelerated to a constant kinetic energy and allowed to travel a certain distance before being collected and analysed. The time-of-flight of an ion species in field free vacuum travel is related to their individual mass.

Two types of SIMS, static SIMS and dynamic SIMS, have been developed. The primary ion beam energy used to scan the surface in static SIMS is low (10^{-9} Acm^{-1}), whereas in dynamic SIMS, the primary beam energy is much higher;[118] the surface is "eroded" by the primary ion beam to reveal the depth chemical profile of the sample. ToFSIMS has been used for characterising the adsorbed protein on surfaces of biomaterials. It can provide composition, conformation, orientation and denaturation information of protein on material surfaces[134] and has been used to identify different amino acids. Since the analysis depth of static SIMS is 10 – 15 Å, the mass spectrum can reveal the amino acid assay of the outer 10 – 15 Å of the adsorbed protein. Therefore static SIMS is a powerful technique for the study of conformational and orientation of proteins.

A disadvantage of SIMS is that it does cause more serious damage than XPS [135]. Furthermore, the quantification of mass spectra requires standards that should be obtained within the same matrix, and such spectral databases are still being developed. Despite this, it has been successfully used in polymer studies involving poly-$_L$-lysine (PLL)[136] and a poly(vinyl chloride)/poly(methyl methacrylate) (PVC/PMMA) blend[137]. More recently, it has also been applied to electrospun poly(caprolactone)/ cetyltrimethylammonium bromide (PCL/CTAB) membranes for the first time with some success.[138] Despite problems with the rough topography, voltage differences and charge build-ups, they were able to detect the major diagnostic ions of both the components and roughly predicte their proportions, with a small loss in mass accuracy and resolution. Future experiments will hopefully build on this, as the ability of SIMS to examine only the top few layers would be particularly relevant to the field of tissue engineering where cells interact primarily with this layer.

Dynamic SIMS can create a depth profile of materials but there are no studies as yet involving Dynamic SIMS and porous/fibrous polymer samples. Recently, a modified SIMS technique was used to improve the resolution of components in blended polymeric materials.[136] In blended polymers, the major characteristic ions in one component are often present in the other component, making it impossible to resolve the separate

components. This can be solved if one of the components in the blend is composed of some deuterium, thus slightly changing the ions formed. This technique may be useful in further studies of blended polymers structures within electrospun membranes if similar problems are encountered.

From the above description of the different analytical techniques available for analysing surfaces, it is apparent that no surface analytical technique provides a full and accurate description of the surface of electrospun membranes. In some circumstances it may be necessary to couple all 3 major techniques mentioned above to obtain the required evaluation of the chemical species on a surface and their distribution.

2.2.7 Surface Energy Analysis

2.2.7.1 Contact Angle Measurements

The contact angle formed at the junction of three phases (i.e. solid, liquid and gas) reflects the liquid surface tension and the solid surface energy through the Young's equation (Eq. 4).[139] The contact angle of a liquid on a solid surface is a direct indication of the wettability of the solid by the liquid. It is a sensitive reflection of changes in physicochemical conditions of the surface, which is linked to surface energy and polarity of the outermost surface (0.3-2 nm).[140]

The surface energy of a solid is determined by the intermolecular forces whose origins are the same as those holding atoms and molecules together in the bulk. An isotropic liquid surface provides a special condition for the surface energy to be directly measured. The surface energy of a pure liquid (which has the units of mJ/m^2, milli Joule per square meter) is equivalent to surface tension (mN/m, milli Newton per metre). However, there is no established method for directly measuring surface energy of a solid surface. The surface energy of the solid can be determined by contact angle methods[140-142] or by

gas adsorption methods, including inverse gas chromatography[143] using liquids with known surface energies.

Under optimal conditions, contact angle measurement can sensitively detect molecular and functional group changes on a solid surface. Contact angle methods have been used to monitor layer-by-layer (LbL) deposition of polymers and proteins on surfaces of electrospun membranes, polymer grafting, plasma treatment induced surface polarity and functional group changes.[95, 144] Contact angle method can only be used on smooth surfaces for surface energy measurements using the Zisman model [145], The Fowkes' geometric means model [142], the Wu's harmonic means model [146] or the Good-van Oss model.[140]

An electrospun membrane has a highly porous structure and therefore also has a surface of nano or micro-scale roughness.[5, 95] Liquid drops on rough and hydrophobic electrospun membranes do not make full contact with the polymer surface (actual contact surface shown in Fig. 3) [147] so contact angle measurements do not correctly reflect the degree of hydrophobicity of the polymer and cannot be used for quantitative or comparison purposes. Zheng *et al*. [148] showed that while the contact angle spin coated polystyrene film has a contact angle with water of around 93˚, the electrospun PS fibre membrane they obtained has a contact angle of 158.1±2.4˚.

The well known models for contact angle corrections are the Wenzel model and the Cassie model. The Wenzel model considers that a liquid drop on a rough surface has a full contact with the surface, i.e. the liquid penetrated into the troughs of the surface texture. Therefore it is useful for contact angle correction for partially wetting situations. In the Wenzel model, the apparent liquid contact angle on a rough solid surface can be described by the follow equation:[149]

$$\cos\theta_{rough} = r\cos\theta_{true} \qquad (10)$$

where r is the roughness factor, which is the ratio of the actual to projected area as expressed below:

$$r = \frac{A_{actual}}{A_{proj}} \quad (11)$$

Nisbet et al. [82] showed that effect of surface roughness on contact angle could be estimated by measuring the solid surface's roughness factor. They used AFM to measure the roughness factors of compression-molded PLGA and P_LLA polymer surfaces and predicted the causes of the contact angle changes by various surface treatments.

When measuring contact angle on a hydrophobic electrospun membrane surface, however, the liquid drop does not make full contact with the surface, but sits on a composite surface comprising of the polymer fibres and air pockets.[148] Such a situation is considered in the Cassie's model as follow:

$$\cos\theta_a = f_1 \cos\theta_1 - f_2 \quad (12)$$

where f_1 is the fraction of the surface that has contact with liquid; f_2 is the fraction that has no contact with the surface.[97] This phenomenon has been widely shown on superhydrophobic surfaces[148, 150] and hydrophobic surfaces, including hydrophobic non-woven polymer materials. Confocal microscopy was employed to visually demonstrate the partial contact of a water drop with the surface of a hydrophobized paper surface.[151]

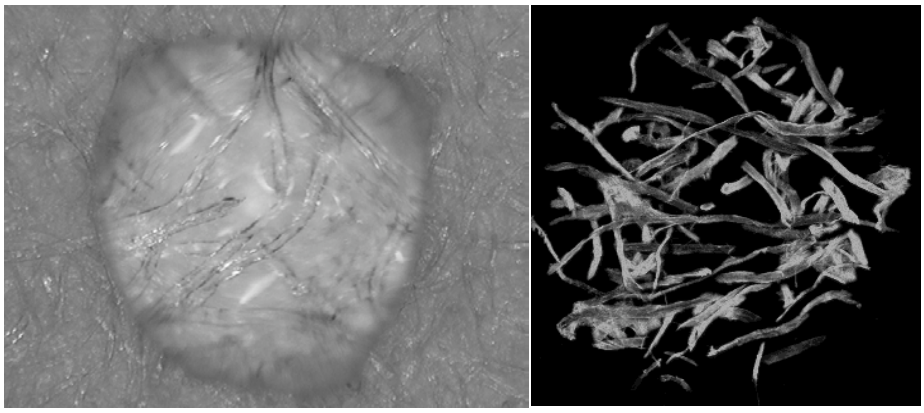

(a) (b)

Figure 3 (a) A water droplet on a paper surface and (b) the actual contact area between a water drop and a paper surface. Reproduced with permission from Elsevier.[147]

Partial contact between a liquid drop and a rough solid surface violates the condition of the Young's equation, which requires the liquid-solid interface being in full contact. Therefore, apparent contact angles observed on rough surfaces will not correctly reflect the real surface condition of the solid and cannot be used for surface energy calculations.[151]

Aspler and co-workers provided an alternative technique of greater precision for determining the surface energies.[152] These authors investigated surface energy of fibrous membranes using a series of water-isopropanol solutions, which have different surface tensions. They observe that generally, a solution of isopropanol and water placed on a non-woven surface is imbibed after a certain time delay. However, a solution with a specific isopropanol concentration (and therefore a specific surface tension) placed on the surface of a non-woven sample, is imbibed into the material immediately. The surface tension of this specific solution is an apparent analogy to the critical wetting surface tension of a solid surface.[140] Although this method was originally proposed for characterising the surface energy of paper,[152] it was recently employed to characterise surface energies of electrospun membranes.[5]

2.2.8 Mechanical Properties (Hardness/Modulus testing)

The mechanical properties of electrospun scaffolds, in particular the hardness and elastic modulus (E), are often of interest. Nanoindentation allows the hardness of specific areas of an electrospun scaffold to be evaluated with very fine resolution, and with minimal preparation.[152] However there are problems with precision and sometimes accuracy when the technique is applied to polymer surfaces, especially fibrous and porous ones. There are now techniques for directly testing the modulus of a single electrospun fibre.[153] Traditional methods of tensile testing have also been applied to scaffolds consisting of many fibres, and their use is reviewed here. When choosing a method, the advantages and disadvantages over nanoindentation should be weighed against the properties, accuracy and time available for measurement.

2.2.8.1 Nanoindentation

Nanoindentation has been the preferred method for investigating mechanical properties for many years. While it requires far less preparation than other techniques and can resolve changes in modulus at different points on a sample, previous studies of polymers have encountered many problems in providing reliable modulus measurements. A comprehensive review of the application of nanoindentation to polymers is provided by Van Landingham *et al.* [152] but its application to nanofibres will be summarised here, along with discussion of several new developments.

Many polymers are too soft to be investigated using nanoindentation, while viscoelastic behaviour (creep) and difficulty in accurately characterising tip shape precludes accuracy using the traditional analysis of Oliver and Pharr.[154] Compared with other methods, modulus values of polymers measured by nanoindentation are often much larger or even

negative in extreme cases, because of the effects of creep,[155] and it is reasonable to assume that this would also be the case for electrospun polymer fibres. Recent attempts to characterise the creep response of polymeric materials[156] suggest that the modulus depends on the speed of the indentation and there is thus no single well-defined value for modulus in these materials. Modulus values also tend to depend on the depth of indentation, with shallower indentations giving larger moduli.[152] Tip shape also seems to affect the measured modulus values. Calibration of the tip-shape area function seems to be a major problem, resolution of which has been attempted using several methods, none of which have resulted in reproducible results.[152] Rough surfaces, as typified by electrospun membranes can also act as a "springy", compliant layer, although a method has been proposed to incorporate this into the analysis.[157] There are several different techniques used for the nanoindentation of polymers, which can be related to electrospun scaffolds. These include Depth-Sensing Indentation (DSI), Atomic Force Microscopy (AFM) and Interfacial Force Microscopy (IFM). A detailed discussion of these techniques is outside the focus of this review, hence interested readers are directed to the following research papers.[109, 158]

2.2.8.2 Dynamic Indentation

Attempts to characterise the viscoelastic behaviour of polymer samples have also used dynamic indentation, using an oscillating tip. Storage and loss moduli were found in studies[159, 160] of different polymer materials which in most cases agreed well with the values determined by dynamic mechanical analysis. We are not aware of studies involving dynamic indentation on porous surfaces but this method does have potential for characterising storage and loss moduli of electrospun scaffolds.

2.2.8.3 Problems faced when determining the moduli of electrospun membranes

There are obvious difficulties for determining the moduli of porous samples. These include ensuring an ideal contact between tip and fibre and that the fibre is adequately

supported to prevent it bending or slipping away from the probe. In one instance scaffolds were compressed prior to indentation,[161] and indentation was then performed on the resulting solid pellet. However, a more common method is to test a single fibre which has been spun onto a hard plate.[162] In this situation it was found that the substrate on which the fibre is mounted can affect the measurement if the fibre diameter is below 300 nm. This study also describes problems involving tip contact with a small-radius fibre; the probe may not contact at 90 degrees or it may slip slightly. The curvature of the fibre should also be considered if this type of analysis is to achieve a more accurate representation of the modulus of the nanofibre scaffold.

While nanoindentation may be a useful and convenient technique for characterising electrospun polymer surfaces, the uncertainties during data analysis must be understood. Therefore, conclusions drawn from nanoindentation data, especially absolute values of hardness or elastic modulus, should be made considering the uncertainties involved.[97, 98] Having said this, nanoindentation experiments have been performed on polymers that have agreed accurately with other testing and accepted values, although as Van Landingham *et al*.[152] noted, care should be taken when comparing to manufacturer's values, as these can vary greatly with crystallinity and other changeable parameters. However, new methods of controlling uncertainties would be invaluable, as nanoindentation has the potential to become a very useful tool for electrospun polymer scaffold characterisation.

2.2.9 Direct Methods for Analysis of Mechanical Properties of Nanofibres

In recent years, several methods have been proposed for the direct testing of the mechanical properties of individual electrospun fibres and the bulk properties of an electrospun matrix. In general these have the advantage of being direct tests of the properties desired, cutting down analysis, and also decreasing the uncertainties in measurements dramatically. Several of these are now discussed.

2.2.9.1 Tensile, Bending, and Cantilever Vibration testing

Individual electrospun fibres have been tested either in tensile testing apparatus or by gluing them to an AFM tip.[163, 164] Such methods have the advantage of producing an entire force-extension curve, allowing the investigation of other properties such as toughness and yield strength. Electrospun fibres are generally strained at a slow rate, in order to allow for viscoelasticity. While this technique is a very reliable way to determine the mechanical properties of individual electrospun fibres, the process of collecting and preparation are very time consuming.

Bending tests have also been performed using an AFM with individual electrospun fibres[157, 165] prepared in a similar way to the direct tensile test. Bending tests only allow the investigation of elastic modulus, and are best for small nanofibres where shear deformation is negligible.[157] A further extension to this method is to suspended individual fibres over pores[166] for the conduct of bend test, which dispenses with the need to collect individual fibres. However, it does require careful searching of the fibre mat in order to find a suitable site for testing that can still be a very time consuming process.

It is well understood that porous structures require a distinction between the properties of solid volumes, produced from solid materials and the behaviour of the sample as a whole. For this reason bulk mechanical tests have also been performed on both electrospun scaffolds [167, 168] and using a microtensile tester. However, one common problem is that the samples are easily damaged whilst loading the specimens into such machines, but, this can be avoided using a protocol similar to that of Huang *et al*..[168] Briefly, this involved preparing samples using a paper template that was fabricated in a manner shown in Figure 4. Double sided tape was applied to the top and bottom sides of the paper template. The electrospun scaffold was then glued to the template and cut along the vertical lines (Figure 4), with additional single sided tape being applied to where the sample is inserted in to the tensile grips for greater rigidity.

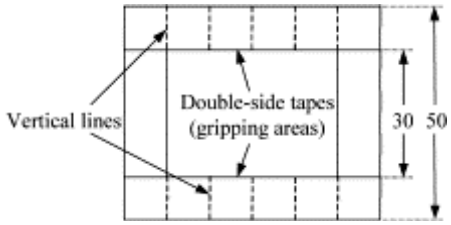

Figure 4 – A paper template proposed to prepare electrospun scaffolds for bulk tensile testing. Employing such a template can avoid structural damage that occurs during sample mounting for these experiments. Reproduced with permission from Elsevier. [168]

When conducting such tensile testing the strength properties of nanofibrous matrices aligned using a spinning mandrels depends on the direction of testing,[169, 170] with increased elastic modulus when tested in a direction parallel to the fibres. Although some studies have reported the absence of such trends [171] this may indicate that in some instances the modulus increase that occurs due to fiber alignment may be influence by material selection (i.e. the orientation of individual molecules within a specific material, which can be calculated using FTIR as discussed above). Tensile testing has been employed to test the bulk properties of electrospun PCL nanofibre scaffolds of random and aligned fibre alignment, which successfully characterised the difference in tensile modulus and maximum strength of these different scaffolds (data shown graphically in Fig. 5).[153] In this instance the sample with random fibre alignment had an isotropic tensile modulus of 12.4 ± 1.3 MPa, whereas for the aligned sample the tensile modulus was 27.3 ± 3.1 MPa parallel to the direction of fibre alignment and 10.2 ± 1.2 MPa in the perpendicular orientation.

PCL fibers have also been strained in tension and have demonstrated a capacity to reorient themselves in the direction of strain, remaining in that orientation after the strain was removed.[170] These observations may explain the difference between strengths in different directions.[170] Strain in the direction of fibre orientation occurred through the strain of individual fibres, while strain in the perpendicular direction was due to the disruption of point bonding between fibres. This development may aid in the

interpretation of results from tensile tests, even for randomly oriented fibres. It also shows the importance of the alignment of fibres when placed in a tensile tester.

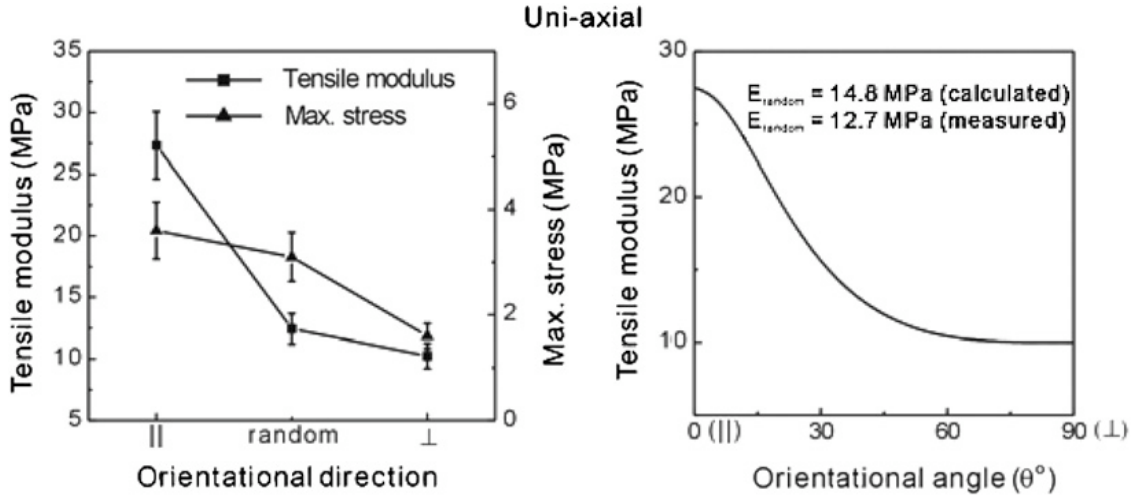

Figure 5 – Tensile moduli and maximum strength of uniaxial random and aligned PCL scaffolds, as well as the angular dependence on the tensile modulus. Reproduced with permission from IOP Journals. [153]

An alternatively way to investigate the bulk mechanical properties of an electrospun matrix other than direct tensile testing is to employ cantilever vibration tests. Such test were designed specifically to allow direct testing of fibres without a time-consuming collection or searching process, [172] whilst still achieving modulus measurements in agreement with the bending test of a single electrospun fibre.[165] Cantilever vibration tests only allow for the determination of elastic modulus, but if this is the only bulk mechanical property required for a fabricated electrospun scaffold this technique may be much more convenient than the others described above.

2.2.10 Alignment Characterisation

The many techniques used to characterise the amount of alignment of the electrospun fibres are all based on statistical methods. It should first be noted that the speed of a rotating mandrel used to align nanofibres should be reported as linear speeds ($m.s^{-1}$) rather than angular speeds (RPM). Angular speed is meaningless unless the diameter of the mandrel is also reported. Strictly speaking, the angle of the fibres is a continuous variable, however most studies[170] have grouped the alignments into discrete subsets and displayed the results as bar charts. Gaussian (normal) distribution may be an alternative choice for modelling the angle of alignment, while the standard deviation could be easily used as a quantifier of the degree of alignment in the nanofibres. This provides a numerical variable for future experiments. Standard deviation can also be used without the assumption of a Gaussian distribution. Obviously if findings deviated from a normal distribution they would have to be reported separately, however we have found no studies where this is significant. The use of discrete statistics causes the loss of a certain amount of information, and is easily replaced with continuous models.

Another alternative method for rapidly measuring the fibre alignment is to employ the 2 dimensional fast Fourier transform (FFT) method. This method generates a mathematical frequency domain from spatial information within an image (typically bright-field images), that are ultimately used to determine the degree of fibre alignment through the formation of a frequency plot.[173] Such a plot consists of grey pixels that are arranged into patterns and used to determine the fibre alignment within the original optical image. This is achieved through the formation of an alignment plot that graphs the FFT alignment verses the principle axis of orientation. On such a graph the peak shape and height are characteristic of the degree of alignment within the scaffold, with the peak position describing the principle axis of orientation. [173] An example of this process is shown in Figure 6 where the initial bright field images are displayed, then the 2D FFT frequency plots that consists of grey pixels and finally the corresponding FFT alignment plots. The only real problem to be aware of when using this method is that uneven illumination within an image can introduce errors into the characterisation of fibre alignment. The interested reader is referred to the following publication that provides an

in-depth description of the utilisation of the 2D fast Fourier transformation method for characterising fibre alignment within electrospun scaffolds.[173]

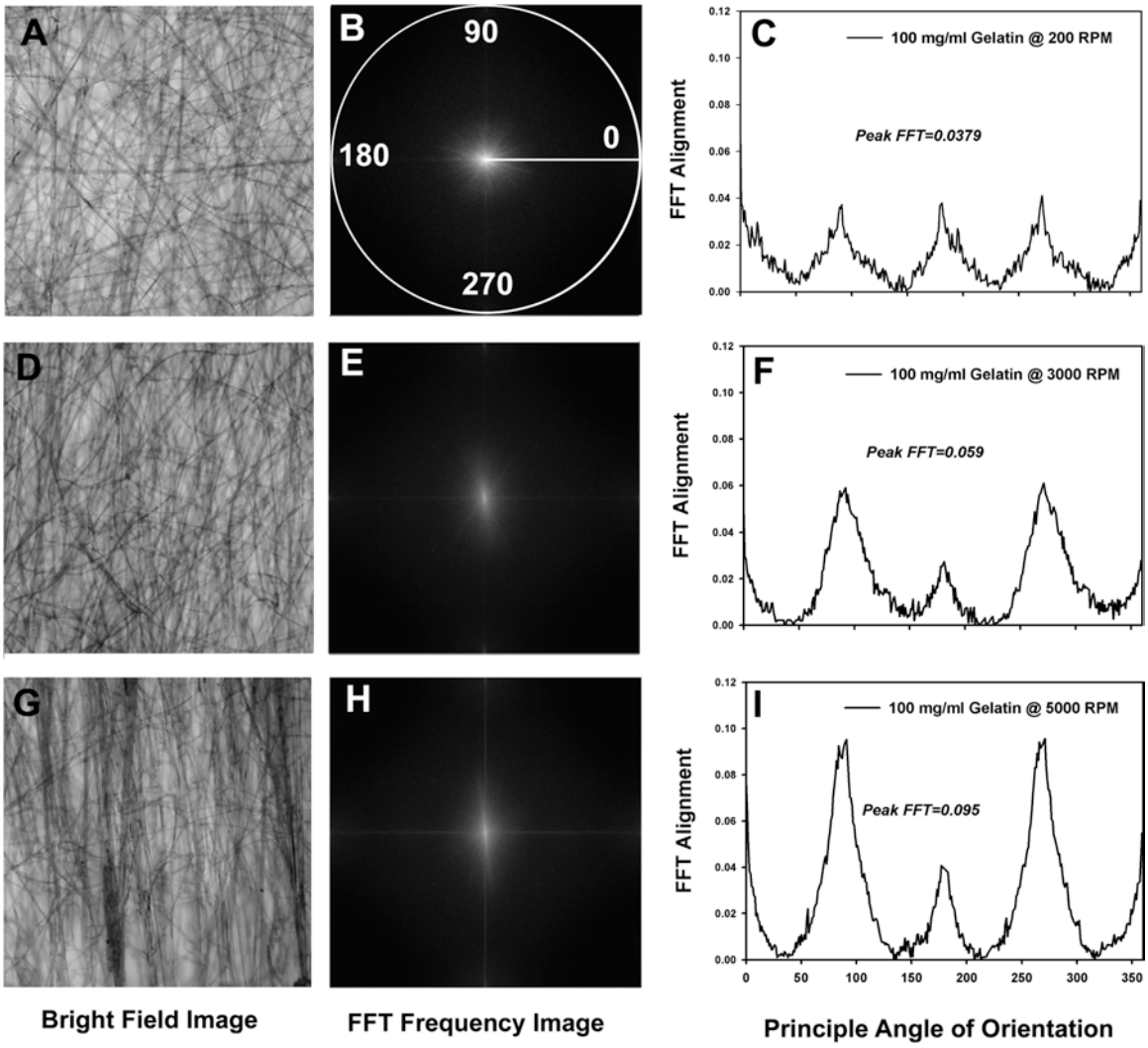

Figure 6 – highlight the analysis used for 2D FFT method to measure fibre alignment. A, D & G are bright field images of the electrospun scaffolds (in this case gelatin). B, E & H are 2D FFT frequency plots that are used to determine the fibre alignment by plotting a FFT alignment plot, which are shown in C, F & I. Reproduced with permission from Brill. [173]

2.2.11 Concluding Remarks

Surface and material sciences play important roles in the characterisation of electrospun scaffolds, as surface and material properties of polymeric scaffolds strongly influence how they interact with their surrounding environment, hence their performance. The important surface properties when dealing with electrospun interfaces are the geometry, topography and the chemical properties of the surface. Geometric and topographical features of electrospun scaffold include the roughness, porosity, pore size, pore size distribution, specific surface area, and intra fibre surface roughness. All these properties influence how an electrospun scaffold will interact with the surrounding environment, as the wettability or hydrophilicity and surface energy are altered. For this reason there is a vast range of analytical tools at the disposal of surface scientists to characterise these properties. We have addressed the current status of characterising electrospun scaffolds in this review and touched on possible improvements in the characterisation of such membranes. Some techniques that have not yet been used for the characterisation of electrospun membranes have also been explored, as we believe that the utilisation of such techniques will dramatically improve upon the way in which electrospun scaffolds are currently characterised.

2.2.12 Acknowledgements

We are grateful to the Australian postgraduate award, and the Cooperative Research Centre (CRC) for Polymers (to DRN), and ARC Discovery (DP0663573) and CRC (to JSF) for funding.

2.2.13 References

[1] M.M. Stevens and J.H. George, *Science* **310** (2005), pp. 1135-1138.

[2] W.E. Teo, W. He and S. Ramakrishna, *Biotechnology journal* **1** (2006), pp. 918-929.

[3] Z. Ma, M. Kotaki, R. Inai and S. Ramakrishna, *Tissue Engineering* **11** (2005), pp. 101-109.

[4] J.B. Chiu, Y.K. Luu, D. Fang, B. Hsiao, B. Chu and M. Hadjiargyrou, *Journal of Biomedical Nanotechnology* **1** (2005), pp. 115-132.

[5] D.R. Nisbet, S. Pattanawong, N.E. Ritchie, W. Shen, D.I. Finkelstein, M.K. Horne and J.S. Forsythe, *Journal of Neural Engineering* **4** (2007), pp. 1-7.

[6] P.D. Dalton, D. Klee and M. Möller, *Polymer* **46** (2005), pp. 611-614.

[7] Z.-M. Huang, Y.-Z. Zhang, M. Kotaki and S. Ramakrishna, *Composites Science and Technology* **63** (2003), pp. 2223-2253.

[8] D. Li, Y. Wang and Y. Xia, *Nano Letters* **3** (2003), pp. 1167-1171.

[9] B. Knight, C. Laukaitis, N. Akhtar, N.A. Hotchin, M. Edlund and A.R. Horwitz, *Current Biology* **10** (2000), pp. 576-585.

[10] L.G. Griffith and M.A. Swartz, *Nature Reviews: Molecular cell biology* **7** (2006), pp. 211-224.

[11] A. Nur-E-Kamala, L. Ahmeda, J. Kamala, M. Schindlerb and S. Meinersa, *Stem Cells* **24** (2006), pp. 426-433.

[12] M. Schindler, I. Ahmed, J. Kamal, A. Nur-E-Kamal, T.K. Grafe, H.Y. Chung and S. Meiners, *Biomaterials* **26** (2005), pp. 5624-5631.

[13] D.R. Nisbet, L.M.Y. Yu, T. Zahir, J.S. Forsythe and M.S. Shoichet, *Journal of Biomaterials Science Polymer Edition* (2007), pp. Accepted 2007.

[14] S.T. Yang and R. Ng, *Materials Today* **10** (2007), pp. 64.

[15] D. Han and P.I. Gouma, *Nanomedicine* **2** (2006), pp. 37-41.

[16] T.K. Borg, *The American Journal of Pathology* **164** (2004), pp. 1141-1142.

[17] T. Hoshiba, M. Wakejima, C.S. Cho, G. Shiota and T. Akaike, *Journal of Biomedical Materials Research Part A* **Published online** (2007), pp. 10.1002/jbm.a.31571.

[18] R. Murugan and S. Ramakrishna, *Tissue Engineering* **13** (2007), pp. 1845-1866.

[19] F. Berthiaume, P.V. Moghe, M. Toner and M.L. Yarmush, *The FASEB Journal* **10** (1996), pp. 1471-1484.

[20] Y. Zhong, X. Yu, R. Gilbert and R.V. Bellamkonda, *Journal of Rehabilitation Research and Development* **38** (2001), pp. 627-632.

[21] D.R. Nisbet, K.E. Crompton, M.K. Horne, D.I. Finkelstein and J.S. Forsythe, *Journal of Biomedical Materials Research: Part B* (2007), pp. Accepted 2007.

[22] D.R. Nisbet, K.E. Crompton, S.D. Hamilton, S. Shirwakawa, R.J. Prankerd, D.I. Finkelstein, M.K. Horne and J.S. Forsythe, *Biophysical Chemistry* **121** (2005), pp. 14-20.

[23] F. Yang, R. Murugan, C. Wang and S. Ramakrishna, *Biomaterials* **26** (2005), pp. 2603-2610.

[24] A. Johansson, C. Carlbergb, N. Danielsenc, L. Monteliusb and M. Kanjea, *Biomaterials* **27** (2006), pp. 1251-1258.

[25] J. Foley, E. Grunwald, P. Nealey and C. Murphy, *Biomaterials* **26** (2005), pp. 3639-3644.

[26] J.M. Corey, D.Y. Lin, K.B. Mycek, Q. Chen, S. Samuel, E.L. Feldman and D.C. Martin, *Journal of Biomedical Materials Research Part A* **83** (2007), pp. 636-645.

[27] I. Kwon, S. Kidoaki and T. Matsuda, *Biomaterials* **26** (2005), pp. 3929- 3939.

[28] W. Li, Y. Guo, H. Wang, D. Shi, C. Liang, Z. Ye, F. Qing and J. Gong, *Journal of Materials Science: Materials in Medicine* **Pubilished online** (2007), pp. 10.1007/s10856-10007-13087-10855.

[29] I. Ahmed, H.Y. Liu, P.C. Mamiya, A.S. Ponery, A.N. Babu, T. Weik, M. Schindler and S. Meiners, *Journal of Biomedical Materials Research* **76** (2006), pp. 851-860.

[30] E. Schnell, K. Klinkhammer, S. Balzer, G. Brook, D. Klee, P.D. Dalton and J. Mey, *Biomaterials* **28** (2007), pp. 3012-3025.

[31] P. Sangsanoh, S. Waleetorncheepsawat, O. Suwantong, P. Wutticharoenmongkol, O. Weeranantanapan, B. Chuenjitbuntaworn, P. Cheepsunthorn, P. Pavasant and P. Supapho., *Biomacromolecules* **8** (2007), pp. 1587-1594.

[32] T.B. Bini, S. Gao, T.C. Tan, S. Wang, A. Lim, L.B. Hai and S. Ramakrishna, *Nanotechnology* **15** (2004), pp. 1459-1464.

[33] T. Matsuda, G. Kagata, R. Kino and J. Tanaka, *Journal of Nanoscience and Nanotechnology* **7** (2007), pp. 852-855.

[34] A. Townsend-Nicholson and S.N. Jayasinghe, *Biomacromolecules* **7** (2006), pp. 3364-3369.

[35] S.N. Jayasinghe and A. Townsend-Nicholson, *Lab on a Chip* **6** (2006), pp. 1086-1090.

[36] R. Rhoades and R. Pflanzer, Human Physiology, 3rd Edt, Saunders College Publishing, Orlando, 1996.

[37] S. Kimakhe, S. Bohic, C. Larrose, A. Reynaud, P. Pilet, B. Giumell, D. Heymann and G. Daculsi, *Journal of Biomedical Materials Research* **47** (1999), pp. 18-27.

[38] S. Stevenson, S.E. Emery and V.M. Goldberg, *Clinical orthopaedics and related research* **324** (1996), pp. 66-74.

[39] V.M. Goldberg and S. Stevenson, *Orthopedics* **17** (1994), pp. 809-810,821.

[40] S.E. Graves, D. Davidson, L. Ingerson, R. P., E.C. Griffith, B.F. McDermott, H.J. McElroy and N.L. Pratt, *The Medical journal of Australia* **180** (2004), pp. S31-34.

[41] M. Shin, H. Yoshimoto and J.P. Vacanti, *Tissue Engineering* **10** (2004), pp. 33-41.

[42] H.W. Kim, J.H. Song and H.E. Kim, *Advanced Functional Materials* **15** (2005), pp. 1988-1994.

[43] C. Li, C. Vepari, H.J. Jin, H.J. Kim and D.L. Kaplan, *Biomaterials* **27** (2006), pp. 3115-3124.

[44] K. Tuslakoglu, N. Bolgen, A.J. Salgado, M.E. Gomes, K. Piskin and R.L. Reis, *Journal of Materials Science: Materials in Medicine* **16** (2005), pp. 1099-1104.

[45] A.S. Badami, M.R. Kreke, M.S. Thompson, J.S. Riffle and A.S. Goldstein, *Biomaterials* **27** (2006), pp. 596-606.

[46] T.B.F. Woodfield, J. Malda, J. de Wijin, F. Peters, J. Riesle and C.A. van Blitterswijk, *Biomaterials* **25** (2004), pp. 4149-4161.

[47] K.J. Shields, M.J. Beckman, G.L. Bowlin and J.S. Wayne, *Tissue Engineering* **10** (2001), pp. 1510-1517.

[48] J. Riesle, A.P. Hollander, R. Langer, L.E. Freed and G. Vunjak-Novakovic, *Journal of Cellular Biochemistry* **71** (1998), pp. 313.

[49] N. Bhattarai, D. Edmondson, O. Veiseh, F.A. Matsen and M. Zhang, *Biomaterials* **26** (2005), pp. 6176-6184.

[50] A. Subramanian, H.Y. Lin, D. Vu and G. Larsen, *Biomedical sciences instrumentation* **40** (2004), pp. 117-122.

[51] A. Subramanian, D. Vu, G. Larsen and H.Y. Lin, *Journal of Biomaterials Science Polymer Edition* **16** (2005), pp. 861-873.

[52] Y.K. Luu, K. Kim, B. Hsiao, B. Chu and M. Hadjiargyrou, *Biomaterials* **89** (2003), pp. 341-353.

[53] W. Li, R. Tuli, C. Okafor, A. Derfoul, K.G. Danielson, D.J. Hall and R.S. Tuan, *Biomaterials* **26** (2005), pp. 599-609.

[54] Y.-Z. Zhang, T.C. Lim, S. Ramakrishna and Z.-M. Huang, *Journal of Materials Science: Materials in Medicine* **16** (2005), pp. 933-946.

[55] B. van der Lei, P. Nieuwenhuis, I. Molenaar and C.R.H. Wildevuur, *Surgery* **101** (1987), pp. 459-467.

[56] H. Sonoda, K. Takamizawa, Y. Nakayama, H. Yasui and T. Matsuda, *Journal of Biomedical Materials Research* **55** (2001), pp. 266-276.

[57] A. Tiwari, H.J. Salacinski, G. Samilton and A.M. Sefalian, *European Journal of Vascular and Endovascular Surgery* **21** (2001), pp. 193-201.

[58] A.M. Seifalian, A. Tiwari, G. Hamilton and H.J. Salacinski, *Artificial Organs* **26** (2002), pp. 301-320.

[59] X. Lian and H.P. Greisler, *Journal of Vascular Surgery* **37** (2003), pp. 472-480.

[60] T.R.S. Kumar and L.K. Krishnan, *Biomaterials* **22** (2001), pp.

[61] R. Rothlein, M.L. Dustin, S.D. Marlin and T.A. Springer, *Journal of Immunology* **137** (1986), pp. 12701274.

[62] Z. Ma, M. Kotaki, T. Yong, W. He and S. Ramakrishna, *Biomaterials* **26** (2005), pp. 2527-2536.

[63] M.R. Williamson, R. Black and C. Kielty, *Biomaterials* **27** (2006), pp. 3608-3616.

[64] J. Stitzel, J. Liu, S.J. Lee, M. Komura, J. Berry, S. Soker, G. Lim, M.V. Dyke, R. Czerw, J.J. Yoo and A. Atala, *Biomaterials* **27** (2006), pp. 1088-1094.

[65] H. Inoguchi, I. Kwon, E. Inoue, K. Takamizawa, Y. Maehara and T. Matsuda, *Biomaterials* **27** (2006), pp. 1470-1478.

[66] X. Zong, H. Bien, C. Chung, L. Yin, D. Fang, B. Hsiao, B. Chu and E. Entcheva, *Biomaterials* **26** (2005), pp. 5330-5338.

[67] X. Zong, H. Bien, C. Chung, L. Yin, K.F. Kim, D, B. Chu, B. Hsiao and E. Entcheva, *Polymer Preprints* **44** (2003), pp. 96-97.

[68] C.Y. Xu, R. Inai, M. Kotaki and S. Ramakrishna, *Biomaterials* **25** (2004), pp. 877-886.

[69] E.D. Boland, J.A. Matthews, K.J. Pawlowski, D.G. Simpson, G.E. Wnek and G.L. Bowlin, *Frontiers in Bioscience* **9** (2004), pp. 1422-1432.

[70] W. He, Y. Ma, T. Yong, W.E. Teo and S. Ramakrishna, *Biomaterials* **26** (2005), pp. 7606-7615.

[71] W. He, T. Yong, W.E. Teo, Z. Ma and S. Ramakrishna, *Tissue Engineering* **11** (2005), pp. 1574-1588.

[72] W. He, T. Yong, Z.W. Ma, R. Inai, W.E. Teo and S. Ramakrishna, *Tissue Engineering* **12** (2006), pp. 2457-2466.

[73] C.Y. Xu, F. Yang, S. Wang and S. Ramakrishna, *Journal of Biomedical Materials Research* **71** (2004), pp. 154-161.

[74] R.K. Li, T.M. Yau, R.D. Weisel, D.A. Mickle, T. Sakai, A. Choi and Z.Q. Jia, *Journal of thoracic and cardiovascular surgery* **119** (2000), pp. 368-375.

[75] M. Shin, O. Ishii, T. Sueda and J.P. Vacanti, *Biomaterials* **25** (2004), pp. 3717-3723.

[76] M. Li, Y. Guo, Y. Wei, A.G. MacDiarmid and P.I. Lelkes, *Biomaterials* **27** (2006), pp. 2705-2715.

[77] E. Yim, K. and K.W. Leong, *Nanomedicine* **1** (2005), pp. 10-21.

[78] S.J. Lee, S.H. Oh, J. Liu, S. Soker, A. Atala and J.J. Yoo, *Biomaterials* **Published Online** (2007), pp. doi:10.1016/j.biomaterials.2007.1011.1024.

[79] J.S. Choi, K.W. Leong and H.S. Yoo, *Biomaterials* **29** (2008), pp. 587-596.

[80] Surface Characterisation of Advanced Polymers, Weinheim, New York, 1993.

[81] Z.M. Huang, Y.Z. Zhang, M. Kotaki and S. Ramakrishna, *Composites Science and Technology* **63** (2003), pp. 2223-2253.

[82] D.R. Nisbet, S. Pattanawong, J. Nunan, W. Shen, M.K. Horne, D.I. Finkelstein and J.S. Forsythe, *Journal of Colloid and Interface Science* **299** (2006), pp. 647-655.

[83] W.J. Li, C.T. Laurencin, E.J. Caterson, R.S. Tuan and F.K. Ko, *Journal of Biomedical Materials Research* **60** (2002), pp. 613-621.

[84] H.L. Schreuder-Gibson, P. Gibson, K. Senecal, M. Sennett and J. Walker, *Journal of Advanced Mat* **34** (2002), pp. 44-55.

[85] B.M. Min, G. Lee, S.H. Kim, Y.S. Nam, T.S. Lee and W.H. Park, *Biomaterials* **25** (2004), pp. 1289-1297.

[86] H.S. Kim, K.H. Kim, H.J. Jin and I.J. Chin, *Macromol Symp* **224** (2005), pp. 145-154.

[87] J.M. Deitzel, W. Kosik, S.H. McKnight, N.C. Beck Tan, J.M. Desimone and S. Crette, *Polymer* **43** (2002), pp. 1025-1029.

[88] J.E. Sanders, S.E. Lamont, A. Karchin, S.L. Golledge and B.D. Ratner, *Biomaterials* **26** (2005), pp. 813-818.

[89] A. Alli, B. Hazer, Y. Manceloglu and S. Suzer, *Eur Polym J* **42** (2006), pp. 740-750.

[90] J.M. Schakenraad, H.J. Busscher, C.R.H. Wildevuur and J. Arends, *Cell Biopys* **13** (1988), pp. 75-91.

[91] D.R. Absolom, C. Thomson, G. Kruzyk, W. Zingg and A.W. Neumann, *Colloids surf* **21** (1986), pp. 447-456.

[92] A. Formhals, *US Patent* (1934), pp. 1,975,504

[93] B.D. Ratner, Surface Characterisation of Biomaterials, Elsevier, New York, 1998.

[94] M. Bognitzki, W. Czado, T. Frese, A. Schaper, M. Hellwig and M. Steinhart, *Advanced Materials* **13** (2001), pp. 70-72.

[95] Z. Ma, M. Kotaki and S. Ramakrishna, *Journal of membrane science* **272** (2006), pp. 179-187.

[96] T. Lin, H.G. Wang, H.M. Wang and X. Wang, *Nanotechnology* **15** (2004), pp. 1375–1381.

[97] A.W. Adamson and A.P. Gast, Physical Chemistry of Surfaces, Wiley-International 6th edition, New York, 1997.

[98] P.A. Webb and C. Orr, Analytical Methods in Fine Particle Technology, Micromeritics Instrument Corporation, USA, 1997.

[99] Y.J. Ryu, H.Y. Kim, K.H. Lee, H.C. Park and D.R. Lee, *European Polymer Journal* **39** (2003), pp. 1883-1889.

[100] R.E. Dehl, *Journal of Biomedical Materials Research* **16** (1982), pp. 715-719.

[101] A.K. Jena and K.M. Gupta, *Journal of Power Sources* **80** (1999), pp. 46-52.

[102] P.V. Grant, C.M. Vaz, P.E. Tomlins, L. Mikhalovska, S. Mikhalovsky, S. James and P. Vadgama, *Springer* **Netherlands** (2006), pp. 215 - 228.

[103] S.J. Gregg and K.S.W. Sing, Adsorption, Surface Area and Porosity, Academic Press, London, 1982.

[104] S.C. Baker, N. Atkin, P.A. Gunning, N. Granville, K. Wilson, D. Wilson and J. Southgate, *Biomaterials* **27** (2006), pp. 3136-3146.

[105] R.R. Rye, J.A. Mann and F.G. Yost, *Langmuir* **12** (1996), pp. 555-565.

[106] Y. Srivastava, I. Loscertales, M. Marquez and T. Thorsen, *Microfluid Nanofluid* **4** (2008), pp. 245–250.

[107] J. Yuh, J.C. Nino and W.M. Sigmund, *Materials Letters* **59** (2005), pp. 3645-3647.

[108] F.K.Y. Gogotsi, A. Ali, N. Naguib, H. Ye, G.L. Yang, C. Li and P. Willis, *Advanced Materials* **15** (2003), pp. 1161 - 1165.

[109] B. Bhusan, H. Fuchs and S. Hosaka, editors. Applied Scanning Probe Methods: Springer, 2004.

[110] J.F. Lübben, G. Fortunato, M. Halbeisen, S. Houis, M. Keller and E. Körner, *Journal of Physics: Conference Series* **61** (2007), pp. 735-739.

[111] R. Garcia and R. Perez, *Surface science reports* **47** (2002), pp. 197-301.

[112] R. García and R. Pérez, *Surface Science Reports* **47** (2002), pp. 197-301.

[113] K.-H. Jung, M.-W. Huh, W. Meng, J. Yuan, S.H. Hyun, J.-S. Bae, S.M. Hudson and I.-K. Kang, *Journal of Applied Polymer Science* **105** (2007), pp. 2816-2823.

[114] A. Hammiche, H. Pollock, M. Reading, M. Claybourn, P. Turner and K. Jewkes, *Applied Spectroscopy* **53** (1999), pp. 810.

[115] I. Koprinarov, A. Hitchcock, W. Li, Y. Heng and H. Stoever, *Macromolecules* **34** (2001), pp. 4424.

[116] R. Jaeger, H. SchOnherr and G.J. Vancso, *Macromolecules* **29** (1996), pp. 7634-7636.

[117] G. Beamson and D. Briggs, High Resolution Xps of Organic Polymers, John Wiely & Sons, Chichester, England, 1992.

[118] H. Liu and T.J. Webster, *Biomaterials* **28** (2007), pp. 354 – 369.

[119] M.S. Wagner, S.L. McArthur, M. Shen, T.A. Horbett and D.G. Castner, *Journal of Biomaterials Science Polymer Edition* **13** (2002), pp. 407-428.

[120] K. Artyushkova and J.E. Fulghum, *Journal of Electron Spectroscopy and Related Phenomena* **121** (2001), pp. 33-55.

[121] P. Rossini, P. Colpo, G. Ceccone, K.D. Jandtb and F. Rossia, *Materials Science and Engineering* **23** (2003), pp. 353 – 358.

[122] Y.Z. Zhang, X. Wang, Y. Feng, J. Li, C.T. Lim and S. Ramakrishna, *Biomacromolecules* **7** (2006), pp. 1049-1057.

[123] P. Zhao, H. Jiang, H. Pan, K. Zhu and W. Chen, *J Biomed Mater Res A* **83** (2007), pp. 372-382.

[124] W. He, Z.W. Ma, T. Yong, W.E. Teo and S. Ramakrishna, *Biomaterials* **26** (2005), pp. 7606-7615.

[125] J.B. Wachtman, *Butterworth-Heinemann* **Boston** (1993), pp. 200 – 220.

[126] A.R. Hind, S.K. Bhargava and A. Mckinnon, *Advanced Colloid and Interface Science* **93** (2001), pp. 91-114.

[127] K.K. Chittur, *Biomaterials* **19** (1998), pp. 357 – 369

[128] R.M. Cornelius, P.W. Wojciechowski and J.L. Brash, *Journal of Colloid and Interface Science* **150** (1992), pp. 121 – 133.

[129] J.D. Schiffman and C.L. Schauer, *Biomacromolecules* **8** (2007), pp. 594-601.

[130] X.L. Deng, G. Sui, M.L. Zhao, G.Q. Chen and X.O. Yang, *Journal of Biomaterials Science Polymer Edition* **18** (2007), pp.

[131] Q. Shi, X. Chen, T. Lu and X. Jing, *Biomaterials* **29** (2008), pp. 1118 – 1126.

[132] M.V. Kakade, S. Givens, K. Gardner, K.H. Lee, D.B. Chase and J.F. Rabolt, *Journal of the American Chemical Society* **129** (2007), pp. 2777-2782.

[133] K.H. Lee, K.W. Kim, A. Pesapane, H.Y. Kim and J.F. Rabolt, *Macromolecules* **41** (2008), pp. 1494-1498.

[134] C.D. Tidwell, D.G. Castner, S.L. Golledge, B.D. Ratner, K. Meyer, B. Hagenhoff and A. Benninghoven, *Surface and Interface Analysis* **31** (2001), pp. 724 - 733.

[135] T. Takahagi, Y. Nakayama, F. Soeda and A. Ishitani, *Journal of Applied Polymer Science* **41** (1990), pp. 1451-1458.

[136] S.K. Tam, J. Dusseault, S. Polizu, M. Ménard, J.-P. Hallé and L.H. Yahia, *Biomaterials* **26** (2005), pp. 6950-6961.

[137] K. Norrman, K.B. Haugshøj and N.B. Larsen, *J Phys Chem B* **106** (2002), pp. 13114-13121.

[138] P.V. Royen, E. Schacht, L. Ruys and L.V. Vaeck, *Rapid Commun Mass Spectrom* **20** (2006), pp. 346-352.

[139] P.C. Hiemenz and R. Rajogopalan, Principles of Colloid and Surface Chemistry, 3rd Ed. Marcel Dekker, New York, 1997.

[140] R.E. Good, Contact Angle, Wetting and Adhesion: A Critical Review, Utrecht, The Netherlands, 1993.

[141] D.K. Owens and R.C.J. Wendt, *Journal of Applied Polymer Science* **13** (1969), pp. 1741.

[142] F.M. Fowkes and M.A. Mostafa, *Ind Eng Chem Prod Res Dev*, **17** (1978), pp. 3.

[143] A. Voelkelk *Critical Rev Anal Chem* **22** (1991), pp. 411 – 439

[144] Q.F. Wei, W.D. Gao, D.Y. Hou and X.Q. Wang, *Applied Surface Science* **245** (2005), pp. 16 – 20.

[145] W.A. Zisman, **ACS series 43** (1964), pp. 1.

[146] S. Wu, *Marcel Dekker* **New York** (1982), pp.

[147] W. Shen, Y. Filonenko, Y. Truong, N. Brack, P. Pigram, I.H. Parker and J. Liesegang, *Colloids and Surfaces A, Physicochemical and Engineering Aspects* **173** (2000), pp. 117-126.

[148] J. Zheng, A. He, J. Li, J. Xu and C.C. Han, *Polymer* **47** (2006), pp. 7095-7102.

[149] R.N. Wenzel, *Ind Eng Chem* **28** (1936), pp. 998-994.

[150] E. Puukilainen, T. Rasilainen, M. Suvanto and T.A. Pakkanen, *Langmuir* **23** (2007), pp. 7263 - 7268.

[151] W. Shen, Y. Filonanko, Y. Truong, I.H. Parker, N. Brack, P. Pigram and J. Liesegang, *Colloid Surf A* **173** (2000), pp. 117-126.

[152] M.R. VanLandingham, J.S. Villarubia, W.F. Guthrie and G.F. Meyers, *Macromolecular Symposia* **167** (2001), pp. 15-43.

[153] G.H. Kim, *Biomedical Materials* **3** (2008), pp. doi:10.1088/1748-6041/1083/1082/025010.

[154] W.C. Oliver and G.M. Pharr, *Journal of Materials Research, v 7, n 6, Jun, 1992, p 1564-1580* **7** (1992), pp. 1564-1580.

[155] B. Briscoe, L. Fiori and E. Pelillo, *J Phys D – Appl Phys* **31** (1998), pp. 2395-2405.

[156] M.L. Oyen, *Acta Materialia* **55** (2007), pp. 3633-3639.

[157] E.P.S. Tan and C.T. Lim. Nanomechanical Testing of Polymeric Nanofibers. In: Quan C, Chau FS, Asundi A, Wong BS and Lim CT, editors. Third Intl Conf on Experimental Mechanics and Third Conf of the Asian Committee on Experimental Mechanics; 2004; Singapore: Proceedings of SPIE; 2004. p. 849-855.

[158] M.R. VanLandingham, J.S. Villarubia, W.F. Guthrie and G.F. Meyers, *Macromolecular Syposia* **167** (2001), pp. 15-45.

[159] G.M. Odegard, T.S. Gates and H.M. Herring, *Experimental Mechanics* **45** (2005), pp. 130-136.

[160] C.C. White, M.R. VanLandingham, P.L. Drzal, N.-K. Chang and S.-H. Chang, *Journal of Polymer Science: Part B: Polymer Physics* **43** (2005), pp. 1812-1824.

[161] S.A. Catledge, W.C. Clem, N. Shrikishen, S. Chowdhury, A.V. Stanishevsky, M. Koopman and Y.K. Vohra, *Biomedical Materials* **2** (2007), pp. 142-150.

[162] E.P.S. Tan and C.T. Lim, *Applied Physics Letters* **87** (2005), pp. 123106.

[163] E.P.S. Tan, S.Y. Ng and C.T. Lim, *Biomaterials* **26** (2005), pp. 1453-1456.

[164] E.P.S. Tan, C.N. Goh, C.H. Sow and C.T. Lim, *Applied Physics Letters* **86** (2005), pp. 073115.

[165] S.-Y. Gu, Q.-L. Wu, J. Ren and G.J. Vancso, *Macromolecular Rapid Communications* **26** (2005), pp. 716-720.

[166] S.-H. Lee, C. Tekmen and W.M. Sigmund, *Materials Science and Engineering A* **398** (2005), pp. 77-81.

[167] W. He, T. Yong, Z.W. Ma, R. Inai, W.E. Teo and S. Ramakrishna, *Tissue Engineering* **12** (2006), pp. 2457-2466.

[168] Z.-M. Huang, Y.Z. Zhang, S. Ramakrishna and C.T. Lim, *Polymer* **45** (2004), pp. 5361-5368.

[169] V. Thomas, M.V. Jose, S. Chowdury, J.F. Sullivan, D.R. Dean and Y.K. Vohra, *J Biomater Sci Polymer Edn* **17** (2006), pp. 969-984.

[170] J. Johnson, A. Ghosh and J. Lannutti, *Journal of Applied Polymer Science* **104** (2007), pp. 2919-2927.

[171] C. Ayres, G. Bowlin, S. Henderson, L. Taylor, J. Shultz, J. Alexander, T. Telemeco and D. Simpson, *Biomaterials*
27 (2006), pp. 5524.

[172] P.A. Yuya, Y. Wen, J.A. Turner, Y.A. Dzenis and Z. Li, *Applied Physics Letters* **90** (2007), pp. 111909.

[173] C. Ayres, B.S. Jha, H. Meredith, J.R. Bowman, G.L. Bowlin, S.C. Henderson and D.G. Simpson, *Journal of Biomedical Science Polymer Edition* **19** (2008), pp. 603-621.

2.1 Characterisation of electrospun membranes

Due to the variety of different applications where electrospun fibres are being used and the specialist and interdisciplinary nature of some fields, often the characterisation aspects are overlooked (tissue engineering is no exception). The composition, surface, morphology and architecture all play critical roles that dictate the performance of the electrospun construct for its particular application. The following review article was targeted to address the scarcity of relevant information surrounding the effective characterisation of electrospun membranes and provides a description of the characterisation methods as well as recommendations on how the technique and/or interpretations can be improved.

Characterisation of electrospun membranes: problems and improvements.

D.R. Nisbet[1,2], A.E. Rodda[1], D.I. Finkelstein[4], M.K. Horne[5], J.S. Forsythe[1,2], W. Shen[3]*

1. Department of Materials Engineering, Division of Biological Engineering , Monash University, PO Box 69M, Victoria 3800, Australia

2. CRC for Polymers, 32 Business Park Drive, Notting Hill, VIC 3168, Australia.

3. Australian Pulp and Paper Institute, Department of Chemical Engineering, Monash University, PO Box 69M, Victoria 3800, Australia

4. The Mental Health Research Institute of Victoria 155 Oak Street, Parkville, Victoria 3052, Australia

5. Howard Florey Institute, Gate 11, Royal Parade, The University of Melbourne, VIC 3010, Australia

2.2.1 Abstract

Electrospun membranes are used in a variety of applications, including filtration systems and sensors for chemical detection and have attracted increased interest in the field of tissue engineering and regenerative medicine. Successful integration of these materials into a specific technology will require understanding of the fibres surface, bulk and architectural properties. Detailed characterisations of these properties are frequently overlooked, particularly in specialised interdisciplinary fields such as tissue engineering. In this article we have reviewed the current status of characterising electrospun scaffolds with a special focus on surface characterisation and recommend improvements in using these techniques to better understand these very interesting nanostructured materials.

2.2.2 Key words

Electrospinning, nanofibre, characterisation, scaffold, fibre mechanical properties

2.2.3 Introduction

As advanced materials are synthesised and fabricated their characterisation by surface science becomes relevant.[1] Characterisation by surface science is paramount to understanding and generating advanced, functional and "smart" materials in modern technologies, such as metallurgy, microelectronics, nanotechnology, corrosion and tissue engineering. This review focuses on the surface characterisation of non-woven polymer membranes that are produced by electrospinning; although the same principles would be relevant to any fibrous membranes fabricated using other processes. We have also addressed the characterisation of modulus and architectural properties of such membranes.

The surface properties of polymeric materials strongly influence their interactions with other materials and interfaces within their surrounding environment and determine the polymer material's suitability for particular engineering applications. The main surface properties of polymeric materials are (a) geometric and topographic and (b) surface chemical properties. Geometric and topographic properties include the roughness of two dimensional polymer surfaces [2-4] as well as the porosity,[5, 6] pore size,[2, 7-9] pore size distribution [7, 10] and specific surface area for porous and non-woven polymer membranes, and intra fibre surface roughness.[11] Surface chemical properties include the chemical composition (which can be different from that of the bulk),[12] which in some instances can be altered by surface modification.[5, 13] This can affect water wettability/hydrophilicity,[3, 5, 6, 14] and surface energetics.[15, 16] In this review, commonly used surface characterisation methods are examined.

2.2.3.1 Current state of surface characterisation in nanofibrous membranes

Although the technology for fabricating electrospun nanofibres was first reported in 1934 [17] , there has been renewed interest in electrospinning because of the growing demand

for nanostructured materials and their unique properties obtained at this length scale, particularly for tissue engineering and regenerative medical technologies. This includes nanostructured drug delivery vessels, cellular microenvironments and conduits for cell regeneration after injury or disease. Successful integration of these materials into a specific technology will require understanding of the fibre surface, bulk and architectural properties.

Biologists will frequently overlook the effect that material surfaces will have on the biological questions they are asking[18] whereas, materials and surface scientists may see biological questions as too complex for the analytical tools at their disposal. This gap between the understandings of interdisciplinary fields can be bridged by assembling interdisciplinary teams, and through the emergence of "new" scientists whose expertise crosses the traditional fields of materials, surface science, engineering and biology. This review is a contribution to bridging this gap and addresses the current status of characterising electrospun scaffolds for use in tissue engineering, highlighting the advantages and disadvantages of analytical techniques in different applications. Where possible, we have recommended improvements in the characterisation of polymer membranes in anticipation of providing a more informed choice of characterisation methods.

2.2.4 Surface characterisation of porous and fibrous polymer materials.

2.2.4.1 Porosity Characterisation

Electrospun scaffolds are highly porous (Fig. 1) and therefore have very large volume to surface ratios, a property central to their use in technologies such as filtration,[19, 20] chemical sensors [21] and tissue engineering.[3, 9, 22] Consequently accurate characterisation of the porosity of these membranes is required for optimal deployment. One simple method for determining porosity of electrospun membranes is by measuring

their apparent weight to volume ratio with the knowledge of bulk polymer density.[20] This results in very basic descriptions of porosity. Other techniques, including mercury porosimetry, capillary flow porosimetry and BET gas adsorption allow for far more detailed characterisation.

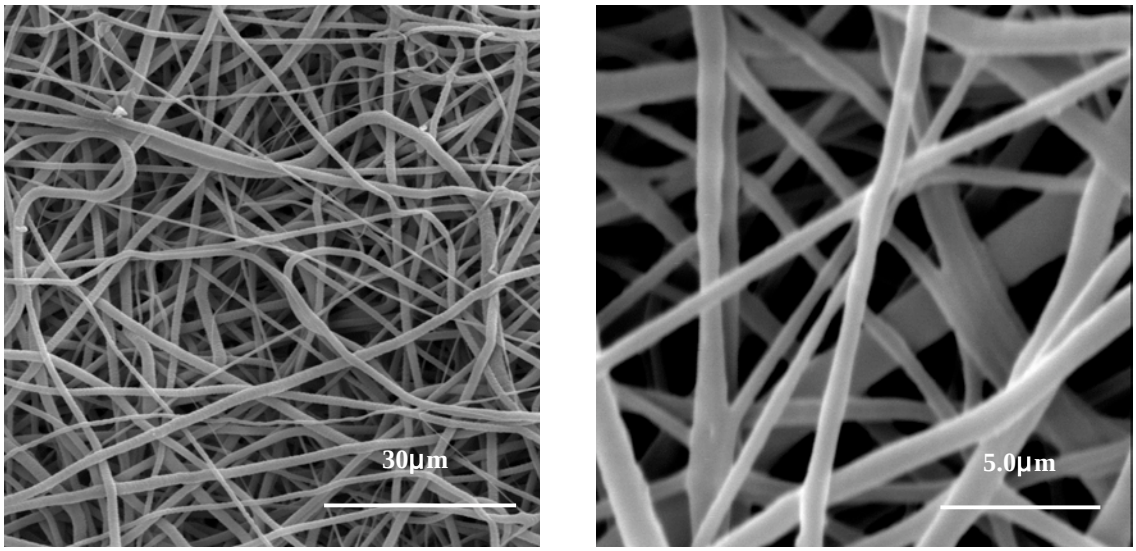

Figure 1 – Polycaprolactone (PCL) scaffolds of highly porous morphology produced by electrospinning. Reproduced with permission from BRILL.[22]

2.2.4.2 Mercury Porosimetry

Mercury porosimetry is a traditional method for characterising porosity and pore size distribution.[10, 16] It is a liquid intrusion method which relies on the principle of the Laplace equation. Mercury has a high surface tension (485.5 dyne/cm at 25˚C) [23] and therefore forms large contact angles with most other materials (≅130˚)[24]. Based on the Laplace equation,[23] mercury does not spontaneously penetrate pores by capillary action. An external pressure must be applied to force mercury into the pores. By assuming that the pores in a porous materials are cylindrical in shape, the pore diameters intruded by mercury can be correlated with the applied pressure according to the following equation (1): [24]

$$D = \frac{-4\gamma \cos\theta}{p} \quad (1)$$

where D is the diameter of the pore, γ is the surface tension of mercury, θ is the contact angle between mercury and the solid and p is the applied pressure. The direct data acquired is the accumulated volume of mercury entering the porous system. A pore size distribution curve is obtained by relating the log differential intrusion volume to log pore diameter, i.e., dV/d(logD). A description of this procedure can be found in reference.[23]

Assuming pores are cylindrical, the pore surface area can also be calculated from the accumulated mercury intrusion volume and the pore diameter data. Since the surface area of a cylindrical pore is πDL and the volume of the pore is $\pi D^2L/4$ (where D and L are the diameter and the length of the cylindrical pore), the wall area of the pore thus equals to:

$$A = \frac{4V}{D} \quad (2)$$

Ryu *et al.* [25] found that mercury porosimetry could detect changes in pore sizes of electrospun nylon-6 membranes of different fibre diameters. Instead of relying on the pore size data obtained directly from the log differential intrusion curve, they calculated the average pore diameters using Eq. 2 with the intrusion volume and pore surface area data obtained by BET measurements. Their pore diameter results ranged from 2.737 – 0.167 μm.[25] Direct volumes of mercury intrusion also provided data on the fraction of voids within the membrane, which ranged from 25 – 80 %.[25] However, assuming that pores are cylindrical is often an over-simplification. The use of Eq. (2) may not provide an accurate surface area measurement, due to a well-known problem associated with the so-called “bottle neck” effect where large cavities behind narrow necks are considered to be pores having the diameter of the neck.[23] Furthermore, high pressure applied to polymer membranes has been reported to cause irreversible structural compression.[26] Thus mercury intrusion method can provide useful representations of porosity and

surface area of polymer nanofibre membranes[11, 23, 25] providing the above caveats are considered.

2.2.4.3 Capillary Flow Porometry

Capillary flow porometry is a liquid extrusion method for measuring pore size.[27] It requires that all pores must first be completely filled with a wetting liquid which is then forced out of the pores by a non-reacting gas. The work done by the gas in forcing liquid out of the pores is assumed to be equal to the surface free energy when the sample-liquid interface is replaced by the sample gas interface.

$$p\,dV = \left(\gamma_{s/g} - \gamma_{s/l}\right) dS \qquad (3)$$

where p is the pressure applied; dV is the displaced volume of liquid by gas; $\gamma_{s/g}$ and $\gamma_{s/l}$ are the surface free energies of solid-gas and solid-liquid; dS is the increase of solid-gas surface area. Jena and Gupta [27] proposed that, by combining Eq. (3) with the Young's equation (Eq. 4), and by replacing the pore cross section area with the equal area circle, a working equation (Eq.5) could be derived:

$$\left(\gamma_{s/g} - \gamma_{s/l}\right) = \gamma_{l/g}\cos\theta \qquad (4)$$

$$p = \frac{4\gamma_{l/g}\cos\theta}{D} \qquad (5)$$

where $\gamma_{l/g}$ is the liquid gas interfacial tension or liquid surface tension; D is the diameter of the equivalent circular area of the pore cross section.[27]

Capillary flow porometry has been used to study the pore size distribution of electrospun fibre membranes.[8, 28] Since capillary flow porometry is a liquid extrusion method, it is more appropriate to use the receding contact angle, which is usually small and leads $\cos\theta$ in Eq. (5) equalling unity. Capillary flow porometry is suitable for measuring "through

pores" that connect one side of the material to the other side, but is not suitable for closed (isolated pores in the matrix) or blind-end pores (connected to the external surface via a single channel or orifice).[28] Like mercury porosimetry, capillary flow porometry is also sensitive to the "bottle neck effect", [28] but unlike mercury porosimetry can not measure blind-end pores.

2.2.4.4 Brunauer-Emmett-Teller (BET) Gas Adsorption

BET gas adsorption method is a well established method for characterising surface area and pore structure of porous materials. The fundamental consideration is the quantity of a single molecular adsorption layer of a known gas. By assuming the Langmuir adsorption model and incorporating the concept of multimolecular layer adsorption, as well as knowing the area occupied by single adsorbed molecule, the surface area of the substrate can be calculated.[23] Gregg and Sing [29] have presented theoretical details of the method. The BET equation is usually written in the following form to allow the determination of values of V_m and C by graphical means:[29]

$$\frac{P}{V_a(P_0 - P)} = \frac{1}{V_m C} + \frac{C-1}{V_m C}\left(\frac{P}{P_0}\right) \qquad (6)$$

Where P and P_0 are the gas pressure and the saturated gas pressure at the temperature of experiment, V_a and V_m are the quantity of gas adsorbed under pressure P and the quantity of gas required for a monolayer adsorption on the sample surface, respectively. C is a constant related to the heat of adsorption of the first molecular layer of gas. By plotting $P/V_a(P_0\text{-}P)$ against (P/P_0). C and V_m can be calculated from the intercept and the slope of the straight line.[29] Since there is no assumption on cylindrical pore geometry, the specific surface area determined by the BET method is more reliable than capillary flow and mercury porsimetry.

Ryu *et al*. [25] used an image analyser to measure the diameters of electrospun fibres (which were controlled by the concentration of polymer solutions and ranged between 90

to 480 nm), and found using BET that the total pore area of nanofibrous membranes to range between 9–51 m^2/g, with the porosity size decreasing within increasing fibre diameter.[25] Based on their specific surface area and porosity data, the authors assumed that pores within the non-woven nanofibrous membranes were fully interconnected when using this method. Although the experimental specific surface area data of nanofibre membrane was smaller, it did not differ greatly from the value calculated using Eq. (2). (by dividing 4 x the volume of the fibres {i.e. membrane mass over polymer density} and the experimental average fibre diameter). The small diameter of the fibres, rather than fibre surface morphology, contributed most to the large specific surface areas found in this study. [25]

2.2.5 Surface and Bulk Morphology: Characterisation and Imaging

2.2.5.1 Scanning Electron Microscopy

Surface morphology is a critical surface parameter that can not only affect the responses of secondary surfaces (such as cells in tissue engineering),[9, 22] but can also affect the characterisation of the material surface.[3] SEM is a method that provides qualitative assessment of fibre diameter distribution, surface roughness and architecture of electrospun polymer membranes.[3, 11, 14, 30] Because this method is very well understood and already extensively used a detailed discussion of this method will not be provided here. However, care must be taken to ensure that fibre diameters and interfibre spacings measured using SEM, are taken on the image plane to ensure that the scale is correct for post analysis. More quantitative evaluation of surface roughness may be obtained using atomic force microscopy (for nano-scale roughness) and a range of contact and non-contact (optical) profilometers (for larger scale roughnesses).[31]

2.2.5.2` Transmission Electron Microscopy

Transmission electron microscopy (TEM) is a characterisation method where the beam of electrons is transmitted through a thin sample and the interaction of the electrons and the sample are used to generate an image. This method has been used on electrospun scaffolds to image core shell structures, shown in Fig. 2 [32], electrospun fibres with incorporated composite particles [33] and carbon nanotubes [34] and the like. Like SEM, this method is well understood and is extensively used to image electrospun scaffolds, so a detailed discussion of the method is not warranted. TEM is a good method to use to image the inclusion of nano-domains within electrospun fibers. One problem with this method is the size of the samples that can be imaged, as they must be ultra thin (less than 1 μm) to allow the focus beam to pass through the sample (generally not an issue for electrospun membranes) and they must be able to withstand high vacuum.

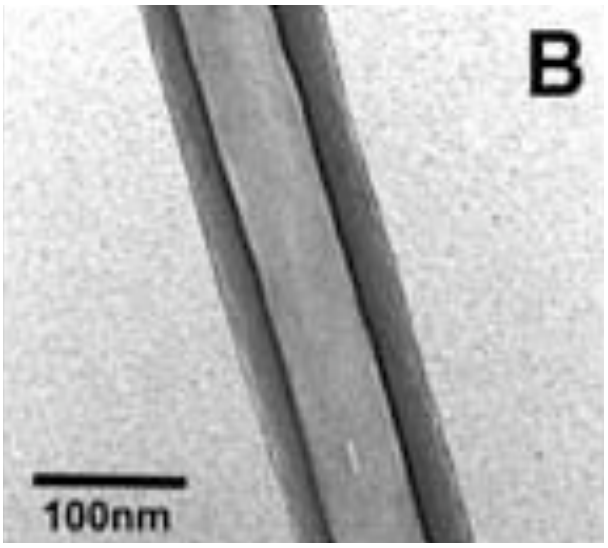

Figure 2 – TEM image of a hollow or core shell electrospun polymer fiber produced from poly(vinylpyrrolidone). Reproduced with permission from Springer-Verlag.[32]

2.2.5.3 Atomic Force Microscopy

Atomic Force Microscopy (AFM) was originally developed to probe the topography of surfaces, and has been used for this purpose on polymer samples, including electrospun

membranes, for many years. However several innovations have allowed the study of other surface properties such as the distribution of a chemical of interest in blended mixtures and the distribution of crystalline and amorphous areas on a surface. The hardness and elastic modulus (through nanoindentation) can also be determined using this technique, and this will be examined in the "Mechanical Properties" section of this review. Thus AFM is very useful for characterising electrospun membranes and indeed any nanoscale surface.

Contact mode is the most conceptually simple form of AFM imaging and is analogous to feeling a surface's texture by running fingers over its surface. However this technique is generally unsuitable for electrospun polymers, as even soft cantilevers have stiffness's comparable or even higher than the stiffness of the bonds in many polymers. Attempts at imaging will therefore cause damage to the sample, due to lateral (frictional) forces.[35] Contact mode has been used[36] to investigate adhesion force on electrospun PET synthetic fibres after the surfaces were modified by plasma treatment. The interested reader is referred to the following excellent review for a more detailed discussion of contact mode AFM imaging.[37]

The AFM mode most often used for polymer imaging and indeed the characterisation of electrospun scaffolds is amplitude modulation, intermittent contact or "tapping" mode. The tip is driven at a fixed frequency, allowing both the amplitude and phase change of the oscillation to be monitored. As the name "tapping" suggests, the tip only briefly enters the contact zone during measurement. Tapping mode copes with large height variations better than the non-contact modes, and also requires smaller forces than contact modes, an important factor when imaging electrospun polymers. Vertical forces are reduced because the tip barely taps the surface, while lateral forces are minimised as the tip is not in constant contact with the surface during scanning. This dramatically reduces surface damage to polymer samples[38]. It is also possible to perform AFM in a liquid surrounding, further reducing requisite forces[35, 38], although the tip response can be more difficult to analyse in such an environment. These advantages of tapping mode (with phase imaging discussed below) have made it the standard for imaging

polymers and characterising electrospun scaffolds.

While amplitude of response is related to surface topography, phase change in the oscillation is loosely related to energy dissipation, although it is not easy to determine the exact contributions from different losses[35]. The phase and topographic image can be conveniently taken and analysed simultaneously. This is advantageous because the fine details on the rough surfaces of fibrous polymers have large height variations[35] **,** and would otherwise remain undetected. The other application for phase imaging is to detect the distribution of composition variation on the surface, even when topography does not change[36, 39]. This could be useful when the distribution of the components of blended electrospun scaffolds, or even electrospun core shell structures are investigated. Some studies have been able to discern differences between crystalline and amorphous areas of a sample based on the phase image, which may also be useful for characterising electrospun scaffolds[35].

It should be noted that phase imaging cannot directly test the chemical makeup of the sample; all of the above techniques rely on changes in mechanical response between the different chemical moities or phases. Thus limited contrast between properties of materials, for example hardness, limits their detection by phase imaging. Attempts at sensing both the physical and chemical makeup of a nano-scale sample have been made by combining AFM with both IR[40] and soft X-ray[41] spectroscopy.

Notwithstanding the power of AFM in surface analysis, users must be aware of its limitations in analysing images of electrospun membranes. AFM images do suffer from small amounts of distortion, in both horizontal and vertical directions. Horizontal images tend to be broadened when a non-ideal tip interacts with the surface. For example, AFM most likely overestimates the diameters of individual electrospun fibres because of the AFM tip geometry,[42] and while the correct choice of tip and a filtering algorithm may reduce this phenomena, it can never be eradicated. While vertical images tend to be compressed by the downward forces exerted on the surface, with appropriate choice of

operating conditions the distortion is usually quite small (0.1 nm) and is unlikely to be a major problem for most polymer-based applications.

Surface roughness measured by AFM can be expressed in many ways, but is most commonly expressed in terms of area average roughness (R_a) and area root-mean-square roughness (R_{ms}).

$$R_a = \frac{1}{N}\sum_{i=1}^{N}\left|Z_i - \overline{Z}\right| \qquad (7)$$

$$R_{ms} = \sqrt{\frac{1}{N}\sum_{i=1}^{N}\left\langle Z_i - \overline{Z}\right\rangle^2} \qquad (8)$$

where N is the total number of data acquired, ($Z_i - \overline{Z}$) is the height (z-value) difference between each data point and the average z-value of all data points. Most AFM software also calculates actual scan area A_{actual} as a ratio of the projected scan area A_{proj},[3] which is a useful index of roughness when calculating the surface energy of the substrate (discussed later in this review).

Providing these limitations of AFM are understood and acknowledged, it is a very useful technique when coupled with SEM, for accurately imaging surface roughness and architecture.

2.2.6 Surface chemical analysis

Techniques for chemical investigation of porous polymeric surfaces include X-ray photoelectron spectroscopy (XPS, also known as electron spectrometry for chemical analysis or ESCA), Fourier Transform Infrared Spectroscopy (FTIR) and Time of Flight Secondary Ion Mass Spectrometry (ToF-SIMS). When using these techniques, their

application to electrospun membranes is similar to a 2D film, which is widely understood, and only a brief description of their use for the surface chemical characterisation of electrospun membranes is warranted.

2.2.6.1 X-ray Photoelectron Spectroscopy

The most commonly used surface chemical analysis technique for polymers and biomedical materials, including electrospun membranes, is X-ray photoelectron spectrum (XPS).[5, 12-14, 30, 43] XPS has been extensively reviewed as an experimental tool for biomaterial research and is a very sensitive surface technique.[44] The main reason for this is that the average mean-free-path of photoelectrons of the relevant kinetic energy range is small; meaning that the sampling depth is therefore localized to around 10 nm below the surface.[43] It has been reported that XPS is capable of a detection limit for protein adsorption of as low as 10 ng/cm^2 at the near surface,[45] highlighting its great potential in the characterisation of electrospun scaffolds.

XPS uses soft X-ray sources, i.e., Mg Kα or Al Kα lines to eject photoelectrons from sample surfaces. It relies on binding energy shifts of photoelectrons ejected from the inner shells of atoms to identify their chemical difference and bonding environment.[46] As spectral resolution is most affected by the energy width of the incident X-ray, it can be improved by use of monochromators.[46] The binding energy shifts of C1s, O1s and N1s have been widely used to derive information of functional groups on surfaces of biomaterials.[45-47] XPS has also been used to investigate whether full encasement has occurred in studies of electrospun polymer membranes with a core shell structure[48, 49] and other similar coatings.[50] However, the binding energy shifts can sometimes be too small to allow full characterisation of the surface; curve fittings must be used to de-convolute XP spectra. Modern XP spectrometers provide computer software for curve fitting using multivariable analysis methods.

Synchrotron radiation sources enable photoelectron surface analysis of greater resolution. However, synchrotron radiation sources are still not widespread and are usually expensive and more complicated than XPS.[51]

2.2.6.2 Attenuated Total Reflection Fourier Transform Infrared Spectroscopy

Fourier Transform Infrared Spectroscopy (FTIR) is a vibrational spectroscopic technique in which infrared radiation interacts with molecules by exciting their bond vibration modes. Attenuated Total Reflection (ATR) FTIR is powerful technique suitable for studying surface properties and surface adsorption.[52] When linearly polarized FTIR light travels through an ATR crystal against the sample surface, it is reflected from the crystal/sample interface, creating an evanescent electric field at each reflection. The depth of penetration of the evanescent field can be determined using the following formula:[52]

$$d_p = \frac{\lambda}{2\pi n_1 \sqrt{\sin^2\theta - (n_2/n_1)^2}} \quad (9)$$

Where λ is the wavelength of the light, n_1 and n_2 are the refractive index of the ATR crystal and the rare medium, θ is the angle of incidence. For germanium n_1 is 4.0. If the angle of incident is 45°, assuming the refractive index of the rare medium being n_2 =1.5 at 1550 cm^{-1} (a typical refractive index for proteins), the depth of penetration is 0.428 μm.[53]

ATR-FTIR has been widely used for surface characterisation of biomedical materials and protein adsorption,[53, 54] and more recently for electrospun membranes surface characterisation to confirm the extent of cross linking in chitosan fibres[55]. It can also be used to investigate the degradation[56] and surface conditions of polymer and co-polymer nanofibrous membranes,[21] antigen immobilisation,[57] layer-by-layer deposition of coatings of different functionalities on the surface of electrospun polymer membranes.

Due to its large penetration depth (approximately 2μm), ATR-FTIR is less surface sensitive than XPS or ToFSIMS. However, if these techniques are used complimentarily, they can provide a good range of detailed surface chemistry information.[20]

Recently polarised FTIR has been used to measure the bulk properties of electrospun polymer fibres. The electrical fields and mechanical forces that are a result of the electrospinning process during the macroscopic nanofibre alignment, also align the polymer chains parallel to the direction of fibre alignment.[58] The degree of alignment of the polymer chains can easily be determined through the analysis of polarised FTIR spectra.[59] While the utilisation of this method for the determination of the molecular orientation within electrospun polymer fibre is recent, polarised FTIR is an established and accurate method that has been extensively used to determine the molecular orientation within polymers. However, generally to determine the degree of polymer molecular alignment, polarised FTIR is coupled with other methods including: polarised Raman spectroscopy and wide angle X-ray diffraction.[58]

2.2.6.3 Secondary Ion Mass Spectrometry (SIMS)

SIMS is a technique with even higher surface sensitivity than XPS with sampling depth of only the top few atomic layers, typically 1 – 2 nm[44, 45] and has an detection limit of 0.1 ng/cm^2.[45] ToFSIMS can also be used to create a spatial distribution, or a map, of the location of different chemical components.[10, 12, 13] Although some advanced XPS and FTIR instruments also have surface mapping functions, these mappings are based on fixed binding energy or fixed wavenumber. SIMS uses a beam of energetic (primary) ions, usually argon or gallium to bombard the surface. As these ions hit the surface, atoms and molecules are removed from the materials surface. A small fraction of the removed atoms and molecules will then be ionized to produce secondary ions, which can be accelerated to a constant kinetic energy and allowed to travel a certain distance before being collected and analysed. The time-of-flight of an ion species in field free vacuum travel is related to their individual mass.

Two types of SIMS, static SIMS and dynamic SIMS, have been developed. The primary ion beam energy used to scan the surface in static SIMS is low (10^{-9} Acm^{-1}), whereas in dynamic SIMS, the primary beam energy is much higher;[44] the surface is "eroded" by the primary ion beam to reveal the depth chemical profile of the sample. ToFSIMS has been used for characterising the adsorbed protein on surfaces of biomaterials. It can provide composition, conformation, orientation and denaturation information of protein on material surfaces[60] and has been used to identify different amino acids. Since the analysis depth of static SIMS is 10 – 15 Å, the mass spectrum can reveal the amino acid assay of the outer 10 – 15 Å of the adsorbed protein. Therefore static SIMS is a powerful technique for the study of conformational and orientation of proteins.

A disadvantage of SIMS is that it does cause more serious damage than XPS [61]. Furthermore, the quantification of mass spectra requires standards that should be obtained within the same matrix, and such spectral databases are still being developed. Despite this, it has been successfully used in polymer studies involving poly-$_L$-lysine (PLL)[62] and a poly(vinyl chloride)/poly(methyl methacrylate) (PVC/PMMA) blend[63]. More recently, it has also been applied to electrospun poly(caprolactone)/ cetyltrimethylammonium bromide (PCL/CTAB) membranes for the first time with some success.[64] Despite problems with the rough topography, voltage differences and charge build-ups, they were able to detect the major diagnostic ions of both the components and roughly predicte their proportions, with a small loss in mass accuracy and resolution. Future experiments will hopefully build on this, as the ability of SIMS to examine only the top few layers would be particularly relevant to the field of tissue engineering where cells interact primarily with this layer.

Dynamic SIMS can create a depth profile of materials but there are no studies as yet involving Dynamic SIMS and porous/fibrous polymer samples. Recently, a modified SIMS technique was used to improve the resolution of components in blended polymeric materials.[62] In blended polymers, the major characteristic ions in one component are often present in the other component, making it impossible to resolve the separate

components. This can be solved if one of the components in the blend is composed of some deuterium, thus slightly changing the ions formed. This technique may be useful in further studies of blended polymers structures within electrospun membranes if similar problems are encountered.

From the above description of the different analytical techniques available for analysing surfaces, it is apparent that no surface analytical technique provides a full and accurate description of the surface of electrospun membranes. In some circumstances it may be necessary to couple all 3 major techniques mentioned above to obtain the required evaluation of the chemical species on a surface and their distribution.

2.2.7 Surface Energy Analysis

2.2.7.1 Contact Angle Measurements

The contact angle formed at the junction of three phases (i.e. solid, liquid and gas) reflects the liquid surface tension and the solid surface energy through the Young's equation (Eq. 4).[65] The contact angle of a liquid on a solid surface is a direct indication of the wettability of the solid by the liquid. It is a sensitive reflection of changes in physicochemical conditions of the surface, which is linked to surface energy and polarity of the outermost surface (0.3-2 nm).[66]

The surface energy of a solid is determined by the intermolecular forces whose origins are the same as those holding atoms and molecules together in the bulk. An isotropic liquid surface provides a special condition for the surface energy to be directly measured. The surface energy of a pure liquid (which has the units of mJ/m^2, milli Joule per square meter) is equivalent to surface tension (mN/m, milli Newton per metre). However, there is no established method for directly measuring surface energy of a solid surface. The surface energy of the solid can be determined by contact angle methods[66-68] or by gas

adsorption methods, including inverse gas chromatography[69] using liquids with known surface energies.

Under optimal conditions, contact angle measurement can sensitively detect molecular and functional group changes on a solid surface. Contact angle methods have been used to monitor layer-by-layer (LbL) deposition of polymers and proteins on surfaces of electrospun membranes, polymer grafting, plasma treatment induced surface polarity and functional group changes.[20, 70] Contact angle method can only be used on smooth surfaces for surface energy measurements using the Zisman model [71], The Fowkes' geometric means model [68], the Wu's harmonic means model [72] or the Good-van Oss model.[66]

An electrospun membrane has a highly porous structure and therefore also has a surface of nano or micro-scale roughness.[9, 20] Liquid drops on rough and hydrophobic electrospun membranes do not make full contact with the polymer surface (actual contact surface shown in Fig. 3) [73] so contact angle measurements do not correctly reflect the degree of hydrophobicity of the polymer and cannot be used for quantitative or comparison purposes. Zheng *et al.* [74] showed that while the contact angle spin coated polystyrene film has a contact angle with water of around 93˚, the electrospun PS fibre membrane they obtained has a contact angle of 158.1±2.4˚.

The well known models for contact angle corrections are the Wenzel model and the Cassie model. The Wenzel model considers that a liquid drop on a rough surface has a full contact with the surface, i.e. the liquid penetrated into the troughs of the surface texture. Therefore it is useful for contact angle correction for partially wetting situations. In the Wenzel model, the apparent liquid contact angle on a rough solid surface can be described by the follow equation:[75]

$$\cos\theta_{rough} = r\cos\theta_{true} \qquad (10)$$

where r is the roughness factor, which is the ratio of the actual to projected area as expressed below:

$$r = \frac{A_{actual}}{A_{proj}} \quad (11)$$

Nisbet et al. [3] showed that effect of surface roughness on contact angle could be estimated by measuring the solid surface's roughness factor. They used AFM to measure the roughness factors of compression-molded PLGA and P_LLA polymer surfaces and predicted the causes of the contact angle changes by various surface treatments.

When measuring contact angle on a hydrophobic electrospun membrane surface, however, the liquid drop does not make full contact with the surface, but sits on a composite surface comprising of the polymer fibres and air pockets.[74] Such a situation is considered in the Cassie's model as follow:

$$\cos\theta_a = f_1 \cos\theta_1 - f_2 \quad (12)$$

where f_1 is the fraction of the surface that has contact with liquid; f_2 is the fraction that has no contact with the surface.[23] This phenomenon has been widely shown on superhydrophobic surfaces[74, 76] and hydrophobic surfaces, including hydrophobic non-woven polymer materials. Confocal microscopy was employed to visually demonstrate the partial contact of a water drop with the surface of a hydrophobized paper surface.[77]

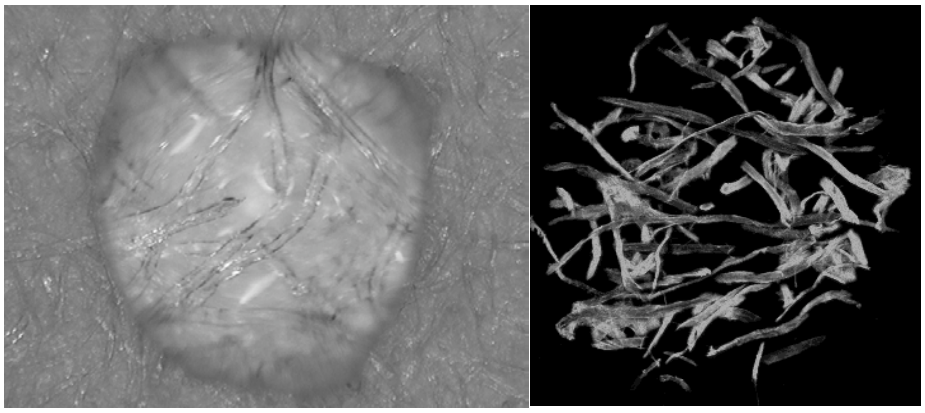

(a) (b)

Figure 3 (a) A water droplet on a paper surface and (b) the actual contact area between a water drop and a paper surface. Reproduced with permission from Elsevier.[73]

Partial contact between a liquid drop and a rough solid surface violates the condition of the Young's equation, which requires the liquid-solid interface being in full contact. Therefore, apparent contact angles observed on rough surfaces will not correctly reflect the real surface condition of the solid and cannot be used for surface energy calculations.[77]

Aspler and co-workers provided an alternative technique of greater precision for determining the surface energies.[78] These authors investigated surface energy of fibrous membranes using a series of water-isopropanol solutions, which have different surface tensions. They observe that generally, a solution of isopropanol and water placed on a non-woven surface is imbibed after a certain time delay. However, a solution with a specific isopropanol concentration (and therefore a specific surface tension) placed on the surface of a non-woven sample, is imbibed into the material immediately. The surface tension of this specific solution is an apparent analogy to the critical wetting surface tension of a solid surface.[66] Although this method was originally proposed for characterising the surface energy of paper,[78] it was recently employed to characterise surface energies of electrospun membranes.[9]

2.2.8 Mechanical Properties (Hardness/Modulus testing)

The mechanical properties of electrospun scaffolds, in particular the hardness and elastic modulus (E), are often of interest. Nanoindentation allows the hardness of specific areas of an electrospun scaffold to be evaluated with very fine resolution, and with minimal preparation.[78] However there are problems with precision and sometimes accuracy when the technique is applied to polymer surfaces, especially fibrous and porous ones. There are now techniques for directly testing the modulus of a single electrospun fibre.[79] Traditional methods of tensile testing have also been applied to scaffolds consisting of many fibres, and their use is reviewed here. When choosing a method, the advantages and disadvantages over nanoindentation should be weighed against the properties, accuracy and time available for measurement.

2.2.8.1 Nanoindentation

Nanoindentation has been the preferred method for investigating mechanical properties for many years. While it requires far less preparation than other techniques and can resolve changes in modulus at different points on a sample, previous studies of polymers have encountered many problems in providing reliable modulus measurements. A comprehensive review of the application of nanoindentation to polymers is provided by Van Landingham *et al.* [78] but its application to nanofibres will be summarised here, along with discussion of several new developments.

Many polymers are too soft to be investigated using nanoindentation, while viscoelastic behaviour (creep) and difficulty in accurately characterising tip shape precludes accuracy using the traditional analysis of Oliver and Pharr.[80] Compared with other methods, modulus values of polymers measured by nanoindentation are often much larger or even

negative in extreme cases, because of the effects of creep,[81] and it is reasonable to assume that this would also be the case for electrospun polymer fibres. Recent attempts to characterise the creep response of polymeric materials[82] suggest that the modulus depends on the speed of the indentation and there is thus no single well-defined value for modulus in these materials. Modulus values also tend to depend on the depth of indentation, with shallower indentations giving larger moduli.[78] Tip shape also seems to affect the measured modulus values. Calibration of the tip-shape area function seems to be a major problem, resolution of which has been attempted using several methods, none of which have resulted in reproducible results.[78] Rough surfaces, as typified by electrospun membranes can also act as a "springy", compliant layer, although a method has been proposed to incorporate this into the analysis.[83] There are several different techniques used for the nanoindentation of polymers, which can be related to electrospun scaffolds. These include Depth-Sensing Indentation (DSI), Atomic Force Microscopy (AFM) and Interfacial Force Microscopy (IFM). A detailed discussion of these techniques is outside the focus of this review, hence interested readers are directed to the following research papers.[35, 84]

2.2.8.2 Dynamic Indentation

Attempts to characterise the viscoelastic behaviour of polymer samples have also used dynamic indentation, using an oscillating tip. Storage and loss moduli were found in studies[85, 86] of different polymer materials which in most cases agreed well with the values determined by dynamic mechanical analysis. We are not aware of studies involving dynamic indentation on porous surfaces but this method does have potential for characterising storage and loss moduli of electrospun scaffolds.

2.2.8.3 Problems faced when determining the moduli of electrospun membranes

There are obvious difficulties for determining the moduli of porous samples. These include ensuring an ideal contact between tip and fibre and that the fibre is adequately

supported to prevent it bending or slipping away from the probe. In one instance scaffolds were compressed prior to indentation,[87] and indentation was then performed on the resulting solid pellet. However, a more common method is to test a single fibre which has been spun onto a hard plate.[88] In this situation it was found that the substrate on which the fibre is mounted can affect the measurement if the fibre diameter is below 300 nm. This study also describes problems involving tip contact with a small-radius fibre; the probe may not contact at 90 degrees or it may slip slightly. The curvature of the fibre should also be considered if this type of analysis is to achieve a more accurate representation of the modulus of the nanofibre scaffold.

While nanoindentation may be a useful and convenient technique for characterising electrospun polymer surfaces, the uncertainties during data analysis must be understood. Therefore, conclusions drawn from nanoindentation data, especially absolute values of hardness or elastic modulus, should be made considering the uncertainties involved.[23, 24] Having said this, nanoindentation experiments have been performed on polymers that have agreed accurately with other testing and accepted values, although as Van Landingham *et al*.[78] noted, care should be taken when comparing to manufacturer's values, as these can vary greatly with crystallinity and other changeable parameters. However, new methods of controlling uncertainties would be invaluable, as nanoindentation has the potential to become a very useful tool for electrospun polymer scaffold characterisation.

2.2.9 Direct Methods for Analysis of Mechanical Properties of Nanofibres

In recent years, several methods have been proposed for the direct testing of the mechanical properties of individual electrospun fibres and the bulk properties of an electrospun matrix. In general these have the advantage of being direct tests of the properties desired, cutting down analysis, and also decreasing the uncertainties in measurements dramatically. Several of these are now discussed.

2.2.9.1 Tensile, Bending, and Cantilever Vibration testing

Individual electrospun fibres have been tested either in tensile testing apparatus or by gluing them to an AFM tip.[89, 90] Such methods have the advantage of producing an entire force-extension curve, allowing the investigation of other properties such as toughness and yield strength. Electrospun fibres are generally strained at a slow rate, in order to allow for viscoelasticity. While this technique is a very reliable way to determine the mechanical properties of individual electrospun fibres, the process of collecting and preparation are very time consuming.

Bending tests have also been performed using an AFM with individual electrospun fibres[83, 91] prepared in a similar way to the direct tensile test. Bending tests only allow the investigation of elastic modulus, and are best for small nanofibres where shear deformation is negligible.[83] A further extension to this method is to suspended individual fibres over pores[92] for the conduct of bend test, which dispenses with the need to collect individual fibres. However, it does require careful searching of the fibre mat in order to find a suitable site for testing that can still be a very time consuming process.

It is well understood that porous structures require a distinction between the properties of solid volumes, produced from solid materials and the behaviour of the sample as a whole. For this reason bulk mechanical tests have also been performed on both electrospun scaffolds [93, 94] and using a microtensile tester. However, one common problem is that the samples are easily damaged whilst loading the specimens into such machines, but, this can be avoided using a protocol similar to that of Huang *et al*..[94] Briefly, this involved preparing samples using a paper template that was fabricated in a manner shown in Figure 4. Double sided tape was applied to the top and bottom sides of the paper template. The electrospun scaffold was then glued to the template and cut along the vertical lines (Figure 4), with additional single sided tape being applied to where the sample is inserted in to the tensile grips for greater rigidity.

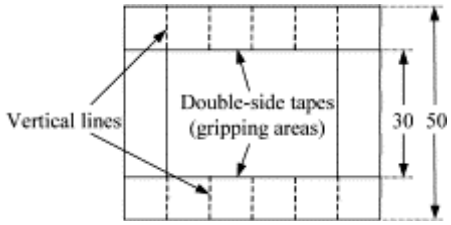

Figure 4 – A paper template proposed to prepare electrospun scaffolds for bulk tensile testing. Employing such a template can avoid structural damage that occurs during sample mounting for these experiments. Reproduced with permission from Elsevier. [94]

When conducting such tensile testing the strength properties of nanofibrous matrices aligned using a spinning mandrels depends on the direction of testing,[95, 96] with increased elastic modulus when tested in a direction parallel to the fibres. Although some studies have reported the absence of such trends [97] this may indicate that in some instances the modulus increase that occurs due to fiber alignment may be influence by material selection (i.e. the orientation of individual molecules within a specific material, which can be calculated using FTIR as discussed above). Tensile testing has been employed to test the bulk properties of electrospun PCL nanofibre scaffolds of random and aligned fibre alignment, which successfully characterised the difference in tensile modulus and maximum strength of these different scaffolds (data shown graphically in Fig. 5).[79] In this instance the sample with random fibre alignment had an isotropic tensile modulus of 12.4 ± 1.3 MPa, whereas for the aligned sample the tensile modulus was 27.3 ± 3.1 MPa parallel to the direction of fibre alignment and 10.2 ± 1.2 MPa in the perpendicular orientation.

PCL fibers have also been strained in tension and have demonstrated a capacity to reorient themselves in the direction of strain, remaining in that orientation after the strain was removed.[96] These observations may explain the difference between strengths in different directions.[96] Strain in the direction of fibre orientation occurred through the strain of individual fibres, while strain in the perpendicular direction was due to the disruption of point bonding between fibres. This development may aid in the interpretation of results from tensile tests, even for randomly oriented fibres. It also shows the importance of the alignment of fibres when placed in a tensile tester.

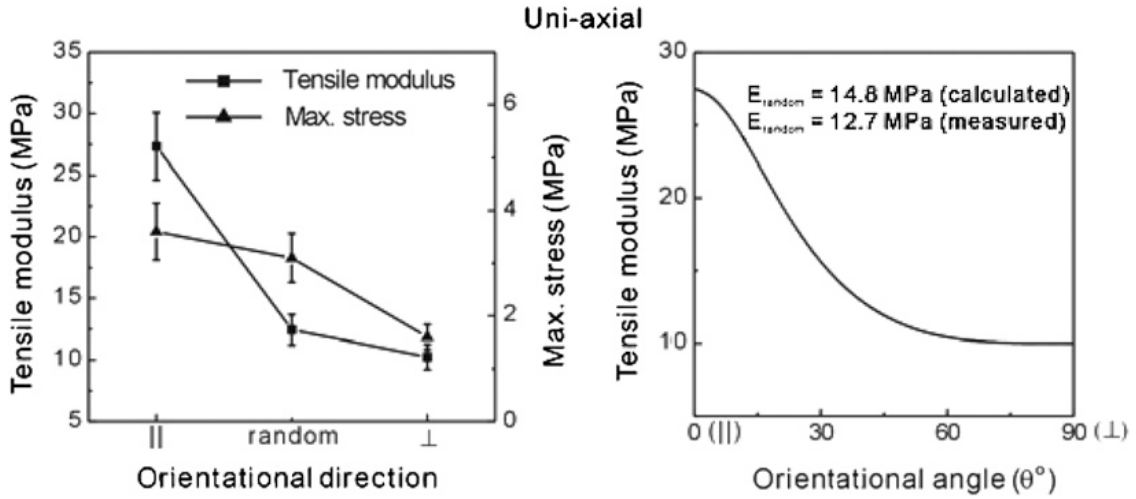

Figure 5 – Tensile moduli and maximum strength of uniaxial random and aligned PCL scaffolds, as well as the angular dependence on the tensile modulus. Reproduced with permission from IOP Journals. [79]

An alternatively way to investigate the bulk mechanical properties of an electrospun matrix other than direct tensile testing is to employ cantilever vibration tests. Such test were designed specifically to allow direct testing of fibres without a time-consuming collection or searching process, [98] whilst still achieving modulus measurements in agreement with the bending test of a single electrospun fibre.[91] Cantilever vibration tests only allow for the determination of elastic modulus, but if this is the only bulk mechanical property required for a fabricated electrospun scaffold this technique may be much more convenient than the others described above.

2.2.10.1 Alignment Characterisation

The many techniques used to characterise the amount of alignment of the electrospun fibres are all based on statistical methods. It should first be noted that the speed of a rotating mandrel used to align nanofibres should be reported as linear speeds ($m.s^{-1}$) rather than angular speeds (RPM). Angular speed is meaningless unless the diameter of

the mandrel is also reported. Strictly speaking, the angle of the fibres is a continuous variable, however most studies[96] have grouped the alignments into discrete subsets and displayed the results as bar charts. Gaussian (normal) distribution may be an alternative choice for modelling the angle of alignment, while the standard deviation could be easily used as a quantifier of the degree of alignment in the nanofibres. This provides a numerical variable for future experiments. Standard deviation can also be used without the assumption of a Gaussian distribution. Obviously if findings deviated from a normal distribution they would have to be reported separately, however we have found no studies where this is significant. The use of discrete statistics causes the loss of a certain amount of information, and is easily replaced with continuous models.

Another alternative method for rapidly measuring the fibre alignment is to employ the 2 dimensional fast Fourier transform (FFT) method. This method generates a mathematical frequency domain from spatial information within an image (typically bright-field images), that are ultimately used to determine the degree of fibre alignment through the formation of a frequency plot.[99] Such a plot consists of grey pixels that are arranged into patterns and used to determine the fibre alignment within the original optical image. This is achieved through the formation of an alignment plot that graphs the FFT alignment verses the principle axis of orientation. On such a graph the peak shape and height are characteristic of the degree of alignment within the scaffold, with the peak position describing the principle axis of orientation. [99] An example of this process is shown in Figure 6 where the initial bright field images are displayed, then the 2D FFT frequency plots that consists of grey pixels and finally the corresponding FFT alignment plots. The only real problem to be aware of when using this method is that uneven illumination within an image can introduce errors into the characterisation of fibre alignment. The interested reader is referred to the following publication that provides an in-depth description of the utilisation of the 2D fast Fourier transformation method for characterising fibre alignment within electrospun scaffolds.[99]

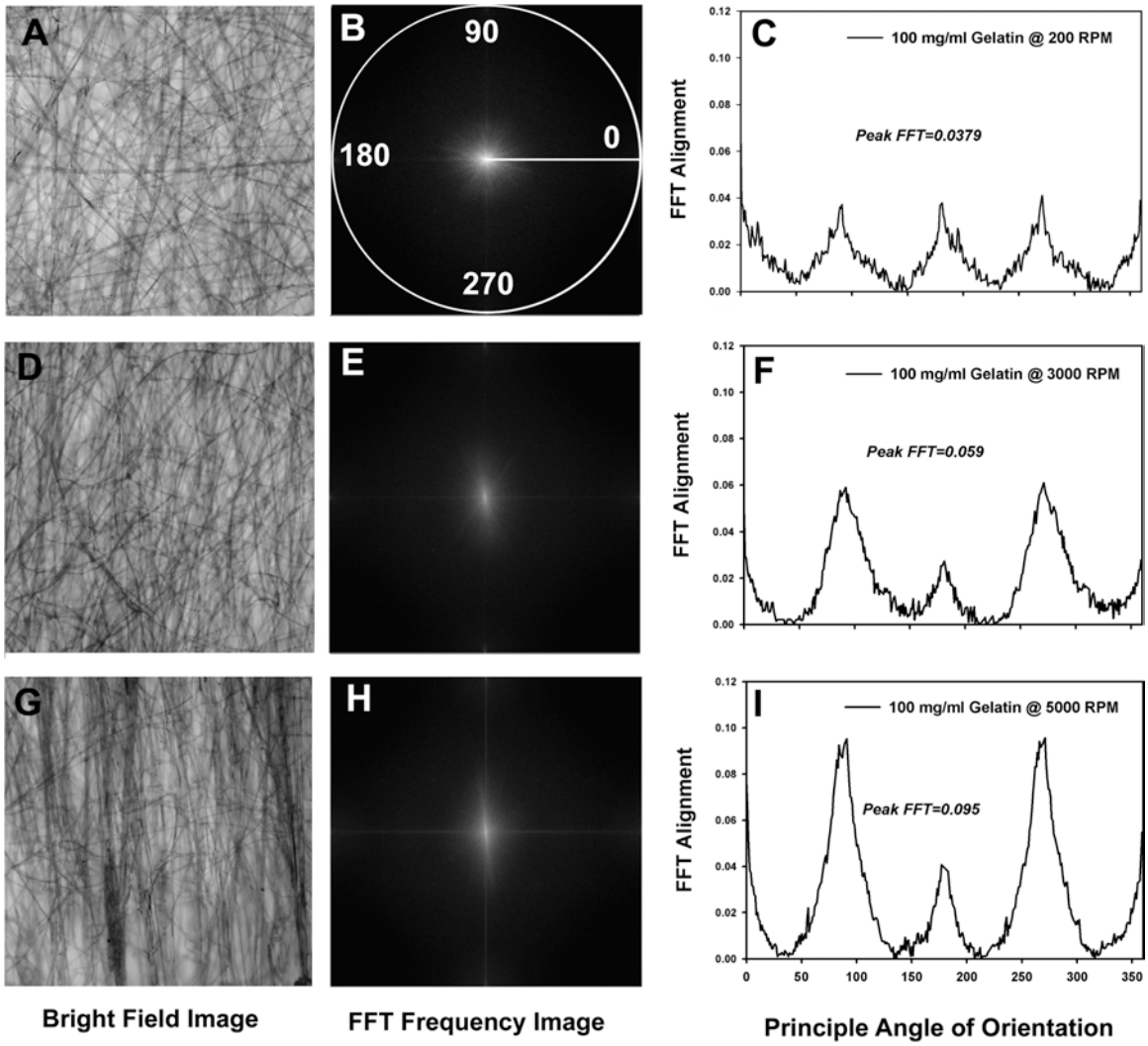

Figure 6 – highlight the analysis used for 2D FFT method to measure fibre alignment. A, D & G are bright field images of the electrospun scaffolds (in this case gelatin). B, E & H are 2D FFT frequency plots that are used to determine the fibre alignment by plotting a FFT alignment plot, which are shown in C, F & I. Reproduced with permission from Brill. [99]

2.2.11 Concluding Remarks

Surface and material sciences play important roles in the characterisation of electrospun scaffolds, as surface and material properties of polymeric scaffolds strongly influence

how they interact with their surrounding environment, hence their performance. The important surface properties when dealing with electrospun interfaces are the geometry, topography and the chemical properties of the surface. Geometric and topographical features of electrospun scaffold include the roughness, porosity, pore size, pore size distribution, specific surface area, and intra fibre surface roughness. All these properties influence how an electrospun scaffold will interact with the surrounding environment, as the wettability or hydrophilicity and surface energy are altered. For this reason there is a vast range of analytical tools at the disposal of surface scientists to characterise these properties. We have addressed the current status of characterising electrospun scaffolds in this review and touched on possible improvements in the characterisation of such membranes. Some techniques that have not yet been used for the characterisation of electrospun membranes have also been explored, as we believe that the utilisation of such techniques will dramatically improve upon the way in which electrospun scaffolds are currently characterised.

2.2.12 Acknowledgements

We are grateful to the Australian postgraduate award, and the Cooperative Research Centre (CRC) for Polymers (to DRN), and ARC Discovery (DP0663573) and CRC (to JSF) for funding.

2.2.11 References

[1] Surface Characterisation of Advanced Polymers (Weinheim, New York, 1993).

[2] Z. M. Huang, Y. Z. Zhang, M. Kotaki and S. Ramakrishna, A review on polymer nanofibers by electrospinning and their applications in nanocomposites, Composites Science and Technology 63 (2003) 2223.

[3] D. R. Nisbet, S. Pattanawong, J. Nunan, W. Shen, M. K. Horne, D. I. Finkelstein and J. S. Forsythe, The effect of surface hydrophilicity on the behaviour of embryonic cortical neurons, Journal of Colloid and Interface Science 299 (2006) 647.

[4] C. Y. Xu, F. Yang, S. Wang and S. Ramakrishna, In vitro study of human vascular endothelial cell function on materials with various surface roughness, Journal of Biomedical Materials Research 71 (2004) 154.

[5] Z. Ma, M. Kotaki, T. Yong, W. He and S. Ramakrishna, Surface engineering of electrospun polyethylene terephthalate (PET) nanofibers towards development of a new material for blood vessel engineering., Biomaterials 26 (2005) 2527.

[6] X. Zong, H. Bien, C. Chung, L. Yin, D. Fang, B. Hsiao, B. Chu and E. Entcheva, Electrospun Fine-textured Scaffolds for Heart Tissue Constructs, Biomaterials 26 (2005) 5330.

[7] W. J. Li, C. T. Laurencin, E. J. Caterson, R. S. Tuan and F. K. Ko, Electrospun nanofibrous strucutre: A novel scaffold for tissue engineering, Journal of Biomedical Materials Research 60 (2002) 613.

[8] H. L. Schreuder-Gibson, P. Gibson, K. Senecal, M. Sennett and J. Walker, Protective textile materials based on electrospun nanofibers, Journal of Advanced Mat. 34 (2002) 44.

[9] D. R. Nisbet, S. Pattanawong, N. E. Ritchie, W. Shen, D. I. Finkelstein, M. K. Horne and J. S. Forsythe, Interaction of embryonic cortical neurones on nanofibrous scaffolds for neural tissue engineering, Journal of Neural Engineering 4 (2007) 1.

[10] B. M. Min, G. Lee, S. H. Kim, Y. S. Nam, T. S. Lee and W. H. Park, Electrospinning of silk fibroin nanofibers and its effect on the adhesion and spreading of normal human keratinocytes and fibroblasts in vitro, Biomaterials 25 (2004) 1289.

[11] H. S. Kim, K. H. Kim, H. J. Jin and I. J. Chin, Morphological characterisation of electrospun nano-fibrous membranes of biodegradable poly(L-lactide) and poly(lactide-co-glycolide), Macromol. Symp. 224 (2005) 145.

[12] J. M. Deitzel, W. Kosik, S. H. McKnight, N. C. Beck Tan, J. M. Desimone and S. Crette, Electrospinning of polymer nanofibers with specific suface chemistry, Polymer 43 (2002) 1025.

[13] J. E. Sanders, S. E. Lamont, A. Karchin, S. L. Golledge and B. D. Ratner, Fibro-porous meshes made from polyurethane micro-fibers: effects of surface charge on tissue response, Biomaterials 26 (2005) 813.

[14] A. Alli, B. Hazer, Y. Manceloglu and S. Suzer, synthesis, characterisation and surface properties of amphiphilic polystyrene-b-polypropylene glycol block copolymers, Eur. Polym. J 42 (2006) 740.

[15] J. M. Schakenraad, H. J. Busscher, C. R. H. Wildevuur and J. Arends, Thermondynamic aspects of cell spreading on solid substrata, Cell Biopys 13 (1988) 75.

[16] D. R. Absolom, C. Thomson, G. Kruzyk, W. Zingg and A. W. Neumann, Adhesion of hydrophilic particles (human erythocytes) to polymer surfaces: effect of pH and ionic strength, Colloids surf. 21 (1986) 447.

[17] A. Formhals, Electrospinning, US Patent (1934) 1.

[18] B. D. Ratner, Surface Characterisation of Biomaterials (Elsevier, New York, 1998).

[19] M. Bognitzki, W. Czado, T. Frese, A. Schaper, M. Hellwig and M. Steinhart, Nanostructured fibres via electrospinning, Advanced Materials 13 (2001) 70.

[20] Z. Ma, M. Kotaki and S. Ramakrishna, Surface modified nonwoven polysulphone (PSU) fiber mesh by electrospinning: A novel affinity membrane, Journal of membrane science 272 (2006) 179.

[21] T. Lin, H. G. Wang, H. M. Wang and X. Wang, The charge effect of cationic surfactants on the elimination of fibre beads in the electrospinning of polystyrene, Nanotechnology 15 (2004) 1375.

[22] D. R. Nisbet, L. M. Y. Yu, T. Zahir, J. S. Forsythe and M. S. Shoichet, Characterization of brain-derived stem cells on electrospun poly(ε-caprolactone)

submicron scaffolds: evaluating their potential in neural tissue engineering., Journal of Biomaterials Science Polymer Edition (2007) Accepted 2007.

[23] A. W. Adamson and A. P. Gast, Physical chemistry of surfaces (Wiley-International 6th edition, New York, 1997).

[24] P. A. Webb and C. Orr, Analytical methods in fine particle technology (Micromeritics Instrument Corporation, USA, 1997).

[25] Y. J. Ryu, H. Y. Kim, K. H. Lee, H. C. Park and D. R. Lee, Transport properties of electrospun nylon 6 nonwoven mats European Polymer Journal 39 (2003) 1883.

[26] R. E. Dehl, On the characterisation of porosity in PTFE-carbon composite implant materials by mercury porosimetry, Journal of Biomedical Materials Research 16 (1982) 715.

[27] A. K. Jena and K. M. Gupta, In-plane compression porometry of battery seperators, Journal of Power Sources 80 (1999) 46.

[28] P. V. Grant, C. M. Vaz, P. E. Tomlins, L. Mikhalovska, S. Mikhalovsky, S. James and P. Vadgama, Physical Characterization of a plycaprolactone tissue scaffold", in Surface chemistry in biomedical and environmental science, Springer Netherlands (2006) 215

[29] S. J. Gregg and K. S. W. Sing, Adsorption, surface area and porosity (Academic Press, London, 1982).

[30] S. C. Baker, N. Atkin, P. A. Gunning, N. Granville, K. Wilson, D. Wilson and J. Southgate, Characterization of electrospun polystyrene scaffolds for three-dimensional in vitro biological studies, Biomaterials 27 (2006) 3136.

[31] R. R. Rye, J. A. Mann and F. G. Yost, The flow of liquids in surface grooves, Langmuir 12 (1996) 555.

[32] Y. Srivastava, I. Loscertales, M. Marquez and T. Thorsen, Electrospinning of hollow and core/sheath nanofibers using a microfluidic manifold, Microfluid Nanofluid 4 (2008) 245.

[33] J. Yuh, J. C. Nino and W. M. Sigmund, Synthesis of barium titanate ($BaTiO_3$) nanofibers via electrospinning, Materials Letters 59 (2005) 3645.

[34] F. K. Y. Gogotsi, A. Ali, N. Naguib, H. Ye, G. L. Yang, C. Li and P. Willis, Electrospinning of Continuous Carbon Nanotube-Filled Nanofiber Yarns, Advanced Materials 15 (2003) 1161

[35] B. Bhusan, H. Fuchs and S. Hosaka, eds., Applied Scanning Probe Methods (Springer, 2004).

[36] J. F. Lübben, G. Fortunato, M. Halbeisen, S. Houis, M. Keller and E. Körner, Characterization of synthetic fibers using the atomic force microscope, Journal of Physics: Conference Series 61 (2007) 735.

[37] R. Garcia and R. Perez, Dynamic atomic force microscopy methods, Surface science reports 47 (2002) 197.

[38] R. García and R. Pérez, Dynamic Atomic Force Microscopy Methods, Surface Science Reports 47 (2002) 197.

[39] K.-H. Jung, M.-W. Huh, W. Meng, J. Yuan, S. H. Hyun, J.-S. Bae, S. M. Hudson and I.-K. Kang, Preparation and Antibacterial Activity of PET/Chitosan Nanofibrous Mats Using an Electrospinning Technique, Journal of Applied Polymer Science 105 (2007) 2816.

[40] A. Hammiche, H. Pollock, M. Reading, M. Claybourn, P. Turner and K. Jewkes, Applied Spectroscopy 53 (1999) 810.

[41] I. Koprinarov, A. Hitchcock, W. Li, Y. Heng and H. Stoever, Macromolecules 34 (2001) 4424.

[42] R. Jaeger, H. SchOnherr and G. J. Vancso, Chain packing in electrospun poly(ethylene oxide) visualized by atomic force microscopy, Macromolecules 29 (1996) 7634.

[43] G. Beamson and D. Briggs, High resolution XPS of organic polymers (John Wiely & Sons, Chichester, England, 1992).

[44] H. Liu and T. J. Webster, Nanomedicine for implants: A review of studies and necessary experimental tools, Biomaterials 28 (2007) 354

[45] M. S. Wagner, S. L. McArthur, M. Shen, T. A. Horbett and D. G. Castner, Limits of detection for time of flight secondary ion mass spectrometry (ToF-SIMS) and X-ray photoelectron spectroscopy (XPS): detection of low amounts of adsorbed protein, Journal of Biomaterials Science Polymer Edition 13 (2002) 407.

[46] K. Artyushkova and J. E. Fulghum, Identification of chemical components in XPS spectra and images using multivariate statistical analysis methods, Journal of Electron Spectroscopy and Related Phenomena 121 (2001) 33.

[47] P. Rossini, P. Colpo, G. Ceccone, K. D. Jandtb and F. Rossia, Surface engineering of polymeric films for biomedical applications, Materials Science and Engineering 23 (2003) 353

[48] Y. Z. Zhang, X. Wang, Y. Feng, J. Li, C. T. Lim and S. Ramakrishna, Coaxial Electrospinning of (Fluorescein Isothiocyanate-Conjugated Bovine Serum Albumin)-Encapsulated Poly(ε-caprolactone) Nanofibers for Sustained Release, Biomacromolecules 7 (2006) 1049.

[49] P. Zhao, H. Jiang, H. Pan, K. Zhu and W. Chen, Biodegradable fibrous scaffolds composed of gelatin coated poly(ε-caprolactone) prepared by coaxial electrospinning, J Biomed Mater Res A 83 (2007) 372.

[50] W. He, Z. W. Ma, T. Yong, W. E. Teo and S. Ramakrishna, Fabrication of collagen-coated biodegradable polymer nanofiber mesh and its potential for endothelial cells growth, Biomaterials 26 (2005) 7606.

[51] J. B. Wachtman, Characterization of materials., Butterworth-Heinemann Boston (1993) 200

[52] A. R. Hind, S. K. Bhargava and A. Mckinnon, At the solid/liquid interface: FTIR/ATR - a tool of choice, Advanced Colloid and Interface Science 93 (2001) 91.

[53] K. K. Chittur, FTIR/ATR for protein adsorption to biomaterial surfaces, Biomaterials 19 (1998) 357

[54] R. M. Cornelius, P. W. Wojciechowski and J. L. Brash, Measurement of protein adsorption kinetics by an in situ, real-time, solution depletion technique., Journal of Colloid and Interface Science 150 (1992) 121

[55] J. D. Schiffman and C. L. Schauer, Cross-Linking Chitosan Nanofibers, Biomacromolecules 8 (2007) 594.

[56] X. L. Deng, G. Sui, M. L. Zhao, G. Q. Chen and X. O. Yang, Poly(L-lactic acid)/hydroxyapatite hybrid nanofibrous scaffolds prepared by electrospinning., Journal of Biomaterials Science Polymer Edition 18 (2007).

[57] Q. Shi, X. Chen, T. Lu and X. Jing, The immobilization of proteins on biodegradable polymer fibers via click chemistry, Biomaterials 29 (2008) 1118

[58] M. V. Kakade, S. Givens, K. Gardner, K. H. Lee, D. B. Chase and J. F. Rabolt, Electric Field Induced Orientation of Polymer Chains in Macroscopically Aligned Electrospun Polymer Nanofibers, Journal of the American Chemical Society 129 (2007) 2777.

[59] K. H. Lee, K. W. Kim, A. Pesapane, H. Y. Kim and J. F. Rabolt, Polarized FT-IR Study of Macroscopically Oriented Electrospun Nylon-6 Nanofibers, Macromolecules 41 (2008) 1494.

[60] C. D. Tidwell, D. G. Castner, S. L. Golledge, B. D. Ratner, K. Meyer, B. Hagenhoff and A. Benninghoven, Static time-of-flight secondary ion mass spectrometry and x-ray photoelectron spectroscopy characterization of adsorbed albumin and fibronectin films, Surface and Interface Analysis 31 (2001) 724

[61] T. Takahagi, Y. Nakayama, F. Soeda and A. Ishitani, Effects of Surface Cleaning and X-Ray Irradiation in XPS Study of Polymers, Journal of Applied Polymer Science 41 (1990) 1451.

[62] S. K. Tam, J. Dusseault, S. Polizu, M. Ménard, J.-P. Hallé and L. H. Yahia, Physicochemical model of alginate–poly-$_L$-lysine microcapsules defined at the micrometric/nanometric scale using ATR-FTIR, XPS, and ToF-SIMS, Biomaterials 26 (2005) 6950.

[63] K. Norrman, K. B. Haugshøj and N. B. Larsen, Lateral and Vertical Quantification of Spin-Coated Polymer Films on Silicon by TOF-SIMS, XPS, and AFM, J. Phys. Chem. B 106 (2002) 13114.

[64] P. V. Royen, E. Schacht, L. Ruys and L. V. Vaeck, Static secondary ion mass spectrometry for nanoscale analysis: surface characterisation of electrospun nanofibres, Rapid Commun. Mass Spectrom. 20 (2006) 346.

[65] P. C. Hiemenz and R. Rajogopalan, Principles of colloid and surface chemistry (3rd Ed. Marcel Dekker, New York, 1997).

[66] R. E. Good, Contact angle, wetting and adhesion: a critical review (Utrecht, The Netherlands, 1993).

[67] D. K. Owens and R. C. J. Wendt, Journal of Applied Polymer Science 13 (1969) 1741.

[68] F. M. Fowkes and M. A. Mostafa, Acid-Base Interactions in Polymer Adsorption, Ind. Eng. Chem. Prod. Res. Dev., 17 (1978) 3.

[69] A. Voelkelk Inverse gas chromatography: characterization of polymers, fibres modified silicas, and surfactants, Critical Rev. Anal. Chem. 22 (1991) 411

[70] Q. F. Wei, W. D. Gao, D. Y. Hou and X. Q. Wang, Surface modification of polymer nanofibres by plasma treatment, Applied Surface Science 245 (2005) 16

[71] W. A. Zisman, Relation of equilibrium contact angle to liquid and solid consititution, ACS series 43 (1964) 1.

[72] S. Wu, Polymer interface and adhesion, Marcel Dekker New York (1982).

[73] W. Shen, Y. Filonenko, Y. Truong, N. Brack, P. Pigram, I. H. Parker and J. Liesegang, Contact angle meausrements and surface energetics of sized and unsized paper, Colloids and Surfaces A, Physicochemical and Engineering Aspects 173 (2000) 117.

[74] J. Zheng, A. He, J. Li, J. Xu and C. C. Han, Studies on the controlled morphology and wettability of polystyrene surfaces by electrospinning or electrospraying Polymer 47 (2006) 7095.

[75] R. N. Wenzel, Resistance of solid surfaces to wetting by water, Ind. Eng. Chem. 28 (1936) 998.

[76] E. Puukilainen, T. Rasilainen, M. Suvanto and T. A. Pakkanen, Superhydrophobic Polyolefin Surfaces: Controlled Micro- and Nanostructures, Langmuir 23 (2007) 7263

[77] W. Shen, Y. Filonanko, Y. Truong, I. H. Parker, N. Brack, P. Pigram and J. Liesegang, Contact angle measurement and surface energetics of sized and unsized paper, Colloid Surf. A 173 (2000) 117.

[78] M. R. VanLandingham, J. S. Villarubia, W. F. Guthrie and G. F. Meyers, Nanoindentation of Polymers: An Overview, Macromolecular Symposia 167 (2001) 15.

[79] G. H. Kim, Electrospun PCL nanofibers with anisotropic mechanical properties as a biomedical scaffold, Biomedical Materials 3 (2008) doi:10.1088/1748.

[80] W. C. Oliver and G. M. Pharr, Improved technique for determining hardness and elastic modulus using load and displacement sensing indentation experiments, Journal of Materials Research, v 7, n 6, Jun, 1992, p 1564-1580 7 (1992) 1564.

[81] B. Briscoe, L. Fiori and E. Pelillo, J Phys D – Appl Phys 31 (1998) 2395.

[82] M. L. Oyen, Sensitivity of Polymer Nanoindentation Creep Properties to Experimental Variables, Acta Materialia 55 (2007) 3633.

[83] E. P. S. Tan and C. T. Lim, in Third Intl. Conf. on Experimental Mechanics and Third Conf. of the Asian Committee on Experimental Mechanics, edited by C. Quan, F. S. Chau, A. Asundi, B. S. Wong and C. T. Lim (Proceedings of SPIE, Singapore, 2004) p. 849.

[84] M. R. VanLandingham, J. S. Villarubia, W. F. Guthrie and G. F. Meyers, Nanoindentation of polymers: An Overview, Macromolecular Syposia 167 (2001) 15.

[85] G. M. Odegard, T. S. Gates and H. M. Herring, Characterization of Viscoelastic Properties of Polymeric Materials Through Nanoindentation, Experimental Mechanics 45 (2005) 130.

[86] C. C. White, M. R. VanLandingham, P. L. Drzal, N.-K. Chang and S.-H. Chang, Viscoelastic Characterization of Polymers Using Instrumented Indentation. II. Dynamic Testing, Journal of Polymer Science: Part B: Polymer Physics 43 (2005) 1812.

[87] S. A. Catledge, W. C. Clem, N. Shrikishen, S. Chowdhury, A. V. Stanishevsky, M. Koopman and Y. K. Vohra, An electrospun triphasic nanofibrous scaffold for bone tissue engineering, Biomedical Materials 2 (2007) 142.

[88] E. P. S. Tan and C. T. Lim, Nanoindentation study of nanofibers, Applied Physics Letters 87 (2005) 123106.

[89] E. P. S. Tan, S. Y. Ng and C. T. Lim, Tensile testing of a single ultrafine polymeric fiber, Biomaterials 26 (2005) 1453.

[90] E. P. S. Tan, C. N. Goh, C. H. Sow and C. T. Lim, Tensile test of a single nanofiber using an atomic force microscope tip, Applied Physics Letters 86 (2005) 073115.

[91] S.-Y. Gu, Q.-L. Wu, J. Ren and G. J. Vancso, Mechanical Properties of a Single Electrospun Fiber and Its Structures, Macromolecular Rapid Communications 26 (2005) 716.

[92] S.-H. Lee, C. Tekmen and W. M. Sigmund, Three-point bending of electrospun TiO_2 nanofibers, Materials Science and Engineering A 398 (2005) 77.

[93] W. He, T. Yong, Z. W. Ma, R. Inai, W. E. Teo and S. Ramakrishna, Biodegradable Polymer Nanofiber Mesh to Maintain Functions of Endothelial Cells, Tissue Engineering 12 (2006) 2457.

[94] Z.-M. Huang, Y. Z. Zhang, S. Ramakrishna and C. T. Lim, Electrospinning and mechanical characterization of gelatin nanofibers, Polymer 45 (2004) 5361.

[95] V. Thomas, M. V. Jose, S. Chowdury, J. F. Sullivan, D. R. Dean and Y. K. Vohra, Mechano-morphological studies of aligned nanofibrous scaffolds of polycaprolactone fabricated by electrospinning, J. Biomater. Sci. Polymer Edn 17 (2006) 969.

[96] J. Johnson, A. Ghosh and J. Lannutti, Microstructure-Property Relationships in a Tissue-Engineering Scaffold, Journal of Applied Polymer Science 104 (2007) 2919.

[97] C. Ayres, G. Bowlin, S. Henderson, L. Taylor, J. Shultz, J. Alexander, T. Telemeco and D. Simpson, Biomaterials
27 (2006) 5524.

[98] P. A. Yuya, Y. Wen, J. A. Turner, Y. A. Dzenis and Z. Li, Determination of Young's modulus of individual electrospun nanofibers by microcantilever vibration method, Applied Physics Letters 90 (2007) 111909.

[99] C. Ayres, B. S. Jha, H. Meredith, J. R. Bowman, G. L. Bowlin, S. C. Henderson and D. G. Simpson, Measuring fiber alignment in electrospun scaffolds: a user’s guide to the 2D fast Fourier transform approach, Journal of Biomedical Science Polymer Edition 19 (2008) 603.

Chapter 3

Part I - Electrospinning
In vitro experimentation

Table of Contents

Declaration

Three publications have been inserted into Chapter 3. Below the reference information and publication status for these publications is provided.

Chapter 3.1

D.R. Nisbet, S. Pattanawong, J. Nunan, W. Shen, M.K. Horne, D.I. Finkelstein, J.S. Forsythe, "The effect of surface hydrophilicity on the behaviour of embryonic cortical neurones", *Journal of Colloid and Interface Science*., 299, pp 647-655 2006.

Chapter 3.2

D.R. Nisbet, S. Pattanawong, N. E. Ritchie, . Shen, D. I. Finkelstein, M. K. Horne, J. S. Forsythe, "Interaction of embryonic cortical neurones on nanofibrous scaffolds for neural tissue engineering", *Journal of Neural Engineering.*, 4, pp 35-41, 2007.

Chapter 3.3

D.R. Nisbet, L.M.Y. Yu, T. Zahir, J.S. Forsythe, M.S. Shoichet, "Characterisation of neural stem cells on electrospun poly(ε-caprolactone) submicron scaffolds: evaluating their potential in neural tissue engineering", Invited Publications, *Journal of Biomaterials Science - Polymer Edition.*, 19, pp623-634, 2008.

Declaration for Thesis Chapter 3.1

Monash University

Declaration by candidate

In the case of Chapter 3.1 the nature and extent of my contribution to the work was the following:

Nature of contribution	Extent of contribution (%)
Experimental design and conduct and article writing.	80

The following co-authors contributed to the work. Co-authors who are students at Monash University must also indicate the extent of their contribution in percentage terms:

Name	Nature of contribution	Extent of contribution (%) for students
S. Patanawong	Assisted in experimentation & corrected manuscript	5
J. Nunan	Assisted in experimentation & corrected manuscript	N/A
W. Shen *	Experimental design and corrected manuscript	N/A
M.K. Horne	Experimental design and corrected manuscript	N/A
D.I. Finkelstein	Experimental design and corrected manuscript	N/A
J.S. Forsythe	Experimental design and corrected manuscript	N/A

Candidate's Signature	[redacted]	**Date** 14/10/2008

Declaration by co-authors

The undersigned hereby certify that:

(1) the above declaration correctly reflects the nature and extent of the candidate's contribution to this work, and the nature of the contribution of each of the co-authors.
(2) they meet the criteria for authorship in that they have participated in the conception, execution, or interpretation, of at least that part of the publication in their field of expertise;
(3) they take public responsibility for their part of the publication, except for the responsible author who accepts overall responsibility for the publication;
(4) there are no other authors of the publication according to these criteria;

(5) potential conflicts of interest have been disclosed to (a) granting bodies, (b) the editor or publisher of journals or other publications, and (c) the head of the responsible academic unit; and
(6) the original data are stored at the following location(s) and will be held for at least five years from the date indicated below:

Name	Location
S. Patanawong	Monash University - Department of Materials Engineering
J. Nunan	Melbourne University - Howard Florey Institute
W. Shen *	Monash University - Australian Pulp and Paper Institute
M.K. Horne	Melbourne University - Howard Florey Institute
D.I. Finkelstein	The Mental Health Research Institute of Victoria
J.S. Forsythe	Monash University - Department of Materials Engineering

Name	Signature	Date
S. Patanawong		14/10/2008
J. Nunan		14/10/2008
W. Shen *	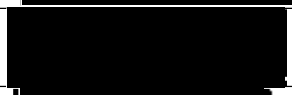	14/10/2008
M.K. Horne	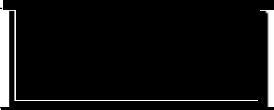	14/10/2008
D.I. Finkelstein		14/10/2008
J.S. Forsythe		14/10/2008

Declaration for Thesis Chapter 3.2

Monash University

Declaration by candidate

In the case of Chapter 3.2 the nature and extent of my contribution to the work was the following:

Nature of contribution	Extent of contribution (%)
Experimental design and conduct and article writing.	75

The following co-authors contributed to the work. Co-authors who are students at Monash University must also indicate the extent of their contribution in percentage terms:

Name	Nature of contribution	Extent of contribution (%) for students
S. Pattanawong	Assisted in experimentation	5
N. Ritchie *	Assisted in experimentation	5
W. Shen	Experimental design and corrected manuscript	N/A
D.I. Finkelstein	Experimental design and corrected manuscript	N/A
M.K. Horne	Experimental design and corrected manuscript	N/A
J.S. Forsythe	Experimental design and corrected manuscript	N/A

Candidate's Signature	[redacted]	**Date** 14/10/2008

Declaration by co-authors

The undersigned hereby certify that:

(7) the above declaration correctly reflects the nature and extent of the candidate's contribution to this work, and the nature of the contribution of each of the co-authors.
(8) they meet the criteria for authorship in that they have participated in the conception, execution, or interpretation, of at least that part of the publication in their field of expertise;
(9) they take public responsibility for their part of the publication, except for the responsible author who accepts overall responsibility for the publication;
(10) there are no other authors of the publication according to these criteria;
(11) potential conflicts of interest have been disclosed to (a) granting bodies, (b) the editor or publisher of journals or other publications, and (c) the head of the responsible academic unit; and

(12) the original data are stored at the following location(s) and will be held for at least five years from the date indicated below:

Name	Location
S. Pattanawong	Monash University - Department of Materials Engineering
N. Ritchie *	Monash University - Department of Materials Engineering
W. Shen	Monash University - Australian Pulp and Paper Institute
D.I. Finkelstein	The Mental Health Research Institute of Victoria
M.K. Horne	Melbourne University - Howard Florey Institute
J.S. Forsythe	Monash University - Department of Materials Engineering

Name	Signature	Date
S. Pattanawong	[redacted]	14/10/2008
N. Ritchie *	[redacted]	14/10/2008
W. Shen	[redacted]	14/10/2008
D.I. Finkelstein	[redacted]	14/10/2008
M.K. Horne	[redacted]	14/10/2008
J.S. Forsythe	[redacted]	14/10/2008

Declaration for Thesis Chapter 3.3

Monash University

Declaration by candidate

In the case of Chapter 3.3 the nature and extent of my contribution to the work was the following:

Nature of contribution	Extent of contribution (%)
Experimental design and conduct and article writing.	85

The following co-authors contributed to the work. Co-authors who are students at Monash University must also indicate the extent of their contribution in percentage terms:

Name	Nature of contribution	Extent of contribution (%) for students
L.M.Y. Yu	Assisted in experimentation and corrected manuscript	N/A
T. Zahir *	Assisted in experimentation and corrected manuscript	N/A
J.S. Forsythe	Experimental design and corrected manuscript	N/A
M.S. Shoichet	Experimental design and corrected manuscript	N/A

Candidate's Signature	[redacted]	Date 14/10/2008

Declaration by co-authors

The undersigned hereby certify that:

(13) the above declaration correctly reflects the nature and extent of the candidate's contribution to this work, and the nature of the contribution of each of the co-authors.
(14) they meet the criteria for authorship in that they have participated in the conception, execution, or interpretation, of at least that part of the publication in their field of expertise;
(15) they take public responsibility for their part of the publication, except for the responsible author who accepts overall responsibility for the publication;
(16) there are no other authors of the publication according to these criteria;
(17) potential conflicts of interest have been disclosed to (a) granting bodies, (b) the editor or publisher of journals or other publications, and (c) the head of the responsible academic unit; and
(18) the original data are stored at the following location(s) and will be held for at least five years from the date indicated below:

Name	Location
L.M.Y. Yu	University of Toronto - Department of Chemical Engineering
T. Zahir *	University of Toronto - Department of Chemical Engineering
J.S. Forsythe	Monash University - Department of Materials Engineering
M.S. Shoichet	University of Toronto - Department of Chemical Engineering

Name	Signature	Date
L.M.Y. Yu	[redacted]	14/10/2008
T. Zahir *	[redacted]	14/10/2008
J.S. Forsythe	[redacted]	14/10/2008
M.S. Shoichet	[redacted]	14/10/2008

3.0 Evaluation of electrospun scaffolds for use in neural tissue engineering

3.1 A biocompatibility investigation on 2D surfaces of poly(α-hydroxy esters)

This chapter investigates the potential of electrospun poly(α-hydroxy esters) for neural track regeneration within the CNS. The capacity of poly(α-hydroxy esters), in particular poly($_L$-lactic-co-glycolic acid) (PLGA) and poly($_L$-lactic acid) (P_LLA) to support cortical neurones was evaluated initially utilising a 2D study i.e. the neurones were cultured on flat surfaces produced from these materials and compared to the controls. This was an important preliminary step to evaluate the potential of producing 3D scaffolds from such materials, as evaluating cell survival, differentiation and morphology on 2D surfaces is much easier than when cells are imbedded within a 3D matrix.

The cellular biocompatibility of the surfaces was investigated both before and after surface modification. This was designed to determine how surface hydrophilicity influenced cellular behaviour on the interface. The morphological and colonisation response to the changes in the surface energies were then determined and compared to that of the controls. Chapter 3.1 was designed as a screening study of cellular responses to different materials with varying hydrophilicity, with the full intention of fabricating 3D fibrous scaffolds from these materials using electrospinning.

The effect of surface hydrophilicity on the behavior of embryonic cortical neurons

D.R. Nisbet[a], S. Pattanawong[a], J. Nunan[b], W. Shen[c], M.K. Horne[b], D.I. Finkelstein[b], J.S. Forsythe[a]*

a *CRC for Polymers, Department of Materials Engineering, Monash University, P.O. Box 69M, Victoria 3800, Australia*

b *Howard Florey Institute, Gate 11, Royal Parade, The University of Melbourne, Victoria 3010, Australia*

c *Australian Pulp and Paper Institute, Monash University, P.O. Box 69M, Victoria 3800, Australia*

3.1.1 ABSTRACT:

The aim of this study was to investigate the interaction of mouse embryonic cortical neurons on PLLA and PLGA substrates, which were partially hydrolysed using potassium hydroxide (KOH). The chemical and topographical properties of the surfaces were characterized, and it was discovered that there was a decrease in the hydrophilicity for the PLLA with increasing concentration of KOH. This was due to chemical modifications to the surfaces of the substrates. Alternatively for the PLGA substrate, only the 0.1 M KOH treated sample had a significantly different hydrophilicity highlighting that surface erosion resulted at higher concentrations. The morphology of the neurons grown on the two substrates were compared to poly-$_D$-lysine (positive control). The neurons formed colonies on all of the substrates, but were dramatically reduced in size in the case of the 0.1 M KOH treated substrates. This finding was attributed to the increases in cell spreading and the size of the cells, as they were larger, more elongated and bipolar like those on the positive control. However, there was a significant decrease in the total number of live cells per unit area. Therefore, on these materials when there was increased cellular spreading there was significantly higher cell death. Furthermore, unlike the 0.0, 0.2, and 0.4 M KOH treated substrates, there was an absence of large bundles of axons that extended between colonies on the 0.1 M sample, instead exhibiting short axons that grew in free space.

3.1.2 KEYWORDS:

Surface hydrophilicity; Neurons; Poly(α-hydroxy esters); Colonization

3.1.3 INTRODUCTION

The growth and distribution of mammalian cells on surfaces is critically influenced by the nature of the biomaterial interface, such as hydrophilicity, chemistry, charge, and topographical cues [1]. The effect of surface hydrophilicity of solid substrates on cell growth and distribution receives specific attention because of its importance in the design of biomaterials [2]. The importance of polymer surface hydrophilicity on cell adhesion was reported by Weiss [3], and subsequently confirmed by other studies. The propensity for cells to spread over or adhere to polymer substrates depends on surface free energy [4]. Cells do not spread and adhere weakly when the surface free energy is low (<5 $ergcm^{-2}$) [4,5].

Poly(lactic acid) (PLA), poly(glycolic acid) (PGA), and poly(lactic-co-glycolic acid) (PLGA) are frequently used polymer substrates for the culture of cells and the proliferation of cells on these substrates varies according to their surface properties [6–10]. Cell proliferation increased on these substrates with increases in surface hydrophilicity. Cell adhesion to surface treated PLGA was greatest when hydrophilicity was moderate and decreased when surfaces were extremely hydrophilic or hydrophobic [7,11,12].

Most research directed at the question of cell proleiferation and adhesions has used fibroblasts or related epithelial cells. The effect of substrata hydrophilicity on neural cells has received considerably less attention although it is a critical parameter for successful neural tissue engineering. The wettability gradient of polyethylene surfaces influenced neurite formation of PC12 cells: a line derived from pheochromocytomas (vascular tumor of the adrenal gland) but having many neuronal characteristics [8]. Neurite formation was inhibited when surfaces were extremely hydrophilic or hydrophobic. The wettability gradient of the polyethylene surfaces may also indirectly influence neurons by affecting adsorption of proteins that influence neurite formation and differentiation. In PC12 cells both differentiation and neurite formation were influenced by serum proteins and growth factors such as a fibronecten, vitronecten, and nerve growth factor (NGF). The wettability

gradient of the polyethylene surfaces may have exerted influence on differentiation and neurite outgrowth as much by affecting adsorption of these proteins as by any effect on surface energy. Furthermore, interpretation of neurite outgrowth cannot be assessed in PC12 cells until they differentiate, which occurs under the influence of the same molecules that induce neurite formation. A study of the effects of wettability gradient and protein absorption on neurite formation and adhesion would be best achieved with primary neuronal cultures, where differentiation is not an issue.

The present study investigates the interaction of mouse embryonic cortical neurons on partially hydrolysed P_LLA and PLGA substrates. The chemical and physical properties of the polymer surfaces were characterized and correlated with the size and number of neural cell colonies and the formation of neurites.

3.1.4 MATERIALS AND METHODS

3.1.4.1 Materials

Poly($_L$-lactic acid) (P_LLA) and poly(lactic-co-glycolic acid) 50:50 copolymer (PLGA) were obtained from Absorbable Polymers, Inc. (AL, USA). Polymers were dried in a vacuum oven overnight at 50 $^\circ$C before being compression-molded at 25 kN for 1 min at 240 $^\circ$C for P_LLA and 180 $^\circ$C for PLGA using polished metal plates with Kapton release film. Each molding was water-quenched to provide a uniform amorphous film approximately 200 μm thick. The samples were cut using a water-jet (Water Jet Solutions) into 15.2 mm diameter discs, which then could be positioned in the bottom of the culture wells. The discs were cleaned in 70% ethanol for 1 min using an ultrasonic bath, before being washed in deionized water. Surface hydrolysis was achieved by immersing in potassium hydroxide KOH solutions (0.1, 0.2 and 0.4 M) for 1 min followed by washing in deionized water. All samples were dried in a vacuum oven overnight at 50 $^\circ$C and stored in a desiccator.

3.1.4.2 Differential scanning Calorimetry

The glass transition temperatures (*T*g) were obtained using a Perkin–Elmer Pyris DSC at a scanning rate of 10 °C/min under a nitrogen atmosphere. Thermal calibration was performed using indium and zinc standards.

3.1.4.3 Water contact angle measurements

Contact angle measurements were performed using a Data Physics Instruments (GmbH OCAH-230) at room temperature using the sessile drop method with deionized water. A 1.2 mm diameter needle was used to introduce a 5 μl water drop onto the sample surface by gravity. The measurements were taken over 5 replicate samples and then averaged. The uncertainty was calculated using a 95% confidence interval from the mean.

3.1.4.4 Scanning electron microscopy and atomic force microscopy

A scanning electron microscope (SEM, S-570 Hitachi Tokyo, Japan), with a 10 kV accelerating voltage was used to characterize the surfaces of the substrates. All samples were gold-coated before imaging. Atomic force microscope (AFM, Explorer, ThermoMicroscope) was used to acquire the information of surface roughness. ULTRASHARP silicon nitride tips (CSC21/50, Micro- Masch) were used at a scanning rate 1 Hz. AFM scans of 100 × 100 μm^2 were performed at room temperature to evaluate the surface roughness changes caused by the KOH treatments. The root-mean-square roughness values of sample surfaces were obtained after the image leveling was performed to remove the signal due to the sample tilt (Table 1). Chemical and topographical changes of the surfaces were characterized, since water contact angles with P_LLA and PLGA were used to reflect changes of the polymer surfaces after the hydrolysis treatment. If a solid surface has a contact angle of <90°, roughening of the surface will cause the contact angle to decrease [13]. Wenzel proposed a simple relationship to quantify the contact angle change due to surface roughness:

$$\cos \theta r = r \cos \theta_0, \quad (1)$$

where θ_0 is the contact angle for a liquid on a smooth solid surface, θ_r is the contact angle for the same liquid on a rough surface of the same solid, r is the roughness factor which is defined as the ratio of the area of the smooth surface (or the project area of the surface), A_0, and the actual area of the surface, Ar [13]:

$$r = A_r/A_0 \quad (2)$$

Values of the projected and the actual areas of the polymer surfaces are obtained using the data analysis software (Thermo-Microscopes, SPMLab Ver 5.1) of the AFM. This software calculates actual area of the surface by calculating the areas of the triangular walls of the prism defined by every four adjacent pixels. The roughness factors obtained using Eq. (2) are listed in Table 1.

3.1.4.5 Attenuated total reflection infrared spectroscopy

Attenuated total reflection (ATR) infrared spectroscopy was preformed using a Perkin–Elmer FTIR Spectrometer 1725X between 4000 and 650 cm^{-1} with 64 scans and a resolution of 4 cm^{-1} under a nitrogen atmosphere. Samples were dried in a vacuum oven overnight at 50 $^{\circ}$C to remove adsorbed water.

3.1.4.6 Mouse cortical neuron culture

C57/B6 type mice (E14) were decapitated, the brains dissected from the skull and cortices dissected and stripped of meninges. The cells were dissociated with 0.025% trypsin in Krebs solutions for 20 min whilst being incubated at 37 $^{\circ}$C (Sigma T-4665). The polymer substrates were immersed in 70% ethanol, allowed to dry, and placed into individual sterile 24-well polystyrene culture dishes in triplicate, soaked in 0.5 ml of Krebs solutions for 2 h, the solution was then removed just before seeding the neurons. Poly-$_D$-lysine (0.05 mg/ml) was coated on 24-well polystyrene tissue culture dishes in

triplicate and served as a positive control. The polystyrene tissue culture dish served as a negative control. Neurons were then seeded onto the culture well at a density of 106 cells/ml in 0.5 ml of modified eagle's medium (MEM, Gibco) and 10% fetal calf serum. After 1 h, the medium was removed and culture medium (1 ml) was added, prepared by 50 ml of Neurobasal medium (NBM, Gibco), 1 ml B27 supplement (Gibco), 125 µl glutamine (200 mM stock), and 50 µl gentamycin (10 µg/ml) (Gibco). The cell number was counted using a hemocytometer and trypan blue exclusion. The cortical neurons were cultured for 6 days at 37 °C with 5% CO_2, the cells were fixed with 2.5% paraformaldehyde (Sigma) solution for 1 min, and then washed in phosphate buffered saline (PBS). After the 6 days period the cultures typically contained 90–95% neurons. Analyses were performed using an Olympus IX71 microscope with attached digital camera (4 mega-pixel resolution, CAMEDIA). Three images were taken randomly on each of the 3 wells using a magnification of 20 times. The density of the colonies (live cells) was then determined by analyzing each of the 9 low magnification images, with a standard unit area of 0.34 mm^2.

3.1.4.7 Statistics

The results were reported as standard error for the triplicate cultures and one-way analysis of variance (ANOVA) was performed on independent samples to determine significant differences between live cell numbers on each of the polymers. Statistical significance was considered at $p < 0.05$.

3.1.5 RESULTS AND DISCUSSION

3.1.5.1 Physiochemical characterization of substrates

Table 1 shows the effect of increasing concentration of KOH on the contact angles of P_LLA substrates. Surface treatment with 0.1 M KOH decreased the water contact angle and with higher KOH concentrations produced further reductions. The contact angle of

PLGA decreased significantly following treatment with 0.1 M KOH, but returned toward untreated values when exposed to higher concentrations of KOH.

The hydrolysis of PLGA occurred via a surface erosion mechanism. The constant T_g of PLGA following the various treatments implies little or no hydrolysis in the bulk of the polymer. The extensively hydrolysed top surface layer produced under strong alkaline conditions may have been removed when washed with water, thus exposing a fresh PLGA surface. Fig. 1 shows extensive pitting for the 0.1 M KOH treated PLGA before the surface was eroded away resulting in smoother surfaces at 0.2 and 0.4 M KOH. AFM results (Table 1) supports this mechanism as the 0.1 M KOH treated PLGA has a significantly higher RMS roughness compared to the other PLGA surfaces. The roughness factor measured from these scans also increased from 1.03 to 1.12 after treatment (Table 1) and there was a 14° decrease in the contact angle. According to the Wenzel model (Eqs. (1) and (2)), changes in surface roughness would only account for 3° reduction in contact angle. It therefore seems likely that changes in the samples surface chemistry due to hydrolysis, contributed most to changes in contact angle.

Table 1

Physical characteristics of the materials before and after KOH treatment

Material	KOH Concentration	Contact angle (°)	ATR ester/CH_3	AFM surface roughness (nm)	Roughness factor	T_g (°C)
P_LLA	0	74 ± 2	5.0	1112	1.04	55
	0.1	66 ±2	4.3	1275	1.06	55
	0.2	64 ±2	3.4	1481	1.03	41
	0.4	64 ±1	3.1	1847	1.01	40
PLGA	0	68 ±2	4.5	1289	1.03	39
	0.1	54 ±1	4.1	1355	1.12	38
	0.2	65 ±2	6.3	1261	1.03	38
	0.4	64 ±2	6.9	1127	1.01	38

Note. Values for contact angle represent the mean ± the standard deviation of the mean of 5 independent measurements per treatment. The surface roughness and glass transition temperature are given as the mean of 3 measurements.

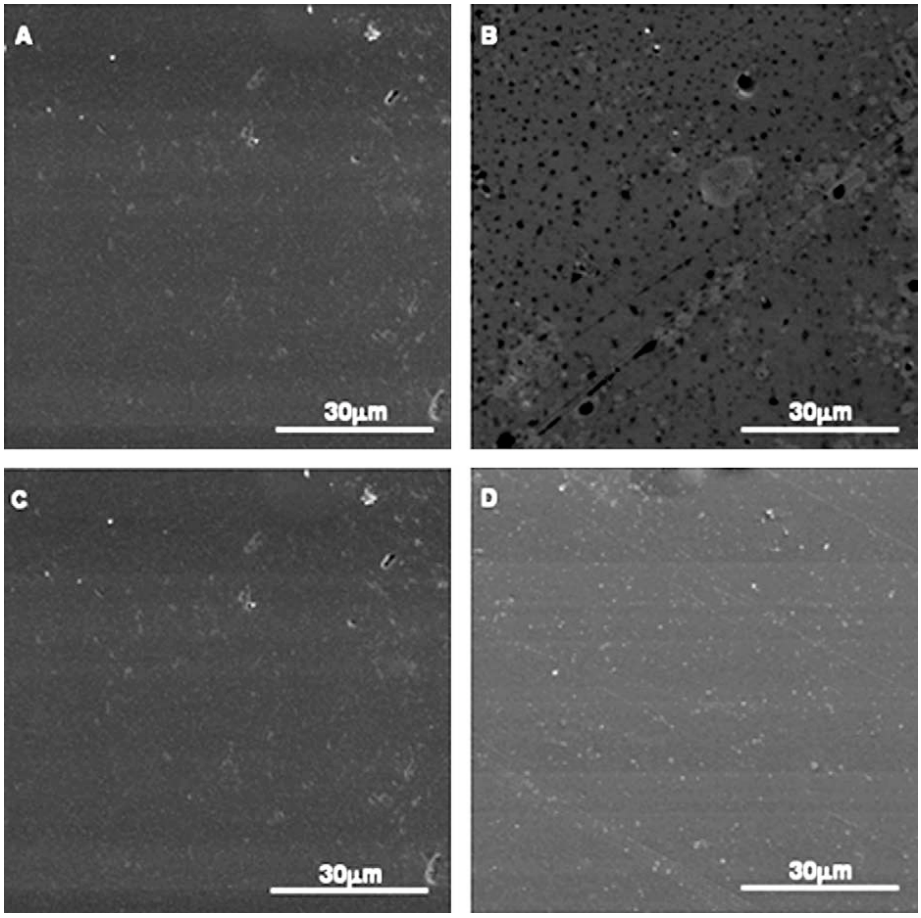

Fig. 1. SEM images of PLGA after the following KOH surface treatments (A) 0, (B) 0.1, (C) 0.2, and (D) 0.4 M.

Treatment of P_LLA with 0.1 M KOH (Table 1) resulted in negligible bulk hydrolysis, reflected by constant glass transition temperatures. However treatment of P_LLA with higher KOH concentrations resulted in a 15 $^{\circ}$C decrease in the glass transition temperature, reflecting a decreased molecular weight throughout the bulk of the material. This is consistent with the known slower rate of hydrolysis for this polyester. The SEM images showed that P_LLA surfaces were less pitted when KOH concentration increased (Fig. 2). AFM measurements (particularly the surface roughness factor) also indicated negligible roughening of the sample surfaces (Table 1).

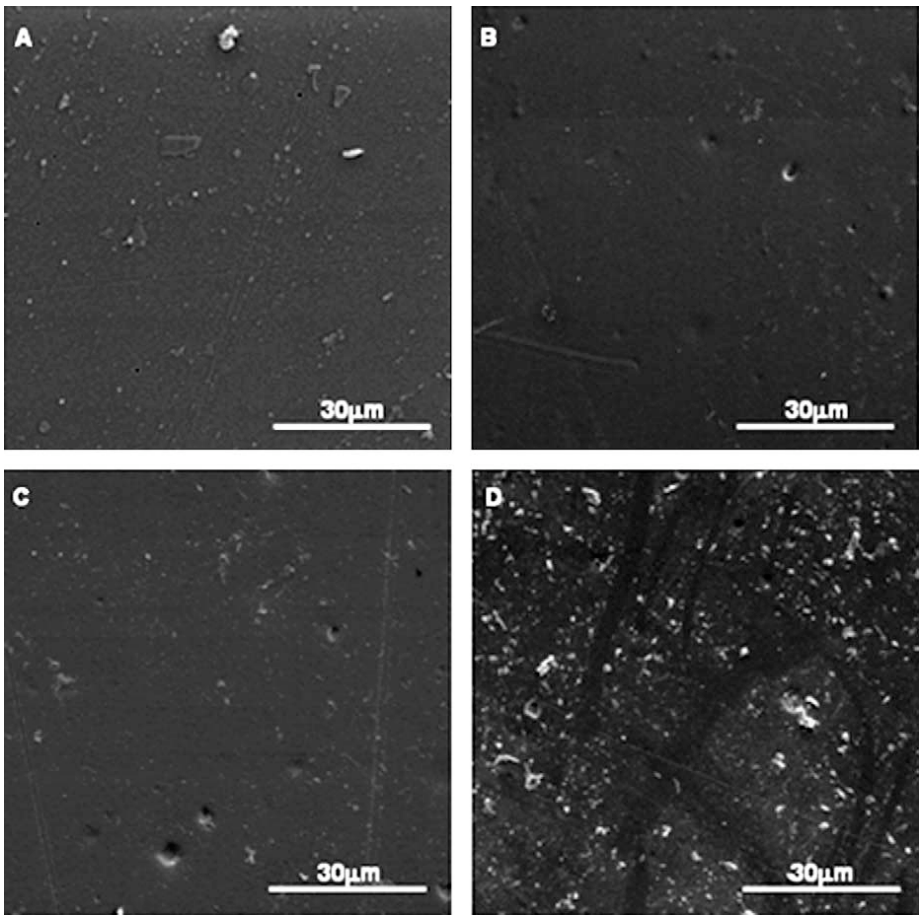

Fig. 2. SEM images of P_LLA after the following KOH surface treatments (A) 0, (B) 0.1, (C) 0.2, and (D) 0.4 M.

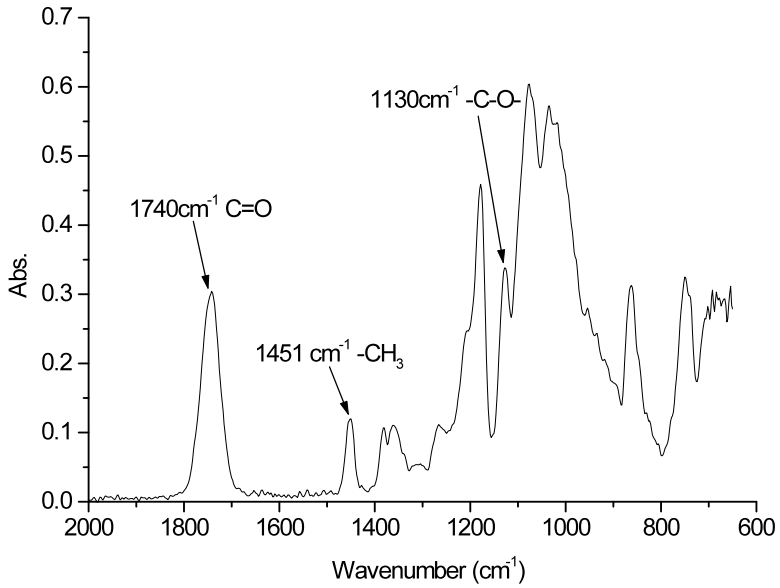

Fig. 3. ATR mid-infrared spectra of unmodified of (A) P_LLA and (B) PLGA.

The extent of hydrolysis of the surfaces was also measured using attenuated total reflectance infrared (ATR-IR) spectroscopy, in the mid-infrared region. The ATR spectra of P_LLA and PLGA (0 M KOH) exhibited a large absorbance at 1740 cm^{-1}, attributed to the carbonyl stretch of the ester, a peak at 1451 cm^{-1} due to $–CH_3$ bending and a peak at 1130 cm^{-1} due to the C–O stretch of the ester groups (Fig. 3). Surface hydrolysis was measured as the C–O ester absorbance at 1130 cm^{-1} expressed as a ratio of the $–CH_3$ absorbance (used as an internal reference). The new carbonyl absorbance from the acid end groups could not be resolved from the ester carbonyl absorbance at 1740 cm^{-1} and therefore was not used. The $C–O/CH_3$ ratios obtained from the ATR of the surfaces of PLGA and P_LLA substrates showed similar trends to the contact angle measurements (Fig. 4). This provided further confirmation that the changes in contact angle were a result of differences in surface chemistry.

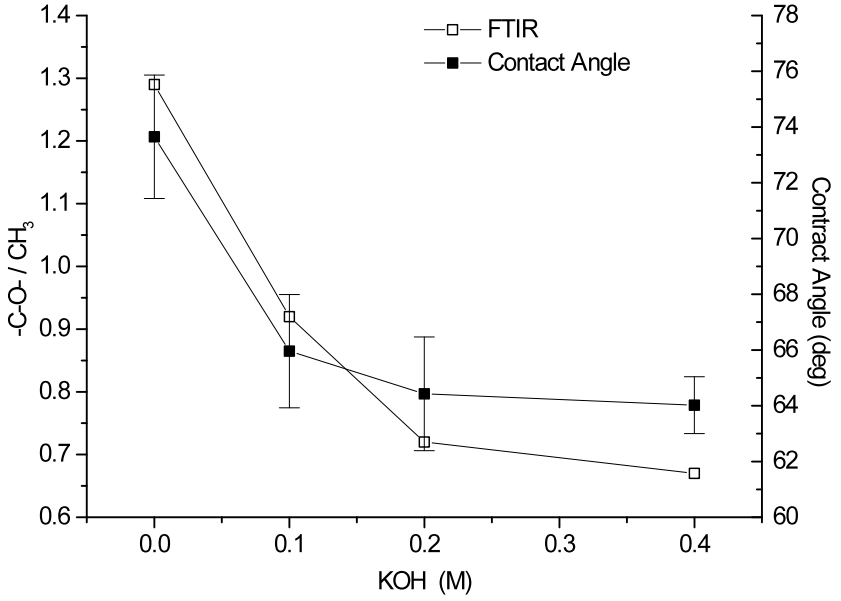

Fig. 4. Variation of ester/CH3 ratio of P_LLA with increasing concentration of KOH. Corresponding water contact angle measurements are shown for comparison.

In summary, only the 0.1 M treatment significantly affects the surface parameters of PLGA because at other molarities, the surface was renewed. In contrast, there was no

renewal of P_LLA surfaces, and consequently the contact angle of the sample decreased with increasing KOH molarities.

3.1.5.2 Culture of mouse cortical neurons on PLLA and PLGA

The morphology of neurons grown on P_LLA and PLGA was compared to neurons grown on polyDlysine (used as a positive reference control). Neurons formed colonies (defined as three or more cells in physical contact) on both the unmodified and surface treated P_LLA and PLGA whereas there were no cell colonies on poly-$_D$-lysine (Figs. 5A and 6A). There was a higher density of colonies on unmodified PLGA than on unmodified P_LLA (28 ± 3 and 15 ± 2, respectively) and an increase in total number of live cells per unit area for unmodified PLGA than on P_LLA (467 ± 60 and 255 ± 46, respectively, and Table 2). Although cells did not clump on the poly$_D$lysine, there were fewer cells than on the unmodified PLGA, implying that cell survival is superior when colonies form. Cell survival on unmodified P_LLA is statically the same as on control poly$_D$lysine.

Figs. 5 and 6 show cortical neurons after 6 days of culture on P_LLA and PLGA, respectively. When plated on P_LLA and PLGA surfaces treated with 0.1 M KOH, cells spread further and were larger and more elongated than those cultured on poly$_D$lysine, particularly when plated on P_LLA. The increased propensity for cells to spread on the 0.1 M modified substrates is reflected by decreased numbers of colonies, and cells per colonies (Table 2). However, increased spreading is associated with a decrease in total cell number. Thus, when the size and number of colonies is reduced, or cells are evenly distributed, the cell death is considerably higher. This further supports the finding that cell colony formation is important for cell survival on these substrates.

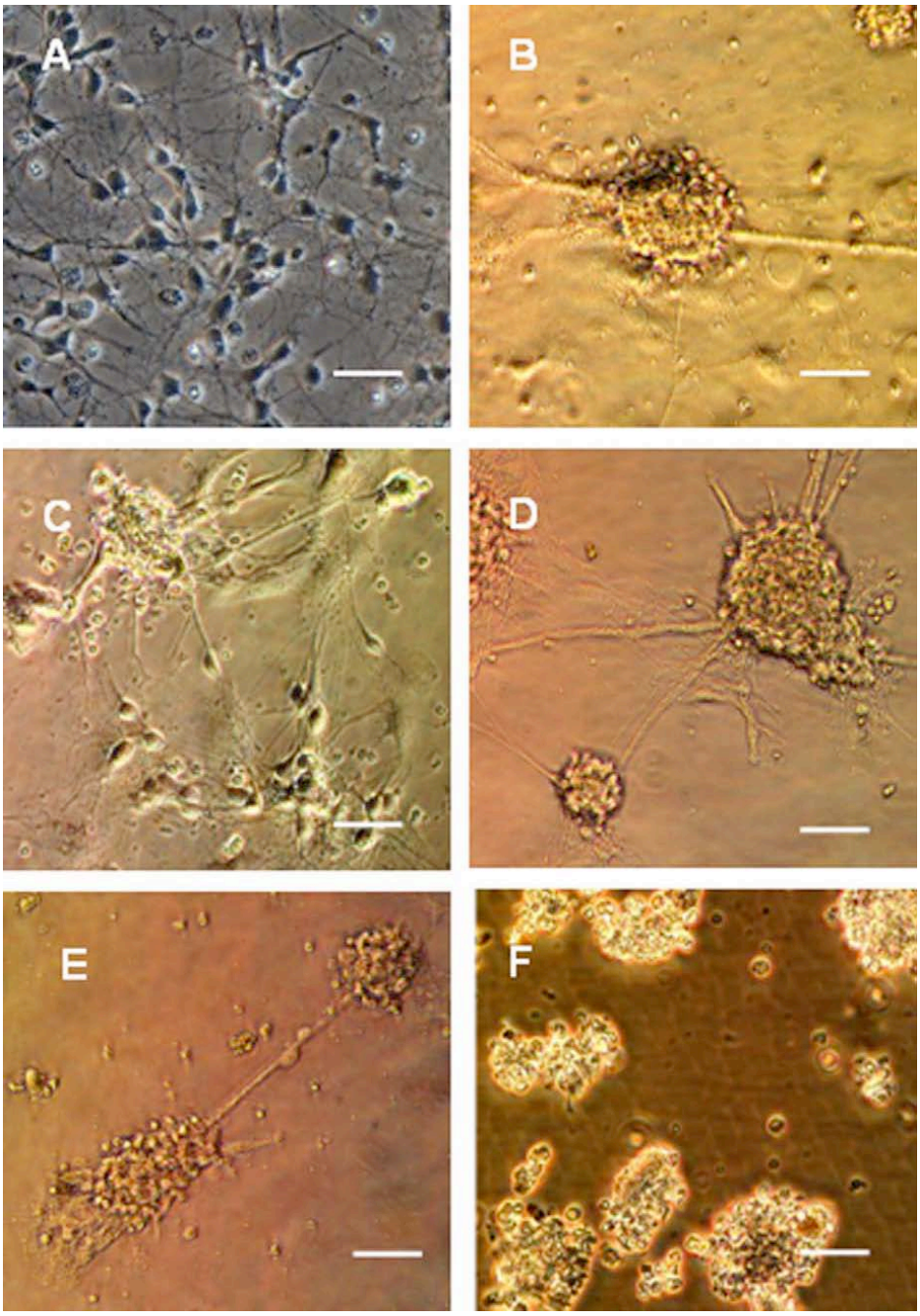

Fig. 5. Phase contrast micrographs of mouse cortical neurons following 6 days of culture on P_LLA. Surfaces were either unmodified (B) or modified (C, D, E) for 1 min in the presence of 0.1, 0.2, and 0.4 M [KOH], respectively. (A) Positive control $poly_D$lysine, (B) unmodified PLLA, (C) 0.1 M [KOH] modified P_LLA, (D) 0.2 M [KOH] modified P_LLA, (E) 0.4 M [KOH] modified P_LLA, (F) negative control polystyrene culture disc. Bar 50 μm.

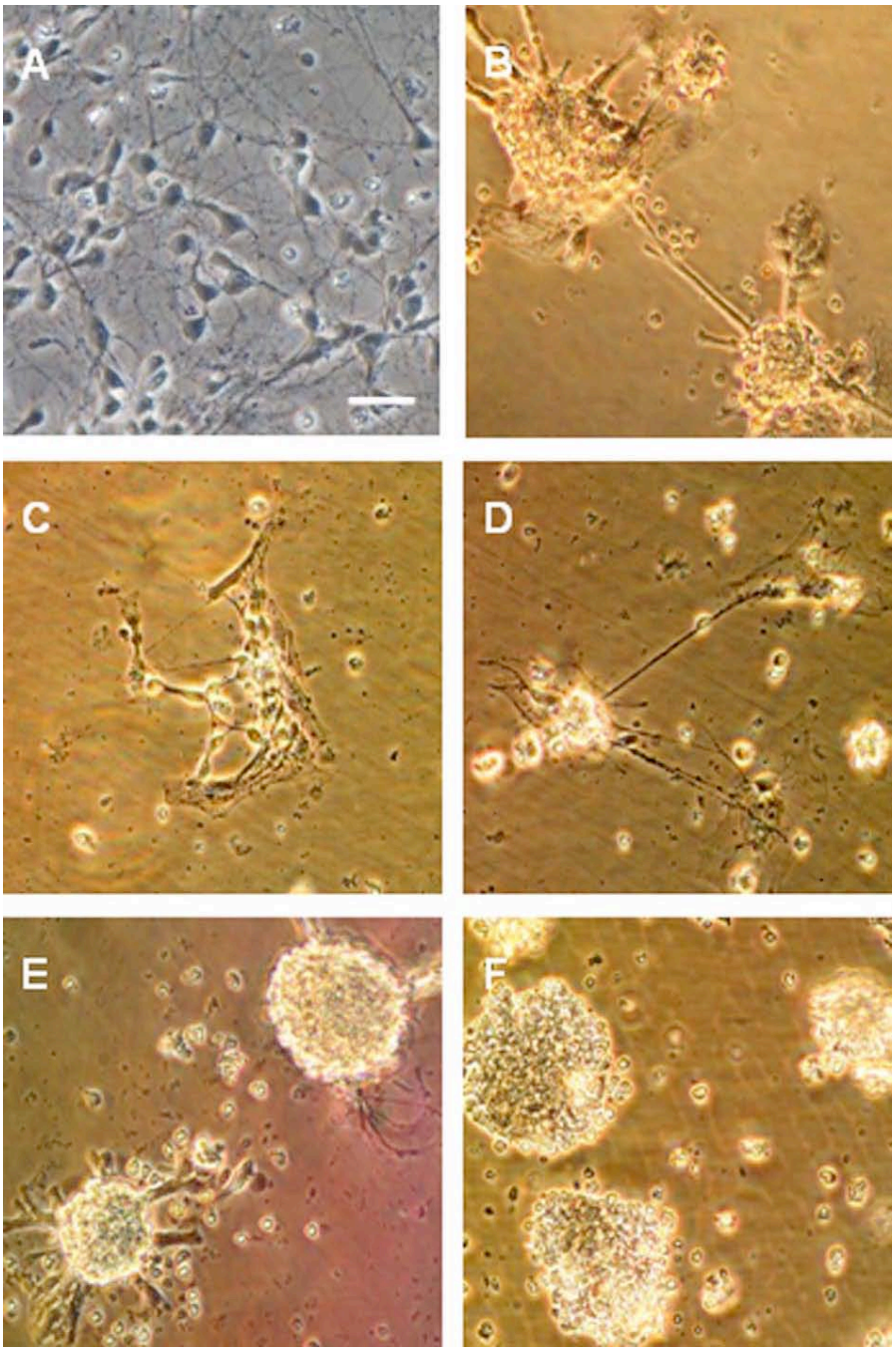

Fig. 6. Phase contrast micrographs of mouse cortical neurons following 6 days of culture on PLGA. Surfaces were either unmodified (B) or modified (C, D, E) for 1 min in the presence of 0.1, 0.2, and 0.4 M [KOH], respectively. (A) Positive control $poly_D$lysine, (B) unmodified PLGA, (C) 0.1 M [KOH] modified PLGA, (D) 0.2 M [KOH] modified PLGA, (E) 0.4 M [KOH] modified PLGA, (F) negative control polystyrene culture disc. Bar 50 μm.

PLGA and P_LLA 0.1 M substrates supported the same (statistically) numbers of colonies and cells (Table 2). However, PLGA 0.0, 0.2, and 0.4 M supported more cells than either P_LLA and poly$_D$lysine, which is approximately equal to that of normal biological density [14]. Contact angles of the 0.2 and 0.4 M samples of PLGA and the 0.1, 0.2, and 0.4 M samples of P_LLA are approximately the same (Figs. 7 and 8) and these substrates have approximately the same surface roughness (Table 1). Therefore the differences in the cell number, cell size, number of colonies and size of colonies (see Table 2) was not solely affected by hydrophilicity, but is also influenced by chemistry of the substrate [15]. Therefore changes in the surface hydrophilicity and chemistry have an impact on the protein adsorption and conformation, hence ultimately influence the cellular behavior [16,17].

Table 2 Cellular response to the materials before and after KOH treatment.

Materials	KOH solution Concentration (M)	Number of Cells / Clump	Total Number of Cells / 0.34mm^2	Total Number of Clumps / 0.34mm^2	Feret clump diameter (μm)	Feret cell diameter (μm)
PLGA	0.0	13 ± 2	467 ± 60	28 ± 3	75 ± 4	12 ± 1
	0.1	8 ± 1	165 ± 21	13 ± 2	69 ± 5	21 ± 2
	0.2	17 ± 2	509 ± 76	30 ± 4	105 ± 10	14 ± 3
	0.4	23 ± 3	520 ± 99	23 ± 2	139 ± 10	13 ± 1
P_LLA	0.0	14 ± 2	255 ± 46	15 ± 2	107 ± 7	11 ± 1
	0.1	8.0 ± 1	171 ± 9	12 ± 1	87 ± 5	16 ± 1
	0.2	13 ± 1	206 ± 26	12 ± 1	142 ± 10	19 ± 1
	0.4	12 ± 2	128 ± 15	9 ± 1	116 ± 6	14 ± 1
Polylysine	N/A	N/A	249 ± 23	N/A	N/A	19.5 ± 1

Note: the values are represented as standard errors.

With increased spreading there was an increase in cell size and individual cells tend to be bipolar. This was most notable on 0.1 M substrates, particularly P_LLA (Fig. 5). However, on all other samples bundles of processes, presumably axons form specific neurite tracks, extend, and join colonies. Examination of the cultures provides the impression that the numbers of axons increase with spreading of cells [8], although technically possible we did not count the number of axons within these large bundles extending between colonies. It appears that the bipolar cells on the 0.1 M samples extended into free space, however, when colonies were formed they were joined by bundles of axons. This may be

a valuable asset of a material to assist in the sending of axons to distant areas. Furthermore, this material allows colonies to form which support a greater number of neurons than conventional culturing materials.

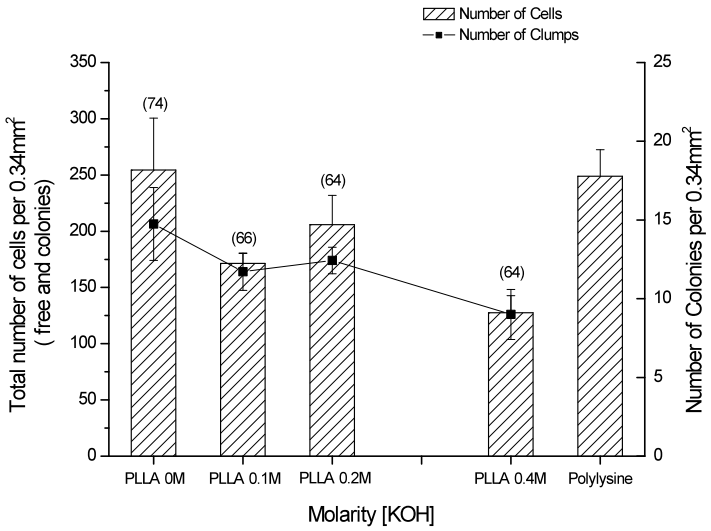

Fig. 7. Colony number and total live cell number/0.34 mm^2 following 6 days culture on unmodified and modified P_LLA. The contact angles are included in parentheses above.

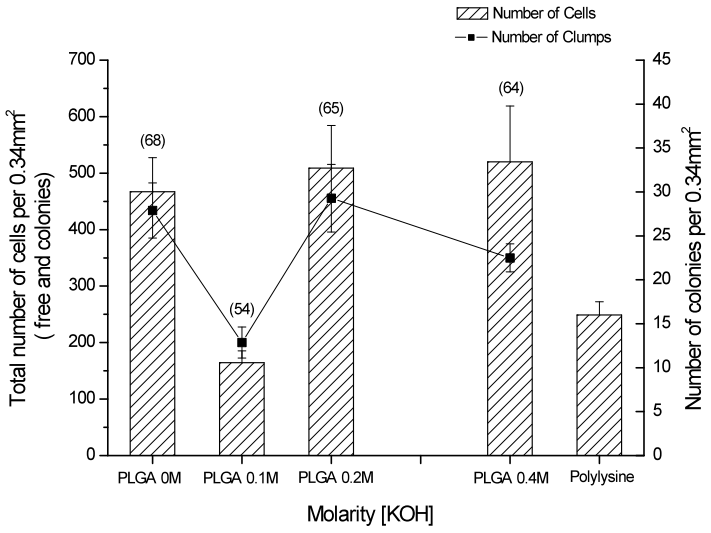

Fig. 8. Colony number and total live cell number/0.3 mm^2 following 6 days culture on unmodified and modified PLGA. The contact angles are included in parentheses above.

3.1.6 SUMMARY

PLGA and P_LLA responded differently to surface hydrolysis with KOH. For the PLGA sample, only the 0.1 M treatment significantly effected the surface energy, as the surface was eroded and hence renewed at other concentrations. Alternatively, minimal surface erosion occurred in the P_LLA sample and consequently the surface energies of the sample decrease with increasing KOH morality. Neurons formed colonies on all substrates. The PLGA substrate, with the exception of the 0.1M sample, supported significantly more cells than the P_LLA and the positive control highlighting that this materials allows for colonization and can support a greater number of neurons than conventional culturing methods. However, in the case of the 0.1 M KOH sample (particularly for the PLGA) the size of the colonies was dramatically reduced due to an increase in cellular spreading. On this sample more cells existed individually and they were larger, bipolar and more elongated, as seen on the positive control. However, with increased spreading there is a considerably higher cell death, as the 0.1 M substrates supported less live cells per unit area than other concentrations of KOH. Furthermore, on the 0.1 M substrates there was an absence of large bundles of axons that extended from, and joined colonies. Instead axons were shorter and existed in free space like those seen on the poly-$_D$-lysine control.

3.1.7 ACKNOWLEDGEMENTS

This project was supported by the CRC for Polymers and ARC Discovery DP0663573.

3.1.8 REFERENCES

[1] D.R. Jung, R. Kapur, T. Adams, K.A. Giuliano, M. Mrksich, H.G. Craighead, D.L. Taylor, Crit. Rev. Biotechnol. 21 (2) (2001) 111–154.

[2] H.B. Lee, J.H. Lee, in: D.L. Wise (Ed.), Encyclopedic Handbook of Biomaterials and Bioengineering, Part A, Dekker, New York, 1995.

[3] L. Weiss, Intl. Rev. Cytol. 9 (1960) 187–225.

[4] P.V.D. Valk, A.W.J.V. Pelt, H.J. Busscher, H.P.D. Jong, C.R.H.Wildevuur, J. Arends, J. Biomed. Mater. Res. 17 (1983) 807–817.

[5] G. Khang, J.H. Choee, J.M. Rhee, H.B. Lee, J. Appl. Polym. Sci. 85 (2002) 1253–1262.

[6] Y. Tamada, Y. Ikada, J. Colloid Interface Sci. 155 (1993) 334–339.

[7] Y. Tamada, Y. Ikada, in: E. Chiellini, P. Giusti, C. Migliaresi, L. Nicolais (Eds.), Polymer in Medicine II, Plenum, New York, 1986, p. 101.

[8] S.J. Lee, G. Khang, Y.M. Lee, H.B. Lee, J. Colloid Interface Sci. 259 (2003) 228–235.

[9] S.J. Lee, G. Khang, Y.M. Lee, H.B. Lee, J. Biomat. Sci. Polym. Ed. 13 (2) (2001) 197–212.

[10] Y. Tamada, Y. Ikada, J. Biomed. Mater. Res. 28 (1994) 783.

[11] F. Grinnell, Intl. Rev. Cytol. 53 (1978) 65–144.

[12] A. Harris, Exp. Cell Res. 77 (1973) 285–297.

[13] A.W. Adamson, A.P. Gast, Physical Chemistry of Surfaces, sixth ed., Wiley–Interscience, New York, 1997.

[14] D. Cotter, D. McKay, S. Frangou, L. Hudson, S. Landau, Br. J. Psychiatry 185 (2004) 258–259.

[15] J. Harrison, S. Pattanawong, J.S. Forsythe, K.A. Gross, D.R. Nisbet, H. Beh, T.F. Scott, A.O. Trounson, R. Mollard, Biomaterials 25 (2004)
4963–4970.

[16] D.R. Lu, K. Park, J. Colloid Interface Sci. 144 (1991) 271–281.

[17] J.M. Schakenraad, H.J. Busscher, C.R.H.Wildevuur, J. Arends, J. Biomed. Mater. Res. 20 (1986) 773–784.

3.2 Investigation into the interaction of cortical neurones with nanofibrous scaffolds.

Cortical neurones were found to be biocompatible with 2D surfaces of P_LLA and PLGA and responded to small changes in surface hydrophilicity. The next stage of investigation was to fabricate 3D scaffolds and assess the biocompatibility of cortical neurones in this environment, compared to the 2D films. Electrospun materials have significantly greater surface areas compared to 2D surfaces, hence the capacity of the scaffold to support neurones is dramatically altered. In this study the cellular biocompatibility following KOH treatment was again investigated within the 3D environment. However, the main focus of this work related to the ability of the scaffold to promote neurite extension with specific focus on the interaction between the growing neurites and the nano-fibres that make up the scaffold matrix. After a 6 day *in vitro* culture, the 3D electrospun scaffold resulted in good cellular adhesion without clumping and promoted appreciable neurite extensions. It was also discovered that changes in the material chemistry and surface tension had significant effects. These results are presented on the follow pages in the form of a publication.

Interaction of embryonic cortical neurons on nanofibrous scaffolds for neural tissue engineering

D R Nisbet[1], S Pattanawong[1], N E Ritchie[1],W Shen[2],
D I Finkelstein[3], M K Horne[3] and J S Forsythe[1*]

1 CRC for Polymers, Department of Materials Engineering, Monash University, PO Box 69M, Victoria 3800, Australia
2 Australian Pulp and Paper Institute, Monash University, PO Box 69M, Victoria 3800, Australia
3 Howard Florey Institute, University of Melbourne, Victoria 3010, Australia

3.2.1 ABSTRACT

The interaction of murine embryonic cortical neurons on randomly orientated electrospun scaffolds of poly($_L$-lactide) (P_LLA) and poly(lactide-co-glycolide) (PLGA) is investigated in this study. The scaffolds were surface treated with different concentrations of KOH to partially hydrolyze the surface and therefore change the surface tension. Hydrophilicity did not significantly influence the number of primary and secondary branches; however, it had a considerable effect on neurite extension. For scaffolds with surface tensions of 40– 47 dyn cm^{-1} there was a significantly greater overall neurite length for both the primary and secondary branches compared with more hydrophilic scaffolds. Another major finding of this work was that the interfibre distance influenced how the neurites extended. When the interfibre distance was greater than approximately 15 μm the neurites followed the fibres and avoided regions of very high fibre density. At interfibre distances less than approximately 15 μm, the neurites traversed between the fibres. Therefore, this study provided little evidence that contact guidance was the dominating cue in directing neurite extension, instead inferring that chemical cues, possibly from adjacent neurons had induced directional change.

3.2.2 INTRODUCTION

Neural tissue engineering is a complex biological phenomenon [1] where many factors, including contact guidance and chemical gradients, influence neurite outgrowth [2, 3]. Cell functions are regulated by biological signals from growth factors, the extracellular matrix, and surrounding cells [4]. The cues perceived by the advancing tip of the neurite are transduced by the growth cone. The challenge presented by substrate/scaffolds used in neural tissue engineering is to present the growth cone with appropriate cues and a permissive environment for axon extensions.

Edges and barriers induce axons to extend and grow in specific directions [2, 5] and behave differently on flat substrates compared with highly tailored three-dimensional surfaces [6]. On 2D PLGA substrates, PC-12 cells produce an average of 2.5 neurites, which sprout in random directions [6]. On the same substrate, primary cortical neurons group together to form colonies, which were often connected by bundles of neurites [7]. In comparison, peripheral nerves do not form colonies on porous three-dimensional nanofibrous scaffolds and grow fewer but longer neurites that presumably use the scaffold as contact guidance conduits [8].

Hydrophilicity has received a lot of attention as a means of optimizing cell adhesion of the surface of biomaterials [9]. Lee *et al* [10] reviewed the effect of the surface hydrophilicity on cell adhesion, and showed that in general, an increase in surface hydrophilicity also resulted in an increase in cell adhesion. Lee *et al* [11] conducted cell interaction studies, on surface modified poly(hydroxy esters) such as poly($_L$-lactide) (P_LLA) and poly(lactide-co-glycolide). However, while cell adherence was found to increase with hydrophilicity, it was also discovered that maximum cellular adherence occurred at intermediate hydrophilicities.

In addition the topography [12] of the scaffold can also be manipulated to control adhesion, proliferation, neurite outgrowth and cell spreading [9]. This is especially relevant in neural tissue engineering because axonal growth is slow in the dynamic

environment of the brain, whereas topography of the scaffold is relatively stable over time [13], and independent of the biochemistry [14]. For example, in nerve regeneration distances of 5 cm or greater may need to be transversed, and axonal regrowth occurs at a rate of approximately 1 mm per day [15]. Ultimately, a scaffold will need to remain *in vivo* for as long as 50 days to encourage axonal extension. Although chemical cues and surface proteins regulate axonal growth, they are tightly regulated with precise timing of production and are relatively short lived [13], making control through contact guidance a particularly attractive tool.

Nanostructured scaffolds for neural tissue engineering have been manufactured using self-assembly techniques [16] and thermally induced phase separation (TIPS) [17]. They can also be conveniently fabricated by electrospinning, which can use a broad range of polymer systems to rapidly produce and manipulate unique sets of spatial and surface structures on the nanoscale [18]. The orientation of the fibres can also be changed using electrospinning by employing different collection devices such as dual rings [19], rapidly rotating drums [20], or a gap method of alignment [21]. Neurons grown on surfaces with parallel nanoscale ridges form neurites that are aligned with the ridges [6]. Johansson *et al* [13] showed that the neurites preferred to grow on ridge edges and elevations rather than in grooves. This leads to the speculation that neurites grow parallel to features to minimize the number of discontinuities encountered by the leading growth cone, or that the initiation of process extensions is less likely perpendicular to topographic features. One reason that neurites prefer nanoscale substrates may be the similarities between the dimensions of the substrates and the structural components found in the native basement membranes, which are comprised of a complex array of extracellular matrix (ECM) components [14, 22].

When poly-α-hydroxy esters were used to create nanofibre scaffolds, consisting of both random and aligned fibres, the direction of neuron growth depended on fibre alignment, with neurite extension parallel to the fibre direction for aligned nanofibre scaffolds [23]. The rate of differentiation into neurons also depended on the fibre diameter, with more cells differentiating on aligned nanofibres than on microfibres [23]. Because neurites

extended into random nanofibrous PLGA scaffold Yang *et al* described the scaffold as providing a 'positive guidance cue' [17]. Therefore, the physical environment provides cues that can be exploited to enhance neurite outgrowth and neurone survival. This study aims to investigate the interaction of neurite extension on three-dimensional scaffolds prepared by electrospinning poly($_L$-lactide) (P_LLA) and poly(lactide-coglycolide) (PLGA). These materials were selected because of their proven biocompatibility with primary cortical neurons [7]. Primary cortical neurons were selected because they are robust under positive culture conditions yet respond to their environment. Therefore, responses to changes in the chemical and physical properties of the scaffold can be monitored. Biocompatibility was investigated following alterations to the surface hydrophilicity of each of the poly-α-hydroxy esters, by comparison of the cell diameter, the number of primary and secondary neurite branches and their length with the poly$_D$lysine positive control.

3.2.3 MATERIALS AND METHODS

3.2.3.1 Materials and scaffold fabrication

P_LLA (MW = 81 090) and PLGA (MW = 160 000) were obtained from Absorbable Polymers, Inc. (AL, USA). Polymer solutions of 10% w/v were prepared by dissolving the polymer in 2 ml of tetrahydrofuran (Merck Pty Ltd, Australia) and dimethylformamide (BDH, UK (ratio 1:1)). The solutions were placed in a 10 ml glass syringe for electrospinning and fitted with an 18 G needle and set at a 0.397 cc h^{-1} flow rate. An accelerating voltage (18 kV) was provided by a high voltage power supply and a working distance of 15 cm was employed. An aluminium container (12 × 10 cm) filled with 20 ml of phosphate buffered saline (PBS) was used as a collector. The non-woven nanofibrous electrospun scaffolds were placed in a vacuum oven for two days at 30 $^{\circ}$C. They were then immersed in potassium hydroxide (KOH) at concentrations of 0.1M, 0.2 M or 0.4 M KOH, rinsed in doubly distilled water and dried again. The electrospun nanofibres were cut into 5 × 5 mm^2 and sterilized just before the cell culture experiment.

3.2.3.2 Scaffold characterization

Scanning electronmicroscopy (SEM) was used to characterize the non-woven scaffolds. Specimens were coated with gold using a sputter coater (Balzers SCD-005, BAL-TEC). The current was 25 mA for a coating time of 180 s. The SEM (Leica 360FE) was operated at 15 kV.

The surface energies of the nanofibre scaffold were determined by a modified contact angle measurement using a Data Physics Instruments GmbH OCAH-200 at room temperature. The sessile drop method was employed using differing concentrations of IPA (isopropyl alcohol, Aldrich, Australia) solutions in milliQ water to determine changes in the hydrophilicity of the surfaces [24]. Fundamentally, when the surface tension of the solution is higher than that of the scaffold, the drop will bead on the surface. As the surface tension becomes equal to that of the scaffold, the drop spreads immediately and penetrates the scaffold. Therefore, the highest concentration of IPA solution that penetrates the scaffold is equal to that of the surface tension of the scaffold.

3.2.3.3 Embryonic cortical neurone cell culture

Cortices from C57/B6-type mice (E14) were dissected, stripped of meninges and olfactory bulbs, and dissociated with 0.025% trypsin in Krebs solutions for 20 min (Sigma T-4665). All the methods conform to the Australian National Health and Medical Research Council published code of practice for the use of animals in research and were approved by the Howard Florey Institute Animal Ethics Committee. The polymer scaffolds were immersed in 70% ethanol and allowed to dry, before being placed into sterile 24-well polystyrene culture dishes in triplicate. They were then soaked in 0.5 ml of Krebs solutions for 2 h. The Krebs solution was removed immediately before seeding of neurons. Poly-$_D$-lysine (0.05 mg ml^{-1}) was coated on glass cover slides, which were placed in the culture dishes in triplicate and served as a positive control. The polystyrene tissue culture dish served as a negative control. Neurons were then seeded at a density of

106 cells ml^{-1} in 0.5 ml of modifed Eagle's medium (MEM, Gibco) and 10% fetal calf serum. After 1 h, the medium was removed and 1 ml of culture medium was added. The culture medium was prepared using 50 ml of Neurobasal medium (NBM, Gibco), 1 ml B27 supplement (Gibco), 125 μl glutamine (200mMstock) and 50 μl gentamycin (10 mg ml^{-1} (Gibco)).

The cortical neurons were cultured for six days at 37 $^{\circ}$C with 5% CO_2, before being fixed with 4.0% formaldehyde (Sigma 37% stock solution) for 10 min at room temperature, and then washed three times in phosphate buffered saline (PBS) for 5 min while being gently rocked. The samples were then stored below 5 $^{\circ}$C prior to reacting with antibodies to neurofilament.

3.2.3.4 Immunohistochemistry for neurofilament

The neurons were again fixed in 10% NBF for 2 min and washed in PBS three times for 5 min while being gently rocked. Non-specific antibody binding was blocked with a solution of 3% normal goat serum (NGS) + 0.3% Triton-x (Sigma) for 20 min at room temperature before washing three times. Primary antibody was rabbit anti-neurofilament (1:300) in 1% NGS (AB1887, Rabbit anti Neurofilament, Chemicon Inc.) plus 0.3% Triton-x (Sigma) was applied and incubated at 37 $^{\circ}$C for 2 h. The material was washed in PBS for 20 min (three times) and secondary goat anti-rabbit tagged with an Alexa Fluor 488 (A11008, molecular probes, 1:600) in PBS, was applied for 2–3 h at room temperature before a final wash in PBS for 10 min (three times) and mounting on slides with Dako fluorescent mounting media.

3.2.3.5 Imaging

Epi-fluorescence (Zeiss Axiovert 200M inverted microscope with FluoArc mercury lamp, Optronics controller and Zeiss 20X lens) was used to image neurons and to determine the cell size and primary and secondary branching. Images were examined for cell diameter, number of primary and secondary branches and a total neurite length using Image J

software (NIH version 1.32). The results were reported as a mean ± standard deviation of means (n = 17) and one-way analysis of variance (ANOVA) was performed on independent samples to determine significant differences between surface modified groups. Statistical significance was considered at $p < 0.05$.

Using laser scanning confocal microscopy (LSCM) (Leica) TCS NT on DMXRE upright, 40X oil lens, NA 1.0–0.5) cells were imaged using 488 nm excitation to acquire a series of optical sections of 0.285 μm steps in the z-direction. In the corresponding focal planes, the reflectance mode of the LSCM was utilized to image the non-fluorescent polymer fibres. The two images at the same depth were combined using Leica software.

3.2.4 RESULTS AND DISCUSSION

3.2.4.1 Electrospinning and surface modification

The average diameter of electrospun PLGA fibre was 0.76 ± 0.30 μm and in the case of P_LLA 0.51 ± 0.38 μm (figure 1 shows SEM images of the PLGA sample). Such variations in the fibre diameters and in particular the interfibre distances have the advantage of presenting a range of topographical features to the axons in a single experiment.

Table 1 Surface energies of the P_LLA and PLGA scaffolds after KOH modifications.

Material	KOH solution concentration (M)	Surface tension (dyn/cm)
P_LLA	0.0	52 ± 2
	0.1	42 ± 2
	0.2	69 ± 5
	0.4	61 ± 3
	0.0	52 ± 2
PLGA		
	0.1	45 ± 2
	0.2	57 ± 3
	0.4	69 ± 5

To examine the effect of surface hydrophilicity on cell growth, the surfaces were modified by partial hydrolysis by immersion in potassium hydroxide (KOH) solutions of varying concentration for 1 min. Table 1 shows the change in surface tension after KOH surface treatments. For both the P_LLA and PLGA scaffolds, treatment with 0.1 M KOH resulted in a drop in the surface tension. This has been attributed to initial hydrolysis and erosion of the fibre surfaces exposing the more hydrophobic underlying layer [7]. However, at higher concentrations of KOH (0.2 and 0.4 M) there were significant increases in the surface tension due to the hydrolysis of the ester moieties and the formation of new acid and alcohol end groups [7]. SEM micrographs of the PLGA scaffold before and after surface treatment (Figure 1) showed that hydrolysis had little effect on the surface roughness.

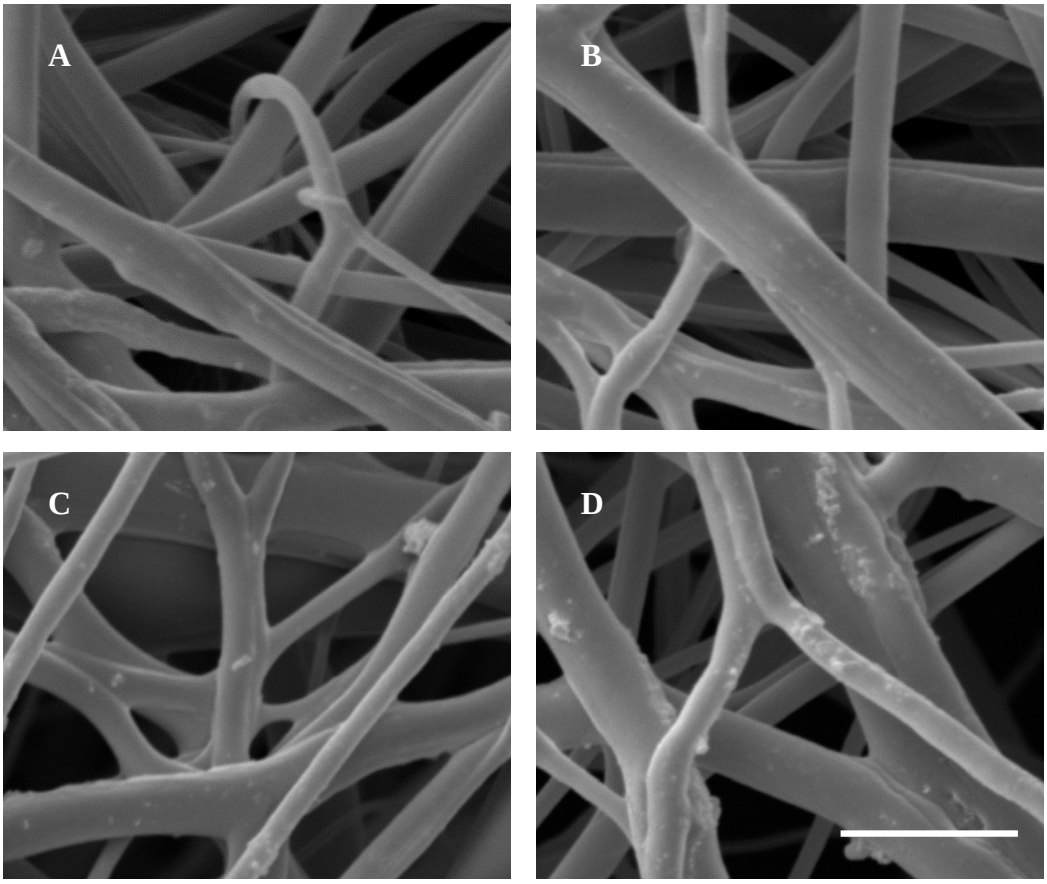

Figure 1. SEM micrographs of unmodified and surface modified PLGA using different concentrations of (KOH). (A) Unmodified; (B) 0.1 M (KOH); (C) 0.2 M (KOH); (D) 0.4 M (KOH) (scale bar = 1 μm).

3.2.4.2 Investigation of embryonic cortical neurons cultured on nanofibrous scaffolds

Embryonic cortical neurons were cultured on PLGA and P_LLA randomly orientated nanofibrous scaffolds and the Feret cell diameter (longest possible distance between the boundary of the cell body), the number of primary and secondary branches and the total length of neurite extensions were measured. Primary branches are defined as axons extending from the cell body and subsequent branching from these axons defined as secondary.

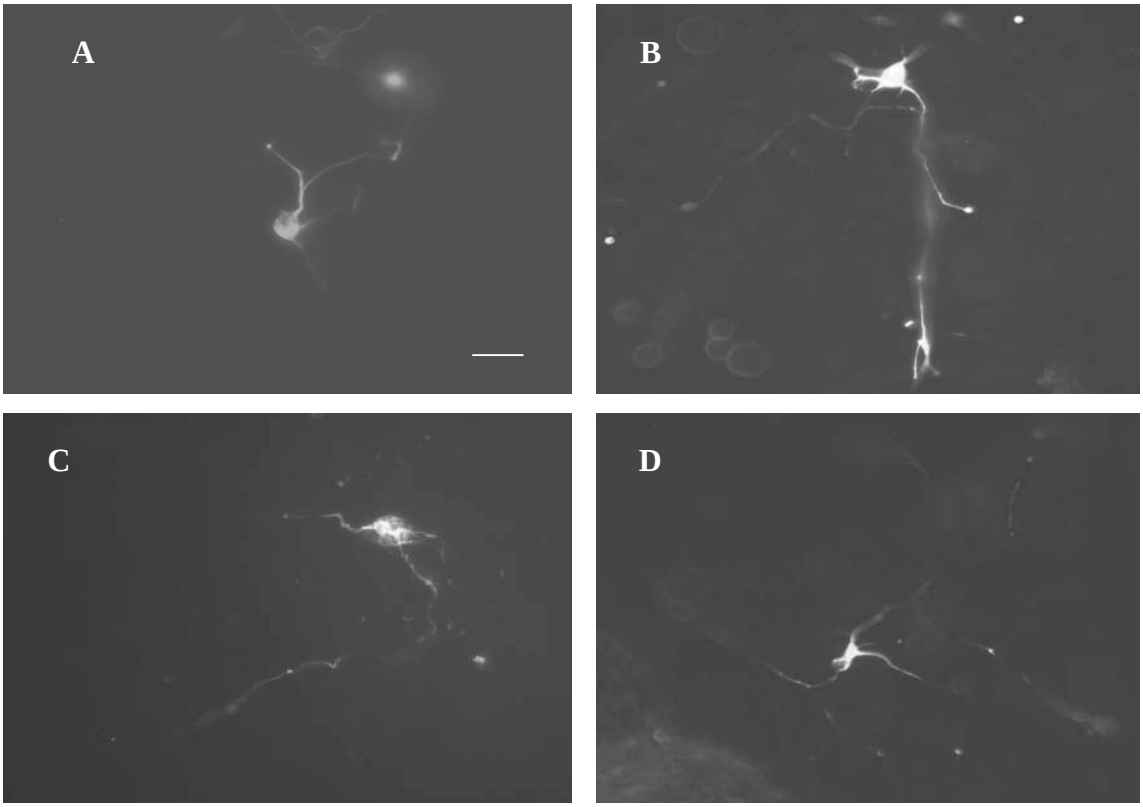

Figure 2. Epifluorescence micrographs of mouse cortical neurons following six days culturing on PLGA. Scaffolds were either unmodified (A) or modified (B), (C) and (D) for 1 min in the presence of 0.1 M, 0.2 M, 0.4 M (KOH), respectively. Bar 25 μm.

Figure 2 shows an epifluorence image of cortical neurons sending out neurite extensions on unmodified and modified PLGA scaffolds. Smooth, round cortical neurons were distributed throughout unmodified PLGA and P_LLA scaffolds. Cell body diameters were

similar on unmodified PLGA and P_LLA nanofibres (20.6 ± 2.5 μm and 20.2 ± 3.4 μm, respectively) and the poly-$_D$-lysine positive control (19.5 ± 1.0 μm). Similarly, there was little difference in the number of primary and secondary branches (number of primary branches; 2.8 ± 1.0 and 2.6 ± 1.0, and number of secondary branches; 2.1 ± 0.8 and 2.0 ± 0.9 for PLGA and P_LLA, respectively). In contrast, large colonies were formed on unmodified flat 2D substrates of the PLGA and P_LLA (figure 3) [7]. This suggests that 3D PLGA and P_LLA nanofibre structures provide appropriate niche environments for cortical neurons to adhere and differentiate.

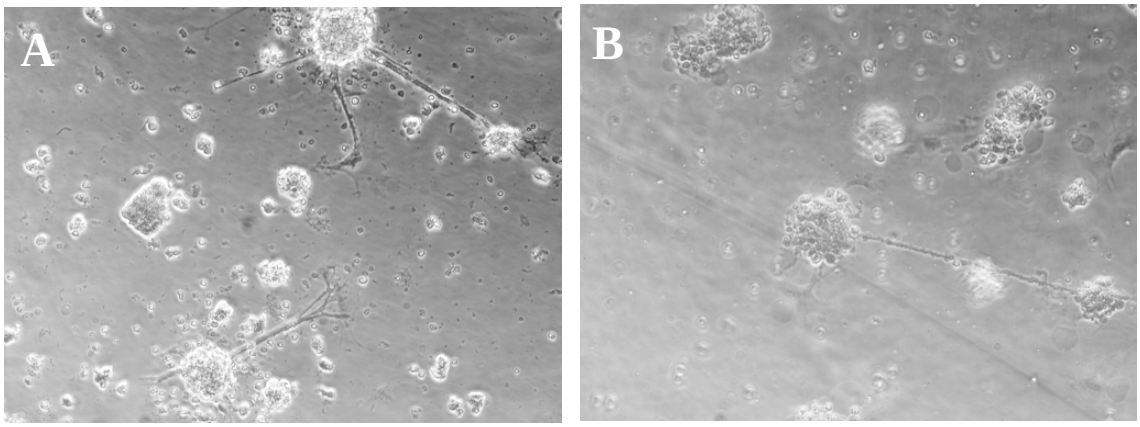

Figure 3. Colony formation on flat 2D substrates of the PLGA (A) and PLLA (B).

Changing the surface tension of the scaffolds did not induce cells to clump on any of the scaffolds (table 1 and figure 2). Most cell bodies were smooth, round to oval and pyramidal with neurites of uniform diameter. The cell diameter and the number of primary and secondary branches did not significantly change with surface tension, with the number of primary branches always being greater than the number of secondary. Furthermore, the number of primary and secondary branches was statistically the same between the P_LLA and PLGA for each concentration of KOH (data not shown).

The correlation between the surface tension of the scaffolds and neurite extension was examined. The length of the neurites on the P_LLA and PLGA scaffolds was statistically the same for each surface tension. However, the neurites for both the P_LLA and PLGA had a statistically larger extension after surface treatment with 0.1M KOH which corresponded to surface tensions of 42 ± 2 and 45 ± 3 dyn cm^{-1}, respectively. Therefore,

scaffolds with the lowest surface tension (i.e. the most hydrophobic) were more conducive to neurite extension. After the 0.2 M and 0.4 M KOH treatments, the scaffolds became more hydrophilic and the total neurite length decreased to that of the untreated scaffold.

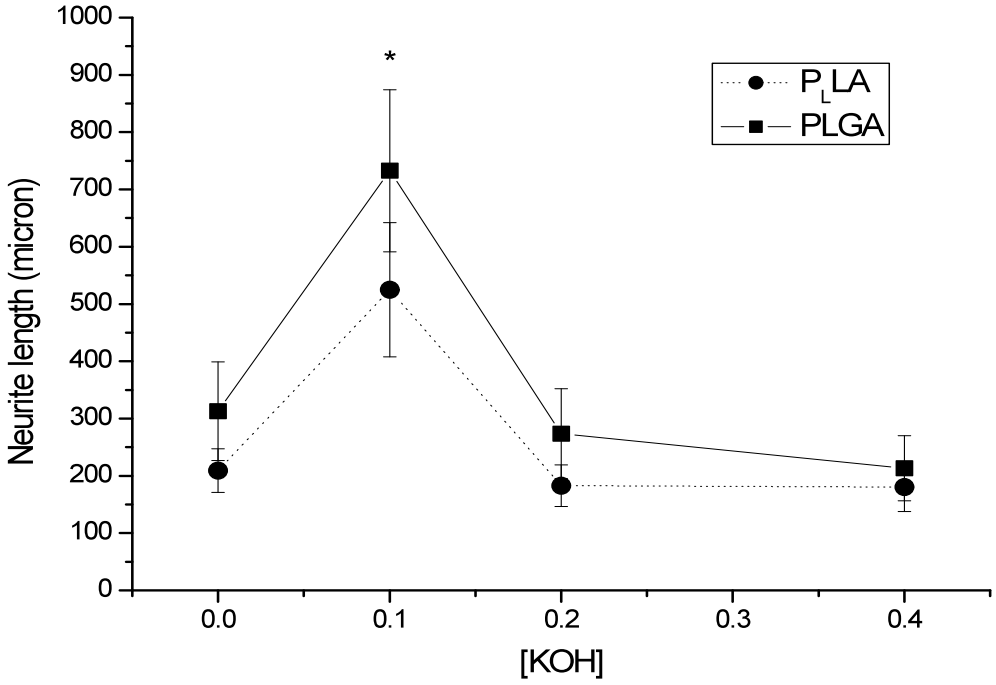

Figure 4. Cortical neurons following six days culturing on P_LLA and PLGA, various degrees of surface modification. Numbers show mean ± standard deviation of mean (*p < 0.05, n = 17).

3.2.4.3 Interaction between neurites and the nanofibrous scaffold

The interaction of the neurites with the nanofibrous scaffolds was investigated using LSCM. Figure 5 shows a typical depth profile of a single neurite extending through a PLGA (0.2 M KOH treated) scaffold. It is evident that the neurite makes contact with the fibres, drapes itself across it and uses this contact as a 'springboard' to a neighbouring fibre. This is in contrast to Foley *et al* who found that neurites follow topographic features to avoid discontinuities because of difficulties crossing voids [6]. However, in this study, scaffolds were randomly orientated and alignment of the fibres may influence

contact guidance. Our results are consistent with Kwon *et al*'s findings that human umbilical vein endothelial cells would be attached to many fibres if the fibres were in close proximity [25], but attached mainly to one fibre when the interfibre distance was large. Figure 6 shows a neurite following a PLGA fibre (0.2M KOH) in a randomly orientated scaffold for approximately 40 μm. The structure of the scaffold in this region was open with the interfibre distance greater than 15 μm. In other areas of the scaffold where the interfibre distance is closer (between 2 and 15 μm) neurites appear to travel from one fibre to another. Similar behaviour was obtained for all scaffolds incorporating different chemistry and surface tension. These preliminary results suggest that neurites follow a fibre when the 'hopping' distance between fibres is too large; however, further observations are required to obtain statistically valid data.

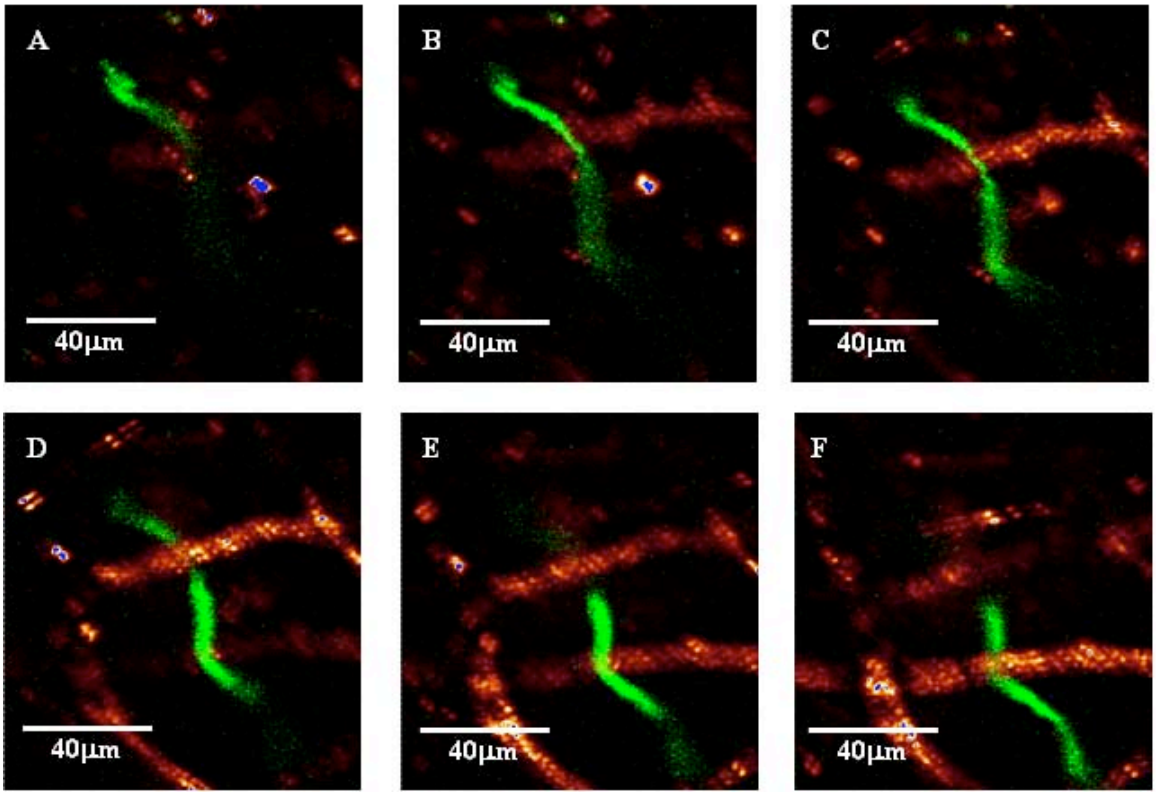

Figure 5. Confocal images of a neurite (green) crossing over two polymer fibres (red). The fibres were imaged using the reflectance mode of the confocal microscope. The *Z* dimension has been changed incrementally with 0.285 μm steps between 0 μm (A) and 4.47 μm (F).

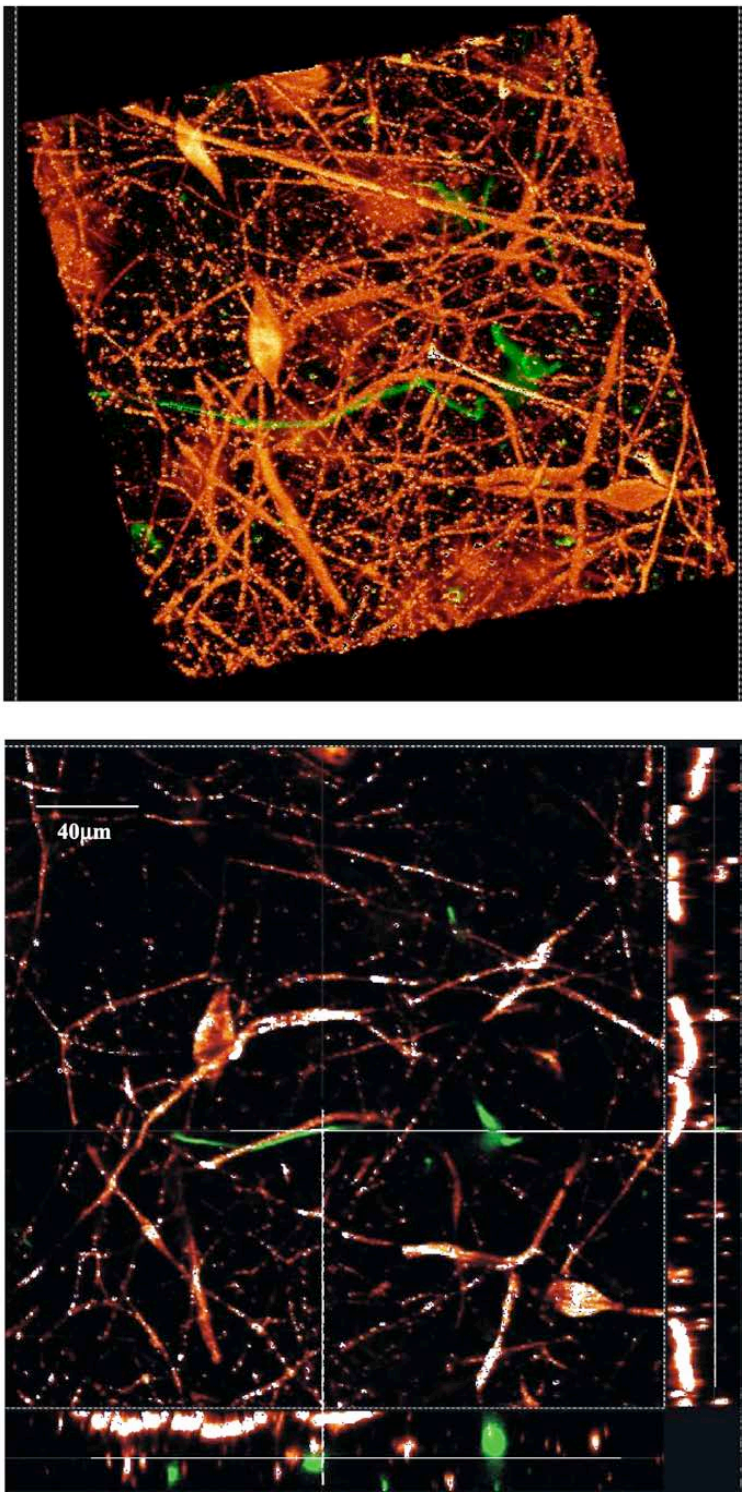

Figure 6. (A) Projection of a neurite briefly growing along a fibre within the PLGA scaffold. (B) Sectioned confocal image of a neurite (green) growing within a scaffold, briefly following the fibre (red). The fibres were imaged using the reflectance mode of the confocal microscope.

Figure 7 is an image of a bundle of PLGA fibres that protrudes from the surface of the scaffold. The bundle forms a much denser fibre network than the majority of the scaffold, with fibres less than 1 μm apart. In this instance the neurite has followed the edge of the bundle as if it were a ledge. There are four clear instances where the neurite has crossed fibres (indicated by white arrows), roughly perpendicular to them, and the small bends present in the neurite are actually undulations where the axon has draped over the three fibres.

This study shows that the fibre network density seems to be an important influence on how a neurite extends. If the network density is low (interfibre distance >15 μm) neurites follow the fibres. On the other hand, neurites seem to avoid regions of greater fibre density within the scaffold. Intermediate fibre densities are traversed perpendicular to the fibre. There were instances where there was no topological cue to explain severe direction changes, implying that a chemical cue, possibly from an adjacent neurone has induced the directional change.

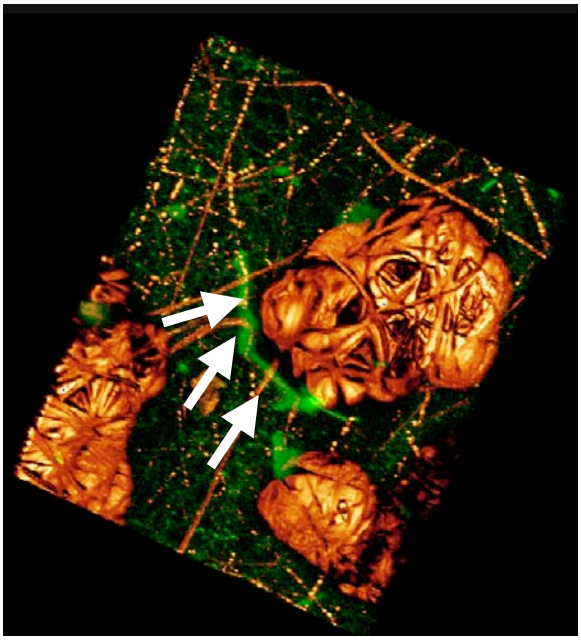

Figure 7. A projection of a neurite (green) growing around a tight bundle of PLGA fibres. The neurite was imaged in confocal mode while the red fibres were imaged ultilizing the reflectance mode.

3.2.5 Conclusions

Three-dimensional non-woven scaffolds were prepared by electrospinning poly($_L$-lactide) (P_LLA) and poly(lactide-coglycolide) (PLGA).While the results indicated that the surface treatments did not change the cell shape and size, or the number of primary and secondary branches, it did affect neurite extension. When the surface tension dropped to its lowest value (between 40–47 dyn cm^{-1} for both samples) there was a significantly greater overall neurite length of both the primary and secondary branches compared to higher surface tensions. Another major finding of this work was that the interfibre distance influenced how the neurite extended. If the interfibre distance was large (>15 μm) the neurites followed the fibres. On the other hand, neurites seem to avoid regions of low interfibre distances (<1 μm) and at intermediate distances neurites traversed perpendicular to the fibres. Therefore, it may be possible to control neurite extension though modifying the architecture of the electrospun scaffolds.

3.2.6 Acknowledgments

This project was supported by the ARC Discovery DP0663573. David Nisbet was supported by an Australian Postgraduate Award and the CRC for Polymers. The authors wish to thank Stephen Firth and Ian Harper of Monash Micro Imaging for assistance with LSCM experiments.

3.2.7 References

[1] Schmidt C E and Baier L J 2003 *Ann. Rev. Biomed. Eng.* **5** 293

[2] Manwaring M E, Walsh J F and Tresco P A 2004 *Biomaterials* **25** 3631

[3] Rabchevsky A G and Streit W J 1997 *J. Neurosci. Res.* **47** 34

[4] Reddi A H 2000 *Tissue Eng.* **6** 351

[5] Maskery S M, Buettner H M and Shinbrot T 2004 *BMC Neurosci.* **2** 22

[6] Foley J, Cgunwald E, Nealey P and Murphy C 2005 *Biomaterials* **26** 3639

[7] Nisbet D R, Pattanawong S, Nunan J, Shen W, Horne M K, Finkelstein D I and Forsythe J S 2006 *J. Colloid Interface Sci.* **299** 647

[8] Bini T B, Gao S, Tan T C, Wang S, Lim A, Hai L B and Ramakrishna S 2004 *Nanotechnology* **15** 1459

[9] Khang G, Choee J-H, Rhee J M and Lee H B 2002 *J. Appl. Polym. Sci.* **85** 1253

[10] Lee H B and Lee J H 1995 Biocompatibility of solid substrates based on surface wettability *Encyclopedic Handbook of Biomaterials and Bioengineering: part A* (New York: Marcel Dekker)

[11] Lee S J, Khang G, Lee Y M and Lee H B 2002 *J. Biomater. Sci. Polym. Ed.* **13** 197

[12] Jung D R, Kapur R, Adams T, Giuliano K A, Mrksich M, Craighead H G and Taylor D L 2001 *Crit. Rev. Biotechnol.* **2** 111

[13] Johansson F, Carlberg P, Danielsen N, Montelius L and Kanje M 2006 *Biomaterials* **27** 1251

[14] Flemming R G, Murphy C J, Abrams G A, Goodman S L and Nealey P F 1999 *Biomaterials* **20** 573

[15] Pfister B J, Iwata A, Meaney D F and Smith D H 2004 *J. Neurosci.* **24** 7978

[16] Silva G A, Czeisler C, Niece K L, Beniash E, Harrington D A, Kessler J A and Stupp S I 2004 *Science* **303** 1352

[17] Yang F, Murugan R, Ramakrishna S, Wang X, Ma Y and Wang S 2004 *Biomaterials* **25** 1891

[18] Zhang Y-Z, Lim T C, Ramakrishna S and Huang Z-M 2005 *J. Mater. Sci. Mater. Med.* **16** 933

[19] Dalton P D, Klee D and Moller M 2005 *Polymer* **46** 611

[20] Huang Z-M, Zhang Y-Z, Kotaki M and Ramakrishna S 2003 *Compos. Sci. Technol.* **63** 2223

[21] Li D, Wang Y and Xia Y 2003 *Nano Lett.* **3** 1167

[22] Xu C Y, Inai R, Kotaki M and Ramakrishna S 2004 *Biomaterials* **25** 877

[23] Yang F, Murugan R, Wang C and Ramakrishna S 2005 *Biomaterials* **26** 2603

[24] Vazquez G, Alvarez E and Navaza J M 1995 *J. Chem. Eng. Data* **40** 611

[25] Kwon I, Kidoaki S and Matsuda T 2005 *Biomaterials* **26** 3929

3.3 Investigation into the interaction of brain derived neural stem cells with the electrospun scaffolds.

Chapter 3.2 demonstrated that cortical neurones are compatible with electrospun fibers and adhere, differentiate and migrate similarly to the way they do *in vivo*. The discovery that cortical neurones sent out longer neurites on more hydrophobic surfaces lead the author to select a poly(α-hydroxy ester) that is inherently more hydrophobic e.g. polycaprolactone (PCL). For the remainder of Part I of the thesis only PCL is utilised in the investigations, although in some instances it has undergone surface modification.

Since cortical neurones had proven biocompatibility with electrospun scaffolds and sent out long process, it was decided to investigate the interaction and differentiation of rat adult brain derived stem cells. The reasoning behind this decision was that for the successful treatment of Parkinson's disease and Spinal Cord Injury it may be necessary to introduce replacement cells i.e. stem cells. The stem cells were cultured on PCL fibres of random orientation that were un-modified and modified with ethylenediamine (ED) to introduce amines on the surface that will later offer sites for the direct immobilisation of growth factors and cell adhesion molecules. The differentiation of the stem cells, considering all four phenotypes that neural stems cells can differentiate towards, was investigated. The results are presented in the following published work.

Characterization of neural stem cells on electrospun poly(ε-caprolactone) submicron scaffolds: evaluating their potential in neural tissue engineering.

D.R. Nisbet[1], L.M.Y. Yu[2, 3], T. Zahir, [2, 3] J.S. Forsythe[1], M.S. Shoichet[2, 3, 4*]

1. Department of Materials Engineering, CRC for Polymers, Monash University, PO Box 69M, Melbourne, Vic, Australia 3800.
2. Department of Chemical Engineering, University of Toronto, 200 College Street, Toronto, ON, Canada M5S 3E5.
3. Institute of Biomaterials and Biomedical Engineering, Terrence Donnelly Center for Cellular & Biomolecular Research, University of Toronto, 160 College Street, RM 514 Toronto, ON, Canada M5S 3E1.
4. Department of Chemistry, University of Toronto, 80 St. George Street, Toronto, ON, Canada M5S 3H6.

3.3.1 ABSTRACT

Development of biomaterials with specific characteristics to influence cell behaviour has played an important role in exploiting strategies to promote nerve regeneration. The effect of three-dimensional (3D) non-woven electrospun poly(ε-caprolactone) (PCL) scaffolds on the behaviour of rat brain-derived neural stem cells (NSCs) is reported. The interaction of NSCs on the randomly orientated submicron (PCL) fibrous scaffolds, with an average fiber diameter of 750 ± 100 nm, was investigated. The PCL scaffolds were modified with ethylenediamine (ED) to determine if amino functionalisation and changes in surface tension of the fibrous scaffolds affected the proliferation and differentiation characteristics of NSCs.

Surface tension of the fibrous scaffold increased upon treatment with ED which was attributed to amine moieties present on the surface of the fibers. Although surface treatment did not change the differentiation of the NSCs, the modified scaffolds were more hydrophilic, resulting in a significant increase in the number of adhered cells, and increased spreading throughout the entirety of the scaffold. When the NSCs were seeded on the PCL scaffolds in the presence of 10% FBS, the stem cells differentiated primarily into oligodendrocytes, indicating that electrospun PCL has the capacity to direct the differentiation of NSCs towards a specific lineage. The data presented here is useful for the development of electrospun biomaterial scaffolds for neural tissue engineering, to regulate the proliferation and differentiation of NSCs.

3.3.2 KEY WORDS

Electrospinning, Neural tissue engineering, Nerve regeneration, Neural stem cells, Oligodendrocyte.

3.3.3 INTRODUCTION

The spinal cord is the main communication channel between the brain and the rest of the body. Consequently when the central nervous system (CNS) is damaged by neurodegenerative diseases or trauma there is minimal-to-no functional recovery with severe physiological consequences for the patient[1-4]. Despite extensive research there is still no definitive treatment for neural tract regeneration in the CNS. Hence, an active area of neural tissue engineering strategies strive to develop a more permissive environment to promote nerve regeneration[3,5]. Moreover, recent advances in neurology, such as the discovery that neurogenesis occurs in adults[6-8], coupled with neural tissue engineering advances in combination strategies may provide a more optimistic outlook.

A wide variety of biomaterials have been evaluated for use in neural tissue engineering to provide a relevant matrix, for cell adhesion and guidance. Poly(α-hydroxy esters) have received considerable attention, as they are bioresorable and have been shown to be biocompatible with many cell types[9-12]. Recent studies have focused on fabricating complex 3-dimensional (3D) scaffolds or hydrogels such as macroporous scaffolds that mimic the extracellular matrix (ECM)[13,14], and injectable hydrogels for localized drug delivery[15]. Other complex 3D scaffolds were fabricated with ledges and fibers in an attempt to guide cell and neurite outgrowth[16,17]. These strategies seek to provide cells with a permissive environment to optimize regeneration. Moreover, nanofibrous scaffolds are particularly attractive in neural tissue engineering as they are inherently porous and have large surface-area-to-volume ratios[18]. Thus these fibrous scaffolds encourage cellular adhesion and proliferation by offering a variety of topographical features to guide an advancing growth cone to adhere. Such scaffolds can be fabricated in a variety of

different ways including self assembly[19] and thermally induced phase separation[9]. Fibrous scaffolds of desired sizes and dimensions can be easily tailored for selected tissue engineering applications using electrospinning[16].

NSCs may play a pivotal role in cell replacement therapies for the repair of the spinal cord and only a handful of studies have been conducted involving the culture of NSCs on electrospun scaffolds. Recent work by Yang *et al.* cultured NSCs (from cerebellum, C17.2) in the presence of 10% fetal calf serum and 5% horse serum on electrospun poly($_L$-lactic acid) scaffolds, and evaluated differentiation on aligned and random nanofibers[16]. They investigated the differentiation of NSCs into neurons and found that when the electrospun fibers were aligned, neurites grew along the aligned fibers. It was also discovered that the differentiation of NSCs into neurons depended on the fiber diameter, with more cells differentiating into neurons on nanofibers than microfibers. This study showed considerable evidence that electrospun scaffolds can promote the preferential differentiation of NSCs based on fiber size.

While the longer term goal is to utilize cell-scaffold constructs that will assist in functional recovery of the damaged spinal cord in vivo, this study investigates the differentiation profile of NSCs within 3D electrospun poly(ε-caprolactone) (PCL) scaffolds in vitro. Stem cell morphology, differentiation and distribution through the electrospun PCL scaffolds were investigated as a function of aminolysis of the PCL fibers. The introduction of amino groups changes the hydrophilicty of the fibers and is also known to affect the level of adhesion and differentiation of hematopoietic stem/progenitor cells.[20] In this study, we are particularly interested in neural stem/progenitor cells derived from the subependyma of the lateral ventricle forebrain in rats because they are capable of self-renewal and are multipotent differentiating into neurons, astrocytes and oligodendrocytes[21,22]. For a regenerative neural tissue engineering strategy of the spinal cord, a combination of cell types will likely be required. For example, the close interaction of axons and oligodendrocytes required for functional regeneration highlights this point[23].

3.3.4 MATERIALS AND METHODS

All chemicals were used as received unless otherwise stated. Distilled and deionized water was obtained using a Millipore Milli-RO 10 Plus and Milli-Q UF Plus (Bedfore, MA) system, and used at 18MΩ resistance.

3.3.4.1 Materials and scaffold fabrication

Poly(ε-caprolactone) (PCL) was obtained from Absorbable Polymers, Inc. (Alabama, USA). Polymer solutions of 10% w/v were prepared by dissolving PCL in 2 ml of chloroform (Merck Pty Ltd, Australia) and methanol (Merck Pty Ltd, Australia) at a ratio of 3:1 (v/v). The solutions were placed into a glass syringe (10 ml) with a 21-guage needle for electrospinning and a flow rate of 0.397 ml/h was set. A 20kV accelerating voltage was applied by a high voltage power supply and a 15 cm working distance was utilized. The scaffolds were collected in an aluminum container (10 cm × 10 cm × 2 cm) filled with 20 ml of phosphate buffered saline (PBS). The non-woven nanofibrous scaffolds were then dried in a vacuum oven for 2 d at 30°C. The scaffolds were then aminolysed in 0.05 M ethylenediamine (ED) (Sigma-Aldrich Pty Ltd) in 2-isopropanol (IPA) (Caledon Laboratories Ltd) and allowed to react at 20°C for 10 to 40 min. The treated samples were then washed 3 times in ice water and soaked for 1 h in distilled water on ice. The samples were dried overnight in a vacuum oven, and cut into 5 mm square scaffolds and disinfected in 70% ethanol for cell culture preparation.

3.3.4.2 Scaffold characterization

The non-woven scaffolds were characterised by scanning electron microscopy (SEM). Scaffolds were gold coated using a sputter coater (Balzers SCD-005, BAL-TEC). A 25 mA current was used for a total coating time of 180 s. The SEM (S-570 Hitachi Toyko, Japan) was operated at 15 kV. The average diameter of the fibers was determined by measuring a total of 20 fibers on three different samples.

The surface tensions of the nano-fiber scaffolds were determined by a modified contact angle measurement using a VCA – optima^{TM} (AST products, Inc) at room temperature. A modified sessile drop method was employed using solutions of different IPA concentrations with milliQ water to detect the changes in drop penetration through the scaffold and the surface tension determined through comparison with standard curves[24,25]. Statistical analysis was conducted using SigmaStat for windows version 3.0.3©, on a sample size (n = 6). A one-way analysis of variance was employed using Tukey's posthoc testing.

Surface functionalization was characterized using X-ray photoelectron spectroscopy (XPS) equipped with a monochromatic A1 Kα source operated at 12kV and 25mA. The samples were placed on round coverslips in preparation for analysis. The XPS was conducted using a Leybold MAX 200 X-ray Photoelectron Spectrometer. The samples were measured at an emission angle of 90° from the surface. Three different areas on each sample were measured.

The surface functionalization of the scaffold was also characterized by fluorescence using 3-(4-carboxybenzoyl)-quinoline-2-carboxaldehyde (CBQCA – Invitrogen^{TM}). The PCL scaffolds that were previously aminolysed were dissolved in a DMSO:THF (19:1) solution at a concentration of 2.6 mg/ml to which a 5 mg/ml of sodium cyanide (NaCN) in a buffer of 0.1M triethanolamine (TEA) was added. The CBQCA was dissolved in DMSO at a concentration of 10 mg/ml. 100 µL of polymer solution and 25 µL of CBQCA and NaCN in buffer were placed in a 96 well plate in triplicate. The samples were then incubated for 48 h while shaking at 37°C. They were then visualized at 560 nm using a fluorescence plate reader (Spectra MAX Gemini EM, Molecular Devices).

3.3.4.3 Isolation and culture of adult brain-derived stem cells

Brain-derived neural stem cells (NSCs) were isolated from the subependymal region of the lateral ventricles of adult rat forebrains as previously described[22]. Brain-derived neurospheres appeared within 2 to 3 weeks of harvesting, after which cells were passaged every week at a 1:3 dilution. The stem/progenitor cells were used after 3 to 5 passages.

The PCL scaffolds (≈ 200 μm thick) were placed into sterile 24-well polystyrene culture dishes in triplicate, and were cut to completely cover the bottom of the wells to ensure that the cells remained on the scaffold during seeding. They were then soaked in Neurobasal Media (NBM) (Invitrogen™) in the absence of mitogens overnight. The NBM contains 2% B27 Supplement (Gibco – Invitrogen™), 2mM L-glutamine (Gibco – Invitrogen™), and 100 ug/ml penicillin-streptomycin (P/S) (Gibco – Invitrogen™). The neurobasal media was removed immediately before the NSCs were seeded.

Laminin was used as a positive control because it has been shown to promote cell attachment. Laminin (0.15 μg/ml) was coated on glass cover slips, by submerging the glass cover slips overnight in the solution and removing it 4 h prior to culture to allow for drying. These cover slips were placed in the culture dishes in triplicate and served as positive controls. NSCs were then dissociated and seeded at a density of 5×10^5 cells/ml on the electrospun scaffolds in proliferating media that consisted of the above NBM with 20 ng/ml each of recombinant human epidermal growth factor (EGF) and recombinant human basic fibroblast growth factor (bFGF), and 2 ng/ml heparin (Sigma-Aldrich). For the laminin controls a density of 5×10^4 cells/ml was employed to avoid over population, as this is a 2D environment. A separate plate with controls was used to study the effect of differentiation media on NSCs. The same cell densities were used, however 10% fetal bovine serum (FBS) was added to the NBM instead of the mitogens. 1 ml of NBM with dissociated cells of the above densities was added to each of the wells.

The NSCs were then cultured for 7 d at 37°C, 5% CO_2, and 100% humidity, before being fixed with 4% paraformaldehyde for 10 min at room temperature. The samples were then washed 3 times in phosphate buffering saline (PBS) (pH 7.4) for 5 min while being

gently rocked. The scaffolds were then mounted on their end using frozen section medium (Stephens Scientific), before being sectioned into 20 μm slices using a cryostat (Leica CM 3050S).

3.3.4.4 Immunocytochemistry

The immunocytochemistry procedures were modified specifically for this application. Sections were firmly attached to glass slides by baking at 37°C for 30 min. The NSCs were again fixed using 4% paraformaldehyde for 2 min and washed in PBS 3 times for 5 min in a static environment. The scaffolds were then permeablised in 0.1% Triton-X for 30 min and washed 3 times in PBS. Non specific antibody binding was then blocked with a solution of 4% normal goat serum (NGS) for 1 h and were then exposed to the following antibodies: mouse anti-nestin (1:1000; BD Pharmingen^{TM}) for undifferentiated cells, mouse anti-GFAP Cy3 conjugate (1:400; Sigma-Aldrich) for astrocytes, mouse anti-CNPase (1:100; Chemicon, Temecula, CA) for oliodendrocytes, and rabbit anti-neurofilament (NF 200) (1:500; Chemicon) for neurons. The primary antibodies were added to PBS containing 1% NGS and 0.1% Triton-X and were allowed to react at 4°C overnight. The sections were then washed 3 times with PBS with 1% Tween (Sigma-Aldrich) added. The secondary antibodies, AlexaFluor 546 Cy3 (1:500; Molecular Probes) for CNPase and nestin, AlexaFluor 647 (1:500; Molecular Probes) for the NF200, were applied for 1 hour before again being washed with the PBS-tween solution. The nuclei were then stained with 10 μM Hoechst 33342 for 5 min, followed by the final 3 washes with the PBS-Tween solution. ProLong Gold anti-fade reagent (Molecular Probes) was then added to the samples and coverslipped. The cells were imaged using a laser scanning confocal microscope (LSCM) (Leica TCS SP2) with a 50X air lens, NA 0.8. The LSCM images presented in this paper (Fig. 4) were pseudo-coloured, meaning that the Cy3 stain used to mark some of the cells (eg. astrocytes in Fig 4C & 4D) are depicted as green rather than the orange-red that it emits. The cell were counted manually and the differentiation statistics were conducted using SigmaStat for windows version 3.0.3© and reported as mean ± standard deviation (n = 9). A pair wise Tukey's *post hoc* test was also employed. The cell numbers are presented as a percentage

differentiation, calculated as a ratio of the number of positively marked cells to the total number of nuceli.

3.3.5 RESULTS AND DISCUSSION

3.3.5.1 Electrospinning and surface modification.

The electrospun PCL scaffolds consisted of randomly orientated non-woven fibers shown in Fig. 1, with the average and standard deviation of fiber diameter throughout the scaffold being 750 ± 100 nm (n=3). To investigate the effect of surface hydrophilicity and chemistry on NSCs adhesion, differentiation and colonization, the surface of the PCL scaffold surfaces were modified by partial aminolysation for 10 to 40 min. While it has been previously shown on 2D surfaces of poly(lactic-co-glycolic acid) (PLGA) that the overall amount of aminolysation did not change after 10 min of reaction with ED[26], we were uncertain whether this would translate to the 3D electrospun PCL scaffold. To assess changes in surface hydrophilicity, we used a modified contact angle measurement technique to calculate the surface tension on the 3D electrospun scaffolds[25]. Using a series of water-IPA solutions of different surface tensions, it has been shown that there is a critical surface tension when a liquid shows no adsorption delay, and that this is analogous to critical wetting surface tension of a solid surface, including fibrous membranes[27]. Table 1 shows the change in surface tension of the PCL electrospun scaffolds after treatment with ED. When the PCL was subjected to treatment for 10 min the surface tension increased from 36 ± 1 dyn/cm to 42 ± 2 dyn/cm. This change was likely to have resulted from nucleophilic attack of carbonyl carbon, which forms a positively charged tetrahedral intermediate[26], and formation of amine (NH_2) moieties on the surface of the fibers. With increasing treatment times the surface tension remained at 42 ± 2 dyn/cm, indicating that 10 min of aminiolysation is sufficient to achieve the maximum surface energy using this method.

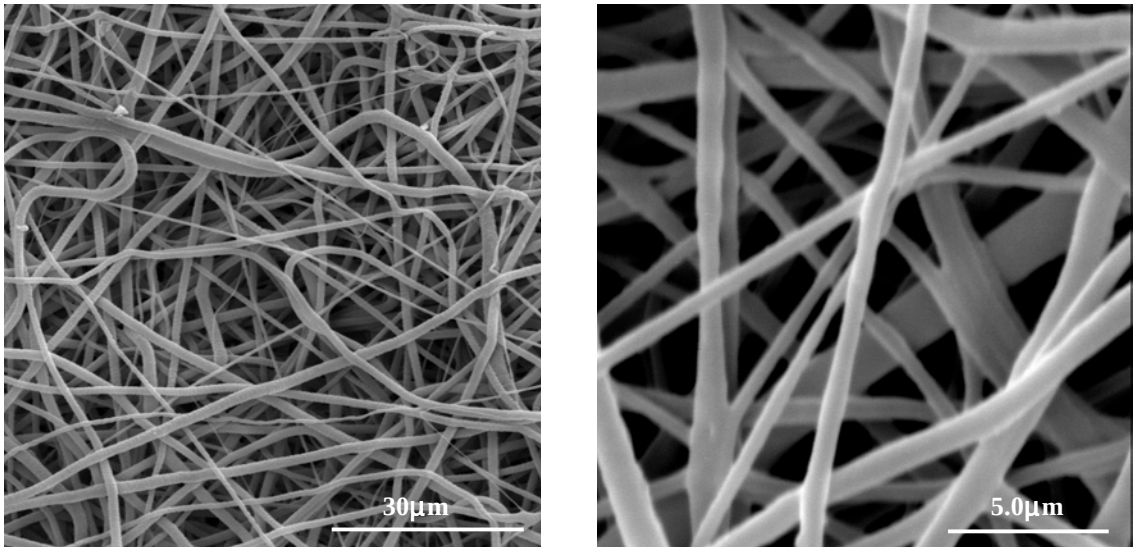

Fig. 1 – SEM images of the electrospun PCL scaffolds at different magnifications. The average fiber size in the PCL scaffolds is 750 ± 100 nm (mean ± standard deviation, n=3).

Table 1 – Surface tension of the PCL scaffolds after ED modification.

Material	Treatment time in ED (min)	Surface tension (dyn/cm)
PCL	No treatment	36 ± 1
	10	42 ± 2*
	20	42 ± 2*
	40	42 ± 2*

Surface tension is represented as mean ± standard deviation (n = 6). ANOVA with Tukey's posthoc test revealed significant differences between each of the treatments and the no treatment (*) p < 0.05.

To gain a greater understanding of the surface chemistry, modified surfaces were characterized by both X-ray photoelectron spectroscopy (XPS) and fluorescence using CBQCA. While the nitrogen (1s) peak was detected by XPS, the difference relative to the background was minimal. This is due to the random error of XPS being 1-2% of the measured value of the elements, and the low concentration of amino groups using ED. For this reason the surface chemistry functionalization was characterized by fluorescence using CBQCA. From the fluorescence intensity of CBQCA, 10 min of aminolysation using 0.05M ED resulted in 0.1 nmol of NH_2/g of PCL polymer. A significant effect on

surface tension can be achieved with a low concentration of amines on the scaffold surface.

3.3.5.2 NSCs response to electrospun scaffolds

To better understand how cells would respond to electrospun PCL scaffolds, dissociated NSCs were plated on PCL scaffolds in either the presence of serum (a differentiation factor) or EGF/FGF2/heparin (mitogens). The survival and colonization of the cells were investigated relative to laminin controls, in an attempt to determine how the dissociated NSCs interacted with the fibrous scaffold. Fig. 2 highlights the distribution of cells (marked with Hoechst 33342) within the unmodified (Fig. 2a) and modified (0.05M ED) (Fig. 2b) scaffolds. On the unmodified scaffold, there is minimal penetration of the NSCs within the scaffold. Furthermore the cells do not remain in their dissociated state, instead forming large spheres on the surface of the scaffold. In contrast, on the modified scaffold, the cells penetrate throughout the entire scaffold and remain dissociated. The greater cell interaction within the modified vs. unmodified scaffold is likely due to the increased hydrophilicity although the concurrent effect of changes in surface chemistry cannot be discounted. As a result there may either be a greater amount of adsorbed proteins on the modified surfaces or the conformation of proteins may be optimal for cell adhesion, spreading, and proliferation. As shown in Table 2, more cells adhered to modified than unmodified scaffolds in both proliferation and differentiation culture conditions. As expected, cells cultured in the mitogens - EGF/bFGF/heparin - had a significantly greater number of adhered cells than those cultured in the differentiating FBS media.

Table 2 – Cell number on the unmodified and modified scaffolds that were subjected to different culture conditions.

Material (PCL scaffold)	Culture condition	Mean cell number (per 84100 μm^2)
Unmodified	Mitogens	190 ± 50
Modified	Mitogens	480 ± 130
Unmodified	10% FBS	30 ± 15
Modified	10% FBS	14 ± 30

The results are reported as mean ± standard deviation (n = 9). ANOVA with pair wise Tukey's posthoc testing revealed all groups are significantly different apart from the cells cultured on the unmodified PCL scaffold in the presence of mitogens compared to the modified PCL in the presence of 10% FBS. $p < 0.05$

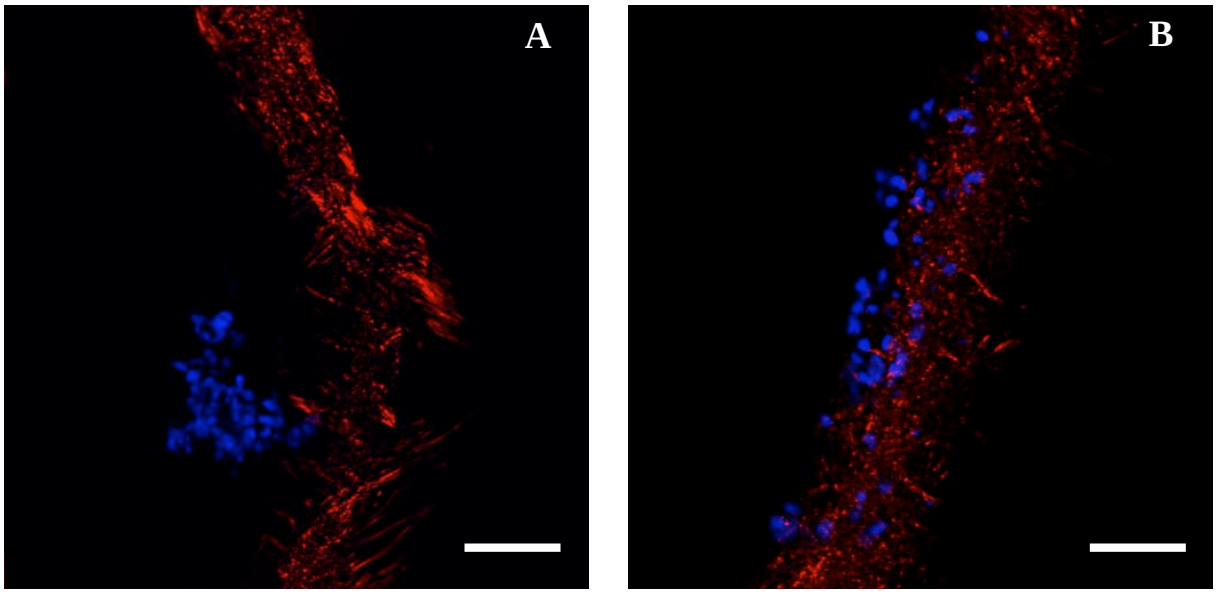

Fig. 2 – The blue represents the nuclei (stained with Hoechst 33342) of NSCs seeded on the PCL scaffolds (imaged using transmission – shown as red). A) A neurosphere is re-formed on the surface of the unmodified PCL scaffold. B) Cell spreading occurs throughout the PCL scaffold after modification with ED. Scale: 50 μm

To gain a greater perspective of the impact of aminolysation of PCL fibers on NSC differentiation, the cells were labeled with antibodies against GFAP (for astrocytes), CNPase (for oligodendrocytes), NF200 (for neurons) and nestin (for neural progenitor cells). As shown in Fig. 3, PCL modification did not impact stem cell differentiation. Interestingly, in differentiating serum, there was evidence of astrocytes,

oligodendrocytes, and neural progenitor cells, but not neurons on PCL scaffolds; however, in control samples cultured on laminin, there was evidence of neurons and the proportion of cells was different. Importantly, there were 75-80% oligodendrocytes on PCL fibers, which is significantly greater than the 40-41% oligodendrocytes on laminin controls. The differentiation to oligodendrocytes in the presence of serum was not significantly different on modified vs. unmodified PCL fibers, suggesting that PCL fibers promote the preferential differentiation to oligodendrocytes. Oligodendrocytes are important for remyelination, making this phenotypic response on PCL of interest. This process of remyelination has recently been observed after adult neural precursor cells were engrafted within the white matter of an injured spinal cord[28]. Delivery of NSCs to a damaged region within the CNS with a highly porous 3D scaffold may be a desirable approach for regeneration.

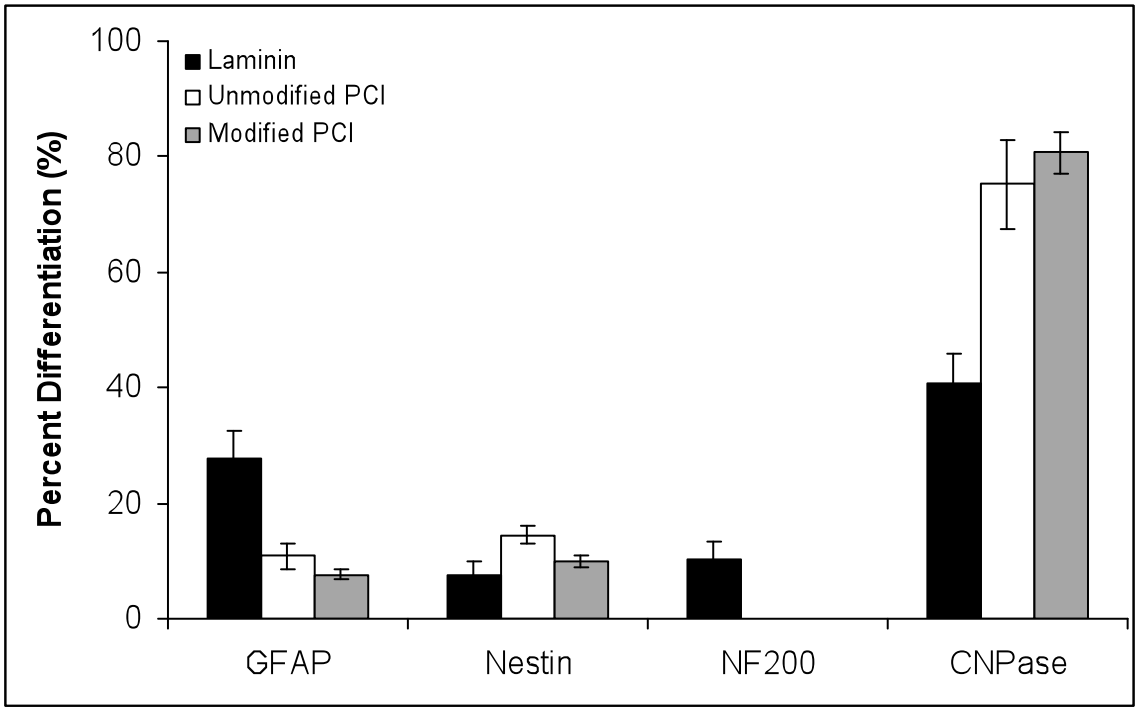

Fig. 3 – Stem cell differentiation on PCL scaffolds and controls cultured in the presence of serum after 7 days *in vitro*. GFAP stains for astrocytes, Nestin for neural progenitor cells, NF200 for neurons and CNPase for oligodendrocytes.

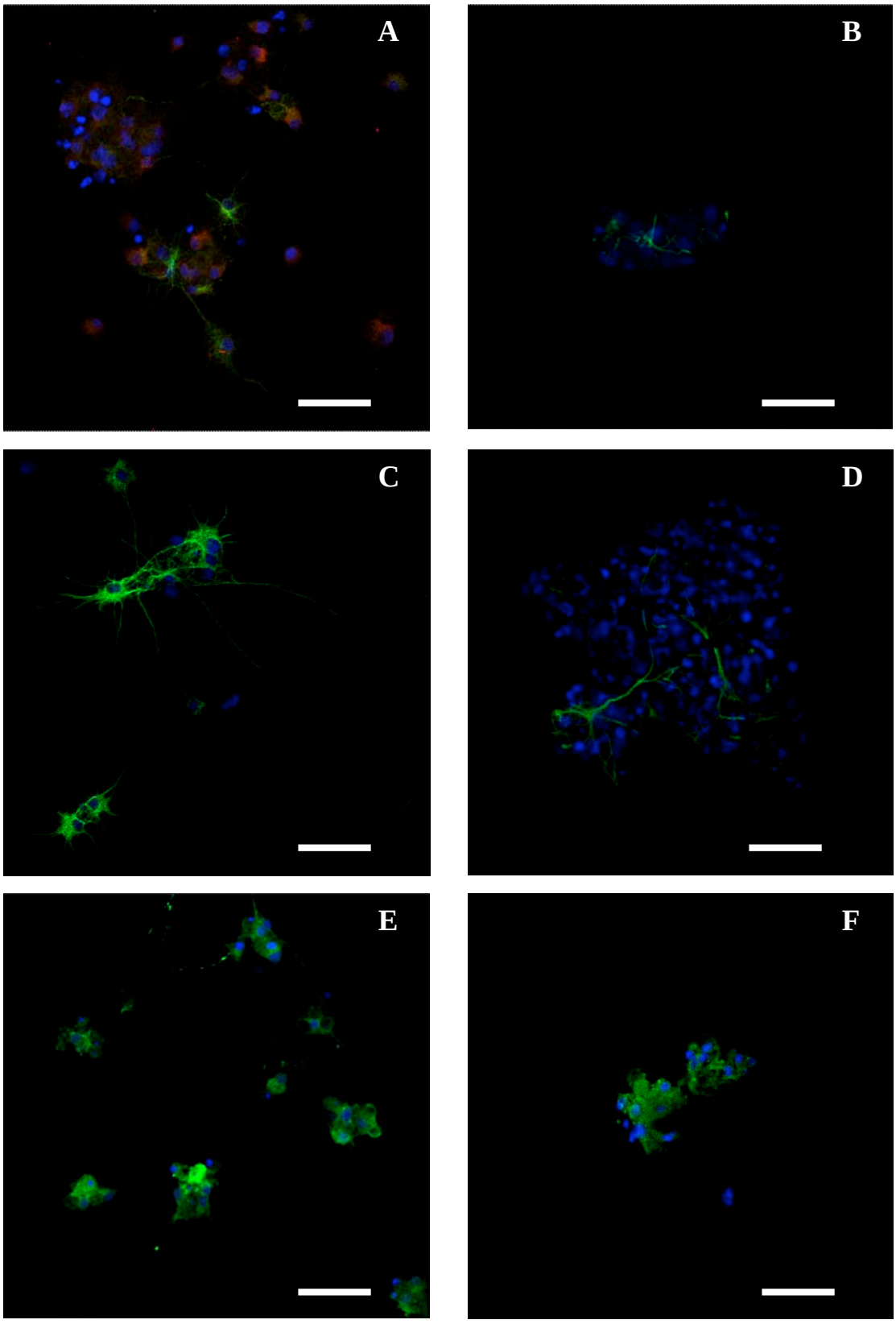
A
B
C
D
E
F

Fig. 4 –Morphology of the differentiated NSCs on the unmodified PCL scaffold culture in the presence of 10% FBS. The images have been pseudocolored. A) Control sample that was dual stained with nestin (Green) and NF200 (Red); B) NSCs cultured on the PCL scaffolds, which were also dual stained but only expressed nestin; C) Control sample that expresses GFAP (Green); D) NSCs cultured on the PCL scaffolds, which also expressed the GFAP marker; E) Control sample that expressed CNPase (Green); F) NSCs cultured on the PCL scaffold, which also expressed the CNPase marker. Scale: 50 μm.

While surface modification did not alter the differentiation profile of the NSCs (*cf.* Fig. 3), the morphologies of the differentiated NSCs cultured on the PCL scaffold were investigated and compared to laminin control sample using LSCM as shown in Fig. 4. Morphologies of the differentiated NSCs, as shown in Fig. 4, agree with the differentiation profile shown in Fig. 3. NSCs differentiated into neurons on laminin control as shown in Fig. 4A by NF200 staining, but no neurons were found on the PCL scaffold (see Fig. 4B). The morphology of astrocytes on laminin and PCL scaffolds have similarities, as shown in Fig. 4C and 4D. NSCs that have differentiated to astrocytes show long thin processes extending from cell bodies regardless of the culturing surface, i.e., laminin or PCL scaffold. However, there was increased cellular spreading on the 2D positive control (Fig. 4C) compared to the 3D PCL scaffold. This is possibly due to there being superior interfacial effects between the cells and the laminin 2D control. Furthermore the density of the cells seeded on the 2D control is much lower, which also results in the appearance of greater spreading. The morphology of the differentiated oligodendrocytes on laminin or PCL scaffold (as shown in Fig. 4E and 4F, respectively) are similar. Thus the differentiation study suggests that neither surface chemistry nor hydrophilicity of PCL has a significant influence on directing stem cell differentiation and morphology, but rather PCL fiber geometry has the dominant effect.

3.3.6 CONCLUSIONS

In this study, 3D non-woven PCL scaffolds were prepared by electrospinning and chemically modified with ED. While this surface modification did not influence NSC differentiation, it had a profound effect on the number of adherent cells. Interestingly PCL electrospun fiber scaffolds influenced the differentiation of NSCs primarily into oligodendrocytes, demonstrating lineage specificity as a function of the scaffold's physical and not chemical properties.

3.3.7 ACKNOWLEDGEMENTS

We are grateful to the Natural Sciences and Engineering Research Council of Canada and the Advanced Food and Materials Network (to MSS), the Australian postgraduate award, the Australasian Society for Biomaterials (ASB), and the Cooperative Research Centre (CRC) for Polymers (to DRN), and ARC Discovery (DP0663573) (to JSF) for funding. We thank Dr. Nic Leipzig for help in immunocytochemistry labeling and Dr. Ying Chen for cell culture support.

3.3.8 REFERENCES

1. Zhang Y-Z, Lim TC, Ramakrishna S, Huang Z-M. Recent development of polymer nanofibers for biomedical and biotechnological applications. Journal of Materials Science: Materials in Medicine 2005;16:933-946.

2. Mukhopadhyay G, Doherty, P., Walsh, F.S., Crocker, P.R., Filbin, M.T. A novel role for myelin-associated glycoprotein as an inhibitor of axonal regeneration. Neuron 1994;13:757-767.

3. Schmidt CE, Baier LJ. Neural tissue engineering: Strategies for repair and regeneration. Annual Review of Biomedical Engineering 2003;5:293-347.

4. McDonald JW. Repairing the damaged spinal cord. Scientific American 1999;281:65-73.

5. Langer R, Vacanti JP. Tissue Engineering. Science 1993;260:920-926.

6. Zhao M, Momma S, Delfani K, Carlen M, Cassidy RM, Johansson CB, Brismar H, Shupliakov O, Frisen J, Janson AM. Evidence for neurogenesis in the adult mammalian substantia nigra. Proc Natl Acad Sc 2003;100:7925-7930.

7. Gould E, Reeves AJ, Graziano MS, Gross CG. Neurogenesis in the neocortex of adult primates. Science 1999;286:548-552.

8. Wang TY, Sen A, Behie LA, Kallos MS. Dynamic behavior of cells within neurospheres in expanding populations of neural precursors. Brain Research 2006;1107:82-96.

9. Yang F, Murugan R, Ramakrishna S, Wang X, Ma Y, Wang S. Fabrication of nano-structured porous PLLA scaffold intended for nerve tissue engineering. Biomaterials 2004;25:1891-1900.

10. Harrison J, Pattanawong S, Forsythe JS, Gross KA, Nisbet DR, Beh H, Scott TF, Trounson AO, Mollard R. Colonization and maintenance of murine embryonic stem cells on poly(α-hydroxy esters). Biomaterials 2004;25:4963-4970.

11. Nisbet DR, Pattanawong S, Nunan J, Shen W, Horne MK, Finkelstein DI, Forsythe JS. The effect of surface hydrophilicity on the behaviour of embryonic cortical neurons. Journal of Colloid and Interface Science 2006;299:647-655.

12. Kim HS, Kim KH, Jin HJ, Chin IJ. Morphological characterisation of electrospun nano-fibrous membranes of biodegradable poly(L-lactide) and poly(lactide-co-glycolide). Macromol. Symp. 2005;224:145-154.

13. Lesvesque SG, Shoichet, M.S. Synthesis of cell-adhesive dextran hydrogels and macroporous scaffolds. Biomaterials 2006;27:5277-5285.

14. Madihally SV, Matthew, H.W. Porous chitosan scaffolds for tissue engineering. Biomaterials 1999;20:1133-1142.

15. Gupta D, Tator, C.H., Shoichet, M.S. Fast-gelling injectable blend of hyaluronan and methylcellulose for intrathecal localized delivery to the injured spinal cord. Biomaterials 2006;27:2370-2379.

16. Yang F, Murugan R, Wang C, Ramakrishna S. Electrospinning of nano/micro scale poly(L-lactic acid) aligned fibers and their potential in neural tissue engineering. Biomaterials 2005;26:2603-2610.

17. Smith LA, MaPX. Nano-fibrous scaffolds for tissue engineering. Colloids and Surfaces B: Biointerfaces 2004;39:125–131.

18. Chiu JB, Luu YK, Fang D, Hsiao B, Chu B, Hadjiargyrou M. Electrospun nanofibrous scaffolds for biomedical applications. Journal of Biomedical Nanotechnology 2005;1:115-132.

19. Silva GA, Czeisler C, Niece KL, Beniash E, Harrington DA, Kessler JA, Stupp SI. Selective differentiation of neural progenitor cells by high-epitope density nanofibers. Science 2004;303:1352.

20. Chua KN, Chai C, Lee PC, Tan YN, Ramakrishna S, Leong KW, Mao HQ. Surface-aminated electrospun nanofibers enhance adhesion and expansion of human umbilical cord blood hematopoietic stem/progenitor cel. Biomaterials 2006;27:6043–6051.

21. Morshead CM, Reynolds BA, Craig CG, McBurney MW, Staines WA, Morassutti D, Weiss S, van der Kooy D. Neural stem cells in the adult mammalian forebrain: a relatively quiescent subpopulation of subependymal cells. Neuron 1994;13:1071-1082.

22. Zahir T, Nomura H, XiaoDong G, Kim H, Tator C, Morshead C, Shoichet M. Bioengineering Brain-Derived Stem-Cell Coated Tubes For Spinal Cord Injury Repair. Cell Transplantaion 2007;Submitted.

23. Bergles DE, Roberts JD, Somogyi P, Jahr CE. Glutamatergic synapses on oligodendrocyte precursor cells in the hippocampus. Nature 2000;405:187.

24. Vazquez G, Alvarez E, Navaza JM. Surface tension of alcohol + water from 20 to 50 C. Journal of Chemical Engineering and Data 1995;40:611-614.

25. Nisbet DR, Pattanawong S, Ritchie NE, Shen W, Finkelstein DI, Horne MK, Forsythe JS. Interaction of embryonic cortical neurones on nanofibrous scaffolds for neural tissue engineering. Journal of Neural Engineering 2007;4:35-41.

26. Croll TI, O'Connor AJ, Stevens GW, Cooper-White JJ. Controllable surface modification of PLGA by hydrolysis or aminolysis 1: physical, chemical and theroretical aspects. Biomacromolecules 2004;5:463-473.

27. Aspler JS. Interactions of ink and water with the paper surface in printing. Nord. Pulp Paper Res. J. 1993;19:68-74.

28. Karimi-Abdolrezaee S, Eftekharpour E, Wang J, Morshead CM, Fehlings MG. Delayed transplantation of adult neural precursor cells promotes remyelination and functional neurological recovery after spinal cord injury. The Journal of Neuroscience 2006;26:3377-3389.

Chapter 4

Part I - Electrospinning

In vivo implantation

Contents

Declaration

One publication has been inserted into chapter 4. Below the reference information and publication status for this publication is provided.

Chapter 4.1

D. R. Nisbet, A. Rodda, M. K. Horne, J. S. Forsythe, D. I. Finkelstein, "Neurite inflitration and inflammatory response of electrospun polycaprolactone scaffolds implanted into the brain", *Acta Biomaterilia.*, manuscript in preparation, 2008.

Declaration for Thesis Chapter 4.1

Monash University

Declaration by candidate

In the case of Chapter 4.1 the nature and extent of my contribution to the work was the following:

Nature of contribution	Extent of contribution (%)
Experimental design and conduct and article writing	80

The following co-authors contributed to the work. Co-authors who are students at Monash University must also indicate the extent of their contribution in percentage terms:

Name	Nature of contribution	Extent of contribution (%) for students
A.E. Rodda	Assisted in experimentation & corrected manuscript	10
M.K. Horne	Experimental design and corrected manuscript	N/A
J.S. Forsythe	Experimental design and corrected manuscript	N/A
D.I. Finkelstein	Experimental design and corrected manuscript	N/A

Candidate's Signature	[redacted]	**Date** 14/10/2008

Declaration by co-authors

The undersigned hereby certify that:

(1) the above declaration correctly reflects the nature and extent of the candidate's contribution to this work, and the nature of the contribution of each of the co-authors.
(2) they meet the criteria for authorship in that they have participated in the conception, execution, or interpretation, of at least that part of the publication in their field of expertise;
(3) they take public responsibility for their part of the publication, except for the responsible author who accepts overall responsibility for the publication;
(4) there are no other authors of the publication according to these criteria;

(5) potential conflicts of interest have been disclosed to (a) granting bodies, (b) the editor or publisher of journals or other publications, and (c) the head of the responsible academic unit; and
(6) the original data are stored at the following location(s) and will be held for at least five years from the date indicated below:

Name	Location
A.E. Rodda	Monash University - Department of Materials Engineering
M.K. Horne	Melbourne University - Howard Florey Institute
J.S. Forsythe	Monash University - Department of Materials Engineering
D.I. Finkelstein	The Mental Health Research Institute of Victoria

Name	Signature	Date
A.E. Rodda		14/10/2008
M.K. Horne	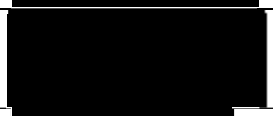	14/10/2008
J.S. Forsythe		14/10/2008
D.I. Finkelstein		14/10/2008

4.0 *In vivo* implantation

4.1 Evaluation of the cellular response to electrospun PCL implanted in the brain

The biocompatibility of neural tissue engineering scaffolds is reflected in the nature in which axons interacted and infiltrate it, coupled with the inflammatory response it elicits *in vivo*. All experiment thus far discussed in Part I of this thesis were performed *in vitro*, but neurite interactions and the resulting level of inflammation can only be assessed *in vivo*. While *in vitro* models are very useful for initial screenings they do not reflect the highly complex cellular interaction that occurs *in vivo*. In this study, electrospun PCL nanofibres, with differing nanofibre alignments, were implanted into the brain of adult rats and their interaction (both with endogenous neurites and within the brain architecture) and the extent of consequent inflammation were assessed.

Neurite infiltration and cellular response to electrospun polycaprolactone nanofibrous scaffolds implantated into the brain

D.R. Nisbet[a], A. Rodda [a], M.K. Horne [b], J.S. Forsythe [a], D.I. Finkelstein [c] *

a *CRC for Polymers, Department of Materials Engineering, Division of Biological Engineering, Monash University, P.O. Box 69M, Victoria 3800, Australia*

b *Florey Neuroscience Institute, Gate 11, Royal Parade and The Centre for Neuroscience, The University of Melbourne, Victoria 3010, Australia*

c *The Mental Health Research Institute of Victoria, Victoria 3010, Australia*

4.1.1 ABSTRACT:

An assessment of axonal infiltration and guidance within neural tissue engineering scaffolds, along with the inflammatory response are critical to determine their potential for facilitating neural repair. Here, the extent of microglial and astrocytic response was measured following implantation of electrospun poly(ε-caprolactone) (PCL) scaffolds into the caudate-putamen of the adult rat brain. The inflammation peaked at around 4 days (microglia) and then subsided to physiological resting levels by 60 days. There was no evidence of microglial encapsulation and indeed neurites had entered the implants, suggesting evidence of scaffold support for neural integration. While the inflammatory response was not influenced by the extent of alignment of the PCL fibres, the extent of neurites entry was. If porosity was large, as was the case with the randomly orientated polymer fibres, neurites could infiltrate and grow within the scaffold. However neuronal process could not penetrate scaffolds when fibres were partially aligned and instead, grew perpendicular to the direction PCL fibre alignment at the interface of the implant and brain tissue i.e. contact guidance was not provided. This investigation shows that electrospun PCL fibres are compatible with brain tissue and provide preliminary insights regarding the influence of microglia and astrocytes in neural integration within such scaffolds.

4.1.2 Keywords

Electrospinning, Neural tissue engineering, Nerve regeneration, *in vivo*, Inflammatory response, neurite.

4.1.3 Introduction

The central nervous system (CNS) is the primary computing area within the body and consists of the brain and spinal cord. It provides the avenue down which motor and sensory information (in the form of electrochemical stimuli) can be passed so that physiological responses desired by the brain can be carried out. While the signalling that underlies this integration is principally electrophysiological and neurochemical, the architectural substrate or "wiring", determined by the way that neurones and axons are connected, determines the effect and efficiency of this signalling. During development, the architecture is established by a highly complex set of guidance cues including cell-cell and cell-extracellular matrix (ECM) interactions and cytotrophic molecules, such as growth factors and guidance molecules.[1-3] When the CNS is damaged by injury or disease, these same factors are induced to re-establish connectivity but their efficiency is severely attenuated and consequently there is limited functional recovery of this complex cellular network. [4-7] As a consequence people with brain and spinal cord injury are left with many major functional disabilities. There are no effective treatments to facilitate neural repair within the adult mammalian CNS [3, 8, 9]; indeed, regeneration or repair of the neural circuitry is actively inhibited by the microenvironment surrounding damaged neurons and axons. [6, 10] Therefore much research, including this study, has focused on the development of neural tissue engineering materials and methods to fabricate permissive microenvironments for regeneration within the CNS.

Whist there are currently many different scaffold materials and designs available PCL nanofibres were selected for this study, due to *in vitro* evidence of the material's ability the support, maintain and control the differentiation of neural stem cells (NSCs). [8] Furthermore the fibres can be easily manipulated to more accurately simulate the native

ECM, through either manipulating the size and or alignment of the fibres. The effect on cellular interactions that results from nanofibre alignment is well reported. Briefly, aligned nanofibrous scaffolds have shown promise in many tissue engineering application including neural tissue engineering, where *in vitro* evidence indicates that they promote neural stem cell (NSCs) differentiation toward the neuronal lineage, and can also provide contact guidance cues and direct axonal outgrowth.[11] The neurites of DRG explants cultured with aligned polymer nanofibres initially grew radially outwards to contact the aligned nanofibres and then turned to follow the fibres.[12, 13] Furthermore, contact guidance is not exclusively controlled by fibre alignment as the diameter of the electrospun fibres also influences contact guidance of neurites [11]. Here, PCL nanofibres were implanted within the caudate putamen of rats to encourage neurite infiltration into the scaffolds *in vivo*. The immune response was also evaluated as a means of assessing the materials biocompatibility and in essence its usefulness as a scaffold for the treatment of CNS disorders such as spinal cord injury and Parkinson's disease.

Injury to the CNS induces an inflammatory reaction, characterised by a chemokine and cytokine response as well as a cellular reaction by astrocytes and microglia.[14-16] The inflammatory reaction consists of several phases which are required to minimise tissue injury and remove damaged cellular debris (the cytotrophic response) and subsequently to restore tissue integrity and cytoarchitecture (cytotrophic response). Part of inflammation is a host defence against foreign tissue and organisms and engages various components of the immune response. Introducing a foreign material such as a scaffold carries the risk of a similar defensive and rejection response. Candidate neural tissue engineering materials must be non-toxic, support tissue growth and have a controlled inflammatory response to provide cytotrophic support for regeneration, whilst also having an appropriate morphology and structure to encourage axonal infiltration.[17, 18]

The main cell types activated during the inflammation in the CNS are astrocytes and microglia, both having distinctly different functions. Microglia are very sensitive to small changes within the extracellular environment and are a component of active inflammation within the CNS[19], participating in phagocytosis of foreign matter that has

directly introduced to the brain [20] or that has crossed the blood-brain-barrier. The response to a stab wound to the brain, such as one required to introduce a scaffold, has two phases. The initial phase typically takes place over the first week and is present to undertake initial repair of breaches of tissue integrity and remove damaged or foreign tissue (by phagocytosis) . Microglia are CNS macrophages and are thus responsible for phagocyte and cytotoxic responses to tissue damage and foreign implanted biomaterials. This is often thought to be a negative or destructive component of inflammation because viable neural tissue can be damaged by a "bystander" effect. In the process of scavenging and phagocytosing debris, microglia excrete cytotoxic molecules to kill viruses, bacteria and neurones infected by viruses: many functioning bystander neurones are also damaged.[19, 20] However, cytotrophic properties of microglia are often overlooked but this phase is essential for regeneration and reconstitution of neural circuitry. After the first phase of cytotoxic inflammation has subsided (a duration of approximately 3 weeks), microglial cells undertake several processes that facilitate neuronal and axonal regeneration. They provide cytotrophic support through the excretion of anti-inflammatory cytokines and are also responsible for synaptic stripping, resulting in the removal of axonal branches locally near damaged tissue in an attempt to facilitate the regrowth of axons.[21] Therefore, to achieve regeneration within the CNS it is important to gain an understanding of the timing of microglial responses during the inflammatory process, and attempt to harness their cytotrophic behaviour while suppressing their cytotoxic effects.

Astrocytes can also have a cytotoxic influence during CNS repair as they too become phagocytic and ingest injured nerve cells. They also proliferate to form a glia scar to maintain the physical integrity of the CNS, but in the process can inhibit neurite outgrowth and circuit repair. This scar can act as a physical barrier to neurite penetration and can release biochemical molecules that inhibit neurite extension.[3] However, astrocytes also contribute a cytotrophic component to repair during inflammation. Astrocytes are responsible for metabolically supporting neurones, [3] as they provide nutrients such as glucose to these cells. They are also critical to the maintenance of the blood brain barrier as they biochemically support the endothelial cells. Astrocytes

undertake many other functions *in vivo*, some of which are not fully understood or even determined, however they are known to include; the expression and release of membrane transporters that are critical to many neurotransmitters;[22] the expression of potassium channels to control the ion levels within the CNS; they have been shown to influence synaptic transmission through quick morphological changes [23] and are involved in the modulation of neuronal blood flow;[24] and they support oligodendrocytes through promoting neurones to release ATP, which is an important stimuli to oligodendrocyte for the production of myelin.[25] Whilst astrocytes can elicit a cytotoxic reaction during inflammation, it is clear that they are also involved in many cytotrophic processes during the regeneration process. The extent and timing of the astrocyte response can provide an initial indication of the cytotoxic and cytotrophic contributions of astrocytes. This is required before commencing on an exhaustive description of the extracellular molecules that are adsorbing to the scaffolds. Measuring the size and timing of the response of astrocytes following the implantation of PCL within the CNS is an important first step in gaining an understanding of how and when to control or harness the reaction of astrocytes and encourage them to play a primarily cytotrophic role in regeneration.

This study investigates the cellular response after the implantation of nanofibrous electrospun scaffolds with different architectures within the caudate putamen of adult rats over different time points. The number of astrocytes, microglia and axonal infiltration was used to assess the potential of PCL nanofibres for neural tissue engineering of the CNS.

4.1.4 Materials and Methods

4.1.4.1 Materials

Poly(ε-caprolactone) (PCL) was purchased from Absorbable Polymers, Inc. (Alabama, USA). Solutions containing 10% w/v polymer were prepared by dissolving PCL in 5 ml of chloroform (Merck Pty Ltd, Australia) and methanol (Merck Pty Ltd, Australia) at a ratio of 75:25 (v/v). The solutions were placed into a 10 ml glass syringe with a 19-guage needle for electrospinning using a flow rate of 0.6 ml/h, an accelerating voltage of 15 kV and a working distance of 12 cm. The scaffolds were collected on an aluminum rotating mandrel (of diameter 5 cm) that rotated at 200 rpm to fabricate the randomly orientated fibres and 4000 rpm to fabricate partially aligned fibres. The nanofibrous scaffolds were then dried in a vacuum oven overnight at 30°C and stored in a desiccator.

4.1.4.2 Scaffold characterisation

The diameter and degree of fibre alignment of the electrospun scaffolds were characterised using scanning electron microscopy (SEM). They were gold coated using a sputter coater (Balzers SCD-005, BAL-TEC) with a 25 mA current for a total coating time of 180 s prior to imaging at 15 kV with the SEM (S-570 Hitachi Toyko, Japan). The diameter of 20 fibres from each sample was measured and averaged and preformed in triplicate. Image J (NIH version 1.32) software was used to measure the angle that 20 fibres from each sample made with the direction of rotation of the mandrel. These measurements were also conducted in triplicate. The percentage of fibres whose alignment with the direction of mandrel rotation was less than or equal to ± 15º was determined as a measurement of fibre alignment.

The surface tensions of the electrospun PCL scaffolds were determined using a modified contact angle measurement, suitable for 3D fibre matrices. The results were obtained

using VCA – optima^{TM} contact angle apparatus (AST products, Inc) at room temperature. As the electrospun scaffold were fibrous, surface tension was measured using a modified sessile drop of differing concentrations of isopropyl alcohol in milliQ water. This demonstrated the interaction between a drop of known surface tension and the scaffold. At a critical surface tension (determined by the specific concentration of the solution), there is no delay in absorption of the drop when it falls onto the surface of the electrospun scaffold. The surface tension of the scaffold was determined at this point when no absorption delay was evident.[26] Statistical analysis was conducted using SigmaStat for windows version 3.0.3©.

4.1.4.3 Animals

In this study a total of 105 male Wistar rats weighing approximately 300 grams were used. All experiments were approved by the Howard Florey Institute Animal Ethics Committee and conformed to the Australian National Health and Medical Research Councils codes of conduct.

4.1.4.4 Materials preparation of in vivo implantation

The nanofibrous membranes were cut into 5 mm square scaffolds, sterilised in 70% ethanol, rolled into a tight tube, inserted into a 21 gauge needle and stored in sterile falcon tubes prior to surgery.

4.1.4.5 In vivo implantation of PCL scaffold

Anaesthesia was induced with 0.25 ml of xylazine hydrochloride (20mg/ml, Toy Labs) and 0.1 ml of atropine in saline, followed by 4 % isoflurane gas, adminstered at 1.5 litres per minute in a closed container for 15 minutes. Rats were placed in a stereotaxic frame and holes were drilled in each side of the skull (from bregma: AP 1.0 mm, lateral

2.5mm). The needles containing the previously sterilised PCL scaffolds were then inserted through these holes to a depth of 7.5 mm below the skull so that most of the scaffold lay in the caudate putamen (CPu). A plunger was then inserted into the needle. This was designed so that as the needle was withdrawn, the scaffold would be extruded, thus remaining at the desired location. A sterilised platinum wire of the same length and diameter as the electrospun PCL scaffolds was inserted into the CPu of control animals. There was a separate control group who received no surgery. Animals were killed with (0.5 mg/g) sodium perntobarbitone (Letho-barb) and were perfused using 250 ml of 0.2M PBS at 37 ºC followed by 4 % paraformaldehyde (Sigma-Aldrich, Australia) at 4 ºC. The brains were then removed and placed in a 30 % sucrose/PBS mixture for 2 days. They where then snap frozen with liquid nitrogen and stored at -80 ºC. The brains were then mounted on a chuck and cut in 40 μm thick sections using a cryostat (Leica) in preparation for immunocytochemistry.

4.1.4.6 Immunocytochemistry

Previously described immunocytochemistry protocols were followed.[2, 9, 27, 28] Each section was baked onto gelatin coated glass slides at 37 °C for 2 hours. The sections were further fixed with 4 % paraformaldehyde for 1 min, washed in PBS (3 x 5 min) and non-specific antibody binding was blocked using a solution of 4% normal goat serum (NGS) and 0.1% Triton-X for 1h at room temperature. The following antibodies were used; rabbit anti-SMI 32 (1:500; Sternberger Monoclonals) for neurites; mouse anti-GFAP Cy3 conjugate (1:400; Sigma-Aldrich) for astrocytes and mouse anti-CD11b FITC conjugated (1:10; Chemicon) for microglia. The primary antibodies in a solution of PBS and 4 % NGS were reacted for 2 hours at 37 ºC. The sections were then washed (3 x 5 min) in PBS before the secondary antibody, AlexaFluor 488 (1:1000; Molecular Probes) was applied for 1 hour at 37 ºC for the SMI 32, all other primary antibodies were conjugated. The samples were again washed (3 x 5 min) in PBS. Dapi (VectorShield ©) was added and sections were coverslipped. The cells were imaged using a laser scanning confocal microscope (LSCM) (Olympus FV1000) with a 20X air lens.

4.1.5 Results and Discussion

4.1.5.1 Materials Characterisation

Two types of PCL scaffolds, one with random and the other with partially aligned non-woven nanofibres, were electrospun to determine if contact guidance of neurones could be achieved *in vivo*. Fibres were categorised as being partially aligned if they formed an angle of less than (±) 15° with the direction of rotation of the electrospinning mandrel. The scaffolds were deemed to be aligned, to a satisfactory level when over 40% of the nanofibres were partially aligned in the direction of mandrel rotation. In the case of the randomly orientated scaffolds, only 22% (n = 8) of the polymer nanofibres were aligned, compared to 47% (n = 8) for the partially aligned scaffolds. The average fibre diameter of the partially aligned scaffold (Figure 1 A) was 450 ± 100 nm and 350 ± 125 nm (n = 8) for the random scaffold (Figure 1 B). The surface tension of the scaffolds was independent of the fibre alignment and in both instances was 36 ± 2 dyn/cm. The two scaffolds are shown in Figure 1.

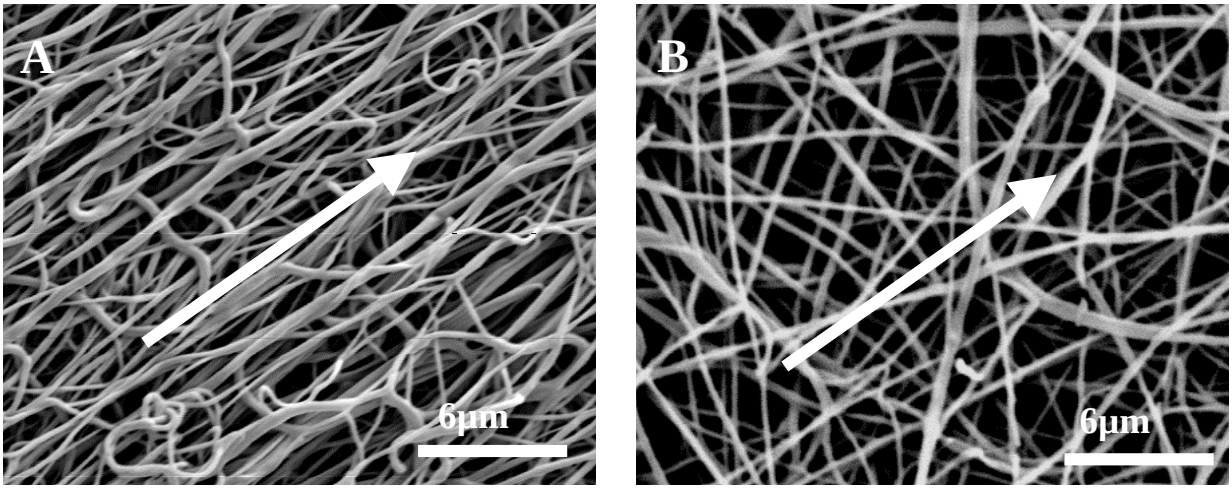

Figure 1 - Partially aligned (A) and random (B) electrospun PCL nanofibrous scaffolds. Arrow shows rotation direction of the mandrel.

4.1.5.2 Cellular response of nanofibrous PCL scaffolds within the caudate putamen

4.1.5.2.1 Experimental design

Animals were divided into 5 experimental groups according to the nature of the implant into the CPu: Partially aligned fibres (n=21), random fibres (n=21), platinum wire (control) (n=21), stab wound without implant (n=21) and non operated animals (n=3). The CPu was selected for the implantation because it is easily accessed by stereotaxic surgery, without causing the animal significant impairment of function. In the first four experimental groups, 3 animals were killed at one of the following intervals after implantation: 1, 3, 7, 14, 21, 28 and 60 days. In each animal, the inflammatory response was quantified by counting the number of microglia and astrocytes. The response to insertion of the scaffold was compared with that which followed a stab wound, insertion of a sterilised platinum wire and the un-operated animals. As the cellular response to random and partially aligned electrospun PCL scaffolds was similar, only the results form the random scaffolds will be described below.

4.1.5.2.2 Cellular response upon implantation of nanofibrous PCL scaffolds

Figure 2 is a 3D graph, plotting the number of activated microglia in the CPu against time (days) after implantation on one axis and distance from the scaffold on the other. Initially there is a large number of activated microglia but the response rapidly subsides to resting levels by approximately 21-28 days after surgery. The number of microglia in the resting CPu (i.e. the normal striatum) was 0.8 ± 0.5 microglia per 10,000 μm^2. In this study we saw no evidence of phagocytosed scaffold material within microglia.

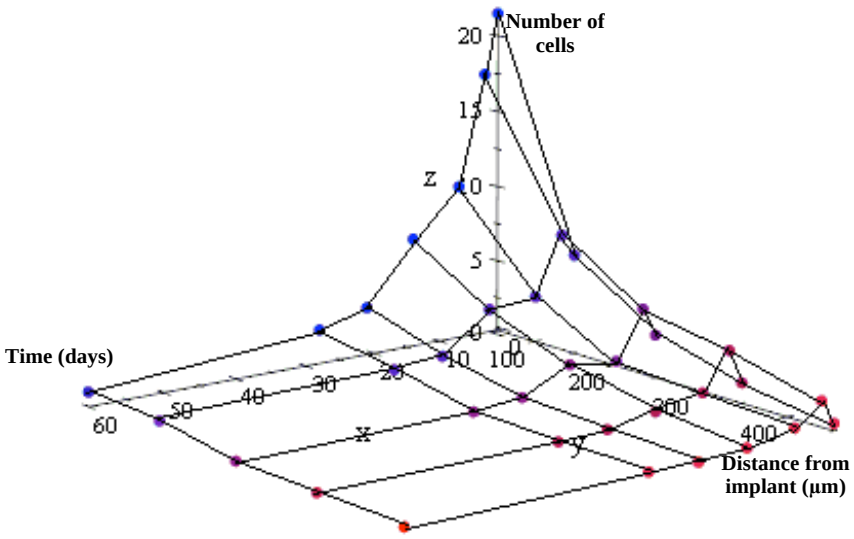

Figure 2 - 3D graph showing the number of activated microglia (z axis), plotted against time in days after implantation (x axis) and distance from the randomly aligned PCL scaffold in µm (y axis). Errors are not included because their presence obscured the figure but the errors in cell number (y direction) for each data point were not greater than ± 2.7 (standard deviation (SD)), apart from day 1 at a distance of 0 – 100 µm from the implant (the first and largest data point) where the error was ± 8 (SD).

Most microglia were within 100 µm of the PCL scaffold (Figure 3 and 4). In Figure 3, this region from the animals with the PCL scaffold implanted and the two control animals (no surgery and the platinum wire) is compared. The number of activated microglia plateaus between 28 and 60 days and is similar to resting levels in animals with implanted scaffolds.

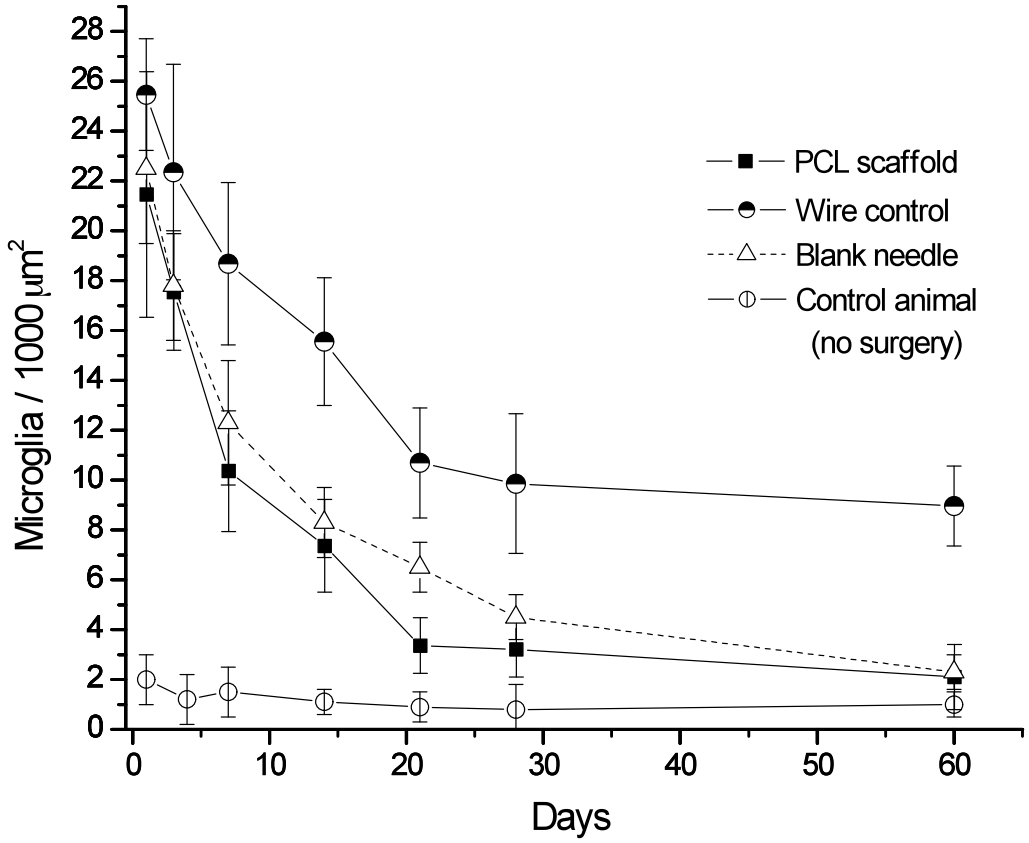

Figure 3 - The number of activated microglia plotted against time after implantation in the region of brain that is less than 100 μm from the scaffold or wire.

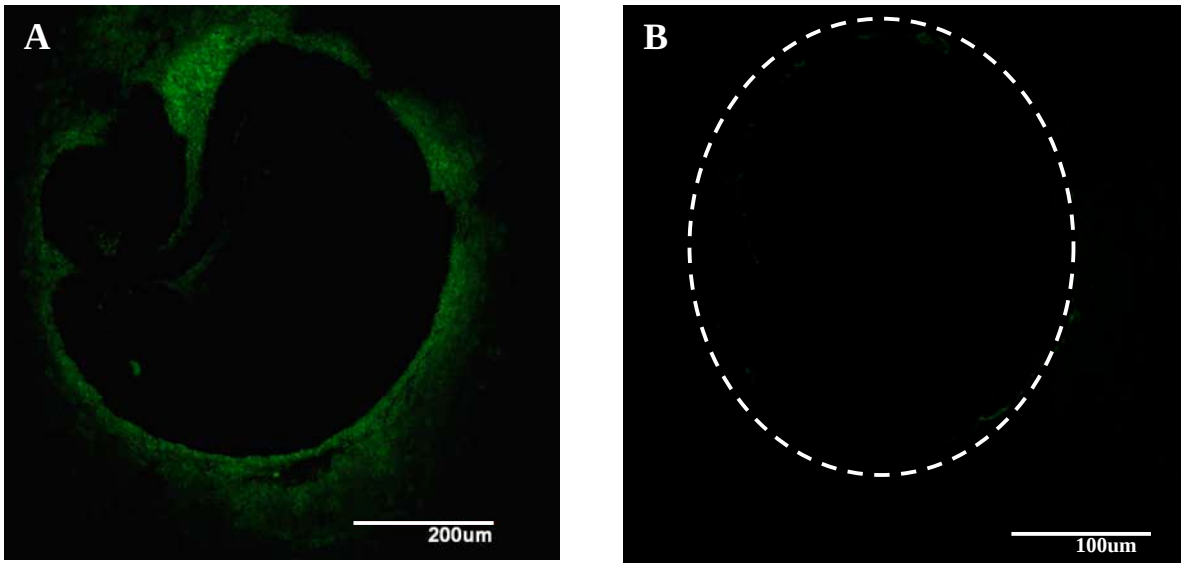

Figure 4 – Confocal images of activated microglia surrounding the randomly aligned PCL scaffold 1 day (A) and 60 days (B) after implantation. The scaffolds were sectioned perpendicular to the PCL fibres, which have not been imaged, hence appear as black amongst the positive microglia cells (green) in (A). Note in (B) there are no activated microglia, hence a white dotted line has been used to indicate the region of the implanted PCL scaffold.

Microglia respond rapidly to injury,[29] and migrate into an injury site before any changes in cell types were observed.[30, 31] This was the case in the present study, with the number of activated microglia peaking immediately within a day of implanting the PCL scaffolds (see figures 2 and 3). Furthermore the inflammatory response of the microglia was typical,[32] being characterised by cell migration towards the injury site and proliferation. This early and rapid increase in microglia density is most likely in response to tissue injury, especially as the response to sham surgery was similar in both cell number and duration of their presence.

Figure 3 also shows microglial reaction to implanted platinum wire control. The microglia remained activated and increased in number, even after 60 days. This is most likely because platinum wire has a higher compliance than surrounding brain; hence

movements cause local micro trauma to adjacent tissue. This is not the case with the electrospun PCL scaffolds *in vivo*.

Injury is also associated with an astrocytic response.[33-35] Following injury, astrocytes migrate and proliferate around an injury site. Their response is often later than the microglial response and associated with a cytotrophic process.[36, 37] Figure 5 is a 3D representation of the number of astrocytes following implantation of a randomly aligned PCL scaffold into the CPu. Astrocyte numbers are plotted against time (days) and different distance (um) from the scaffold. The initial activation of the astrocytes is a little slower than the microglia response, peaking approximately 3 days after implantation and remaining elevated for 14 days before subsiding. However, figure 6 shows that the astrocyte density remained elevated until some time between 28 and 60 days. Again, most activated astrocytes were close to the surface of the implanted PCL scaffold (within the first 100 μm, figure 7).

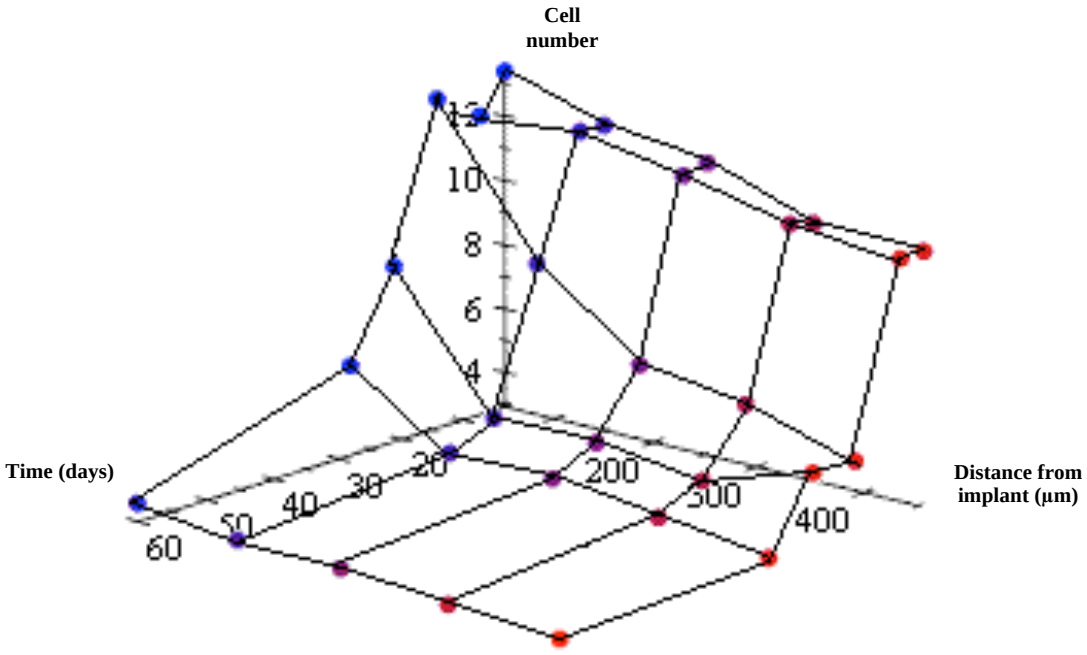

Figure 5 - 3D representation of the number of activated astrocytes (z axis), plotted against time in days after implantation (x axis) and distance in μm from the randomly aligned nanofibrous scaffold (y axis). Because day 1 measurements remained at

physiological resting levels they have not been plotted. Errors are not shown as they obscure the image. However, the errors (in y direction for cell number) for each data point were not greater than ± 2 (SD) for all data points.

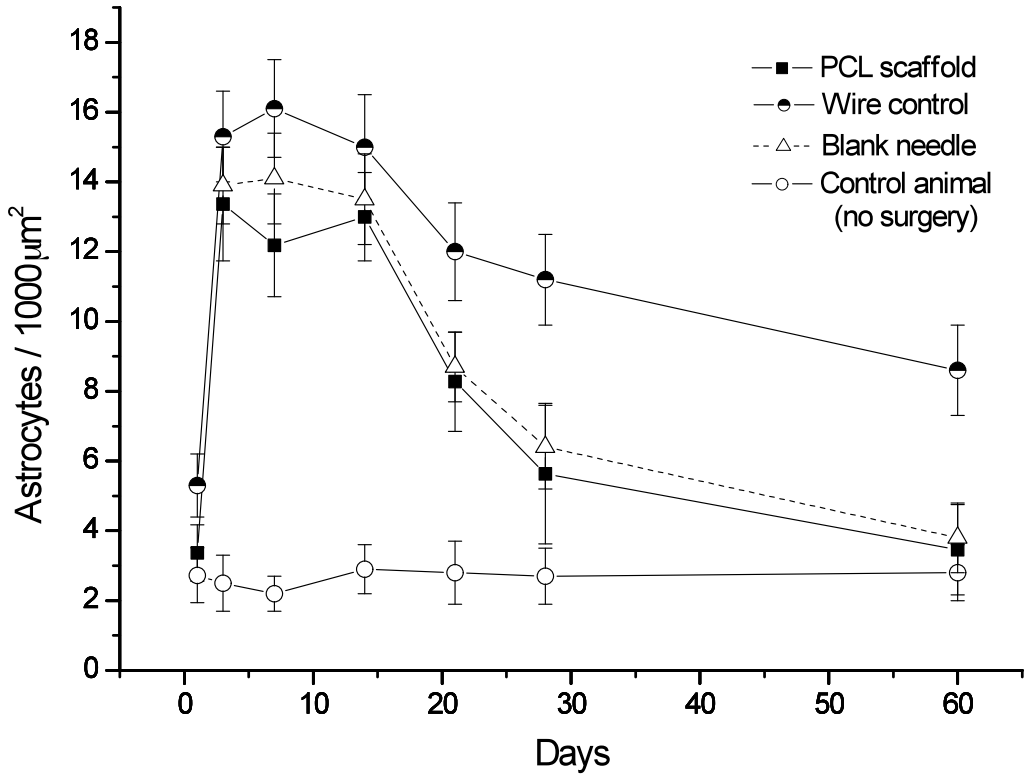

Figure 6 - Number of astrocytes plotted against time after implantation time in the region of brain that is less than 100 μm from the scaffold or wire.

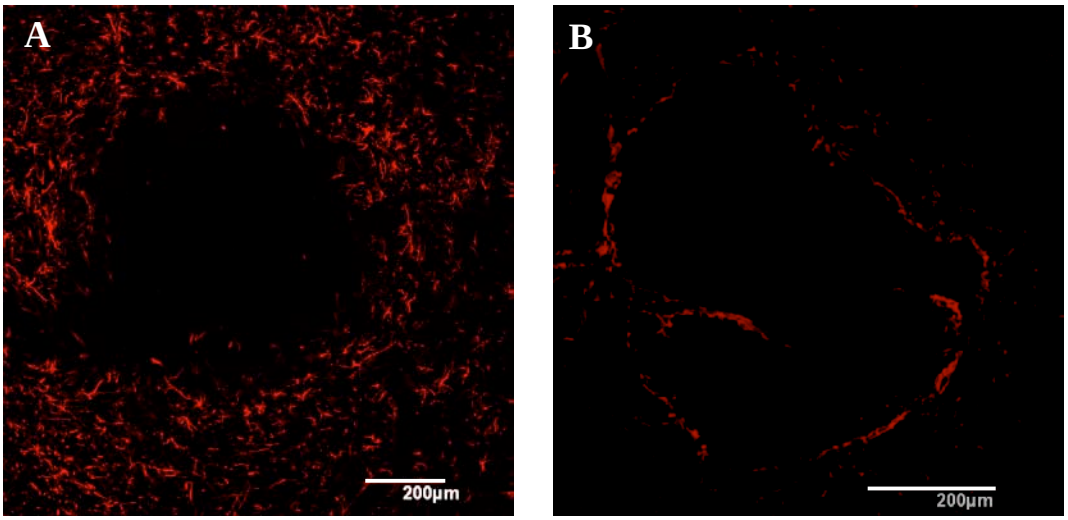

Figure 7 - Confocal images of astrocytes surrounding the randomly orientated nanofibrous scaffold 3 days (A) and 60 days (B) after implantation. The scaffolds were sectioned perpendicular to the PCL fibres, which have not been stained for using GFAP that was conjugated with Cy-3, hence appear red.

As has been reported previously, the response of astrocytes post-injury is characterised by hyperplasia and hypertrophy of the cell bodies (Figure 7).[31, 38] The role of astrocytes in neural repair remains under considerable debate within the neural tissue engineering field. Some studies have shown the proliferation of astrocytes during inflammation inhibiting neural repair, as the astrocytes produce cytokines that are toxic to neurones [39-42] and assist in the formation of scars that acts as a physical and biochemical barrier.[3] Alternatively, other research has shown that astrocytes have a positive persuade in the neural repair process. In these instances astrocytes facilitated neuronal sprouting[3, 34] and provide a cytotrophic effect on neurones through the excretion of growth factors and guidance molecules.[43, 44]

In the current work we have shown that excessive scarring has not formed from the implantation of nanofibrous PCL scaffolds (Figure 7), and after approximately 60 days the inflammation has subsided as the numbers of astrocytes have returned to physiological resting levels. This is significant considering that the astrocyte number remained elevated for more than 60 days in the case of the wire control. Furthermore,

this coupled with the fact that microglia are not attempting to engulf the scaffolds indicates that the PCL scaffold does not elicit a prolonged foreign body reaction.

The capacity for neurites to enter random and partially aligned PCL scaffold was examined (Figure 8A). Neurites were only observed entering randomly orientated (Figure 8A) and not into partially aligned nanofibrous scaffolds, where the nanofibres remained at the interface between the scaffold and adjacent brain parenchyma (Figure 8B & C). This is shown in a high magnification image of the interface between the electrospun PCL scaffold and the brain parenchyma (Figure 9) In this image the scaffold has been sectioned parallel to the fibre alignment and shows very few neurites growing in that direction. The most likely reason is the smaller interfibre distance of the partially aligned nanofibrous scaffold. When the neurites grew along the interface between the scaffold and the striatal parenchyma they cross the PCL fibres perpendicularly (shown schematically in Figure 8D).

Evidence of perpendicular contact guidance has been reported on surfaces of quartz plates presenting aligned groves of different widths and depths. CNS neuroblasts cultured on these surfaces extended processes perpendicular to the alignment of the groves when the spacing between them was less than 4 μm.[45] Contact guidance of CNS neuroblast in the direction of grove alignment was only evident when the groves had spacing greater than 4 μm.[45] We have also reported a similar response from primary cortical neurones cultured on electrospun scaffolds where the interfibre within different regions of scaffolds with random fibre alignment influenced the direction of neurite extension (i.e. perpendicular or parallel to the direction of the fibres).[28] Our study therefore provides valuable scaffold architectural information for guided axonal outgrowth in the CNS and raises the idea of building “ladder-like” structures to guide axons to target sites via perpendicular contact guidance.

The other interesting discovery was the timing of the neurites entering the scaffold. Endogenous neurites began to enter random scaffolds after approximately 7 days, corresponding with the decline in the number of activated microglia and the peak in

astrocyte numbers. Therefore, in this instance the role of microglia in neural repair may not be positive, as the cells may have been delivering neurotoxic signals. Hence, once the number of these cells began to decrease, and there was a maximum number of astrocytes present to deliver neurotropic signals to biochemically and physically support neurones, neurite extension into the scaffold began. The fact that neurite extension within the scaffolds occurred indicated that the electrospun PCL has integrated within the brain circuitry and is not being encapsulated by fibrous tissue.

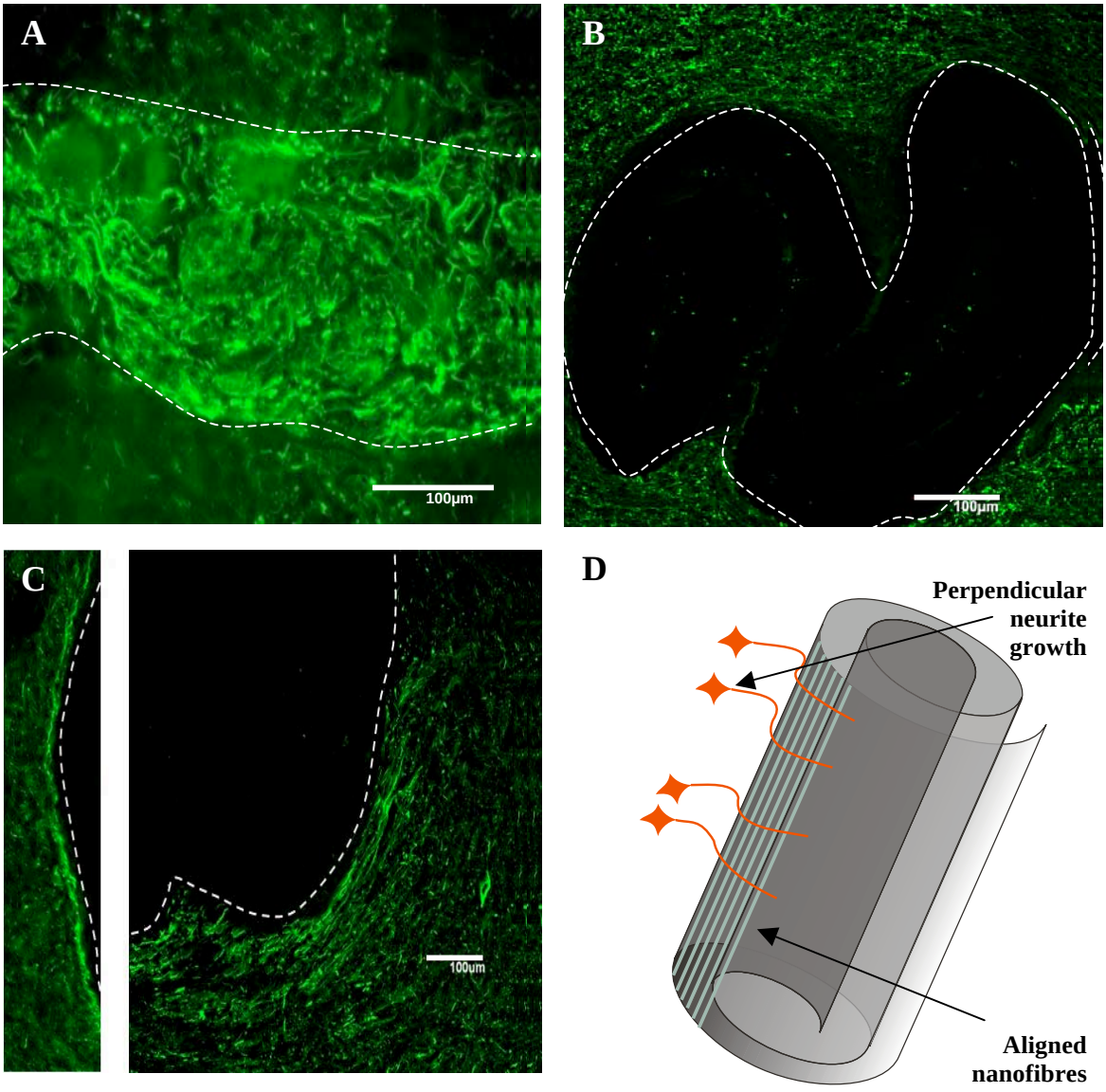

Figure 8 - Neurites interacting with the electrospun PCL scaffolds 60 days after implantation. The nanofibrous scaffolds have not been imaged and the neuritis have been stained with a 488 secondary antibody, hence neural growth appears green. A) PCL scaffold with random fibre alignment and has been sectioned parallel to the implantation to show the extent of neurite infiltration into the scaffold; B) partially aligned fibres sectioned perpendicular to the scaffold; C) is a split image (having the same scale bars) of higher magnification showing neuritis growing on an additional partially aligned fibrous scaffold ; and D) is a schematic of how the neurites are interacting with the partially

aligned fibres. The white dotted lines in the images represent the interface between the scaffold and the endogenous tissue.

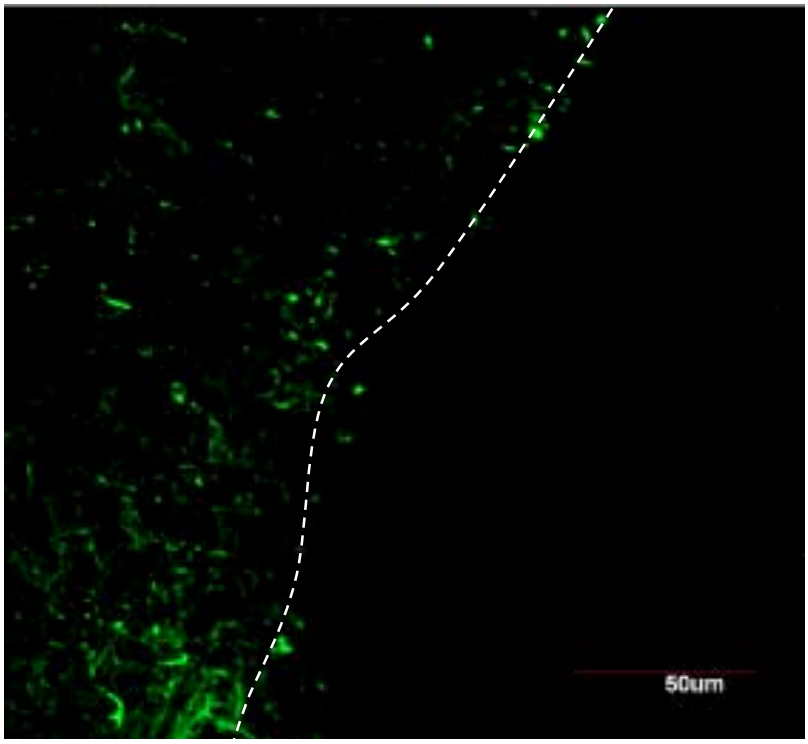

Figure 9 - Neurites interacting with a partially aligned nanofibrous scaffold that has been sectioned parallel to the fibre alignment. This image highlights that there is minimal evidence of neurite infiltration. The white dotted lines in the images represent the interface between the scaffold and the endogenous tissue.

4.1.6 Conclusion

In this investigation, partially aligned and randomly orientation PCL scaffolds were fabricated using electrospinning. These scaffolds were then implanted into the brain of adult rats and the resulting cellular response was measured. Microglial peak occurred 3

days after implantation, and had attenuated to resting levels by 28 days. Astrocytes' activation began later but peaked at a similar time to microglia, remaining elevated for 14 days, after which time the inflammation begins to subside. The astrocytes number remained elevated for longer than that of the microglia. However, after 60 days the scaffold was not encapsulated by fibrous tissue or a microglia scar and did not seem to elicit a foreign body reaction.

It was also discovered that neurites were able to infiltrate the randomly orientated electrospun scaffolds, but could not penetrate the partially aligned scaffolds. Interestingly, when endogenous neurites grew along the interface between the partially aligned nanofibrous scaffold and the brain tissue the neurites actually crossed the PCL fibres perpendicular to the direction of fibre alignment, ie. exhibiting perpendicular contact guidance, consistent with some other *in vitro* studies.[28, 45]

The timing when the endogenous neurites entered the randomly orientation PCL scaffold was also investigated. Neurites began to infiltrate the scaffold after approximately 7 days. This time also correlated to when the number of activated microglia was beginning to decline, whilst correlating to the maximum number of astrocytes activation. Therefore, it is possible that the role of microglia in neural repair may not be positive, as the cells may have been delivering neurotoxic signals and that it is only when there are many astrocytes delivering neurotropic signals to biochemically and physically support neurones that neurite infiltration begins. This discovery is being investigated further.

4.1.7 Acknowledgements

We are grateful to the Australian postgraduate award and the Cooperative Research Centre (CRC) for Polymers (to DRN), and ARC Discovery (DP0663573) (to JSF) and the CRC (to AER) for funding.

4.1.8 References

[1] H.W. Cheng, T. Jiang, S.A. Brown, G.M. Pasinetti, C.E. Finch, McNeill, Response of Striatal Astrocytes to Neural Deafferentation: An Immunocytochemical and Ultrastructural Study, Neuroscience, 62 (1994) 425-439.

[2] D.R. Nisbet, S. Pattanawong, J. Nunan, W. Shen, M.K. Horne, D.I. Finkelstein, J.S. Forsythe, The Effect of Surface Hydrophilicity on the Behaviour of Embryonic Cortical Neurons, J Colloid Interface Sci, 299 (2006) 647-655.

[3] D.R. Nisbet, K.E. Crompton, M.K. Horne, D.I. Finkelstein, J.S. Forsythe, Neural Tissue Engineering of the CNS Using Hydrogels – a Review, J Biomed Mater Res B Appl Biomater, 87 (2008) 251-263.

[4] Y.-Z. Zhang, T.C. Lim, S. Ramakrishna, Z.-M. Huang, Recent Development of Polymer Nanofibers for Biomedical and Biotechnological Applications, Journal of Materials Science: Materials in Medicine, 16 (2005) 933-946.

[5] G. Mukhopadhyay, Doherty, P., Walsh, F.S., Crocker, P.R., Filbin, M.T., A Novel Role for Myelin-Associated Glycoprotein as an Inhibitor of Axonal Regeneration, Neuron, 13 (1994) 757-767.

[6] C.E. Schmidt, L.J. Baier, Neural Tissue Engineering: Strategies for Repair and Regeneration, Annual Review of Biomedical Engineering, 5 (2003) 293-347.

[7] J.W. McDonald, Repairing the Damaged Spinal Cord, Scientific American, 281 (1999) 65-73.

[8] D.R. Nisbet, L.M.Y. Yu, T. Zahir, J.S. Forsythe, M.S. Shoichet, Characterization of Brain-Derived Stem Cells on Electrospun Poly(ε-Caprolactone) Submicron Scaffolds: Evaluating Their Potential in Neural Tissue Engineering., Journal of Biomaterials Science Polymer Edition, 19 (2008) 623-634..

[9] D.R. Nisbet, D. Moses, J.S. Forsythe, D.I. Finkelstein, M.K. Horne, Enhancing Neurite Outgrowth from Primary Neurones and Neural Stem Cells Using Thermoresponsive Hydrogel Scaffolds for the Repair of Spinal Cord Injury, Journal of Biomedical Materials Research - Part A, In Press (2008) 10.1002/jbm.a.31962.

[10] R. Langer, J.P. Vacanti, Tissue Engineering, Science, 260 (1993) 920-926.

[11] F. Yang, R. Murugan, C. Wang, S. Ramakrishna, Electrospinning of Nano/Micro Scale Poly(L-Lactic Acid) Aligned Fibers and Their Potential in Neural Tissue Engineering, Biomaterials, 26 (2005) 2603-2610.

[12] J.M. Corey, D.Y. Lin, K.B. Mycek, Q. Chen, S. Samuel, E.L. Feldman, D.C. Martin, Aligned Electrospun Nanofibers Specify the Direction of Dorsal Root Ganglia Neurite Growth, Journal of Biomedical Materials Research Part A, 83 (2007) 636-645.

[13] E. Schnell, K. Klinkhammer, S. Balzer, G. Brook, D. Klee, P.D. Dalton, J. Mey, Guidance of Glial Cell Migration and Axonal Growth on Electrospun Nanofibers of Poly-ε-Caprolactone and a Collagen/Poly-ε-Caprolatone Blend, Biomaterials, 28 (2007) 3012-3025.

[14] K.E. Crompton, D. Tomas, D.I. Finkelstein, M. Marr, J.S. Forsythe, M. Horne, Inflammatory Response on Injection of Chitosan/GP to the Brain, J Mater Sci - Mater Med, 17 (2005) 633-639.

[15] M.J. Smith, D.C. Smith, K.L. White, G.L. Bowlin, Immune Response Testing of Electrospun Polymers: An Important Consideration in the Evaluation of Biomaterials, Journal of Engineered Fibers and Fabrics, 2 (2007) 41-47.

[16] A.M. Fagan, F.H. Gage, Mechanisms of Sprouting in the Adult Central Nervous System: Cellular Resonses in Areas of Terminal Degeneration and Reinnervation in the Rat Hippocampus, Neuroscience, 58 (1994) 705-725.

[17] T.K. Borg, It's the Matrix!, The American Journal of Pathology, 164 (2004) 1141-1142.

[18] L.G. Griffith, M.A. Swartz, Capturing Complex 3D Tissue Physiology *In Vitro*, Nature Reviews: Molecular cell biology, 7 (2006) 211-224.

[19] J. Gehrmann, Y. Matsumoto, G.W. Kreutzberg, Microglia: Intrinsic Immunoeffector Cell of the Brain, Brain Research Reviews, 20 (1995) 296-287.

[20] F. Aloisi, Immune Function of Microglia, Glia, 36 (2001) 165-179.

[21] M.R. Ritta, E. Banin, S.K. Moreno, E. Aguilar, M.I. Dorrel, M. Friedlander, Myeloid Progenitors Differentiate into Microglia and Promote Vascular Repair in a Model of Ischemic Retinopathy, Journal of Clinical Investigation, 116 (2006) 3266-3276.

[22] M. Santello, A. Vloterra, Synaptic Modulations by Astrocytes Via Ca($^{2+}$) Dependent Glutamate Release, Neuroscience, Early View (2008) doi:10.1016/j.neruoscience.

[23] R. Piet, L. Vargova, E. Sykova, D. Poulain, S. Oliet, Physiological Contribution of the Astrocytic Environment of Neurons to Intersynaptic Crosstalk, Proc Natl Acad Sci, 101 (2004) 2151-2155.

[24] R. Parri, V. Crunelli, An Astrocyte Bridge from Synapse to Blood Flow, Nature Neurosciece, 6 (2003) 5-6.

[25] T. Ishibashi, K. Dakin, B. Stevens, P. Lee, S. Kozlov, C. Steward, R. Fields, Astrocytes Promote Myelination in Response to Electrical Impulses, Neuron, 49 (2006) 823-832.

[26] G. Vazquez, E. Alvarez, J.M. Navaza, Surface Tension of Alcohol + Water from 20 to 50 °C, Journal of Chemical Engineering and Data, 40 (1995) 611-614.

[27] D.R. Nisbet, L.M.Y. Yu, T. Zahir, J.S. Forsythe, M.S. Shoichet, Characterization of Brain-Derived Stem Cells on Electrospun Poly(ε-Caprolactone) Submicron Scaffolds: Evaluating Their Potential in Neural Tissue Engineering., Journal of Biomaterials Science Polymer Edition, 19 (2008) 623-634..

[28] D.R. Nisbet, S. Pattanawong, N.E. Ritchie, W. Shen, D.I. Finkelstein, M.K. Horne, J.S. Forsythe, Interaction of Embryonic Cortical Neurones on Nanofibrous Scaffolds for Neural Tissue Engineering, Journal of Neural Engineering, 4 (2007) 1-7.

[29] W.J. Streit, The Role of Microglia in Brain Injury, Neurotoxicology 17 (1996) 671–678.

[30] G.W. Kreutzberg, Microglia: A Sensor for Pathological Events in the CNS, Trends in neuroscience, 19 (1996) 312–318.

[31] D. Stanic, W. Tripanichkul, J. Drago, D.I. Finkelstein, M.K. Horne, Glial Responses Associated with Dopaminergic Striatal Reinnervation Following Lesions of the Rat Substantia Nigra Brain Research, 1023 (2004) 83-91.

[32] M.B. Jensen, B. Gonzalez, B. Castellano, J. Zimmer, Microglial and Astroglial Reactions to Anterograde Axonal Degeneration: A Histochemical and Immunocytochemical Study of the Adult Rat Fascia Dentata after Entorhinal Perforant Path Lesions, Experimental Brain Research, 98 (1994) 245-260.

[33] H. Asada, N.Y. Ip, L. Pan, N. Razack, P. M.M., P. R.J., Time Course of Ciliary Neurotrophic Factor MRNA Expression is Coincident with the Presence of Protoplasmic Astrocytes in Traumatized Rat Striatum, , J Neurosci Res, 40 (1995) 22-30.

[34] P.E. Batchelor, G.T. Liberatore, J.Y. Wong, M.J. Porritt, F. Frerichs, G.A. Donnan, D.W. Howells, Activated Macrophages and Microglia Induce Dopaminergic Sprouting in the Injured Striatum and Express Brain-Derived Neurotrophic Factor and Glial Cell Line-Derived Neurotrophic Factor., J Neurosci, 19 (1999) 1708-1716.

[35] K.M. Guthrie, A.G. Woods, N. T., C.M. Gall, Astroglial Ciliary Neurotrophic Factor MRNA Expression is Increased in Fields of Axonal Sprouting in Deafferented Hippocampus, , J Comp Neurol, 386 (1997) 137-148.

[36] O. Isacson, W. Fischer, K. Wictorin, D. D., A. Bjorklund, Astroglial Response in the Excitotoxically Lesioned Neostriatum and its Projection Areas in the Rat, Neuroscience, 20 (1987) 1043–1056.

[37] J.N. Kay, M. Blum, Differential Response of Ventral Midbrain and Striatal Progenitor Cells to Lesions of the Nigrostriatal Dopaminergic Projection, Developmental Neuroscience, 22 (2000) 56–67.

[38] C.L. Parish, Finkelstein, D.I., Tripanichkul, W., Satoskar, A.R., Drago, J. and Horne, M.K., The Role of Interleukin-1, Interleukin-6, and Glia in Inducing Growth of Neuronal Terminal Arbors in Mice, J Neurosci, 22 (2002) 8034-8041.

[39] G.T. Liberatore, D.I. Finkelstein, J.Y. Wong, M.K. Horne, M.J. Porritt, G.A. Donnan, D.W. Howell, Sprouting of Dopaminergic Axons after Striatal Injury: Confirmation by Markers Not Dependent on Dopamine Metabolism, Exp Neurol, 159 (1999) 565–573.

[40] R.B. Banati, J. Gehrmann, P. Schubert, G.W. Kreutzberg, Cytotoxicity of Microglia, Glia, 7 (1993) 111-118.

[41] P.E. Batchelor, D.W. Howells, CNS Regeneration: Clinical Possibility or Basic Science Fantasy, Journal of Clinical Neuroscience, 10 (2003) 523-534.

[42] X. Yu, R.V. Bellamkonda, Dorsal Root Ganglia Neurite Extension is Inhibited by Mechanical and Chondroitin Sulfate-Rich Interfaces., J Neurosci Res, 66 (2001) 303-310.

[43] P.E. Batchelor, G.T. Liberatore, M.J. Porritt, G.A. Donnan, D.W. Howells, Inhibition of Brain-Derived Neurotrophic Factor and Glial Cell Line-Derived

Neurotrophic Factor Expression Reduces Dopaminergic Sprouting in the Injured Striatum, Eur J Neurosci, 12 (2000) 3462–3468.

[44] P.E. Batchelor, M.J. Porritt, P. Martinello, C.L. Parish, G.T. Liberatore, G.A. Donnan, D.W. Howells, Macrophages and Microglia Produce Local Trophic Gradients That Stimulate Axonal Sprouting toward but Not Beyond the Wound Edge, Mol Cell Neurosci, 21 (2002) 436–453.

[45] I. Nagata, A. Kawana, N. Nakatsuji, Perpendicular Contact Guidance of CNS Neuroblasts on Artificial Microstructures, Development, 117 (1993) 401-408.

Part II
Hydrogel

Chapter 5

Part II - Hydrogel

Literature Review

Contents

Declaration

One publication has been inserted into chapter 5. Below the reference information and publication status of this publication is provided.

Chapter 5.1

D.R. Nisbet, K.E. Crompton, M.K. Horne, D.I. Finkelstein, J.S. Forsythe, "Neural tissue engineering of the CNS using hydrogels – A Review", *J. Biomed. Mat. Res*, 87B, pp 251-263, 2008.

Declaration for Thesis Chapter 5.1

Monash University

Declaration by candidate

In the case of Chapter 5.1 the nature and extent of my contribution to the work was the following:

Nature of contribution	Extent of contribution (%)
Planning, research and article writing..	45

The following co-authors contributed to the work. Co-authors who are students at Monash University must also indicate the extent of their contribution in percentage terms:

Name	Nature of contribution	Extent of contribution (%) for students
K.E. Crompton	Planning, research and article writing.	45
M.K. Horne	Assisted in planning & corrected manuscript	N/A
D.I. Finkelstein	Assisted in planning & corrected manuscript	N/A
J.S. Forsythe	Assisted in planning & corrected manuscript	N/A

Candidate's Signature	[redacted]	**Date** 14/10/2008

Declaration by co-authors

The undersigned hereby certify that:

(1) the above declaration correctly reflects the nature and extent of the candidate's contribution to this work, and the nature of the contribution of each of the co-authors.
(2) they meet the criteria for authorship in that they have participated in the conception, execution, or interpretation, of at least that part of the publication in their field of expertise;
(3) they take public responsibility for their part of the publication, except for the responsible author who accepts overall responsibility for the publication;
(4) there are no other authors of the publication according to these criteria;

(5) potential conflicts of interest have been disclosed to (a) granting bodies, (b) the editor or publisher of journals or other publications, and (c) the head of the responsible academic unit; and
(6) the original data are stored at the following location(s) and will be held for at least five years from the date indicated below:

Name	Location
K.E. Crompton	Monash University - Department of Materials Engineering
M.K. Horne	Melbourne University - Howard Florey Institute
D.I. Finkelstein	The Mental Health Research Institute of Victoria
J.S. Forsythe	Monash University - Department of Materials Engineering

Name	Signature	Date
K.E. Crompton		14/10/2008
M.K. Horne	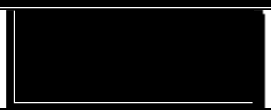	14/10/2008
D.I. Finkelstein		14/10/2008
J.S. Forsythe	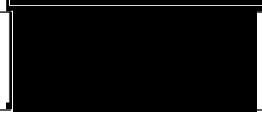	14/10/2008

5.0 Literature Review

5.1 Hydrogels for neural tissue engineering applications.

Chapter 5 is the first chapter in Part II of this thesis. It consists of a literature review of hydrogel scaffolds that have been utilised in neural tissue engineering applications. This article begins by providing a brief introduction into the neuroscience involved in neural tissue engineering by introducing the importance of the growth cone, glia and glia scars and cell adhesion molecules. It is touches on how adhesion factors and the physical environment can also influence nerve regeneration. The remainder of the article is a literature review of both natural and synthetic hydrogels that have been used in neural tissue engineering. One of the naturally derived hydrogels is xyloglucan which is the focus of Part II of this thesis.

Neural tissue engineering of the CNS using hydrogels – A Review

D.R. Nisbet[a,b,1], K.E. Crompton[a,b,1], M.K. Horne[c],
D.I. Finkelstein[d], J.S. Forsythe[a,b*]

a. Department of Materials Engineering, Monash University, Wellington Rd, Clayton, VIC 3800, Australia
b. CRC for Polymers, 32 Business Park Drive, Notting Hill, VIC 3168, Australia
c. Howard Florey Institute, The University of Melbourne, VIC 3010, Australia
d. The Mental Health Research Institute of Victoria, 155 Oak Street, Locked Bag 11, Parkville, VIC 3052, Australia

5.1.1 ABSTRACT

Current therapies have limited capacity to curtail disease progression or damage of the central nervous system (CNS) of adult mammals and successful regeneration following injury or disease does not occur. Regeneration of the CNS is limited by physical and chemical inhibitory barriers within the injured environment and the absence of positive cues that elicit and guide repair. Neural tissue engineering strategies focus on developing scaffolds that artificially generate favourable cellular microenvironments that attempt to tip the balance in favour of regeneration. Some recent advances using scaffolds to promote regeneration within the CNS, particularly in conjunction with stem cells, has generated promising results. This review focuses on hydrogel scaffolds which have been used extensively in neural tissue engineering applications and addresses the physical and chemical modifications of these materials to promote nerve regeneration

5.1.2 KEY WORDS

Neural tissue engineering, Nerve regeneration, Hydrogel, Central nervous system

5.1.3 INTRODUCTION

Physical injury to the CNS and chronic neurodegenerative diseases (e.g. Parkinson's Disease and Alzheimer's disease) disrupt brain architecture, resulting in loss of neuronal cell bodies, axons and associated glia support. In the case of haemorrhage, ischaemia and trauma, there is often associated disruption to blood supply. The functional consequences are severe because the CNS has limited capacity (and in some sites none) to replace neurones lost through injury or disease and because of the associated inflammatory response which results in glial scarring. This inflammation is characterised by microglial infiltration and subsequent astrocyte proliferation. It is the combination of this glia scarring, with an attenuated neuronal proliferative response that limits the capacity for the CNS to repair itself following trauma or other CNS disorders that induce inflammation. Neurones of the peripheral nervous system (PNS) have a greater capacity than CNS neurones to regrow axons after damage.[1] The contrasting capacities have been attributed to the growth permissive Schwann cells in the PNS and the growth inhibitory environment of the oligodendrocytes in the CNS.[2]

For newly formed neurones to participate in repair they must become incorporated into functional brain circuitry. This will be the case for both intrinsically derived neurones or those implanted as part of cell based therapies. There must be cues and signals for cell migration, acquisition of the relevant neuronal phenotype, axon guidance to the relevant target and synapse formation. While these cues may be present in the developing brain, they will be largely absent in the adult CNS, where reparative and proliferative process are suppressed. In other adult organs, such as the gut, skin, blood and liver, replacement and repair occurs through the regulated provision of adult stem cells by the microenvironment of stem cell niches.[3-5] The regulatory balance between suppression and proliferation is provided by support cells and basement membranes in the immediate proliferative environment. In the case of the adult brain, the support cells, namely oligodendrocytes and astrocytes are heavily biased toward suppression of proliferation and axon growth.[6] Thus the challenge facing tissuing engineering of the CNS is to

overcome the obstacles of lack of a proliferative source of cells, lack of guidance cues and excess inhibition. This review initially focuses on the biochemical and biophysical factors that are known to induce axon extension and guidance, specifically gradients of trophic signalling factors, cell surface signals, interactions with extracellular matrix (ECM) molecules and the physical environment. The review then sets out to examine hydrogel scaffolds used in neural tissue engineering, highlighting how biochemical and biophysical cues have been incorporated into these structures.

5.1.3.1 THE GROWING AXON

Most information about chemical guidance cues comes form studies of the development of the nervous system.[7] During development, neurones first migrate to their appropriate locations and then send out axons to make connections with targets. Various environmental cues guide these migrating neurones and growing axons. The tip of the extending neurite, known as a growth cone (GC), is enlarged and has many protrusions, or filopodia, which are supported by microfilaments. The entire GC area is sensitive to the local environment, but it is the filopodia that react negatively or positively to these cues. GC extension is cyclical, through search, displacement and rest phases rather than steady progression.[8] During the search and displacement phases, filopodia retract when positive cues are absent, or to negative cues, such as a glial scar tissue or inhibitory molecules. Extension of the neurite toward the appropriate growth-inducing chemicals in its environs is known as chemotaxis.[9] These chemical signals are gradients of diffusible trophic factors but may also be chemicals bound to cell surfaces or ECM.[9] These are collectively known as guidance molecules but adhesion molecules that regulate adhesion of the GC and their microspikes to their substrate can regulate elongation of the neurite but also guide direction, usually by cell to cell adhesion.[10]

5.1.3.2 GUIDANCE MOLECULES

There are several important ligand-receptor pairs that guide axons and neurones in

development. Four classical guidance molecules include semaphorins, netrins, NoGo and the ephrins.[10,11] Also growth factors , neurotrophins, neurotransmitters, cytokines and changes in calcium can either guide or act as regulators of axonal outgrowth. [12-14] Recently morphogens such as the wnts have also been recognized as having guidance capacity.[15] It is outside the scope of this review to touch on all of these candidates and the interested reader is directed to the following excellent reviews.[16-20] However from a tissue engineering point of view the classic guidance molecules hold the most interest. This is because they are anchored along the path of the growing GC and form gradients or cues to repel or attract the neurite. NoGo in particular has received considerable attention for the repair of the CNS. NoGo is expressed on the surface of oligodendrocytes that form myelin and has a powerful repulsive effect on GCs.[21-26] Myelin does not form early in the developing brain, but is plentiful in the adult brain. During development the presence of the various types of NoGo receptor are present before the developing axons arrives in its target area, and acts to arrest growth when the target has been reached.[27] Adult mammalian axons cannot spread across oligodendrocytes because of myelin associated glycoprotein (MAG) and NoGo. Following injury to the adult brain, administration of NoGo-A blocking reagents enhances regeneration, compensatory sprouting, structural reorganization and functional recovery.[26,28] The receptor complex for myelin derived proteins consist of at least three elements: the p75 receptor (p75NTR), the NoGo receptor and LINGO-1.[29] These receptor molecules activate the RhoA and Rho kinase intracellular pathways, which are major regulators of axonal extension.[30] Rho activation arrests axon growth, and its suppression permits axonal extension and may thus be an important mediator of repair.

5.1.3.3 ADHESION FACTORS AND THE PHYSICAL ENVIRONMENT

Adhesion factors also promote axon growth. At the simplest level, this is an interaction between the GC and the substrate, with the rate of extension a reflection of how strongly F-actin filaments in the GC adhere with the substrate: axons extend more readily on substrates that bind F-actin strongly. Differential adhesion can therefore direct growth

and this selective adhesion can occur through cell-cell interactions via Cell adhesion Molecules (CAMs), or through cell-substrate interactions via (SAMs). There are in fact a relatively large number of CAMS that are specific to certain pathways and neurone types. These include molecules such as amalgam, fasciclin II, Ng-Cam and contactin. These are found in specific neurones and specific tracts and even at specific times in pathfinding. [15,17,31-34] With respect to axon guidance, laminin and fibronectin are two important SAMs. Both can promote the adhesion and extension of neurites and bind with the integrin receptor protein. Binding with integrins induces the clustering of a number tyrosine protein kinase and activation of intracellular signalling.[35] Mechanical stimuli also provide cues for neurite growth. This is most apparent in tissue culture, where mechanical and structural cues can be readily studied but are probably equally important *in vivo*. For instance the pioneering work by the Bellamkonda group showed a definitive relationship between hydrogel pore size and neurite outgrowth.[36] Substrate elasticity influences focal-adhesions and the cyctoskeleton, and is a key factor in regulating stem cell differentiation and proliferation.[37] For example, when mesenchymal stem cells were grown on soft substrates with stiffness similar to that of brain tissue, the cells exhibited neuronal phenotype.[37] Substrate elasticity also regulates neurite outgrowth although it is unresolved as to whether neurite outgrowth increases with decreasing hydrogel stiffness [38,39] or decreases.[40] Confounding factors may be unintentional changes in ligand density upon changes in hydrogel crosslink density as well as differences in neuronal phenotype.

5.1.3.4 GLIA AND GLIA SCARS

Microglia provides both neurotrophic signals to aid axon guidance [41] and cell survival as well as neurotoxic signals that lead to cell death especially in the immediate aftermath of injury. Microglia are also sources of trophic factors including the Glial cell line-Derived Neurotrophic Factor (GDNF) and the neurotrophins. Astrocytes and oligodendrocytes also provide important signals that guide and also inhibit axon outgrowth.[26] When a GC reaches these landmark cells, the filopodia of the GC penetrate the landmark cell. The meaning of this event is not clear but it is likely that it induces a change in the molecular expression at the surface of the GC and or neurite so that it responds differently to the

cues surrounding it. For example, astrocytes guide dopaminergic (DA) neurite outgrowth, both *in vitro,*[42] and *in vivo,*[41] and this observation has been used to argue that the growth of astrocytes into the matrix results in the consequent growth of neurites into a synthetic hydrogel.[43] The other important consequence of injury in the adult CNS is the aggregations of oligodendrocytes, which as discussed above inhibit axon extension. Glia scars are composed of fibrous astrocytes with interwoven processes and basement membrane proteins such as collagen type IV and chondroitin sulfate proteoglycans.[44,45] The glia scar can be considered to act as a mechanical and biochemical barrier [45] suppressing regeneration in the CNS, although there is some debate as to the relative contributions of each.[44] Hydrogels have been useful in constructing *in vitro* models of glia scars. For instance neurite extension is inhibited when presented with elasticity mismatches (mechanical barrier) or chondroitin sulphate-rich (biochemical barrier) hydrogel interfaces. [45]

5.1.4 HYDROGEL SCAFFOLDS

Hydrogels may be classified as either natural or synthetic in origin. They have many advantages over alternative scaffold materials, such as high oxygen and nutrient permeabilities and low interfacial tensions. The latter attribute minimises barriers to cells migrating into the scaffold from surrounding soft tissue, or processes from cells within or out of the material crossing the scaffold-tissue boundary.[46] The morphology of hydrogel scaffolds used in neural tissue engineering are generally macroporous or become macroporous after degradation, to allow room for neurite outgrowth. The mechanical properties of hydrogels are similar to those of soft tissue so that the load on cells in the area will be distributed normally and cells within the gel receive appropriate structural growth cues. The elasticity of hydrogels is also tuneable by controlling the crosslink density. Another advantage of many hydrogels is that they easily conform to any defect shape, whilst they can be functionalised to include NTs for the control of neuronal cell adhesion, proliferation and axonal extension. Cell replacement therapies in the CNS may also greatly benefit using hydrogels that provide artificial 3D stem cell niches for

controlled proliferation and differentiation – an area of considerable activity in regenerative medicine.

Testing tissue engineering scaffolds, including hydrogels, for their viability, functionality and the influence on the differentiation characteristics of cells *in vitro* and i*n vivo* underpins neural tissue engineering. This review does not cover the use of animal models in evaluating the effectiveness of scaffolds in neurobiological studies. However the authors direct interested readers to the following reviews concerning scaffolds and animal models used in for nerve regeneration. [44,47,48]

5.1.5 Biologically derived hydrogels

Many biologically derived hydrogels have similarities to substances found in the body (for example polysaccharides and glycosaminoglycans GAGs), which enhances their biocompatibility in neural tissue engineering applications. Furthermore, natural materials generally have intrinsic biological activity, hence in some cases may provide appropriate signalling to cells without the need to add growth factors. They are also more likely to be degraded by naturally occurring enzymes. The main class of naturally occurring hydrogels is polysaccharides.

5.1.5.1 Agarose

Agarose is a linear polysaccharide derived from red algae. It is often used for three dimensional cell cultures, as it is biocompatible with many cell types. Agarose has been employed in neural tissue engineering [36,49,50] with good results and its gel properties optimised, such as stiffness, porosity (both composition related) [39,51] and biocompatibility. Bellamkonda *et al.* [36] optimised the concentration (1 w/v%) of agarose for neurite extension. PC12 cells and chick dorsal root ganglia (DRG) produced neurites averaging 900 μm in length, and in three-dimensions (3D), when cultured within this hydrogel for 4 days. Agarose can also be used to guide cell adhesion and neurite

outgrowth in vitro.[52] The biocompatibility of agarose scaffolds were also improved by immobilising various laminin oligopeptides, increasing the gels capacity to promote neurite extension.[52,53] Freeze-dried agarose containing nerve growth factor (NGF) was used in vitro [54] and encouraged axonal regeneration within the CNS. Stokols et al. incorporated brain-derived neurotrophic factors (BDNF) into freeze dried agarose scaffolds which promoted axonal growth through the scaffold in a linear fashion.[50] Agarose hydrogels containing microtubules that release BDNF were inserted across the defect in a lesioned rat spinal cord and neurites extended into the scaffold.[55] This suggests that agarose scaffolds can induce axonal regeneration that will cross an injury site. However, a major disadvantage of agarose for tissue engineering is that it is not biodegradable.

5.1.5.2 Alginate

Alginate is a negatively charged linear polysaccharide [51] that forms a gel when divalent cations such as Ca^{2+} are added and is well-established in tissue engineering applications.[56-59], including its use in peripheral nerve repair. Schwann cells seeded on alginate gels, remained viable whilst inducing neurite extension from DRG cells seeded within the scaffold.[60,61] Consequently alginate gels were employed to transport Schwann cells into a nerve guidance conduit.[62] However, contradictory evidence over the usefulness of alginate for Schwann cells prevents its broader use in the PNS.[61] Because of properties such as biodegradability, biocompatibility, hydrophilicity and low toxicity, alginate hydrogels have also been used to fill cavities caused by injury to spinal cords.[63,64] A 2 mm gap between two ends of a completely transected infant rat spinal cord was bridged by regenerating axons following implantation of cross-linked alginate sponge. Axons grew into the implant without assistance of implanted growth factors, while glial numbers, and consequent glial scar formation, decreased.[65] The mechanism of alginate action was not determined. Aliginate gels have a net negative charge which inhibits protein adsorption and reduces cellular adhesion, however bioactive molecules such as arginine-glycine-aspartic acid (RGD) and fibronectin have been immobilized within the hydrogel to facilitate improved adhesion of cells.[61,66]

5.1.5.3 Xyloglucan

Xyloglucan is a structural polysaccharide of the cell walls of all higher plants.[67,68] The neutrally charged β-1,4-linked D-glucan backbone of xyloglucan is partially substituted at the *O-6* position of its glucopyranosyl residue with α-D-xylopyranose residue. In tamarind seed xyloglucan, this latter residue is partially substituted at the *O-2* position with *β-D*-galactopyranose residue (in which case the branch may also be known as (1,2)-*β-D*-galactoxylopyranose). [69-71] Modification of xyloglucan with fungal *β*-galactosidase causes thermal gelation at physiological temperatures when the removal ratio of galactose residue is larger than 35%.[68,70] The gelation of xyloglucan occurs by the hydrophobic associations of the glucan backbone, hence the gelation properties can be easily modified by changing the galactose removal ratio. During gelation, xyloglucan forms flat structures caused by the lateral stacking of rod-like chains.[68] The authors have begun to investigate the response of embryonic cortical neurones on xyloglucan scaffolds that have been modified with immobilized poly-$_L$-lysine. Preliminary studies show that functionalization with polylysine may control and optimize the cell number, diameter, migration and the neurite density. The interaction of xyloglucan scaffold with neural stem cell (NSC) cultures is also being investigated to establish whether xyloglucan is useful in controlled development of NSCs *in vitro* (Figure 1 M.K. Horne Personal Communication).

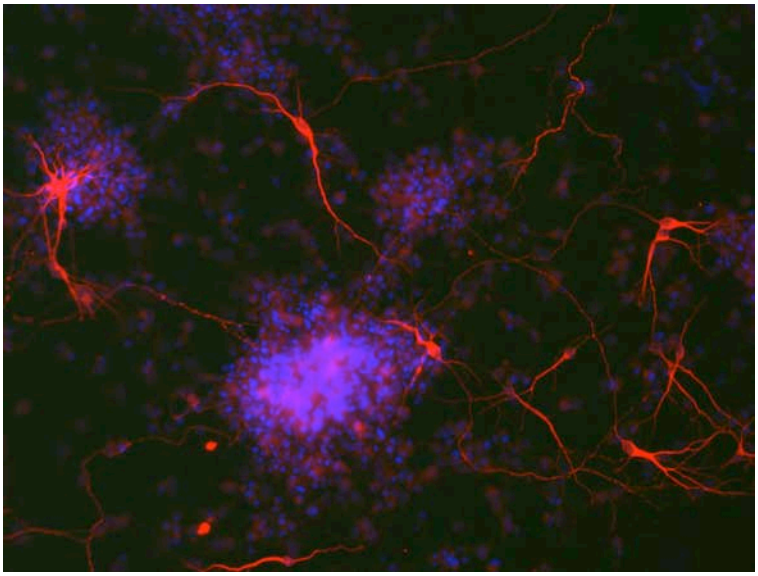

Figure 1 Epi-fluorescence images of neurospheres cultured on 2D samples of 100% xyloglucan-graft-PDL, with an immobilisation of approximately 1 PDL molecule per galactose residue. The red is a positive neuronal stain (βIII-tubulin) and the blue is a positive stain for cell nuclei.

5.1.5.4 Methylcellulose

Cellulose is a hydrophilic water-insoluble crystalline material. It can be modified with a hydrophobic side-group, such as a short saturated hydrocarbon, that allows aqueous dissolution and thermo-responsive gelation. Methylcellulose is the most simple, and common of these. The methyl group is substituted, often heterogeneously, along the backbone to attain a certain degree of substitution characterising the system (it is usually between 1 and 2). The gelation is a kinetic process that produces a turbid, phaseseparated gel.[72] The temperature of gelation is normally around 60 °C or higher, [73] but can be reduced by altering composition and salt content to make it more physiologically useful.[74,75] Methylcellulose induces a minimal inflammatory response when injected to a brain lesion but does not easily adsorb proteins and is thus relatively non-bioactive.[74] However, the bioactivity of methylcellulose can be increased through binding of adhesive molecules such as laminin.[75]

Methocel A is a 2% methylcellulose system accepted by the FDA [76] for use as a nerve guide for the peripheral nervous system.[76] Its effectiveness was enhanced when used with platelet-derived growth factor (PDGF). The biocompatibility of methylcellulose with astrocytes and neurones was evaluated using a ratio of live to dead cells (rather than neurite outgrowth) and found to be biocompatible in a range of compositions.[74] The *in vivo* biocompatibility was determined by injecting the gel into rats brains at room temperature and allowing it to gel within the organ at 37 °C.[74] Inflammation in the area injected with methylcellulose was no greater than that around the control injections and it was concluded that methylcellulose was suitably biocompatible for use in the brain. Unfortunately, methylcellulose is not readily broken down in closed tissue compartments.[76]

5.1.5.5 Hyaluronan

Hyaluronan (hyaluronic acid, hyaluronate) is a high molecular weight glycosaminoglycan (GAG) found naturally in the ECM of humans, primarily in mesenchymal tissue and the CNS.[77] It is negatively charged and comprised of alternating glucuronic acid and N-acetylglucosamine. Hyaluronan hydrogels support the proliferation and viability of Schwann cells, and have been used in conjunction with nerve guidance conduits for peripheral nerve repair, in a similar fashion to aliginate gels.[60,78,79] More recently, it was implanted as a solid sponge to treat traumatic brain injury.[80] Hyaluronan alone was not very successful, but when modified with between 10-25% polylysine, neurones moved into the scaffold, forming long neurites *in-vitro*, and when implanted *in-vivo* the neurones were accompanied by astrocytes. Various chemical modifications have been made to hyaluronan in order to vary its properties. These include esterification (a material commercially known as Hyaff), [81] crosslinking the gel to modify mechanical properties,[82,83] binding with gelatin [84] or collagen [85] to further mimic ECM molecules, or with polyethylene glycol (PEG) derivatives for improved gelation.[86] The esterified hyaluronan Hyaff resorbs within around 90 days of subcutaneous implantation to rats, depending on the chemistry of the hyaluronan.[81] Hyaluronan has also been modified with biological molecules to increase the probability of neural repair on implantation. In

particular, Tian and co workers [87] prevented inhibition of neural repair via NoGo receptors by attaching a receptor antibody to the hyaluronan hydrogel.

5.1.5.6 Chitosan

Chitosan is a (1,4)-linked 2-amino-2-deoxy-β-D-glucan [88], produced by alkaline deacetylation of chitin (N-acetyl-D-glucosamine). Chitin is a structural polysaccharide found in crab shell and many shellfish. The degree of deacetylation (DD), and therefore the positive charge affects cell adhesion, as DD increases, inflammation decreases and biocompatibility increases.[89,90] Chitosan is enzymatically biodegraded by lysozyme.[91,92] Lysozyme acts at the acetylated groups [93] with degradation slowed by higher degrees of deacetylation.[90,91,94] Chitosan has been used in encapsulation devices, which protect non-

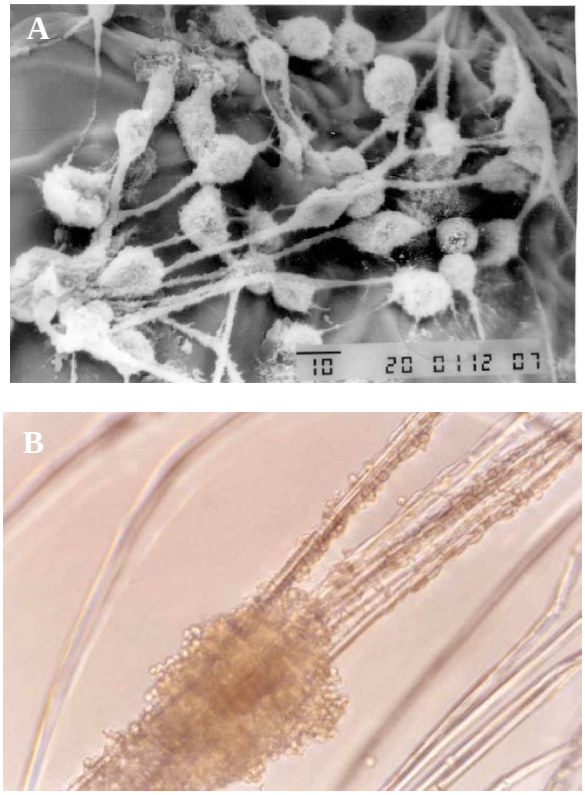

Figure 2 A) is an SEM micrograph of Schwan cells that have been cultured on a chitosan membrane. They have a round morphology with many microvilli. B) respresents Schwann cells that have been cultured on chitosan fibers for 7 days. Reference, reproduced by permission from Elsevier[69]

autologous implanted cells from the immune system.[95,96] Zielinski *et al.* showed that a chitosan matrix, inside an encapsulating sheath for example, immobilised PC12 cells.[96] They further showed that, *in-vitro*, PC12 cells embedded in the material and exposed to nerve growth factor sent neurites out through the matrix. Hence, although the cell bodies of neurones were immobilised in the chitosan matrix, the neurites could penetrate and potentially form synapses. Chitosan supports the growth in culture of neurones and glia, including Schwann cells [97], although C17.2 neuronal stem cells did not survive.[98] Although the viability of nerve cells on chitosan could be improved, neurite outgrowth was not as well supported.[99,100] Chitosan channels have been employed for spinal cord injuries and repair of the sciatic nerve has been documented in rodents [101] and dogs.[102] Schwann cells have also been transplanted in chitosan tubes, which improved peripheral nerve repair (Figure 2). [103]

Chitosan mixed with basic polyol salts such as glycerophosphate (GP) salt remains in solution at neutral pH at room temperature but importantly, becomes thermally responsive upon heating to 37 °C.[90,104] The authors recently cultured foetal mouse cortical neurones in 2D and 3D chitosan/GP hydrogels.[105] Cell adhesion and neurite extension were dramatically improved with the immobilisation of polylysine at an optimum concentration of 0.1%. The morphology of neurones also more closely resembled neurones *in vivo* when cultured in 3D. However, chitosan activates macrophages through the receptor-mediated binding of Nacetylglucosamine, increasing the inflammatory response.[106-108] This will limit its applications as a scaffold in the CNS. It will most likely be rapidly resorbed and the presence of activated microglia may substantially and possibly adversely affect the response of neurones.[108]

5.1.5.7 Matrigel

The introduction of Schwann cells is known to promote spinal cord and peripheral nerve regeneration,[109-111] and in most instances, poly(acrylonitrile-co-vinyl chloride) PAN/PVC tubes are deployed when filled with Schwann cells mixed with Matrigel™.[111,112]

Matrigel™ is the trade name of a product produced by BD Biosciences, which is a gelatinous protein mixture that is secreted by mouse tumour cells. Matrigel™ is a complex mixture of proteins that resemble the extracellular matrix found in much tissue, hence making Matrigel™ a suitable substrate for cell culture. Often cells that are cultured on this substrate demonstrate complex cellular behaviour that would otherwise be difficult to observe under normal in vitro conditions. Matrigel™ mixed in with the Schwann cells promotes the adhesion of the cells to the inner wall of the tube.[113] A PAN/PVC tube, filled with Schwann cells isolated from adult rat sciatic nerves mixed with Matrigel™, was implanted across the gap between fully transected spinal cord and induced axonal outgrowth across the gap.[111,114] One month later, the stumps were joined by a tissue bridge that contained Schwann cells, myelinated axons, blood vessels, fibroblast and macrophages.[115-117] It was estimated that 25% of the fibres within the tissue bridge were myelinated by Schwann cells [114] rather than oligodendrocytes, which normally myelinate CNS axons. However, in all these studies there was loss of tissue in the stumps that were placed into the tubes. To address this problem PAN/PVC grafts were filled with Schwann cells and antiinflammatory glucocortico steroid (methlprednisolone) was added.[115] This reduced tissue loss within the stumps and increased the number of axons in the tissue bridge, most likely by reducing the microglial invasion that follows the introduction of the bridge. Schwann cells have been combined with BDNF, NT3 or GDNF in an attempt to enhance the growth of myelinated axons across a spinal cord lesion.[118] In some instances PAN/PVC tubes filled with hydrogels (Matrigel™, fibrin and the like) have also been used to encapsulate neural cells lines and they have the potential to be used to deliver molecules such as catecholamines in cell-based therapies to promote neural outgrowth.

5.1.6 SYNTHETIC HYDROGELS

5.1.6.1 Methacrylate based hydrogels

The chemical and spatial architecture of methacrylate based hydrogels can be tailored to produce similar mechanical properties to neural tissue. The main hydrogel in this class used with neurones is poly(2-hydroxyethyl methacrylate) (pHEMA). pHEMA on its own is not adhesive or attractive to neurones but it has been modified with molecules such as adhesive protein-derived oligopeptides, [119] aminosugars or collagen, [120] greatly improving its *in vitro* and *in vivo* biocompatibility with neurones. pHEMA has been extensively used in neural tissue engineering for spinal cord injuries. pHEMA sponges implanted into the injured spinal cord enhanced axonal regrowth,[121] and with the addition of oriented channels, the hydrogel showed great potential for neural repair.[122] The Shoichet group have also worked on textured poly(2-hydroxy-ethyl methacrylate-comethyl methacrylate) (pHEMA-MMA) hydrogel channels.[123] pHEMA-MMA channels filled with FGF-1 used to bridge transection of the sciatic nerve induced axons to cross a 10 mm gap between the fully separated stumps of nerve, [124] and was superior to implanted pHEMA sponges.[121] Figure 3 shows the transacted stumps placed within the pHEMA-MMA channel and shows the small tubes within the large channel encouraging spinal cord regeneration.[125] However, a major problem with the pHEMA and Phemamma channels was partial collapse after implantation.[126,127] This problem was addressed by implanting coil reinforced pHEMA-MMA/pHEMA channels, [128] loaded with FGF-1, providing equivalent performance in a complete spinal cord transection to autografts. Nerve growth factor (NGF) had been photochemically bound to pHEMA scaffolds for in vitro testing.[129] The NGF immobilized onto the scaffold was found to be bioactive and the percentage of cell population that responded to the bound NGF was statistically similar to cells cultured on collagen with soluble NGF present.[129] In a later study, concentration gradients of neurotrophic factors NGF and neurotrophin-3 (NT-3) were incorporated into the scaffolds to guide neurite outgrowth from primary neurones.[130] The concentration gradient of NT-3 required to guide DRG neurites was significantly less than for NGF (200 ng/mL/mm and 310 ng/mL/mm respectively).[130]

Poly(hydroxypropyl methacrylate) (pHPMA) is more biocompatible than pHEMA [131] and shows great promise in aiding regeneration following lesions of the CNS.[120,132,133] pHPMA hydrogels are often used with other molecules, such as attached adhesive

peptides.[134,135] They have a colloidal-type structure with microspheres 3-5 μm in diameter in a loosely-packed structure forming a three-dimensional network.[131] Implanting pHPMA into the cavity that forms in the rat spinal cord 3 months after a severe injury not only reduced the volume of the cavity but also induced axonal growth throughout the graft, resulting in functional recovery.[132] Addition of adhesion promoting peptides (RGD) to the pHPMA hydrogels mediated binding to integrin receptors, ultimately resulting in more axonal ingrowth[133,136,137] and a reduction in the expression of stress proteins.[138] Additionally, pHPMA used to bridge the gap between ends of the transected spinal cord model induced outgrowth of axons which were myelinated with Schwann cells.[139] pHPMA hydrogels demonstrated good integration and weak glyosis when implanted in lesions between the septum and hippocampus.[140] The bioadhesiveness was increased by incorporation of an amino sugar into the backbone of the hydrogel and promoted astrocyte and acetylcholinesterase-positive axonal penentration although there was a lack of reinnervation to the hippocampus.[140] Further studies also investigated the capacity of homotopic grafts of septal cells combined with pHPMA hydrogels to bridge lesions between the septum and hippocampus.[141] The grafts induced the recovery of some hippocampal function however, there was no significant recovery of sensorimotor or cognitive function.

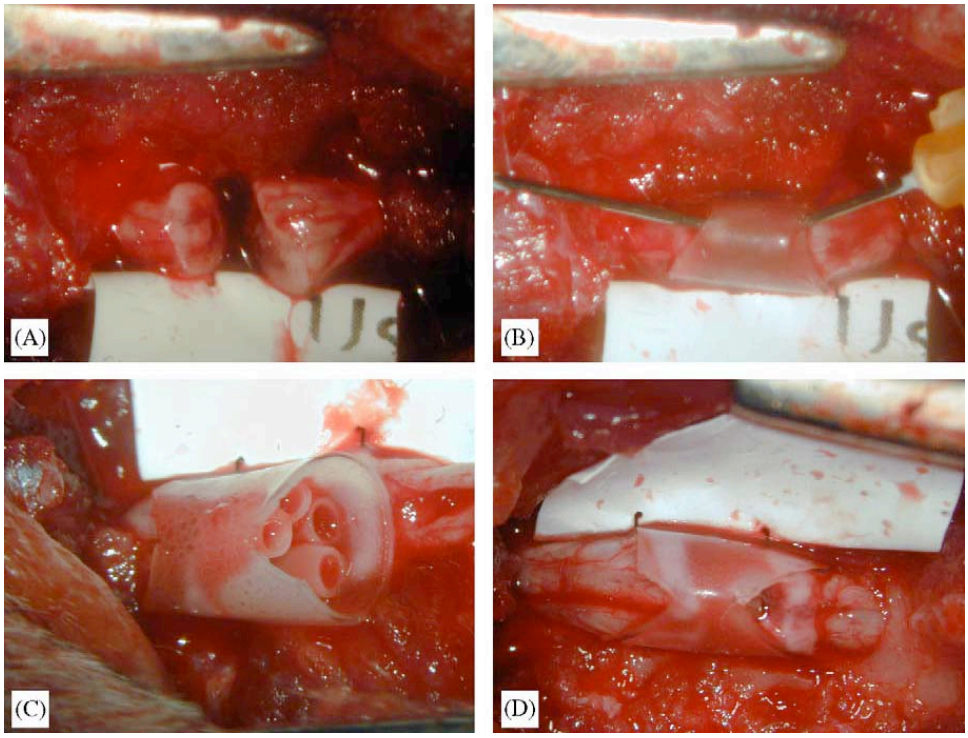

Figure 3 A) Complete transection of the spinal cord. B) two stumps after being placed into the pHEMA-MMA channel. C) pHEMA-MMA tubes within the larger pHEMA-MMA channel. D) the two stumps placed into the pHEMA-MMA channels with the pHEMA-MMA tubes within the construct. Reproduced by permission from Elsevier[75]

NF160-positive axons respond similarly to pHPMA and pHEMA hydrogels implanted into the brain of rats however there was a greater amount of connective tissue growth into the pHPMA hydrogel compared to the pHEMA.[142] Immobilisation of the xIKVAVx (isoleucine-lysine-valine-alanine-valine) peptide on pHPMA hydrogels provided structural continuity across cavities made in the adult rat cerebrum, resulting in a more favourable wound repair and subsequently axonal growth throughout the hydrogel.[135] RGD has also been immobilised on pHPMA143 but with the intention of promoting fibroblast growth. The fibroblasts were genetically modified to produce Brain-derived Neurotrophic Factor (BDNF), Ciliary Neurotrophic Factor (CNTF) or both, which invoked axonal outgrowth of retinal neurones when implanted to the optic tract of rats. A drawback with using methacrylate based hydrogels is that they are not biodegradable.

5.1.6.2 Polyethylene glycol

Polyethylene glycol (PEG) is a hydrophilic polymer that adheres only weakly to protein and cells, is non-toxic and has been trialled in neural tissue repair [144-146] with encouraging results. PEG solutions administered 72 hours after spinal cord injury prevented nerve cells from rupturing by repairing initial membrane damage.[144] Paralysis was prevented in 3 out of 4 animals tested. Severed medial giant earthworm axons could be fused, suggesting that a variant of this technique might be useful for the rapid repair of mammalian-myelinated axons.[147] However, while these preliminary findings suggested that PEG is neuroprotective due to its ability to seal damaged cells/membranes following injury [148] and suppress oxidative stress, [149] it can only be applied when the nerve ends are adjacent to each other and prior to the formation of glial scarring and thus early after injury.

Gunn *et a*l. evaluated the functionalization of PEG hydrogels with RGDS, IKVAV and YI GSR (tyrosine-isoleucine-glycine-serine-arginine) on the neurite extensions from PC12 cells.[150] They found that the longest neurites were seen on scaffolds that incorporated RGDS, with no neurites present on YIGSR scaffolds.[150] This may be useful for the regeneration of larger nerve defects. Biodegradable and photocrosslinkable PEG based hydrogels have been investigated as a vehicle for delivering neurotrophins to the spinal cord.[151,152] Neural precursor cells have been photoencapsulted within a degradable PEG hydrogel and by changing the degradation rate of the hydrogel, it was possible to control the time-scale over which the neural cells extended axons.[153] Figure 4 shows the response of the neural cells in the degradable hydrogel.[153]

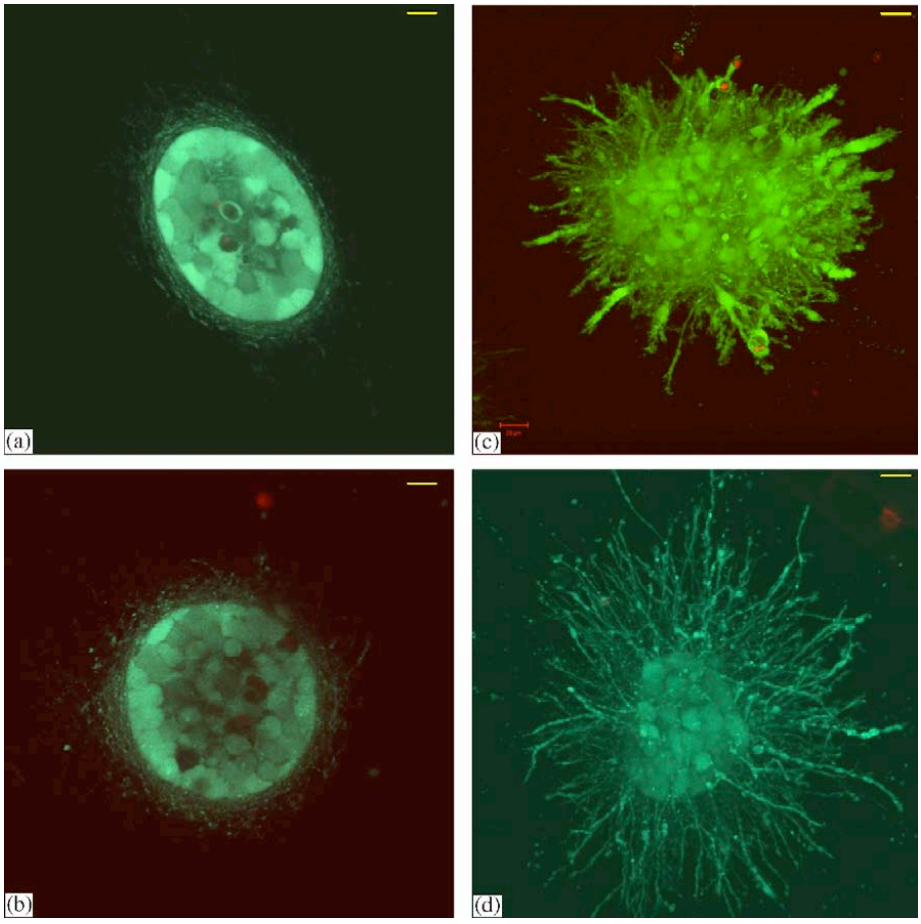

Figure 4 – These images were taken during a 2 week culture. The neural cells were stained using calcein (green – live cells) and the red represents dead cells (stained using ethidium bromide). Figures a) and b) represents a projection of 5 optical sections that were 2 μm thick on day 10 and 12 of culture respectively. At this stage in the degradation process the neurites grow in a shell wrapping themselves around the tissue. In figures c) and d) a projection of 50-60 optical sections that were 1 μm thick were constructed on a single piece of tissue on day 14 and 16 of culture respectively. At this stage of degradation many processes emerge radially from the aggregates. Reference reproduced by permission from Elsevier[107]

5.1.7 Summary

There are many different types of hydrogels that have been used for neural tissue engineering applications. Clearly the selection of a hydrogel for a specific application depends on the cellular response to the materials, which is influenced by its chemical and physical properties. Due to the recognition that longer neurite extensions often exist on 2D surfaces, [48] the possibility of incorporating 2D surfaces in macroporous hydrogels to generate "composite scaffolds" can be conceived.

However, thus far research has mainly focused on the physical and chemical properties of hydrogels and the viability of cells on these materials. Directed axonal outgrowth using hydrogel scaffolds as focussed in this review is not the end of the story for successful repair of neural pathways since the integration of the graft to restore function may require the extensive rehabilitation, physical therapy and learning to reuse the new part of the body. Up till now, the quality of a scaffold has been expressed in the relatively crude terms of cell survival or proliferation and the capacity to form neurites in comparison to conventional culture media. Furthermore the use of scaffolds has mainly been restricted to the concept of a surgical aid to breach a physical defect in the integrity of axonal tracts. However the sophistication in understanding of how the extracellular environment supports and regulates axonal extension and cell survival has meant that neural tissue engineers are looking to ways to experimentally manipulate this environment. With the knowledge that chemical gradients are powerful guidance cues for axons and also for differentiation, comes the possibility of using scaffolds to provide these gradients. Similarly the physical nature of the environment in terms of scaffold pore size, elasticity and capacity to bind surface active molecules can be exploited in favour of axon extension over cell entry. Thus it becomes possible to conceive of three dimensional models of brain nuclei connected by axonal tracts. These would be invaluable in understanding internal circuitry and the processes that regulate plasticity and synapse formation. These *in vitro* applications to support the understanding of fundamental mechanisms of neuronal interactions may be the most important use for scaffolds in the next few years. The use of biomaterials in treatment of brain disorders and spinal cord injury may require advances in both neurobiology and scaffolds, but advances in *in vitro* uses will almost certainly underpin therapeutic applications.

5.1.8 Acknowledgements

This project was funded by an Australian Postgraduate Award, the CRC for Polymers and ARC Discovery DP0450618.

5.1.9 References

1. Harvey AR, Plant GW, Tan MM. Schwann cells and the regrowth of axons in the mammalian CNS: a review of transplantation studies in the rat visual system. Clin Exp Pharmacol Physiol. 1995;22:569-579.

2. Klapka N, Muller HW. Collagen matrix in spinal cord injury. Journal of Neurotrauma 2006;23:422-435.

3. Yin T, Li L. The stem cell niches in bone. The Journal of Clinical Investigation 2006;116:1195-1201.

4. Nystul TG, Spradling AC. Breaking out of the mold: diversity within adult stem cells and their niches. Current Opinion in Genetics & Development 2006;16:463-468.

5. Moore KE, Mills JF, Thornton MM. Alternative sources of adult stem cells: a possible solution to the embryonic stem cell debate. Gender Medicine 2006;3:161-168.

6. Yiu G, He Z. Glial inhibition of CNS axon regeneration. Nature Reviews Neuroscience 2006;7:617-627.

7. Nakai Y, Kamiguchi H. Migration of nerve growth cones requires detergentresistant membranes in a spatially defined and substrate-dependent manner. Journal of Cell Biology 2002;159:1097–1108.

8. Zhong Y, Yu X, Gilbert R, Bellamkonda RV. Stabilizing electrode-host interfaces: a tissue engineering approach. Journal of Rehabilitation Research and Development 2001;38:627-632.

9. Lundborg G, Nerve Injury and Repair, Churchill Livingstone, Hampshire, 1988.

10. Yu TW, Bargmann CI. Dynamic regulation of axon guidance. Nature Neuroscience 2001;4 suppl:1169-1176.

11. Goldshmit Y, McLenachan S, Turnley A. Roles of Eph receptors and ephrins in the normal and damaged adult CNS. Brain Research Reviews 2006;52:327-345.

12. Deister C, Schmidt CE. Optimizing neurotrophic factor combinations for neurite outgrowth. Journal of neural engineering 2006;3:172-179.

13. Kiryushko D, Berezin V, Bock E. Regulators of neurite outgrowth: role of cell adhesion molecules. Annals of the New York Academy of Sciences 2004;1014:140-154.
14. Koert CE, Spencer GE, van Minnen J, Li KW, Geraerts WPM, Syed NI, Smit AB, van Kesteren RE. Functional implications of neurotransmitter expression during axonal regeneration: serotonin, but not peptides, auto-regulate axon growth of an identified central neuron. Journal of Neuroscience 2001;21:5597-5606.
15. Waimey KE, Cheng HJ. Axon pruning and synaptic development: how are they perplexin? Neuroscientist 2006;12:398-409.
16. Zou Y, Lyuksyutova AI. Morphogens as conserved axon guidance cues. Current opinion in neurobiologyl 2007;17:22-28.
17. Maness PF, Schachner M. Neural recognition molecules of the immunoglobulin superfamily: signaling transducers of axon guidance and neuronal migration. Nature Neuroscience 2007;10:19-26.
18. Butler SJ, Tear G. Getting axons onto the right path: the role of transcription factors in axon guidance. Development 2007;134:439-448.
19. Yamashita T, Mueller BK, Hata K. Neogenin and repulsive guidance molecule signaling in the central nervous system. Current opinion in neurobiologyl 2007;17:29-34.
20. Quinn CC, Wadsworth WG. Axon guidance: ephrins at WRK on the midline. Current Biology 2006;16:954-955.
21. Chen Y, Aulia S, Tang BL. Myelin-associated glycoprotein-mediated signaling in central nervous system pathophysiology. Molecular Neurobiology 2006;34:81-91.
22. Liu BP, Cafferty WB, Budel SO, Strittmatter SM. Extracellular regulators of axonal growth in the adult central nervous system. Philosopical trasaction of the royal society of london: Series B, biological sciences 2006;361:1593-1610.
23. Fontoura P, Steinman L. Nogo in multiple sclerosis: growing roles of a growth inhibitor. Journal of the Neurological Sciences 2006;245:201-210.
24. Cui Q. Actions of neurotrophic factors and their signaling pathways in neuronal survival and axonal regeneration. Molecular Neurobiology 2006;33:155-179.
25. Zurn AD, Bandtlow CE. Regeneration failure in the CNs: cellular and molecular mechanisms. Advances in Experimental Medicine and Biology 2006;557:54-76.

26. Buchli AD, Schwab ME. Inhibition of Nogo: a key strategy to increase regeneration, plasticity and functional recovery of the lesioned central nervous system. Annals of Medicine 2005;37:556-567.

27. Meier S, Brauer AU, Heimrich B, Schwab ME, Nitsch R, Savaskan NE. Molecular analysis of Nogo expression in the hippocampus during development and following lesion and seizure. The FASBE journal 2003;17:1153-1155.

28. Ji B, Li M, Wu WT, Yick LW, Lee X, Shao Z, Wang J, So KF, McCoy JM, Pepinsky RB, Mi S, Relton JK. LINGO-1 antagonist promotes functional recovery and axonal sprouting after spinal cord injury. Molecular and cell neurosciences 2006;33:311- 320.

29. Yamashita T, Fujitani M, Yamagishi S, Hata K, Mimura F. Multiple signals regulate axon regeneration through the nogo receptor complex. Molecular Neurobiology 2005;32:105-111.

30. Alabed YZ, Pool M, Tone SO, Fournier AE. Identification of CRMP4 as a convergent regulator of axon outgrowth inhibition. The Journal of Neuroscience 2007;27:1702-1711.

31. Chen Y, Aulia S, Li L, Tang BL. AMIGO and friends: an emerging family of brain-enriched, neuronal growth modulating, type I transmembrane proteins with leucinerich repeats (LRR) and cell adhesion molecule motifs. Brain Research Reviews 2006;51:265-274.

32. Kruger RP, Aurandt J, Guan KL. Semaphorins command cells to move. Nature Reviews Molecular and Cell Biology 2005;6:789-800.

33. Sakisaka T, Takai Y. Cell adhesion molecules in the CNS. Journal of Cell Science 2005;118:5407-5410.

34. Waites CL, Craig AM, Garner CC. Mechanisms of vertebrate synaptogenesis. Annual review of neuroscience 2005;28:251-274.

35. Nakamoto T, Kain KH, Ginsberg MH. Neurobiology: New connections between integrins and axon guidance. Current Biology 2004;14:R121-123.

36. Bellamkonda R, Ranieri JP, Bouche N, Aebischer P. Hydrogel-based threedimensional matrix for neural cells. Journal of Biomedical Materials Research 1995;29:663-671.

37. Engler AJ, Sen S, Sweeney HL, Discher DE. Matrix elasticity directs stem cell lineage specification. Cell 2006;126:677-689.

38. Willits RK, Skornia SL. Effect of collagen gel stiffness on neurite extension. J Biomater Sci Polym Ed. 2004;15:1521-1531.

39. Balgude AP, Yu X, Szymanski A, Bellamkonda R. Agarose gel stiffness determines rate of DRG neurite extension in 3D cultures. Biomaterials 2001;22:1077- 1084.

40. Leach JB, Brown XQ, Jacot JG, DiMilla PA, Wong JY. Neurite outgrowth and branching of PC12 cells on very soft substrates sharply decreases below a threshold of substrate rigidity. Journal of neural engineering 2007;4:26-34.

41. Batchelor PE, Liberatore GT, Wong JY, Porritt MJ, Frerichs F, Donnan GA, Howells DW. Activated macrophages and microglia induce dopaminergic sprouting in the injured striatum and express brain-derived neurotrophic factor and glial cell linederived neurotrophic factor. The Journal of Neuroscience 1999;19:1708-1716.

42. Johansson S, Strömberg I. Guidance of dopaminergic neuritic growth by immature astrocytes in organotypic cultures of rat fetal ventral mesencephalon. Journal of Comparative Neurology 2002;443:237-249.

43. Woerly S, Marchand R, Lavallée C. Interactions of copolymeric poly(glyceryl methacrylate)-collagen hydrogels with neural tissue: effects of structure and polar groups. Biomaterials 1991;12:197-203.

44. Batchelor PE, Howells DW. CNS regeneration: Clinical possibility or basic science fantasy. 2004;

45. Yu X, Bellamkonda RV. Dorsal root ganglia neurite extension is inhibited by mechanical and chondroitin sulfate-rich interfaces. Journal of neuroscience Research 2001;66:303-310.

46. Ratner BD, Hoffman AS. in Hydrogels for Medical and Related Applications; J. D. Andrade, Ed.; ACS, Washington D.C., 1976, p 1-36.

47. Kwon BK, Oxland TR, Tetzlaff W. Animal models used in spinal cord regeneration research. Spine 2002;27:1504-1510.

48. Bellamkonda R. Peripheral nerve regeneration: An opinion on channels, scaffolds and anisotropy. Biomaterials 2006;27:3515-3518.

49. Stokols S, Tuszynski MH. The fabrication and characterization of linearly oriented nerve guidance scaffolds for spinal cord injury. Biomaterials 2004;25:5839– 5846.

50. Stokols S. Freeze-dried agarose scaffolds with uniaxial channels stimulate and guide linear axonal growth following spinal cord injury. Biomaterials 2006;27:443-451.

51. Dillon GP, Yu Z, Sridharan A, Ranieri JP, Bellamkonda RV. The influence of physical structure and charge on neurite extension in a 3D hydrogel scaffold. Journal of Biomaterials Science, Polymer Edition 1998;9:1049-1069.

52. Luo Y, Shoichet MS. A photolabile hydrogel for guided three-dimensional cell growth and migration. Nature Materials 2004;3:249-253.

53. Bellamkonda R, Ranieri JP, Aebischer P. Laminin oligopeptide derivatized agarose gels allow three-dimensional neurite extension in-vitro. Journal of Neuroscience Research 1995;41:501-509.

54. Yu X, Dillon GP, Bellamkonda RV. A laminin and nerve growth factor-laden three-dimensional scaffold for enhanced neurite extension. Tissue Engineering 1999;5:291-304.

55. Jain A, Kim Y-T, McKeon RJ, Bellamkonda RV. In situ gelling hydrogels for conformal repair of spinal cord defects, and local delivery of BDNF after spinal cord injury. Biomaterials 2006;27:497-504.

56. Awad HA, Wickham MQ, Leddy HA, Gimble JM, Guilak F. Chondrogenic differentiation of adipose-derived adult stem cells in agarose, alginate, and gelatin scaffolds. Biomaterials 2004;25:3211-3222.

57. Barralet JE, Wang L, Lawson M, Triffitt JT, Cooper PR, Shelton RM. Comparison of bone marrow cell growth on 2D and 3D alginate hydrogels. Journal of Materials Science: Materials in Medicine 2005;16:515-519.

58. Dvir-Ginzberg M, Gamlieli-Bonshtein I, Agbaria R, Cohen S. Liver tissue engineering within alginate scaffolds: Effects of cell-seeding density on hepatocyte viability, morphology, and unction. Tissue Engineering 2003;9:757-766.

59. Lai HL, Abu'Khalil A, Craig DQM. The preparation and characterisation of drug-loaded alginate and chitosan sponges. International Journal of Pharmaceutics 2003;251:175-181.

60. Mosahebi A, Simon M, Wiberg M, Terenghi G. A novel use of alginate hydrogel as Schwann cell matrix. Tissue Engineering 2001;7:525-534.

61. Novikova LN, Mosahebi A, Wiberg M, Terenghi G, Kellerth JO, Novikov LN. Alginate hydrogel and matrigel as potential cell carriers for neurotransplantation. Journal of Biomedical Materials Research (Applied Biomaterials) 2006;77:242-252.

62. Mosahebi A, Fuller P, Wiberg M, Terenghi G. Effect of allogeneic Schwann cell transplantation on peripheral nerve regeneration. Experimental Neurology 2002;173:213-223.

63. Freier T, R. M, Shan Koh H, Shoichet MS. Chitin-based tubes for tissue engineering in the nervous system. Biomaterials 2005;26:4624-4632.

64. Suzuki Y, Kitaura M, Wu S, Kataoka K, Suzuki K, Endo K, Nishimura Y, Ide C. Electrophysiological and horseradish peroxidase-tracing studies of nerve regeneration through alginate-filled gap in adult rat spinal cord. Neuroscience Letters 2002;318:121-124.

65. Kataoka K, Suzuki Y, Kitada M, Ohnishi K, Suzuki K, Tanihara M, Ide C, Endo K, Nishimura Y. Alginate, a bioresorbable material derived from brown seaweed, enhances elongation of amputated axons of spinal cord in infant rats. Journal of Biomedical Materials Research 2001;54:373-384.

66. Park KH, Na K, Lee KC. Immobilization of Arg-Gly-Asp (RGD) sequence in sugar containing copolymer for culturing of pheochromocytoma (PC12) cells. Journal of bioscience and bioengineering 2004;97:207-211.

67. Reiter W-D. Biosynthesis and properties of the plant cell wall. Current Opinion in Plant Biology 2002;5:536-542.

68. Nisbet DR, Crompton KE, Hamilton SD, Shirakawa M, Prankerd RJ, Finkelstein DI, Horne M, Forsythe JS. Morphology and gelation of thermosensitive xyloglucan hydrogels. Biophysical Chemistry 2005;121:14-20.

69. Miyazaki S, Suisha, F., Kawasaki, N., Shirakawa, M., Yamatoya, K. and Attwood, D. Thermally reversible xyloglucan gels as vehicles for rectal drug delivery. Journal of Controlled Release 1998;56:75-83.

70. Shirakawa M, Yamatoya K, Nishinari K. Tailoring of xyloglucan properties using an enzyme. Food Hydrocolloids 1998;12:25-28.

71. Yamatoya K, Shirakawa M, Kuwano K, Suzuki J, Baba O. Hypolipidemic effects of hydrolyzed xyloglucan. Macromolecular Symposia 1997;120:231-236.

72. Desbrières J, Hirrien M, Ross-Murphy SB. Thermogelation of methylcellulose: rheological considerations. Polymer 2000;41:2451–2461.

73. Kobayashi K, Huang C-i, Lodge TP. Thermo-reversible gelationof aqueous methyl cellulose solutions. Macromolecules 1999;32:7070-7077.

74. Tate MC, Shear DA, Hoffman SW, Stein DG, LaPlaca MC. Biocompatibility of methylcellulose-based constructs designed for intracerebral gelation following experimental traumatic brain injury. Biomaterials 2001;22:1113-1123.

75. Stabenfeldt SE, Garcia AJ, LaPlaca MC. Thermoreversible lamininfunctionalized hydrogel for neural tissue engineering. Journal of biomedical materials research part A 2006;77:718-725.

76. Wells MR, Kraus K, Batter DK, Blunt DG, Weremowitz J, Lynch SE, Antoniades HN, Hansson H-A. Gel matrix vehicles for growth factor application in nerve gap injuries repaired with tubes: A comparison of Biomatrix, collagen, and methylcellulose. Experimental Neurology 1997;146:395–402.

77. Mori M, Yamaguchi M, Sumitomo S, Takai Y. Hyaluronan-based biomaterials in tissue engineering. Acta Histochemica et Cytochemica 2004;37:1-5.

78. Seckel BR, Jones D, Hekimian KJ, Wang KK, Chakalis DP, Costas PD. Hyaluronic acid through a new injectable nerve guide delivery system enhances peripheral nerve regeneration in the rat. Journal of Neuroscience Research 1995;40:318- 324.

79. Mann BK. Biologic gels in tissue engineering. Clinics in plastic surgery 2003;30:601-609.

80. Tian WM, Hou SP, Ma J, Zhang CL, Xu QY, Lee IS, Li HD, Spector M, Cui FZ. Hyaluronic acid-poly-D-lysine-based three-dimensional hydrogel for traumatic brain injury. Tissue Engineering 2005;11:513-525.

81. Benedetti L, Cortivo R, Berti T, Berti A, Pea F, Mazzo M, Moras M, Abatangelo G. Biocompatibility and biodegradation of different hyaluronan derivatives (Hyaff) implanted in rats. Biomaterials 1993;14:1154-1160.

82. Leach JB, Bivens KA, Patrick CW, Jr., Schmidt CE. Photocrosslinked hyaluronic acid hydrogels: Natural, biodegradable tissue engineering scaffolds. Biotechnology and Bioengineering 2003;82:578-589.

83. Burdick JA, Chung C, Jia F, Randolph MA, Langer R. Controlled degradation and mechanical behavior of photopolymerized hyaluronic acid networks. Biomacromolecules 2005;6:386-391.

84. Shu XZ, Liu Y, Palumbo FS, Prestwich GD. Disulfide-crosslinked hyaluronangelatin hydrogel films: a covalent mimic of the extracellular matrix for in vitro cell growth. Biomaterials 2003;24:3825-3834.

85. Segura T, Anderson BC, Chung PH, Webber RE, Shull KR, Shea LD. Crosslinked hyaluronic acid hydrogels: a strategy to functionalize and pattern. Biomaterials 2005;26:359–371.

86. Shu XZ, Liu Y, Palumbo FS, Luo Y, Perestwich GD. In situ crosslinkable hyaluronan hydrogels for tissue engineering. Biomaterials 2003;25:1339-1348.

87. Tian WM, Hou SP, Ma J, Zhang CL, Zu QY, Lee IS, Li HD, Spector M, Cui FZ. Hyaluronic acid-poly-D-lysine-based three dimensional hydrogel for traumatic brain injury. Tissue Engineering 2005;11:513-525.

88. Lee KY, Ha WS, Park WH. Blood compatibility and biodegradability of partially N-acetylated chitosan derivatives. Biomaterials 1995;16:1211-1216.

89. Hidaka Y, Ito M, Mori K, Yagasaki H, Kafrawy AH. Histopathological and immunohistochemical studies of membranes of deacetylated chitin derivatives implanted over rat calvaria. Journal of Biomedical Materials Research 1999;46:418-423.

90. Chenite A, Chaput C, Wang D, Combes C, Buschmann MD, Hoemann CD, Leroux JC, Atkinson BL, Binette F, Selmani A. Novel injectable neutral solutions of chitosan form biodegradable gels in situ. Biomaterials 2000;21:2155-2161.

91. Hirano S, Tsuchida H, Nagao N. N-acetylation in chitosan and the rate of its enzymic hydrolysis. Biomaterials 1989;10:574-576.

92. Jarry C, Chaput C, Chenite A, Renaud M-A, Buschmann M, Leroux J-C. Effects of steam sterilization on thermogelling chitosan-based gels. Journal of Biomedical Materials Research (Applied Biomaterials) 2001;58:127-135.

93. Vårum KM, Holme HK, Izume M, Stokke BT, Smidsrød O. Determination of enzymatic hydrolysis specificity of partially N-acetylated chitosans. Biochimica et Biophysica Acta 1996;1291:5-15.

94. Shigemasa Y, Saito K, Sashiwa H, Saimoto H. Enzymatic degradation of chitins and partially deacetylated chitins. International Journal of Biological Macromolecules 1994;6:43-49.

95. Li RH, White M, Williams S, Hazlett T. Polymers for Tissue Engineering, CytoTherapeutics, Inc., Lincoln, RI, USA., 1998, pp 235-254.

96. Zielinski BA, Aebischer P. Chitosan as a matrix for mammalian cell encapsulation. Biomaterials 1994;15:1049-1056.

97. Yuan Y, Zhang P, Yang Y, Wang X, Gu X. The interaction of Schwann cells with chitosan membranes and fibers in vitro. Biomaterials 2004;25:4273-4278.

98. Bini TB, Gao S, Wang S, Ramakrishna S. Development of fibrous biodegradable polymer conduits for guided nerve regeneration. Journal of Materials Science: Materials in Medicine 2005;16:367-375.

99. Gong HP, Zhong YH, Li JC, Gong YD, Zhao NM, Zhang XF. Studies on nerve cell affinity of chitosan-derived materials. Journal of Biomedical Materials Research 2000;52:285.

100. Cheng MY, Gong K, Li J, Gong YD, Zhao NM, Zhang XF. Surface modification and characterization of chitosan film blended with poly-L-lysine. Journal of Biomaterials Applications 2004;19:59-75.

101. Itoh S, Yamaguchi I, Suzuki M, Ichinose S, Takakuda K, Kobayashi H, Shinomiya K, Tanaka J. Hydroxyapatite-coated tendon chitosan tubes with adsorbed laminin peptides facilitate nerve regeneration *in vivo*. Brain Research 2003;993:111-123.

102. Rosales-Cortes M, Peregrina-Sandoval J, Banuelos-Pineda J, Castellanos- Martinez EE, Gomez-Pinedo UA, Albarran-Rodriguez E. [Regeneration of the axotomised sciatic nerve in dogs using the tubulisation technique with Chitosan biomaterial preloaded with progesterone]. Reviews in Neurological Disease 2003;36:1137-1141.

103. Yuan T, Zhang P, Yang Y, Wang X, Gu X. The interaction of Schwann cells with chitosan membranes and fibers *in vitro*. Biomaterials 2004;25:4273-4278.

104. Chenite A, Buschmann M, Wang D, Chaput C, Kandani N. Rheological characterisation of thermogelling chitosan/glycerol-phosphate solutions. Carbohydrate Polymers 2001;46:39-46.

105. Crompton KE, Goud JD, Bellamkonda RV, Gengenbach TR, Finkelstein DI, Horne MK, Forsythe JS. Polylysine-functionalised thermoresponsive chitosan hydrogel for neural tissue engineering. Biomaterials 2006;doi:10.1016/j.biomaterials.2006.1008.1044.

106. Nishimura K, Nishimura S, Seo H, Nishi N, Tokura S, Azuma I. Macrophage activation with multiporous beads prepared from partially deacetylated chitin. Journal of Biomedical Materials Research 1986;20:1359-1372.

107. Peluso G, Petillo O, Ranieri M, Santin M, Ambrosio L, Calabró D, Avallone B, Balsamo G. Chitosan-mediated stimulation of macrophage function. Biomaterials 1994;15:1215-1220.

108. Crompton KE, Tomas D, Finkelstein DI, Marr M, Forsythe JS, Horne M. Inflammatory response on injection of chitosan/GP to the brain. Journal of Materials Science: Materials in Medicine 2005;

109. Bunge RP. Expanding roles for the Schwann cell:ensheathment, myelination, trophism and regeneration. Current opinion in neurobiologyl 1993;3:805-809.

110. Bunge MB. Bridging areas of inury in the spinal cord. Neuroscienctist 2001;7:325-339.

111. Xu XM, Guenard V, Kleitman N, Bunge MB. Axonal regeneration into Schwann cell-seeded guidance channels grafted into transected adult rat spinal cord. Journal of Comparative Neurology 1995;351:145-160.

112. Xu XM, Guenard V, Kleitman N, Aebischer P, Bunge MB. A combination of BDNF and NT-3 promotes supraspinal axonal regeneration into Schwann cell grafts in adult rat thoracic spinal cord. Experimental Neurology 1995;134:261-272.

113. Flanagan LA, Ju YE, Marg B, Osterfield M, Janmey PA. Neurite branching on deformable substrates. Neuroreport 2002;13:2411-2415.

114. Xu XM, Chen A, Guenard V, Kleitman N, Bunge MB. Briding Schwann cell transplants promote axonal regeneration from both the rostral and caudal stumps of transected adult rat spinal cord. Journal of Neurocytology 1997;26:1-16.

115. Chen A, Xu XM, Kleitman N, Bunge MB. Methylprednisolone administration improves axonal regeneration into Schwann cells grafts in trasected adult rat thoracic spinal cord. Experimental Neurology 1996;138:261-276.

116. Oudega M, Xu XM, Guenard V, Kleitman N, Bunge MB. A combination of insulin-like growth factor and platelet derived growth factor enhances myelination but diminishes axonal regereation into Schwann cell grafts in the adult rat spinal cord. Glia 1997;19:247-258.

117. Jones LL, Oudega M, Bunge MB, Tuszynski MH. Neurotrophic factors, cellular bridges and gene therapy for spinal cord injury. Journal of physiology 2001;533:83-89.

118. Iannotti C, Li H, Yan P, Lu X, Wirthlin L, Xu XM. Glial cell line-derived neurotrophic factor-enriched bridging transplants promote propriospinal axonal regeneration and enhance myelination after spinal cord injury. Experimental Neurology 2003;183:379-393.

119. Yu TT, Shoichet MS. Guided cell adhesion and outgrowth in peptide-modified channels for neural tissue engineering. Biomaterials 2005;26:1507-1514.

120. Giannetti S, Lauretti L, Fernandez ES, F.; Tamburrini, G.; Pallini, R. Acrylic hydrogel implants after spinal cord lesion in the adult rat. Neurological Research 2001;23:405-409.

121. Tsai EC, Dalton PD, Shoichet MS, Tator CH. Synthetic hydrogel guidance channels facilitate regeneration of adult rat brainstem motor axons after complete spinal cord transection. Journal of Neurotrauma 2004;21:789-804.

122. Flynn L, Dalton PD, Shoichet MS. Fiber templating of poly(2-hydroxyethyl methacrylate) for neural tissue engineering. Biomaterials 2003;24:4265-4272.

123. Dalton PD, Flynn L, Shoichet MS. Manufacture of poly(2-hydroxyethyl methacrylate-co-methyl methacrylate) hydrogel tubes for use as nerve guidance channels. Biomaterials 2002;23:3843-3851.

124. Midha R, Munro CA, Dalton PD, Tator CH, Shoichet MS. Gorwht factor enhancement of periheral nerve regeneration through a novel synthetic hydrogel tube. Journal of neurosurgery 2003;99:555-565.

125. Tsai EC, Dalton PD, Shoichet MS, Tator CH. Matrix inclusion within synthetic hydrogel guidance channels improves specific supraspinal and local axonal regeneration after complete spinal cord transection. Biomaterials 2006;27:519-533.

126. Nomura H, Tator CH, Shoichet MS. Bioengineered strategies for spinal cord repair. Journal of Neurotrauma 2006;23:496-507.

127. Belkas JS, Munro CA, Shoichet MS, Johnston M, Midha R. Long-term in vivo biomechanical properties and biocompatibility of poly(2-hydroxyethyl methacrylate-comethyl methacrylate) nerve conduits. Biomaterials 2005;26:1741-1749.

128. Katayama Y, Montenegro R, Freier T, Midha R, Belkas JS, Shoichet MS. Coilreinforced hydrogel tubes orinite berve regeneration equivalent to that of nerve autografts. Biomaterials 2006;27:505-518.

129. Kapur TA, Shoichet M. Chemically-bound nerve growth factor for neural tissue engineering applications. Journal of Biomaterials Science, Polymer Edition 2003;14:383-394.

130. Moore K, MacSween M, Shoichet M. Immobilized concentration gradients of neurotrophic factors guide neurite outgrowth of primary neurons in macroporous scaffolds. Tissue Engineering 2006;12:267-278.

131. Woerly S, Pinet E, de Robertis L, Bousmina M, Laroche G, Roitback T, Vargová L, Syková E. Heterogeneous PHPMA hydrogels for tissue repair and axonal regeneration in the injured spinal cord. Journal of Biomaterials Science, Polymer Edition 1998;9:681-711.

132. Woerly S, Doan VD, Evans-Martin F, Paramore CG, Peduzzi JD. Spinal cord reconstruction using NeuroGel™ implants and functional recovery after chronic injury. Journal of Neuroscience Research 2001;66:1187-1197.

133. Woerly S. Restorative surgery of the central nervous system by means of tissue engineering using NeuroGel implants. Neurosurgical Review 2000;23:59-77.

134. Plant GW, Woerly S, R HA. Hydrogels containing peptide or aminosugar sequences implanted into the rat brain: influence on cellular migration and axonal growth. Experimental Neurology 1997;143:287-299.

135. Cui FZ, Tian WM, Fan YW, Hou SP, Xu QY, Lee I-S. Cerebrum repair with PHPMA hydrogel immobilized with neurite-promoting peptides in traumatic brain injury of adult rat model. Journal of Bioactive and Compatible Polymers 2003;18:413-432.

136. Woerly S, Pinet E, de Robertis L, Van Diep D, Bousmina M. Spinal cord repair with PHPMA hydrogel containing RGD peptides (NeuroGel). Biomaterials 2001;22:1095-1111.

137. Woerly S. Porous hydrogels for neural tissue engineering. Materials Science Forum 1997;250:53-68.

138. Woerly S, Awosika O, Zhao P, Agbo C, Gomez-Pinilla F, de Vellis J, Espinosa-Jeffrey A. Expression of heat shock protein (HSP)-25 and HSP-32 in the rat spinal cord reconstructed with Neurogel. Neurochemical Research 2005;30:721-735.

139. Woerly S, Doan VD, Sosa N, de Vellis J, Espinosa-Jeffrey A. Prevention of gliotic scar formation by NeuroGel allows partial endogenous repair of transected cat spinal cord. Journal of Neuroscience Research 2004;75:262-272.

140. Duconseille E, Stephane W, Kelche C, Will B, Cassel JC. Polymeric hydrogels placed into a fimbria-forniz lesion cavity promote fiber (re_growth: a morphological study in rat. Restorative Neruology and Neuroscience 1998;13:193-203.

141. Duconseille E, Carrot SN, Woerly S, Kelche C, Will B, Cassel JC. Homotopic grafts of septal neurons combined to polymeric hydrogels placed into a fimbria-fornix lesion cavity attenuate locomotor hyperactivity but not mnemonic dysfunctions in rats. Restorative Neruology and Neuroscience 2001;18:39-51.

142. Lesný P, De Croos J, Prádný M, Vacík J, Michálek J, Woerly S, Syková E. Polymer hydrogels usable for nervous tissue repair. Journal of Chemical Neuroanatomy 2002;23:243-247.

143. Loh NK, Woerly S, Bunt SM, Wilton SD, Harvey AR. The regrowth of axons within tissue defects in the CNS is promoted by implanted hydrogel matrices that contain BDNF and CNTF producing fibroblasts. Experimental Neurology 2001;170:72-84.

144. Laverty PH, Leskovar A, Breur GJ, Coates JR, Bergman RL, Widmer WR, Toombs JP, Shapiro S, Borgens RB. A preliminary study of intravenous surfactants in paraplegic dogs: polymer therapy in canine clinical SCI. Journal of Neurotrauma 2004;21:1767-1777.

145. Lore AB, Hubbell JA, Bobb DSJ, Ballinger ML, Loftin KL, Smith JW, Smyers ME, Garcia HD, Bittner GD. Rapid induction of functional and morphological continuity between severed ends of mammalian or earthworm myelinated axons. Neuroscience 1999;19:2442-2454.

146. Schmidt CE, Leach JB. Neural tissue engineering: stratergies for repair and regeneration. Annual Review of Biomedical Engineering 2003;5:293-347.

147. Krause TL, Bittner GD. Rapid morphological fusion of severed myelinated axons by polyethylene glycol. Proc, Natl, Acad. Sci 1990;87:1471-1475.

148. Borgens RB, Shi R, Bohnert D. Behavioral recovery from spinal cord injury following delayed application of polyethylene glycol. Journal of experimental neurology 2002;205:1-12.

149. Luo J, Shi R. Diffusive oxidation stress following acute spinal cord injury in guinea pigs and its inhibition by polyethylene glycol. Neuroscience Letters 2004;359:167-170.

150. Gunn JW, Turner SD, Mann BK. Adhesive and mechanical properties of hydrogels influence neurite extension. Journal of Biomedical Materials Research (Applied Biomaterials) 2005;72:91-97.

151. Piantino J, Burdick JA, Goldberg D, Langer R, Benowitz LI. An injectable, biodegradable hydrogel for trophic factor delivery enhances axonal rewiring and improves performance after spinal cord injury. Experimental Neurology 2006;201:359-367.

152. Burdick JA, Ward M, Liang E, Young MJ, Langer R. Stimulation of neurite outgrowth by neurotrophins delivered from degradable hydrogels. Biomaterials 2006;27:452-459.

153. Mahoney MJ, Anseth KS. Three-dimensional growth and function of neural tissue in degradable polyethylene glycol hydrogels. Biomaterials 2006;27:2265-2274.

Chapter 6

Part II - Hydrogel
In vitro experimentation

Contents

Declaration

Two publications have been inserted into Chapter 6. Below the reference information and publication status for these publications is provided.

Chapter 6.1

D.R. Nisbet, K.E. Crompton, S.D. Hamilton, S. Shiwakawa, R.J. Prankerd, D.I. Finkelstein, M.H. Horne, J.S. Forsythe, "Thermosensitive xyloglucan hydrogels: Morphology and gelation, *Biophys. Chem*. 121, pp 14-20 2006.

Chapter 6.2

D.R. Nisbet, D. Moses, T.R. Gengenbach, J.S. Forsythe, D.I. Finkelstein, M.K. Horne. "Enhancing neurite outgrowth from primary neurones and neural stem cells using thermoresponsive hydrogel scaffolds for the repair of spinal cord injury", *J. Biomed. Mat. Res.,* In Press, (10.1002/jbm.a.31962) 2008.

Declaration for Thesis Chapter 6.1

Monash University

Declaration by candidate

In the case of Chapter 6.1 the nature and extent of my contribution to the work was the following:

Nature of contribution	Extent of contribution (%)
Experimental design and conduct and article writing.	75

The following co-authors contributed to the work. Co-authors who are students at Monash University must also indicate the extent of their contribution in percentage terms:

Name	Nature of contribution	Extent of contribution (%) for students
K.E. Crompton	Assisted in experimentation & corrected manuscript	10
S.D. Hamilton	Assisted in experimentation & corrected manuscript	5
S. Shirakawa *	Supplied xyloglucan & corrected manuscript	N/A
R. Prankerd	Assisted in result interpretation and corrected manuscript	N/A
D.I. Finkelstein	Experimental design and corrected manuscript	N/A
M.K. Horne	Experimental design and corrected manuscript	N/A
J.S. Forsythe	Experimental design and corrected manuscript	N/A

Candidate's Signature	[redacted]	Date 14/10/2008

Declaration by co-authors

The undersigned hereby certify that:

(1) the above declaration correctly reflects the nature and extent of the candidate's contribution to this work, and the nature of the contribution of each of the co-authors.
(2) they meet the criteria for authorship in that they have participated in the conception, execution, or interpretation, of at least that part of the publication in their field of expertise;
(3) they take public responsibility for their part of the publication, except for the responsible author who accepts overall responsibility for the publication;

(4) there are no other authors of the publication according to these criteria;
(5) potential conflicts of interest have been disclosed to (a) granting bodies, (b) the editor or publisher of journals or other publications, and (c) the head of the responsible academic unit; and
(6) the original data are stored at the following location(s) and will be held for at least five years from the date indicated below:

Name	Location
K.E. Crompton	Monash University - Department of Materials Engineering
S.D. Hamilton	Monash University - Department of Materials Engineering
S. Shirakawa *	Dainippon Sumitomo Pharmaceutics - Japan
R. Prankerd	Monash University - Department of Pharmaceutics
D.I. Finkelstein	The Mental Health Research Institute of Victoria
M.K. Horne	Melbourne University - Howard Florey Institute
J.S. Forsythe	Monash University - Department of Materials Engineering

Name	Signature	Date
K.E. Crompton	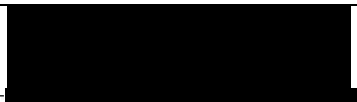	14/10/2008
S.D. Hamilton	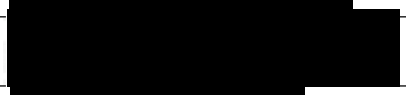	14/10/2008
S. Shirakawa *	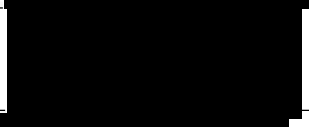	14/10/2008
R. Prankerd	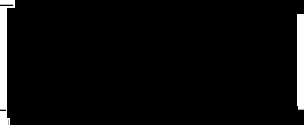	14/10/2008
D.I. Finkelstein	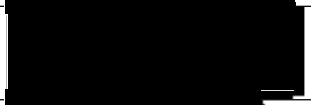	14/10/2008
M.K. Horne	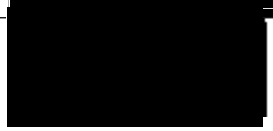	14/10/2008
J.S. Forsythe		14/10/2008

Declaration for Thesis Chapter 6.2

Monash University

Declaration by candidate

In the case of Chapter 6.1 the nature and extent of my contribution to the work was the following:

Nature of contribution	Extent of contribution (%)
Experimental design and conduct and article writing.	85

The following co-authors contributed to the work. Co-authors who are students at Monash University must also indicate the extent of their contribution in percentage terms:

Name	Nature of contribution	Extent of contribution (%) for students
D. Moses	Assisted in experimentation & corrected manuscript	N/A
T.R. Gengenbach	Assisted in experimentation & corrected manuscript	N/A
J.S. Forsythe	Experimental design and corrected manuscript	N/A
D.I. Finkelstein	Experimental design and corrected manuscript	N/A
M.K. Horne	Experimental design and corrected manuscript	N/A

Candidate's Signature	[redacted]	Date 14/10/2008

Declaration by co-authors

The undersigned hereby certify that:

(7) the above declaration correctly reflects the nature and extent of the candidate's contribution to this work, and the nature of the contribution of each of the co-authors.
(8) they meet the criteria for authorship in that they have participated in the conception, execution, or interpretation, of at least that part of the publication in their field of expertise;
(9) they take public responsibility for their part of the publication, except for the responsible author who accepts overall responsibility for the publication;
(10) there are no other authors of the publication according to these criteria;
(11) potential conflicts of interest have been disclosed to (a) granting bodies, (b) the editor or publisher of journals or other publications, and (c) the head of the responsible academic unit; and

(12) the original data are stored at the following location(s) and will be held for at least five years from the date indicated below:

Name	Location
D. Moses	Melbourne University - Howard Florey Institute
T.R. Gengenbach	CSIRO, Molecular and Health Technologies
J.S. Forsythe	Monash University - Department of Materials Engineering
D.I. Finkelstein	The Mental Health Research Institute of Victoria
M.K. Horne	Melbourne University - Howard Florey Institute

Name	Signature	Date
D. Moses	[redacted]	14/10/2008
T.R. Gengenbach	[redacted]	14/10/2008
J.S. Forsythe	[redacted]	14/10/2008
D.I. Finkelstein	[redacted]	14/10/2008
M.K. Horne	[redacted]	14/10/2008

6.0 *In vitro* experimentation

6.1 Studying the morphology and gelation of xyloglucan hydrogels for tissue engineering applications.

In addition to the poly (α-hydroxyl esters) that have been discussed in Part I of this thesis, the potential for using thermally sensitive xyloglucan hydrogels was investigated, as it provides a minimally invasive means of deploying the scaffold via injection. Ultimately both the electrospun scaffolds (Part I) and the xyloglucan (Part II) will be combined into a 'composite' scaffold. This will be discussed in greater detail within Part III of this thesis.

This study investigates the thermal and rheological properties of xyloglucan with considerations of using it as an injectable scaffold for neural tissue engineering. The effect of ionic strength on the gelation temperature was investigated and for the first time the morphology of the hydrogel is presented.

Morphology and gelation of thermosensitive xyloglucan hydrogels

D.R. Nisbet [a,b], K.E. Crompton [a,b], S.D. Hamilton [a], S. Shirakawa [e], R.J. Prankerd [c], D.I. Finkelstein [d], M.K. Horne [d], J.S. Forsythe [a,b*]

a Department of Materials Engineering, Monash University, Wellington Rd, Clayton, VIC 3800, Australia
b CRC for Polymers, 32 Business Park Drive, Notting Hill, VIC 3168, Australia
c Department of Pharmaceutics, Monash University, 381 Royal Parade, Parkville, VIC 3052, Australia
d Howard Florey Institute, Gate 11, Royal Parade, The University of Melbourne, VIC 3010, Australia
e Research and Development,, Dainippon Sumitomo Pharma Co. Ltd. 5-51, Ebie 1-chome, Fukushima-ku Osaka, 553-0001, Japan

6.1.1 Abstract

Galactose modified xyloglucan is a thermally reversible hydrogel that is increasingly used in the biomedical field due to the ease of altering the gelation time and temperature by modifying the galactose removal ratio. However there is little information concerning the morphology and rheological properties of the hydrogel under physiological conditions. Differential scanning microcalorimetry (DSµC) showed the thermal gelation process to occur over a broad temperature range (5–50 °C). The rheological properties of the hydrogels were investigated as a function of concentration, temperature and ionic strength. The final elastic moduli of the hydrogels increased with increases in concentration. Isothermal rheology suggests that the gelation occurred in two distinct stages, which was influenced by the solution media. Scanning electron microscopy (SEM) was used to characterize the morphology of the xyloglucan which were thermally gelled at 37 °C. The resultant morphology was strongly dependent on the concentration of the hydrogel. Strong hydrogels were only obtained at 3 wt.% at 37 °C, and the morphology characterized by an open 3-dimensional network, comprised of thin membranes. It is proposed that the first stage of the isothermal gelation is the formation

and growth of the thin membranes, followed by the formation of a three dimensional network.

6.1.2 Keywords:

Xyloglucan; Hydrogel; Rheology; Scanning electron microscopy; Morphology

6.1.3 Introduction

There has been growing interest in the use of thermally sensitive in situ forming, physical hydrogels for biomedical applications [1,2] as minimally invasive scaffolds for tissue engineering. Because of their low interfacial tension and high molecular and oxygen permeability, hydrogels are ideal tissue engineering constructs [3]. Consequently, hydrogels have been investigated for cell gene therapy [4], enzyme and cell encapsulation [5–7], drug delivery [8–11], joint cushioning and lubrication [8,12] and as environmental shape memory materials [4]. The utility of hydrogels as tissue engineering scaffolds appears to be related to microscopic [13] and macroscopic [14] porosity within the structure of hydrogels. Microscopic pore interconnectivity and the volume of water phase present within the hydrogel ensures cellular viability, permits cell migration, increases transportation of nutrients, oxygen and metabolites [15], and influences drug release profiles and enzymatic degradation [8]. The shape and size distribution of the pores also influence cellular function [8]. By exploiting these features it may be possible to mimic features of the natural extracellular matrix, and control tissue structure and cellular functions [16].

Xyloglucan is a neutral, non-toxic polysaccharide [17], whose degradation products consist of naturally occurring saccharides and are assumed non-toxic, although the experimental evidence for this conclusion is limited. Xyloglucan is extracted from the tamarind seed and is a major component of higher plant cell walls [18]. It is composed of

a β-1,4 linked D-glucan backbone where the *O-6* positions of the glucopyranosyl residue are partially substituted with α-D-xylopyranose residue [11,19]. Fig. 1 shows the backbone structure of xyloglucan and Fig. 2 presents the structure of the galactopyranose, glucopyranose and xylopyranose which make up the polysaccharide.

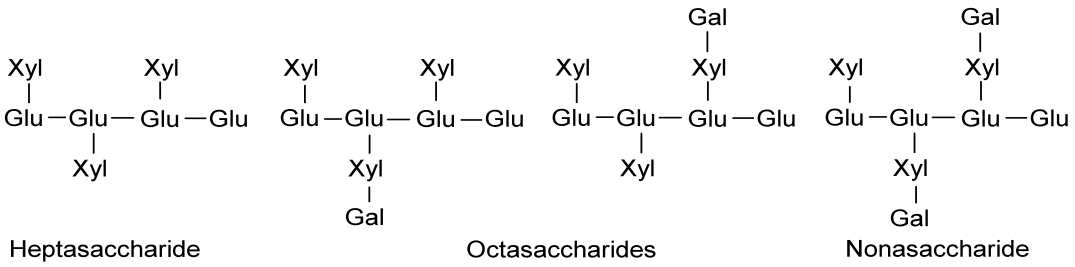

Figure 1 : Backbone structure of xyloglucan [17]

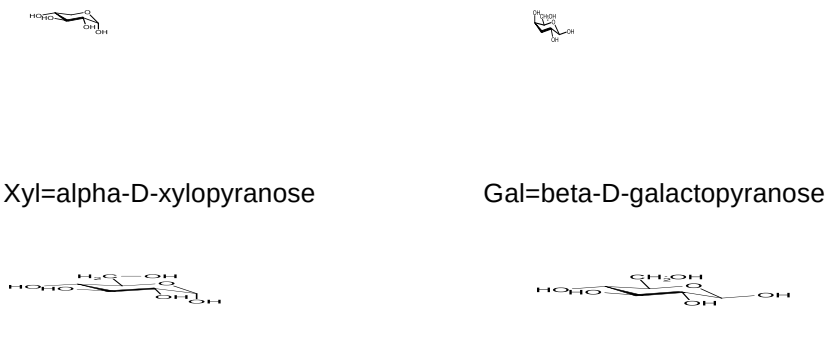

Figure 2: Glucose units that exist in the three oligomer structures in xyloglucan

Thermally responsive xyloglucan is formed using fungal β-galactosidase to remove more than 35% of the galactose residue [17]. Shirakawa *et al.* [17] found that the optimum removal ratio was between 35% and 50%. Using DSC and rheology they related gelation temperature to the concentration of xyloglucan in the pre-gel solution. Miyazaki *et al.* [11] found that increasing the concentration of the pre-gel solution from 1% to 2% decreased gel temperature from 27 to 22 °C as well as the gel time. A lower and upper transition from sol–gel and gel–sol, respectively, were found, and the gel was shown to

be thermo-reversible upon cooling. It was also determined that with a higher galactose removal ratio there was an increase in temperature range of the gelation peaks, hence a broader gelation range [17].

While tissue engineering applications for xyloglucan are not extensive, it has been used as skin patches [20], oral and rectal delivery of drugs [11], and for intraperitoneal injections [21]. It was drug loaded in the latter two applications and was found to provide stronger bioavailability of the relevant drug and longer residence times than previous commercial suppositories [22] Importantly there was no apparent tissue damage [11] implying that xyloglucan hydrogel is a biocompatible material that can be implanted non-invasively via injection in tissue engineering applications.

X-ray scattering studies of the gel nano-structure of galactose-modified xyloglucan, showed that flat structures were formed from lateral stacking of rod-like chains [23] whereas the addition of ethanol to the solution created a random structure consisting of condensed phase aggregates amongst dilute, single chain areas [24].

This study aims to investigate the thermal, Rheological properties of thermally gelling xyloglucan with a galactose removal ratio of 48% with consideration of its use as an injectable tissue engineering scaffold. The effect of changing the ionic strength of solution media on the properties of the hydrogel were determined by comparing deionised water and phosphate buffered saline (PBS) as solution media. This study also presents for the first time, the morphology of the gel networks as determined using electron microscopy.

6.1.4 Methodology

6.1.4.1 Materials

Xyloglucan with a 48% galactose removal ratio was prepared by enzymatic modification from tamarind seed xyloglucan, according to previous method [17]. It was purified by dissolving 1 wt.% xyloglucan in deionized water with a magnetic stirrer at a temperature between 0 and 5 °C. The solution was then precipitated out in 60% ethanol at room temperature and washed with 60% ethanol through a sintered glass filter and flask with attached vacuum pump. An additional wash was conducted using acetone. The precipitate was then dried at room temperature for two days in a vacuum oven.

6.1.4.2 Sample preparation

Sample solutions were prepared by dissolving the purified xyloglucan in either deionised water or PBS at concentrations of 0.5, 1.0, 1.5, 2.0, 2.5 and 3.0 wt.% and stirred in an ice bath until no particles were visible, and stored at 0–5 °C.

6.1.4.3 Rheology

Rheological measurements of the elastic (G′) and viscous (G″) shear moduli and gelation temperature were taken for solutions of 2.0, 2.5 and 3.0 wt.% in both deionised water and PBS using a Bohlin CS-50 rheometer in parallel plate configuration, and within the linear viscoelastic region of the gels. Measurements were conducted using frequencies of 0.1, 0.316, 1.0, 3.19 and 10 Hz with the strain rate held at 1.25% with an initial stress of 0.245 MPa. The isothermal studies were conducted at 37 °C to determine the induction time of gelation, or the time where the phase shift was independent of frequency. For this experiment the sample was placed into the rheometer at 5 °C and allowed to rest for 90 s

before raising to 37 °C. Rheology was also conducted using temperature ramping of 1 °C intervals over the range 5–50 °C.

6.1.4.4 Differential scanning microcalorimetry

Differential scanning microcalorimetry (DSμC) was used to determine the gelation temperature at the lower concentrations (0.5, 1.0 and 1.5 wt.%) in deionised water and PBS solutions. The samples equilibrated for 30 min before the temperature was ramped from 5 to 50 °C at 1 °C/min, using a N-DSC II differential scanning microcalorimetry (Model 6100, Calorimetry Sciences Corporation; baseline noise range, 30nW). Aliquots of xyloglucan solution and an appropriate control (deionised water and PBS solution, respectively) were used. The scan was conducted under atmospheric pressure to avoid damaging the delicate hydrogel networks by pressure-influenced thermal events [8]. To avoid significant evaporation the maximum temperature was limited to 50 °C. The samples were scanned in triplicate and the baseline was subtracted from the heat flow, which was normalized against the xyloglucan weight.

6.1.4.5 Scanning electron microscopy (SEM)

Samples were gelled at 37 °C on a microscope slide before being quenched with liquid nitrogen and freeze dried under vacuum for 48 h. The sections were then sputter-coated with gold using a Bal-Tec SCD 005, Balzers for 180 s before SEM was preformed using a Hitachi S-570 SEM with an accelerating voltage of 15 kV and a magnification ranging from 50 to 1000 times.

6.1.5 Results and discussion

6.1.5.1 Thermal and rheological characterization

The gelation characteristics of the xyloglucan hydrogels at concentrations ranging from 0.5 to 3 wt.% were studied using DSµC and rheology in both water and PBS to determine if there was a change in the gelation behavior due to changes in ionic strength. At concentrations less than 2.0 wt.%, Rheological characterisations showed that the physical gels were weak and their elastic modulus, (E′), did not increase as temperature increased. Consequently, DSµC was used to study the gelation behavior at concentrations below 2 wt.% (at higher concentrations this technique was inadequate because the gels became viscous, even at low temperature, making their insertion and removal from the apparatus difficult).

Table 1 : Elastic/viscous modulus cross-over point obtained using scanning rheometry.

Concentration wt%	Cross over point at 0.1 Hz (°C)		Gel temperature (°C)		Maximum elastic modulus (MPa)	
	Water *	PBS*	Water*	PBS*	Water**	PBS**
2.0	18 ± 2	23 ± 2	37 ± 2	36 ± 2	0.15 ± 0.03	0.17 ± 0.04
2.5	17 ± 2	21 ± 2	35 ± 2	36 ± 2	0.20 ± 0.06	0.25 ± 0.04
3.0	18 ± 2	20 ± 2	34 ± 2	35 ± 2	0.48 ± 0.05	0.32 ± 0.07

**** Errors estimated from the best possible resolution of the tan δ graphs.***

***** Errors were calculated using the standard deviation of the mean method (95% confidence interval)***

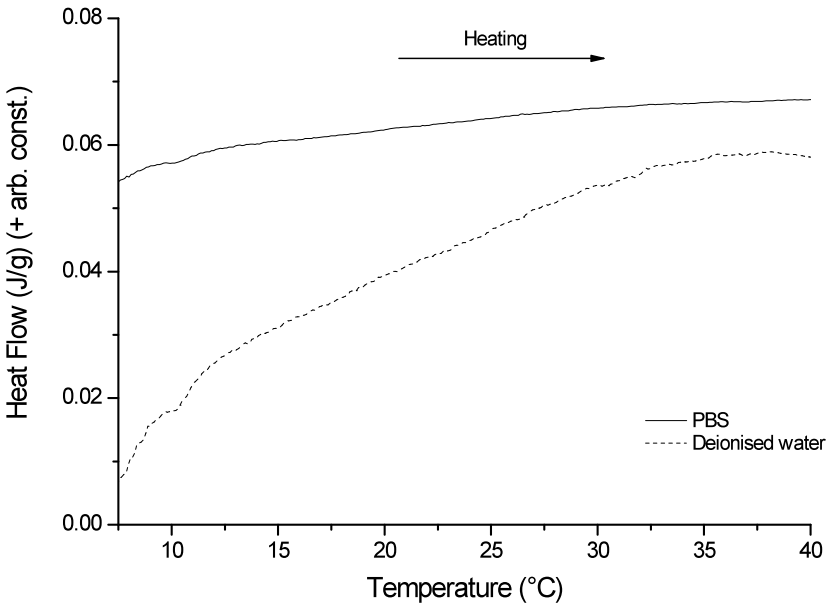

Figure 3: DSµC heating curve for 0.5 wt% xyloglucan in deionised water and PBS (arbitrary constant on Y scale).

Figs. 3 and 4 show the DSµC heating and cooling curves, respectively, of the 0.5 wt.% solutions in both deionised water and PBS. The thermograms in both media exhibited a broad and non-resolved endotherm during heating between 9 and 50 °C indicating that the gelation process occurred slowly over this temperature range and began at low temperatures (Fig. 3). However, the endotherm of the PBS media was not as pronounced as that of the deionised water media. The cooling thermograms are shown in Fig. 4. Exotherms were observed in all the samples and the area of these exotherms increased with increasing concentration of xyloglucan (for example 1 wt.% PBS Fig. 4). The temperature onset of the exotherm was increased in PBS, indicating that the ionic strength was accelerating the gel to sol transition. Due to the low temperature limitations of the DSµC instrument, some of the exotherms could not be resolved.

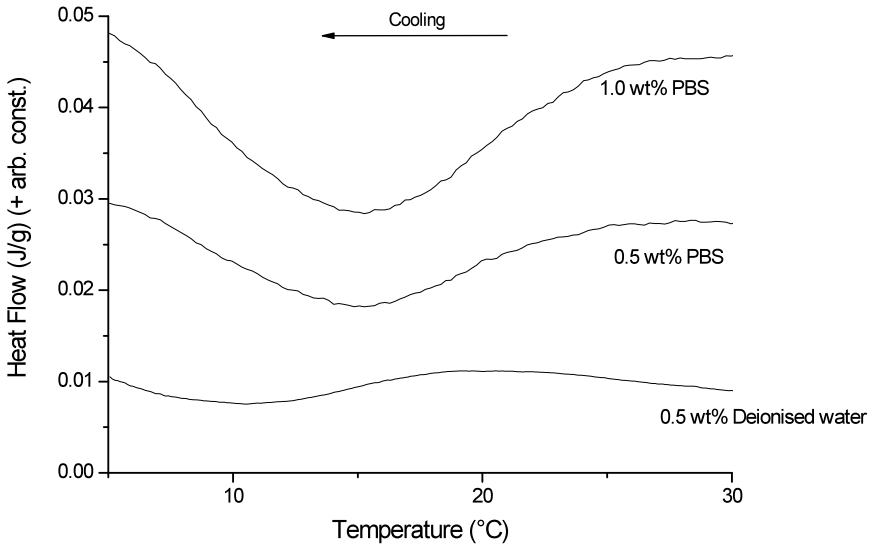

Figure 4: DSμC cooling curve for 0.5 wt% xyloglucan in deionised water and PBS (arbitrary constant on Y scale).

Fig. 5 shows the change in the elastic modulus (E′) and the viscous modulus (E″) as a function of temperature for the 3 wt. % xyloglucan in PBS. The cross over point of the E′ and E″ gives an indication of the transition from the initial dominant viscous liquid-like behavior to elastic solid or gel-like behavior [25]. All compositions exhibited a cross-over point in the temperature range of 17–23 °C and was largely insensitive to concentration and solution media in the ranges investigated (Table 1). The samples exhibited frequency dependence prior to the cross-over point, i.e., increasing E′ with increasing frequency, indicating the presence of a weak gel at these low temperatures. Following the cross-over point, there was a rapid increase in the E′ attributed to the formation of the network gel structure. The gel point, as determined by the frequency independence in tan δ (Fig. 6, Table 1), was also insensitive to the composition of xyloglucan and ionic strength of the solution media in the concentration ranges investigated. At temperatures above 40 °C, the maximum elastic moduli were achieved for all samples (Table 1) and was found to increase with increasing concentration. Interestingly, the maximum elastic moduli were also insensitive to the ionic strength, except for the 3 wt.% solution which formed a

significantly weaker gel (0.32±0.07 in PBS compared to 0.48±0.05 for water). In this instance, the higher ionic strength may be interfering with the hydrophobic associations of the xyloglucan.

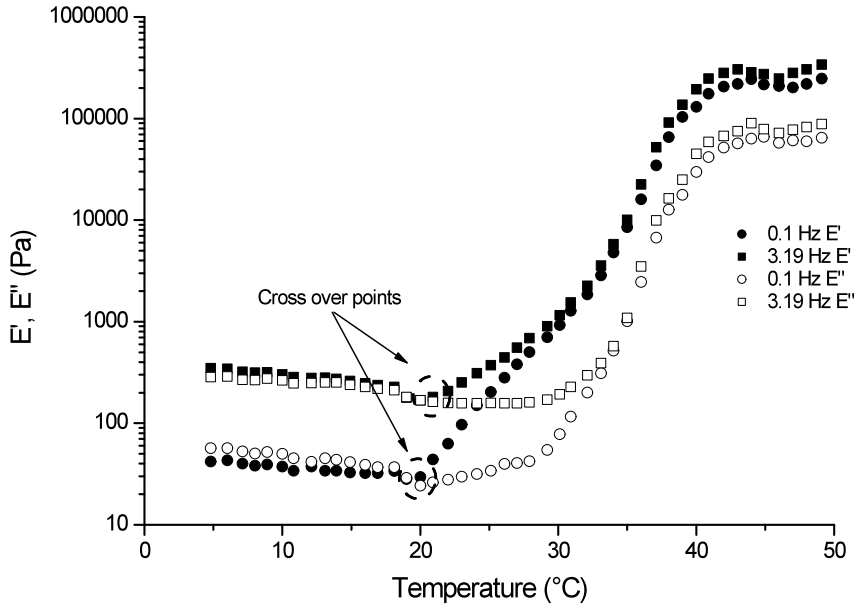

Figure 5: Modulus versus Temperature for a 3 wt% xyloglucan in PBS solution.

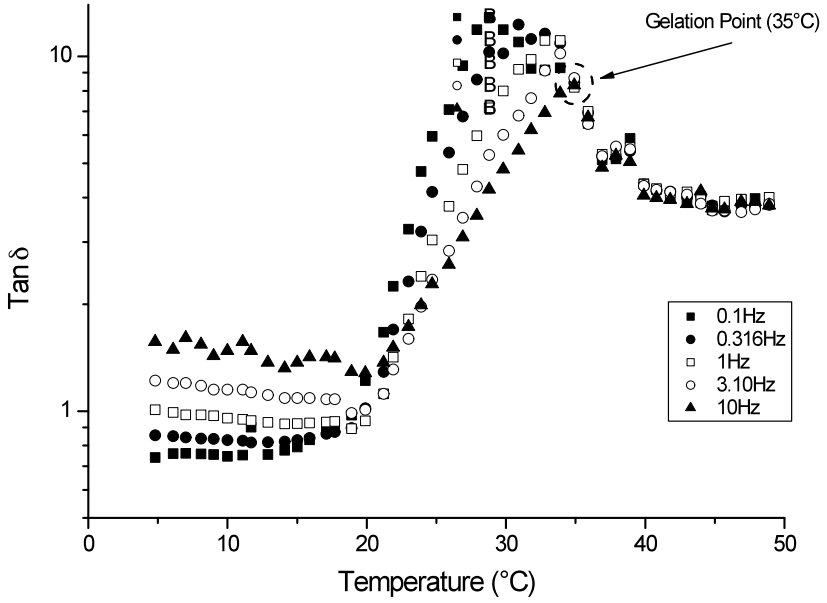

Figure 6: Tan δ verses temperature curves for 3 wt% xyloglucan in PBS solution.

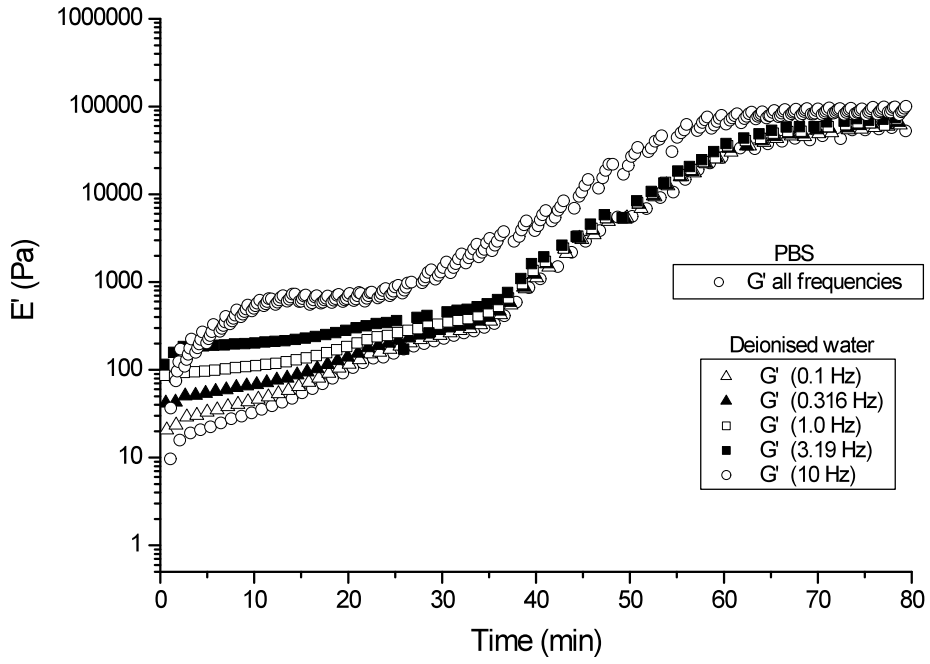

Figure 7: Isothermal gelation (37°C) of xyloglucan showing the elastic modulus E' as a function of time and solution media.

Isothermal rheological experiments were also conducted at 37 °C with consideration of future *in vivo* studies where the sol will be injected into the body and allowed to gel *in situ.* Concentrations less than 3 wt.% failed to form strong physical gels at 37 °C regardless of the type of solution media and hence only the 3 wt.% compositions were investigated. Fig. 7 shows the elastic modulus as a function of time for the deionised water and PBS solutions. The deionised water sample exhibited a steady rise in E′ which was also frequency dependent up to the gel point at (44.7 min, frequency independence of tan δ, Fig. 8) at which point there was a dramatic increase in E′. The introduction of PBS as the solution media had a significant effect on the isothermal gelation behavior. Fig. 7 shows that the PBS has an initially higher elastic modulus which is frequency independent at all times compared to the deionised water solution. The corresponding tan δ curves (Fig. 8) indicate that both systems exhibit similar gelation times (formation of a 3 dimensional network), however the elastic modulus is dominating both before and after gelation. The PBS also decreased the time to reach the maximum elastic modulus (60min compared to 73min for deionised water). The final elastic moduli for the 3wt.%

xyloglucan gels were insensitive to solution media and were approximately 100,000 Pa. This value is several orders of magnitude higher than other biological or synthetic physical hydrogels (Table 2).

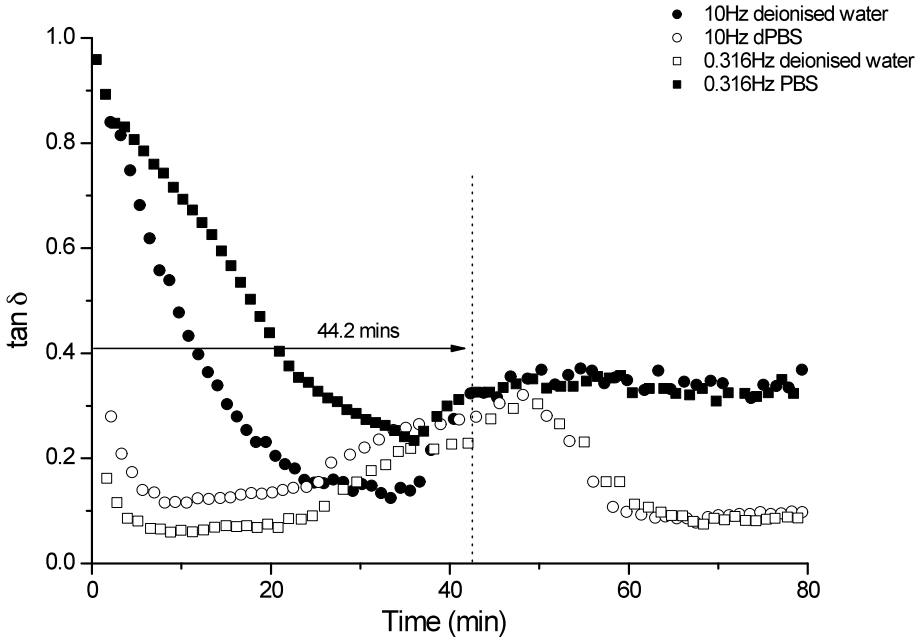

Figure 8: Isothermal tan δ curves of 3.0wt% xyloglucan in deionised water and PBS at 37°C. The induction time for gelation for both media is shown.

Table 2: Comparison of shear modulus with other hydrogels.

Material	*Modulus (Pa)*	*Reference*
Xyloglucan	E' = 150000-480000	Experimental
2 w/v% chitosan/GP	E' = 6,000	Chenite *et al.* [27]
Chitosan/xanthan (MW=10^6 g/mol)	E' = 60,000	Magnin *et al.* [28]
1 w/v% agarose	E^* = 12.5	Balgude *et al.*[29]
Matrigel (basal) Matrigel (crosslinked)	E' = 34 E' = 118	Semler *et al.* [30]
Biomatrix I (ECM)	E' = 20-35	Snyder *et al.* [31], Parsons *et al.* [32]
Type I collagen	E' = 5-60	Knapp *et al.* [33], Parsons *et al.* [32]
PHPMA	E^* = 250 E' = 2600	Woerly *et al.* [34]
1 w/v% Pluronic-PAA	E' = 100	Huibers *et al.* [35]
Polylysine-b-polyleucine copolymer	E = 12-4273	Breedveld *et al.*

Note E* is the storage modulus (i.e. E* = E' + iE").

6.1.5.2 Microstructure characterization and gelation mechanism

Macro-porous hydrogels can be examined using scanning electron microscopy (SEM) after freeze drying [22] when the material has an adequate modulus to avoid the structural collapse during dehydration [26]. The morphology of xyloglucan gels, whose temperature was held at 37 °C for approximately 5000 s prior to quenching in liquid nitrogen, was examined using SEM. Fig. 9 shows SEM of a range of concentrations (2.0, 2.5 and 3 wt. %) of xyloglucan gels. The SEM of 2.0 wt.% shows the gel structure collapsed, confirming that only weak gels formed at this concentration. However, some large flat sheets approximately 150 μm in length and 80 μm in width are present. A lath sheet-like structure was formed within the 2.5 wt.% sample and sheets were more numerous, larger (200 μm in length and 100 μm in width) with inclusions of macropores. There was almost no interconnection between laths and it is possible that the large sheets were torn. However, a significantly stronger gel was formed which did not collapse upon freeze drying when the concentration of xyloglucan was further increased to 3 wt.%. The SEM images showed a sheet-like or membrane structure with significant interconnection forming a 3-dimensional network (an example of this is highlighted in Figs. 10–11). The

morphology of the final hydrogel was insensitive to the solution media. Fig. 10 also shows membranes fused together forming an interconnected cellular 3-dimensional network. In many instances, the membranes appear to be torn, probably as a result of the freeze drying process. The average pore ranged between 50 and 150 μm in size.

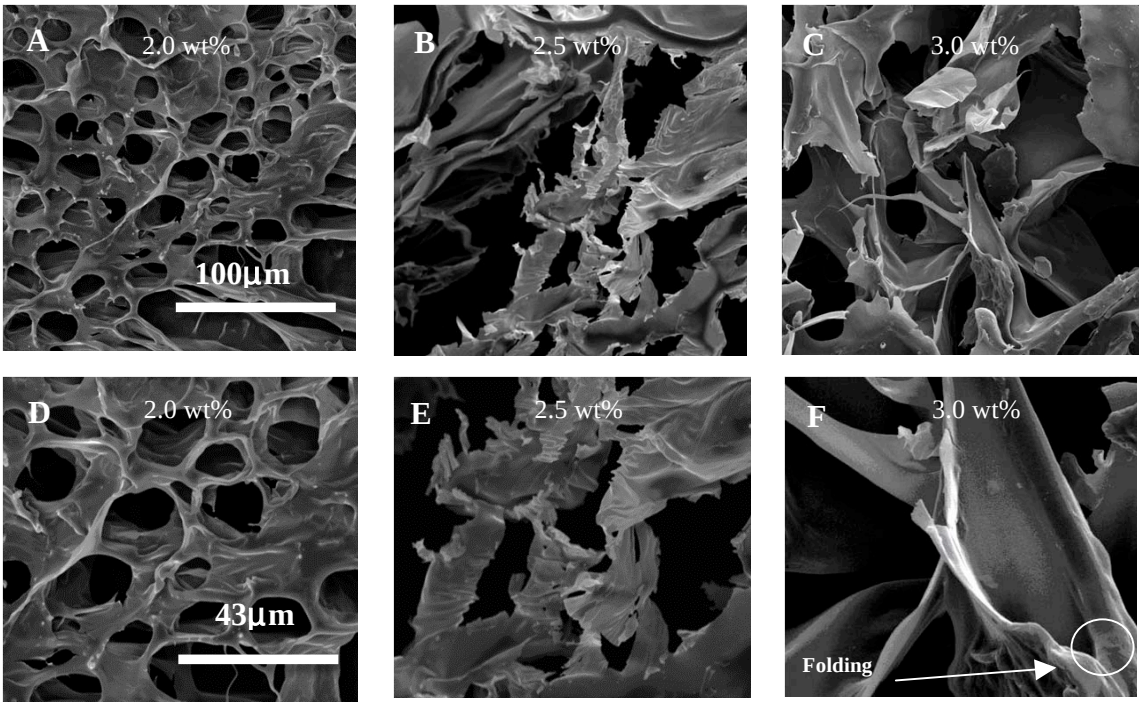

Figure 9: SEM images of the surface morphology of xyloglucan at different concentration and magnifications. Note that A-C and D-E all have the same magnification hence error bar size.

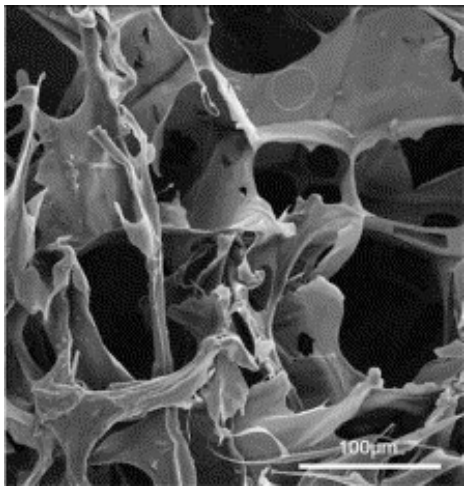

Figure 10: A high magnification image of 3wt% xyloglucan in water.

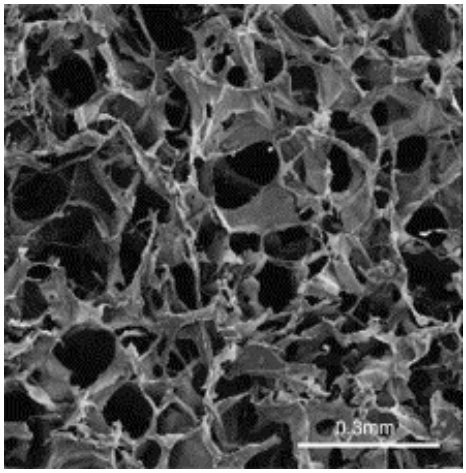

Figure 11: A high magnification image of 3wt% xyloglucan in water.

6.1.6 Conclusion

Xyloglucan is a thermally reversible hydrogel that has a significantly higher modulus than most other hydrogels. In this study the microstructural and rheological results indicated that the gelation of xyloglucan occurs as a 2 stage process. The first step, which is not concentration dependent, is the initial formation of large membrane structures in the pre gel. This accounts for the initially high modulus and, as the sheets refract light, also explains why the pre-gel solution is opaque. The formation of the membrane structures appears to be accelerated by the presence of ions in the PBS. The second stage involves the joining of membranes into a very strong 3-dimensional network. This process and the final morphology is independent of the solution media.

6.1.7 Acknowledgements

I would like to thank W.D. Cook for use of the rheometer, and I. Harper for use of the SEM. This project was funded by the CRC for Polymers and the ARC project DP0450618.

6.1.8 References

[1] A.S. Hoffman, Hydrogels for biomedical applications, Adv. Drug Deliv. Rev. 43 (2002) 3–12.

[2] J.M. Rosiak, F. Yoshii, Hydrogels and their medical applications, Nucl. Instrum. Methods Phys. Res., Sect. B, Beam Interact. Mater. Atoms 151 (1–4) (1999) 56–64.

[3] B.D. Ratner, A.S. Hoffman, Synthetic hydrogels for biomedical applications, Hydrogels for Medical and Related Applications, 1976, pp. 1–36.

[4] P. Petrini, S. Fare, A. Piva, M.C. Tanzi, Design, synthesis and properties of polyurethane hydrogels for tissue engineering, J. Mater. Sci., Mater. Med. 14 (2003) 683–686.

[5] P. Aebischer, L.Wahlberg, P.A. Tresco, S.R.Winn, Macroencapsulation of dopamine-secreting cells by coextrusion with an organic polymer solution, Biomaterials 12 (1991) 50–56.

[6] D.F. Emerich, S.R. Winn, L. Christenson, M.A. Palmatier, F.R. Gentile, P. R. Sanberg, A novel approach to neural transplantation in Parkinson's disease: use of polymer-encapsulated cell therapy, Neurosci. Biobehav. Rev. 16 (1992) 437–447.

[7] B.A. Zielinshi, P. Aebischer, Chitosan as a matrix for mammalian cell encapsulation, Biomaterials 15 (1) (1994) 1049–1056.

[8] K.E. Crompton, R.J. Prankerd, D.M. Paganin, T.F. Scott, M.K. Horne, D.I. Finkelstein, K.A. Gross, J.S. Forsythe, Morphology and gelation of thermosensitive chitosan hydrogels, Biophys. Chem. 117 (2005) 43–49.

[9] D. Cohn, A. Sosnik, A. Levy, Improved reverse thermo-responsive polymeric systems, Biomaterials 24 (2003) 3707–3714.

[10] J.L. Drury, D.L. Mooney, Hydrogels for tissue engineering: scaffold design variables and applications, Biomaterials 24 (2003) 4337–4351.

[11] S. Miyazaki, F. Suisha, M. Kawasaki, M. Shirakawa, K. Yamatoya, D. Attwood, Thermally reversible xyloglucan gels as vehicles for rectal drug delivery, J. Control. Release 56 (1998) 75–83.

[12] R. Barbucci,., Hyaluronic acid hydrogel in the treatment of osteoarthritis, Biomaterials 23 (2002) 4503–4513.

[13] L.M. Pakstis, B. Ozbas, K.D. Hales, A.P. Nowak, T.J. Deming, D. Pochan, Effect of chemistry and morphology on the biofunctionality of selfassembling diblock copolypeptide hydrogels, Biomacromolecules 5 (2004) 312–318.

[14] H.R. Oxley, P.H. Corkhill, J.H. Fitton, B.J. Tighe, Macroporous hydrogels for biomedical applications: methodology and morphology, Biomaterials 14 (14) (1993) 1064–1072.

[15] A.L. Sieminski, K.J. Gooch, Biomaterial-microvasculature interactions, Biomaterials 21 (2000) 2233–2241.

[16] K.Y. Lee, D.J. Mooney, Hydrogels for tissue engineering, Chem. Rev. 101 (7) (2001) 1869–1879.

[17] M. Shirakawa, K. Yamotoya, K. Nishinari, Tailoring of xyloglucan properties using an enzyme, Food Hydrocoll. 12 (1998) 25–28.

[18] W.D. Reiter, Biosynthesis and properties of the plant cell wall, Curr. Opin. Plant Biol. 5 (6) (2002) 536–542.

[19] K. Yamatoya, M. Shirakawa, K. Kuwano, J. Suzuki, O. Baba, Hypolipidemic effects of hydrolyzed xyloglucan, Macromol. Symp. 120 (1997) 231–236.

[20] F.M. Strickland, Y. Sun, A. Darvill, S. Eberhard, M. Pauly, P. Albersheim, Preservation of the delayed-type hypersensitivity response to alloantigen by xyloglucans or oligogalacturonide does not correlate with the capacity to reject ultraviolet-induced shin tumors in mice, J. Invest. Dermatol. 116 (1) (2001) 62–68.

[21] F. Suisha, N. Kawasaki, S. Miyazaki, M. Shirakawa, K. Yamatoya, M. Sasaki, D. Attwood, Xyloglucan gels as sustained release vehicles for the intraperitoneal administration of mitomycin C, Int. J. Pharm. 172 (1–2) (1998) 27–32.

[22] E. Ruel-Gariepy, A. Chenite, C. Chaput, S. Guirguis, J.C. Leroux, Characterization of thermosensitive chitosan gels for the sustained delivery of drugs, Int. J. Pharm. 203 (2000) 89–98.

[23] Y. Yuguchi, The carious types of gelation mechanisms of xyloglucan, Cellul. Commun. 9 (2) (2002) 76–80.

[24] S. Yamanaka, Y. Yuguchi, H. Urakawa, K. Kajiwara, M. Shirakawa, K. Yamatoya, Felation of tamarind seed polysaccharide xyloglucan in the presence of ethanol, Food Hydrocoll. 14 (125–128) (2000).

[25] M. Shirakawa, Y. Uno, K. Yamatoya, K. Nishinari, Rheological and thermal studies on the sol–gel transition of aqueous solutions of enzymically modified xyloglucan, Spec. Publ.- R. Soc. Chem., 218 (Gums and Stabilisers for the Food Industry 9) (1998) 94–103.

[26] R. Bellamkonda, J.P. Ranieri, N. Bouche, P. Aebischer, Hydrogel-based three-dimensional matrix for neural cells, J. Biomed. Mater. Res. 29 (5) (1995) 663–671.

[27] A. Chenite, M. Buschmann, D.Wang, C. Chaput, N. Kandani, Rheological characterisation of thermogelling chitosan/glycerol–phosphate solutions, Carbohydr. Polym. 46 (2001) 39–46.

[28] D. Magnin, J. Lefebvre, E. Chorbet, S. Dumitriou, Physicochemical and structural characterization of a polyionic matrix of interest in biotechnology, in the pharmaceutical and biomedical fields, Carbohydr. Polym. 55 (2004) 437–453.

[29] A.P. Balgude, X. Yu, A. Szymanski, R. Bellamkonda, Agarose gel stiffness determines rate of DRG neurite extension in 3D cultures, Biomaterials 22 (10) (2001) 1077–1084.

[30] E.J. Semler, C.S. Ranucci, P.V. Moghe, Mechanochemical manipulation of hepatocyte aggregation can selectively induce or repress liver-specific function, Biotechnol. Bioeng. 69 (4) (2000) 359–369.

[31] J. Snyder, A new instrument for evaluating the stresses hepatocytes produce during aggregation, Mechanical Engineering and Engineering Science, University of North Carolina at Charlotte, Charlotte, 1999.

[32] J.W. Parsons, R.N. Coger, A new device for measuring the viscoelastic properties of hydrated matrix gels, J. Biomech. Eng. 13 (18) (2002) 145–154.

[33] B. Knapp, V. Barocas, A. Moon, K. Yoo, L. Petzold, R. Tranquillo, Rheology of reconstituted type I collagen gel in confined compression, J. Rheol. 41 (1997) 971–993.

[34] S.Woerly, E. Pinet, L. de Robertis, M. Bousmina, G. Laroche, T. Roitback, L. Vargová, E. Syková, Heterogeneous PHPMA hydrogels for tissue repair and axonal regeneration in the injured spinal cord, J. Biomater. Sci., Polym. Ed. 9 (7) (1998) 681–711.

[35] P.D.T. Huibers, L.E. Bromberg, B.H. Robinson, T.A. Hatton, Gelation in semidilute aqueous solutions of associative polymers: a small-angle neutron scattering study, Macromolecules 32 (15) (1999) 4889–4894.

[36] V. Breedveld, A.P. Nowak, J. Sato, T.J. Deming, D.J. Pine, Rheology of block copolypeptide solutions: hydrogels with tunable properties, Macromolecules 37 (10) (2004) 3943–3953.

6.2 Investigating the interaction of neurons and stem cells with thermosenisitive xyloglucan for neural tissue engineering.

Xyloglucan scaffolds had a suitable morphology and gelation properties for neural tissue engineering applications; hence the next step was to investigate the cellular biocompatibility of cortical neurones and neural stem cells, cultured on and encapsulated within the scaffold.

The capacity of xyloglucan to support neurones and neural stem cells was first evaluated utilizing a 2D study. The cellular biocompatibility was investigated for 3 wt% xyloglucan, and 3 wt% xyloglucan with poly-$_D$-lysine immobilised. The density of the cells, their size, and shape and colonisation response was evaluated. The density of the neural process and differentiation of the NSCs towards neurones was also investigated.

Enhancing neurite outgrowth from primary neurones and neural stem cells using thermoresponsive hydrogel scaffolds for the repair of spinal cord injury

D. R. Nisbet [1 2], D. Moses [3], T. R. Gengenbach [4], J. S. Forsythe [1 2], D. I. Finkelstein [5], M. K. Horne [3 *]

[1]*Department of Materials Engineering, Division of Biological Engineering, Monash University, Victoria 3800, Australia*
[2]*CRC for Polymers, 8 Redwood Drive, Notting Hill, Victoria 3168, Australia*
[3]*Howard Florey Institute, University of Melbourne, Victoria 3010, Australia*
[4]*CSIRO, Molecular and Health Technologies, Bag 10, Clayton South, Victoria 3168, Australia*
[5]*The Mental Health Research Institute of Victoria, 155 Oak Street, Locked Bag 11, Parkville, Victoria 3052, Australia*

6.2.1 ABSTRACT

In this study, thermoresponsive xyloglucan hydrogel scaffolds were investigated as candidates for neural tissue engineering of the spinal cord. The hydrogels were optimized to provide similar mechanical properties to that of native spinal cord, although also being functionalized through the immobilization of poly-$_D$-lysine to promote neurone adhesion and neurite outgrowth. Under 2D and 3D culture conditions, xyloglucan scaffolds supported the differentiation of primary cortical neurones. Furthermore, functionalization provided a means of controlling and optimizing the cell diameter, number, migration and the neurite density, and the direction of growth. The interaction of neural stem cells (NSCs) was also investigated on the xyloglucan scaffolds *in vitro*. The survival of the NSCs and the axonal extensions on the scaffolds were similar to that of the primary cortical neurones. These findings suggest that xyloglucan-based materials are suitable for providing a neurotrophic milieu.

6.2.2 KEY WORDS

hydrogel • neural tissue engineering • nerve regeneration • stem cell • spinal cord

6.2.3 INTRODUCTION

Neurones within the spinal cord create complex functional networks. When injured by trauma, the recovery of these networks is limited by the inability of the nervous system to self repair.[1-4] Regeneration of the spinal cord is prevented in part by glial scars,[2][5] inhibiting molecules[3] and lack of relevant stimulatory cues. Artificial scaffolds have been investigated as a means of addressing these inhibitory stimuli.[6][7] They can also be designed to provide a physical cellular microenvironment containing signaling molecules that promote cell attachment, while regulating and guiding axonal extension. There has been growing interest in the use of hydrogels as scaffolds that achieve these aims.[8-11] Thermoresponsive hydrogels, both natural and synthetic, are particularly attractive as these hydrogels undergo solution-gelation transitions and hence can be delivered by minimally invasive injection.[12]

Hydrogels consist of a highly interconnected three-dimensional (3D) porous network, which promotes cell viability by permitting migration and increasing the transportation of nutrients, oxygen and metabolites.[13] Pore size can be regulated to allow regenerating neural processes to penetrate the scaffold, as neurite outgrowth is inhibited when pore size is too narrow. Conversely, the cellular microenvironment may not be optimal when the scaffold pores are too large. The pore size of hydrogels can be designed to change with time to either initiate or assist neurites to extend. For instance, the degradation of polyethylene glycol 3D hydrogels have been used to directly control neurite outgrowth by the creation of macropores over time.[7]

Techniques successfully employed in the peripheral nervous system, such as the formation of guidance channels are now being employed to induce spinal cord regeneration. These attempts involve fabricating tubes from hydrogels such as chitosan[14] and poly(2-hydroxyethyl methacrylate-*co*-methyl methacrylate),[15] and scaffolds made from macroporous hydrogels such as agarose.[16] Although these

scaffolds provide physical pathways for regeneration, Schwann cells have been incorporated to provide molecular and cellular guidance within the tubes.[17]

Physiochemical and structural characteristics of hydrogel scaffolds also influence neuronal behavior. The length of a neurite extension is directly proportional to the magnitude of charge on a hydrogel scaffold with a positively charged scaffold inducing longer neurites.[18] However, neurite outgrowth is inhibited if the concentration of positively charged molecules exceeds the optimum levels, for example the presentation of poly-D-lysine (PDL).[19][20] Neurite outgrowth is also affected by substrate elasticity, but it is unresolved whether decreasing hydrogel stiffness increases[21][22] or decreases[23] the length of axons. Substrate elasticity and the 3D structure of the scaffold are important regulators of neuronal differentiation from both neuronal precursors and stem cells.[24]

Xyloglucan is a polysaccharide hydrogel used in biomedical applications.[25-28] However, it is only when 35-50% of galactose groups are removed that the xyloglucan is capable of forming a thermally sensitive hydrogel. The partial removal of galactose groups reduces steric hindrance, allowing the polysaccharide chains to form hydrophobic associations of the glucan backbone and thermal gelation results.[29] Gelation of xyloglucan occurs as a two-stage process[30]; initially large membrane structures form in the "pre gel" which continue to form three-dimensional networks with a final modulus ranging between 150 and 480 kPa, depending on the concentration.[30] When used as a synthetic extracellular matrix, the galactose moieties within the xyloglucan side chain bind with asialoglycoprotein receptors on hepatocytes, providing excellent adhesion and spheroid formation.[31]

The ultimate goal of this study is to use thermoresponsive xyloglucan as a cell-scaffold construct to assist in the regeneration of the injured spinal cord. These experiments investigated the biocompatibility of murine embryonic cortical neurones with xyloglucan and the capacity of embryonic neurosphere differentiation on two-dimensional (2D) and 3D xyloglucan scaffolds. In this study, the cell numbers, neurite density and neurite length for both cell phenotypes were measured. The scaffolds were then modified by the

immobilization of poly-D-lysine to improve the neuronal affinity of the hydrogel. The ability to culture isolated cortical neurones and neuronal precursors with these hydrogels was examined. The long term aim is to provide neural stem cells (NSCs) with a scaffold that acts as a proliferative niche to support differentiation and to reduce glial scarring, thus facilitating repair by direct cell replacement.[32]

6.2.4 EXPERIMENTAL

6.2.4.1 Materials

Thermoresponsive xyloglucan with 48% galactose groups removed was kindly supplied by Dainippon Sumitomo Pharma, 5-51, Ebie 1-chome, Fukushima-ku Osaka, 553-0001, Japan and was prepared by enzymatic modification of tamarind seed xyloglucan according to previous methods.[29] A previous study revealed the unit structures of xyloglucan (with 48% galactose removed) to be 48, 31, and 21 mol % hepta-saccharide, octa-saccharide and nona-saccharide, respectively, as shown in Figure 1.[25] Sample solutions were prepared by dissolving the xyloglucan in either deionized water or PBS at a concentration of 3.0 wt %, by stirring the solution in an ice bath until no particles were visible. The solutions were then stored between 0 and 5°C prior to the experimentation.

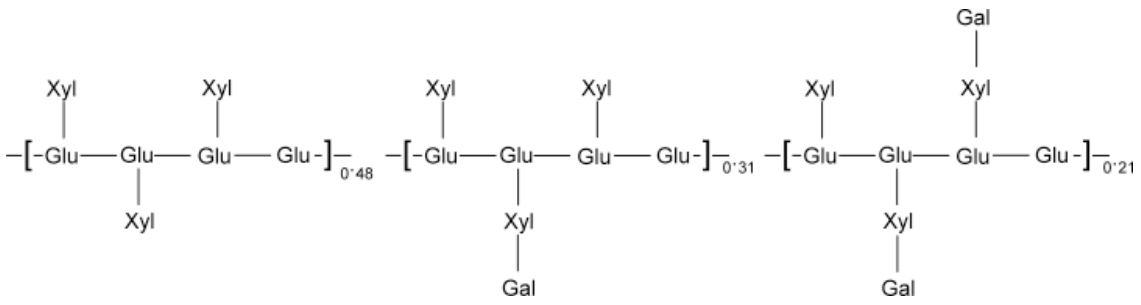

Figure 1. The chemical structure of xyloglucan.

6.2.4.2 Immobilization of poly-D-lysine on xyloglucan

Poly-D-lysine was photocoupled to the xyloglucan using a modified version of Chen et al.'s protocol.[33] This process involved mixing 50 mg of poly-D-lysine, 152 mg of *N*-(3-dimethylaminopropyl)-*N'*-ethylcarbodiimide hydrochloride (EDAC) and 56 mg of 4-azidoaniline in 140 mL of ddH_2O at a molar ratios of 40:1 (EDAC:PDL) and 4:1 4-azidoaniline:EDAC. The mixing was conducted at 4°C for 4 h. To remove the unreacted species, the solutions were dialyzed through a 500 Da MWCO cellulose ester membrane (Spectrum) before being lyophilized for 48 h. The next step was to attach the PDL-photoreactive species to the xyloglucan (shown schematically in Fig. 2). Briefly, the reactive species was dissolved in PBS (6 mL), before being added to 2 g of xyloglucan powder. The xyloglucan-PDL solution was placed into a polystyrene container (Falcon) and irradiated with UV light (Dymax® ultraviolet light source 2000-EC; wavelength ~ 360 nm) for 2 min. The xyloglucan-graft-PDL was then washed in ddH_2O to remove unbound polylysine, frozen then lyophilized.

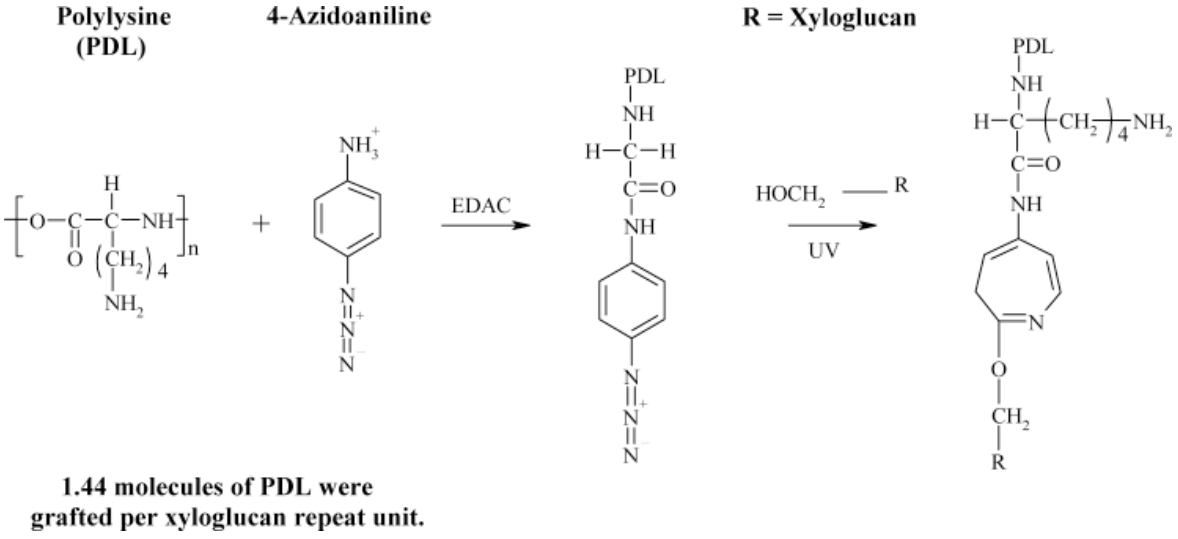

Figure 2. The attachment procedure of polylysine to azidoaniline (the photoreactive species), followed with the attachment to xyloglucan.

6.2.4.3 X-ray photoelectron spectroscopy analysis

Samples for X-ray photoelectron spectroscopy (XPS) were prepared by placing 3 wt % solutions of xyloglucan and xyloglucan-PDL onto round coverslips, allowing the solution to air dry before being scanned. The XPS analysis was conducted using an AXIS-HSi spectrometer (Kratos Analytical) with a monochromated Al K_{α} source at a power of 144 W (12 kV × 12 mA), and 1 × 0.5 mm aperture. The samples were measured at an emission angle of 0° from the surface normal. A survey spectrum was performed to identify all elements present, before high resolution scans at 40 eV pass energy were undertaken to resolve individual peaks. The data was curve-fitted using a minimization algorithm to determine the contributions from specific functional groups. Four different areas on each sample were scanned and an average taken.

6.2.4.4 Isothermal rheology

A Rheometric Scientific^{TM} rheometer was used to investigate the effect of the addition of PDL on the thermal gelation and final modulus. Isothermal rheology was conducted within the linear viscoelastic region of the hydrogels using parallel plate configuration at frequencies of 0.1, 0.3, 1.0, 3.1, and 10.0 Hz with the strain rate held at 1.25% with an initial stress of 0.245 MPa. Rheology was also employed to determine the time to reach the final modulus of the 3 wt % xyloglucan and 3 wt % xyloglucan-graft-PDL. The samples were placed into the rheometer at 4°C and allowed to rest for 60 s before being ramped to 37°C.

6.2.4.5 Scanning electron microscopy

2D and 3D hydrogel samples were prepared for scanning electron microscopy (SEM) by placing 200 μL of solution onto a microscope slide. The samples were then gelled for 50 min at 37°C before they were quenched with liquid nitrogen and freeze dried under vacuum for 48 h. The sections were then sputter-coated with gold using a Bal-Tec SCD 005, Balzers for 180 s before SEM was performed using a Hitachi S-570 SEM with an accelerating voltage of 15 kV and a magnification ranging from 50 to 1000 times.

6.2.4.6 Primary cortical neurone culture - Sample preparation

Xyloglucan powder was blended with xyloglucan-graft-PDL at ratios of 90 and 50 wt/wt %. Samples of 100% xyloglucan, 100% xyloglucan-graft-PDL and the blends were then sterilized in 70% ethanol and allowed to dry in a C2 laminar flow fume hood for 20 min. The solutions were then prepared as previously described to 3 wt % in autoclaved milliQ water.[30] In the 2D experiments, round coverslips were placed in the wells of a 24-well plate and were coated, in triplicate, with the solutions and allowed to gel for 50 min prior to cell seeding (replicating the sample preparation for SEM). In preparation for the 3D culture, the solutions were stored at 4°C until the cells were ready to be mixed in. At this point 200 μL of solutions was added to each well and mixed with the cells before they were incubated at 37°C for 50 minutes to allow for gelation. Poly-D-lysine (0.05 mg/mL) was coated on glass coverslips in a 24-well polystyrene tissue culture dish in triplicate and served as a positive control. The uncoated glass cover slip served as a negative control.

6.2.4.7 Primary cultures of embryonic cortical neurones

Embryonic cortices were harvested from time-pregnant C57/B6 type mice at embryonic day 14 according to previous protocols.[34][35] These studies conformed to the Australian National Health and Medical Research Council guidelines for use of animals in research, and were approved by the Howard Florey Institute Animal Ethics Committee. Briefly, the cells were dissociated with 0.025% trypsin for 20 min while being incubated at 37°C (Sigma T-4665). For both the 2D and 3D experiments cortical neurones were seeded at a density of 10^6 cells/mL (calculated by counting with a hemocytometer), in 0.5 mL of Modifed Eagle's Medium (MEM, Gibco) and 10% fetal calf serum. After 1 h, the medium was removed and culture medium (1 mL) added. The culture medium contained 50 mL of Neurobasal medium (NBM, Gibco), 1 mL B27 supplement (Gibco), 125 μL glutamine (200 m*M* stock) and 50 μL gentamycin (10 μg/mL) (Gibco).

After a 6-day period, the culture medium was removed and the samples washed in sterile PBS. For the cortical neurones cultured in 2D the cells were fixed 2.5%

paraformaldehyde (Sigma) solution for 1 min and washed three times in PBS for 10 min in a static environment. Non-specific antibody binding was then blocked in 3 % normal goat serum (NGS) and 0.3% Triton-X for 20 min at room temperature, before being washed again. Primary antibody (AB1887 Chemicon) was rabbit anti-neurofilament (1:300) in 1% NGS plus and 0.3% Triton-X (Sigma), which was applied and incubated at 37°C for 2 h. The 2D samples were then washed in PBS and secondary goat anti-rabbit tagged with an Alexa Fluor 488 (A11008, Molecular Probes, 1:600), applied in PBS for 2-3 h at room temperature before the final wash. The coverslips were then removed from the tissue culture wells and mounted on slides with Dako fluorescent mounting media. Epi-fluorescence microscopy was conducted using a Zeiss Axiovert 200M inverted microscope with FluoArc mercury lamp and Zeiss 20× lens.

Because 3D cultures could not be removed from their culture wells, a live stain was conducted and the cells were imaged in the wells. An assay solution containing 2 μ*M* calcein acetoxymethyl ester (calcein AM, Molecular Probes) in PBS, was used to stain these cultures. 250 μL of this solution was then added to each well before incubating at 37°C, 5% CO_2 for an additional 30 min. The samples were then washed twice in sterile PBS to remove the dye, before being imaged in the wells using an Olympus IX71 microscope with digital camera (4 mega-pixel, CAMEDIA). Three images at random locations were taken on an *x-y* plane that was 100 μm from the bottom of the culture well. The neurite lengths and cell diameters where then measured using Image J (1.32j, National Institute of Health, USA) software. In each case 10 random measurements from each image ($n = 30$), were measured. The neurite density was analyzed using a template of five lines in random orientation and neurites in contact with the line were counted. The cell numbers were counted manually in the same images. All of the statistics were preformed using SigmaStat for windows version 3.0.3© and reported as mean ± standard deviation. Statistical significance was considered at $p < 0.05$.

6.2.4.8 Neurosphere generation

Embryos were collected from time-pregnant C57/BL6 strain mice at embryonic day 10-11. The method of neurosphere generation used has been described in detail

elsewhere.[36] Briefly, embryonic cortices were collected and subjected to enzymatic dissociation with trypsin. To generate primary neurospheres, 25×10^4 cells/mL were plated in uncoated 25 cm^2 flasks (Falcon) at a final volume of 5 mL. The incubation medium consisted of DMEM/F12/2.5 m*M* Glutamine (Gibco, Cat. No.: 11320-033), 1% N2 supplement (Gibco), 0.6% glucose, penicillin (Gibco, 50 IU/mL) and streptomycin (Gibco, 50 μg/mL) (referred to as neurosphere medium) supplemented with FGF2 (10 ng/mL, Peprotech) or EGF (10 ng/mL, Peprotech). Neurospheres were passaged twice before plating in culture conditions that replicated the 2D cortical neurone study. The neurospheres were then collected, trypsinized in bulk and seeded at a density of 5×10^4 cells/mL in the presence of FGF2 and EGF. Differentiation was induced by mitogen withdrawal following plating on the surfaces in question. Notably, no growth factors were present in the differentiation medium. This procedure was repeated to produce tertiary neurospheres that were subsequently used for experimentation.

6.2.4.9 Differentiation assay

Intact tertiary neurospheres were plated onto 4-well chamber slides (Nunc), precoated with poly-L-lysine (PLL, Sigma) (as described previously)[36] or with the xyloglucan samples (using the same procedure as for the cortical neurones). Attached spheres were then incubated in neurosphere medium for 5 days and 30% of the incubation medium was replaced once at 3 days *in vitro*.

6.2.4.10 Fluorescent immunocytochemistry

Differentiated neurospheres were fixed for 15 min with chilled 4% paraformaldehyde (Sigma) in 0.1M PBS, pH 7.3. Fixed cells were permeabilized by incubation in 100% methanol at -20°C for 10 min. Cultures were washed in PBS, blocked in 10% normal goat serum (NGS) in PBS for 1 h at room temperature and then incubated for 24 h at 4°C with primary antibody diluted in blocking solution neurone-specific[37] mouse monoclonal anti-β-tubulin-III (clone TU-20, MAB1637, Chemicon), 1:400. Cultures were washed in PBS and blocked again with 10% NGS, followed by application of secondary $F(ab)_2$ goat anti-mouse 594 fluorescent antibody (Molecular Probes) for 1 h at

room temperature. To identify cell nuclei Hoescht-33258 (5 μg/mL, Sigma) was applied for 10 min. After an additional PBS wash, slides were cover-slipped with DAKO fluorescent mounting medium. The neurite lengths and cell diameters were again measured using Image J (1.32j, National Institute of Health, USA) software. Statistics were preformed using SigmaStat for Windows version 3.0.3© and reported as mean ± standard deviation.

6.2.5 RESULTS AND DISCUSSION

6.2.5.1 Materials functionalization and characterization

XPS was used to determine the extent of PDL grafting to the xyloglucan. Figure 3 shows a survey spectrum of PDL and the unmodified and modified xyloglucan, where the appearance of the nitrogen peak on the modified material is highlighted. The extent of grafting was determined using the nitrogen to carbon ratio of the xyloglucan-graft-PDL, which was 0.062 ± 0.003 indicating immobilization of ~1.44 PDL molecule per xyloglucan repeat unit. Isothermal rheological experiments (Fig. 4) were conducted to determine the composition at which the elastic modulus of the xyloglucan hydrogels matched the modulus of neural tissue in the spinal cord (~520,000 Pa).[38] The compliance of 3 wt % xyloglucan scaffolds provided the best match with spinal cord compliance (Fig. 5).

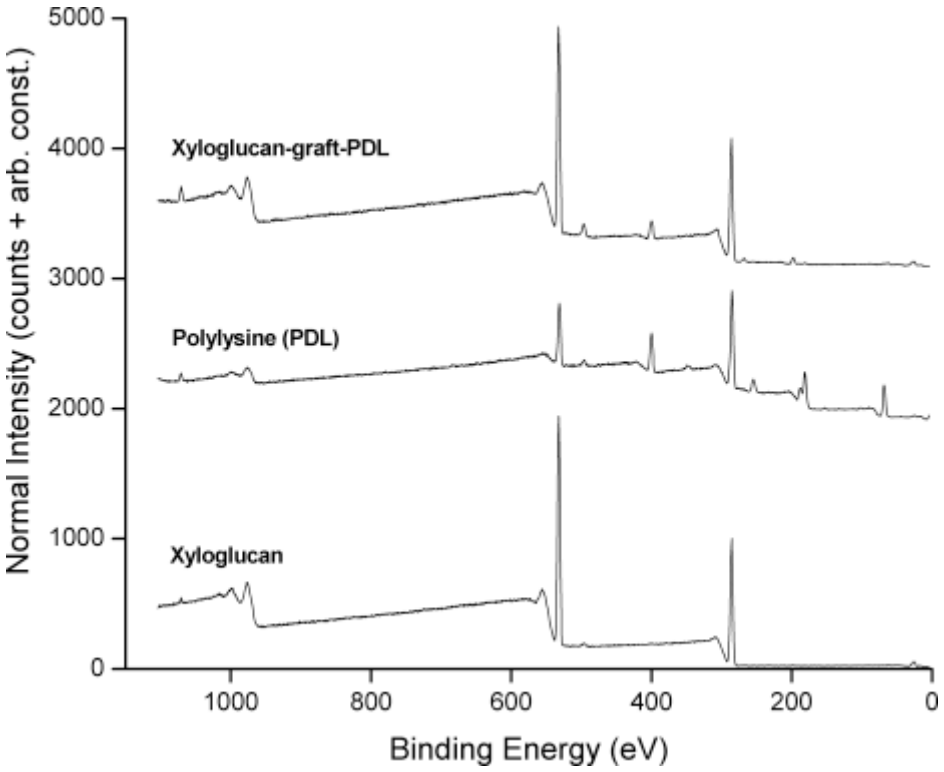

Figure 3. A survey spectrum of the unmodified xyloglucan, polylysine and the modified xyloglucan. The *N* 1s peak is present at ~400 eV, which was used to calculate the amount of PDL immobilized on the xyloglucan scaffold.

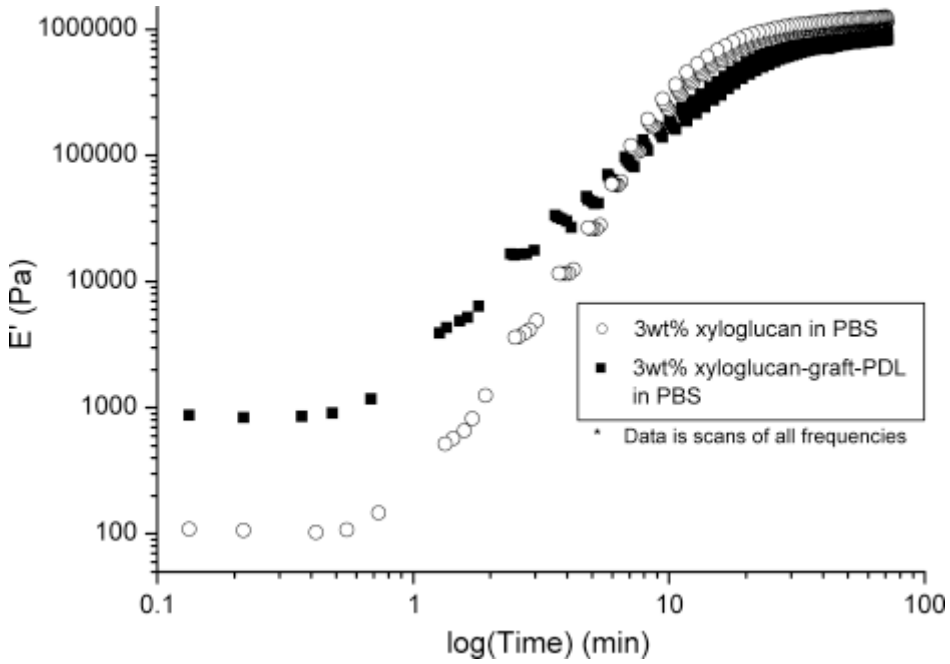

Figure 4. Isothermal gelation (37°C) of xyloglucan and xyloglucan-graft-PDL, showing the elastic modulus E' as a function of time.

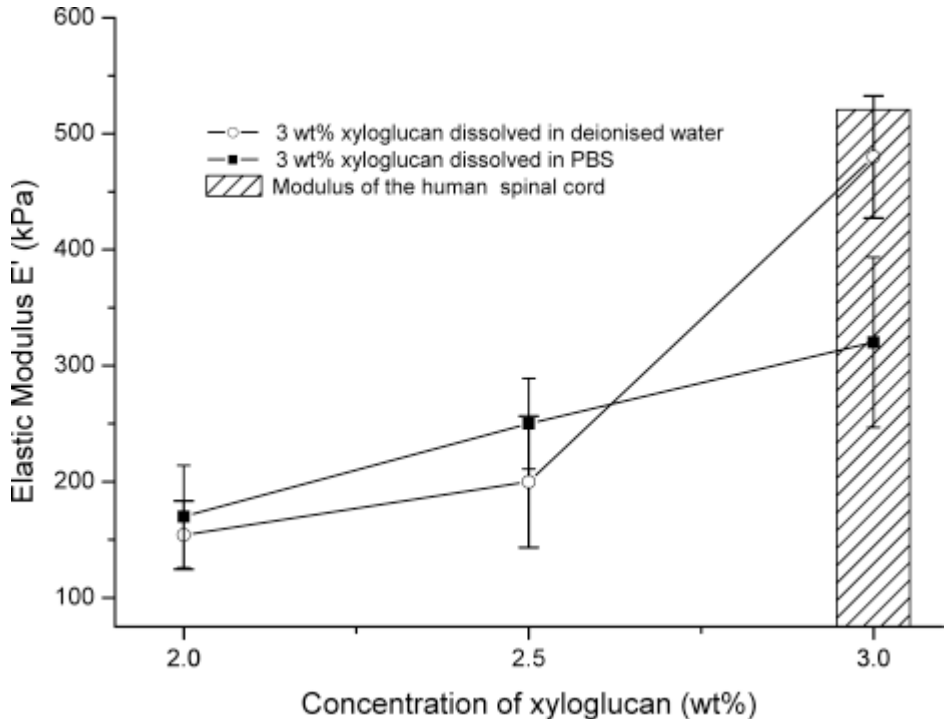

Figure 5. Relationship between the modulus and concentration (wt %) of xyloglucan produced from PBS and deionized water. This figure also shows the similarity between the modulus of the human spinal cord and that of the 3 wt % xyloglucan hydrogel in both media.

The immobilization of PDL resulted in a pregel with an increased initial elastic modulus. Although the final modulus of both the materials were similar (≈100 kPa), the time to reach the final modulus was more rapid in the absence of PDL (~25 min compared with 44 min in the case of the xyloglucan-graft-PDL sample). The time to reach the final modulus was taken as the start of the plateau region in Figure 4. The addition of PDL onto the polysaccharide may have increased the steric hindrance, thus increasing the time required for the hydrophobic associations of the glucose backbone to occur.

In preparation for 2D cultures, a thin film of xyloglucan was induced to completely cover a glass coverslip and then gelled (images not shown). Larger volumes of xyloglucan were used to obtain the 3D gel structure. SEM images of the 3D hydrogel scaffolds showed an

ordered stacking of membranes (Fig. 6), which were insensitive to the presence of PDL grafts. Hydrogels formed in ddH_2O, exhibited membrane spacing of 10 ± 2 μm. However, the spacing between membranes increased to 48 ± 7 μm, in the presence of PBS. Furthermore, holes formed within the gel membranes in the presence of PBS [Fig. 6(C,D)], which had diameters of approximately 5 ± 1 μm. This was possibly caused by the increase in ionic strength accelerating the rate of gelation.[39] The only significant effect produced by immobilizing PDL was the loss of strands connecting the membranes [see Fig. 6(A,C)].

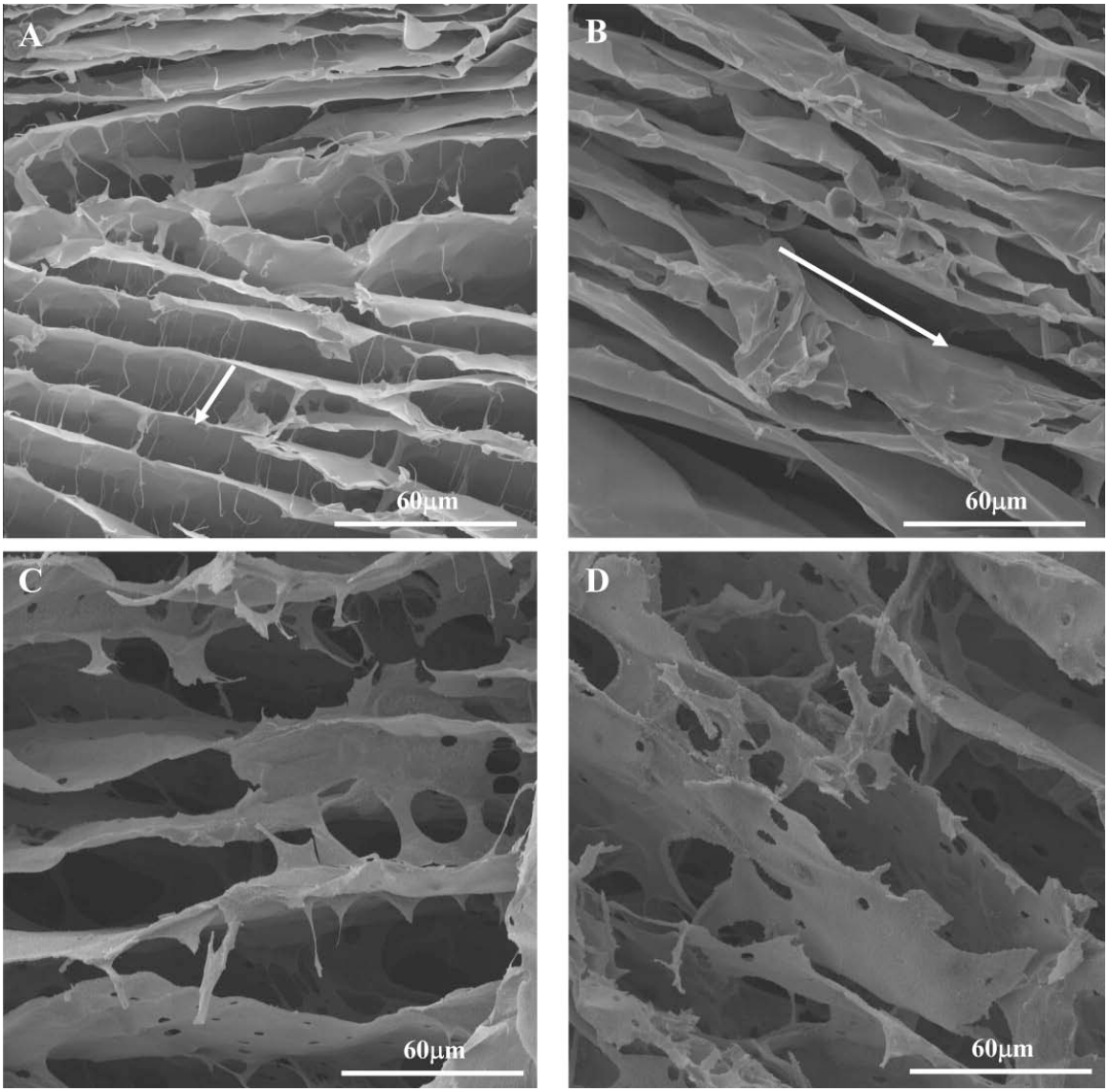

Figure 6. SEM images of the morphology of 3 wt % xyloglucan and xyloglucan-graft-PDL. A: 3 wt % xyloglucan produced with deionized water. B: 3 wt % xyloglucan-graft-PDL produced with deionized water. C: 3 wt % xyloglucan produced with PBS and (D) 3 wt % xyloglucan-graft-PDL produced with PBS. The white arrow in image (A) is parallel to the strands and the arrow in image (B) parallel to the large flat sheets for those particular images.

6.2.5.2 2D cortical neurone cellular study

In these studies, our interest was directed primarily at the affinity of neurones to the materials and their capacity to form extensions. Consequently, our attention was directed toward cells immunoreacting to β-tubulin^{III} and neurofilament antibodies. Primary cortical neurones cultures were grown on the xyloglucan, xyloglucan-graft-PDL and the blends 50:50 and 90:10 (xyloglucan to xyloglucan-graft-PDL). Cellular morphology was compared with neurones grown on poly-D-lysine (positive reference control) and glass coverslips (negative control) (Fig. 7). On all the samples, cells grew as flat, elongated neurones, sending out many long processes (up to 5-6 per cell and ranging between 150 and 500 μm in length). Cell diameter was greater on the PDL control (22 ± 0.5 μm), than on either the 100% xyloglucan or the 90:10 (xyloglucan to xyloglucan-graft-PDL) blend [17 ± 0.5 μm and 19 ± 0.5 μm, respectively, Fig. 8(A)]. The diameter of cells grown on 100% xyloglucan-graft-PDL (20.8 ± 0.3 μm) was marginally smaller but the diameter of the cells cultured on the 50:50 (xyloglucan to xyloglucan-PDL) blend was higher (24 ± 0.5 μm). Cell diameter correlated strongly with neurite density [Fig. 8(B)]. As the amount of xyloglucan-graft-PDL in the sample increased, cells spread further, became larger, more elongated and sent out more processes (Fig. 7). Thus, the diameter of the cells and density of the neurites on the surface could be controlled by modifying the concentration of immobilized PDL through the addition of xyloglucan-graft-PDL [Fig. 8(A,B)].

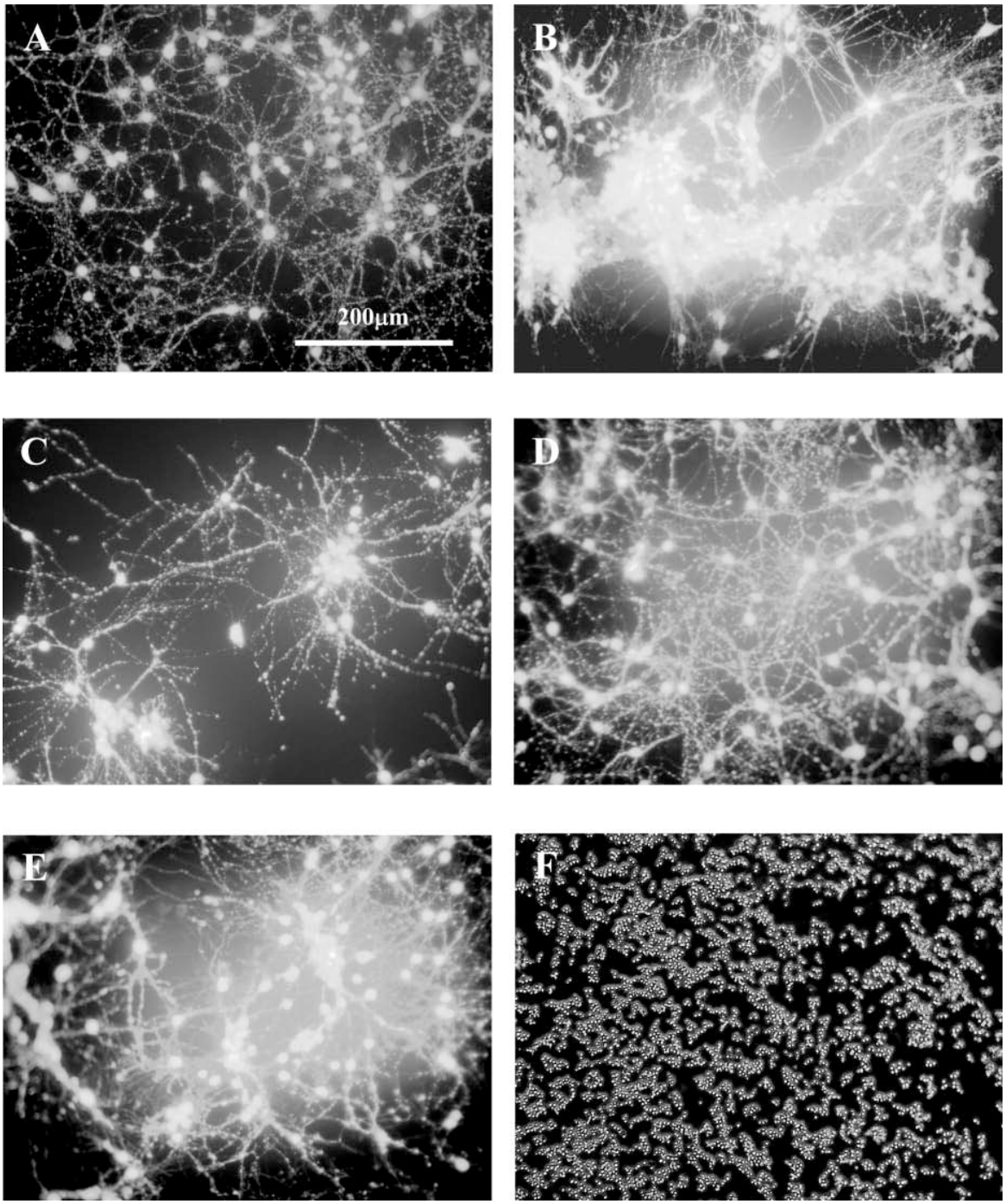

Figure 7. Epifluorescence images of cortical neurons cultured in 2D on (A) polylysine positive control, (B) 100% xyloglucan, (C) 90:10 xyloglucan to xyloglucan-graft-PDL blend, (D) 50:50 xyloglucan to xyloglucan-graft-PDL blend, (E) 100% xyloglucan-graft-PDL, and (F) negative control (glass coverslip).

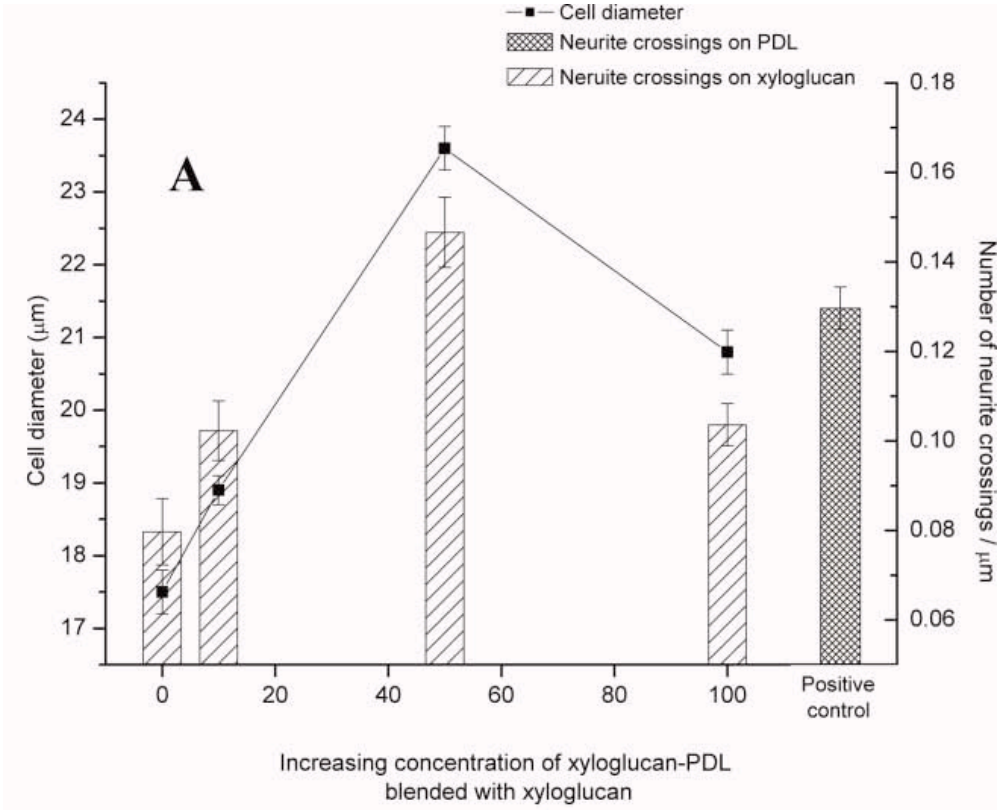
Cell diameter
Neurite crossings on PDL
Neruite crossings on xyloglucan
A
Cell diameter (μm)
Number of neurite crossings / μm
0
20
40
60
80
100
Positive control
Increasing concentration of xyloglucan-PDL blended with xyloglucan

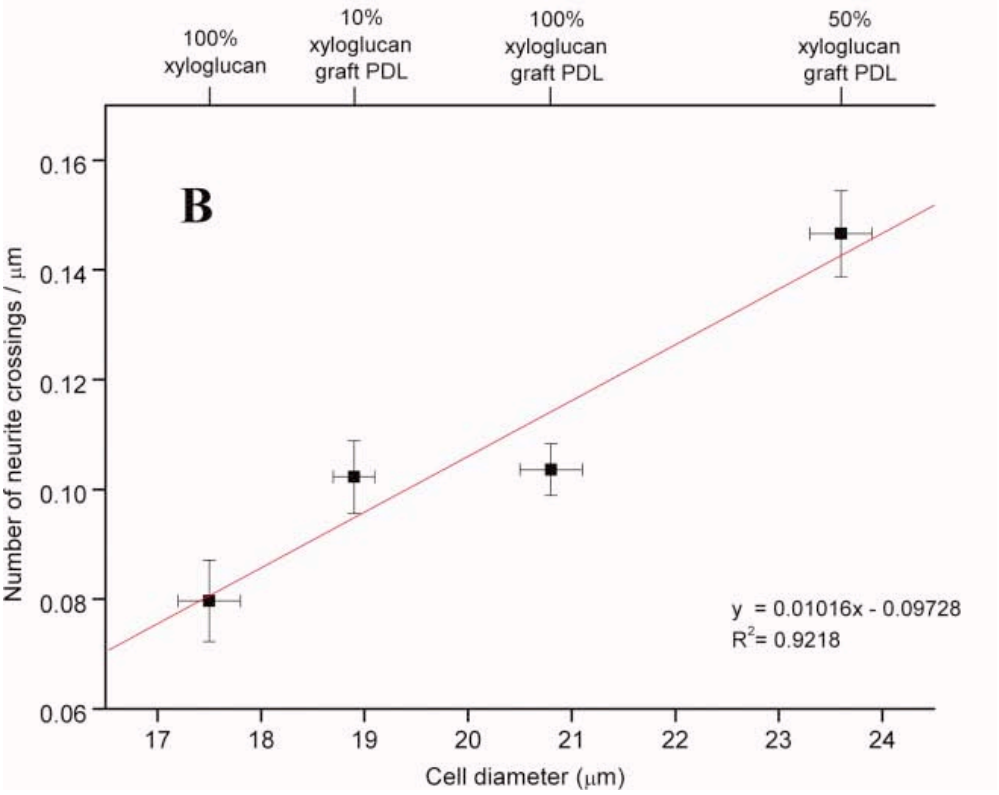
100% xyloglucan
10% xyloglucan graft PDL
100% xyloglucan graft PDL
50% xyloglucan graft PDL
B
Number of neurite crossings / μm
Cell diameter (μm)
y = 0.01016x - 0.09728
R2= 0.9218

Figure 8. A: represents the cell diameter and neurite density of cortical neurones as a function of PDL-graft-xyloglucan content. The results are reported as mean ± standard deviation. For the neurite density data an ANOVA with pair wise Tukey's *post hoc* testing revealed all groups are significantly different apart from sample 90:10 xyloglucan:xyloglucan-graft PDL and 100% xyloglucan-graft-PDL, which were statistically the same. The cell diameter of all groups was found to be statistically different. B: represents the relationship between the cell diameter and neurite density on 2D surfaces as a function of PDL-graft-xyloglucan content.

Twice the number of neurones survived on 100% xyloglucan sample (205 ± 20 per 0.34 mm^2) than on any of the modified materials. This number was similar to number that grew on the positive control (poly-D-lysine, Fig. 9). Neuronal survival increased linearly from 90 ± 10 to 160 ± 10 per 0.34 mm^2 as the concentration of immobilized PDL in the sample was increased. The higher density of colonies on unmodified xyloglucan may lead to increased live cell number per unit area, as they were exposed to higher concentrations of trophic factors released from adjacent cells. Cellular migration increased as the amount of xyloglucan-graft-PDL in the blend was increased (Fig. 7), and cellular migration may influence survival. This study shows that it is possible to control, and in some instances optimize, the number of surviving neurones, migration, areas/diameters of the surviving cells and the neurite density, through functionalization of 2D surfaces of xyloglucan.

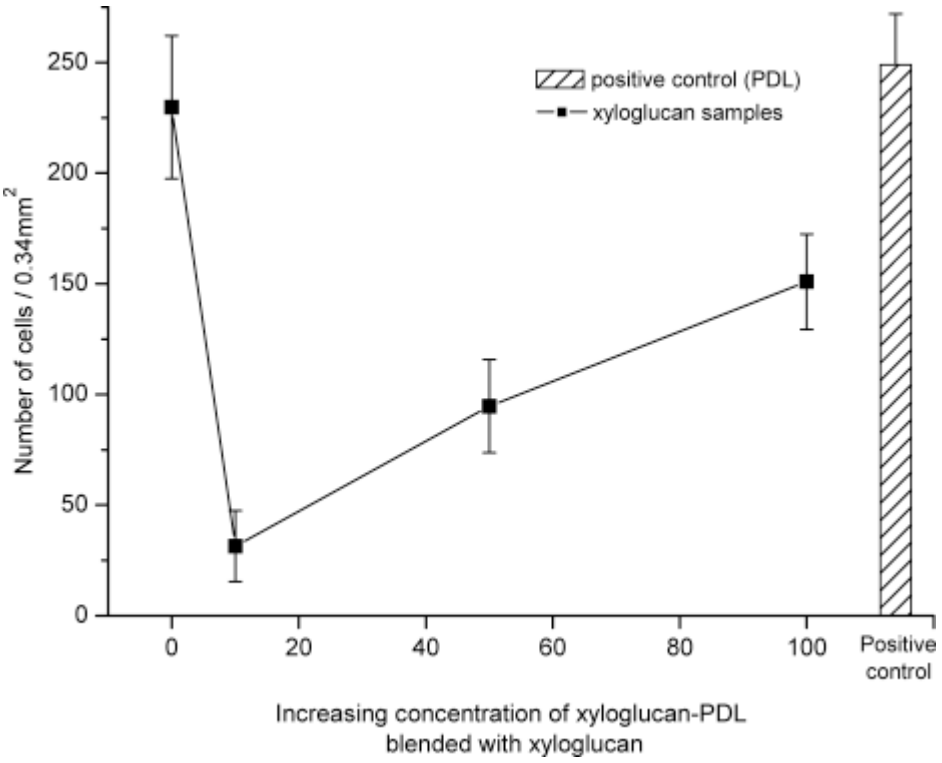

Figure 9. Number of cells/0.34 mm^2 as a function of PDL-graft-xyloglucan content. The results are reported as mean ± standard deviation. ANOVA with pair wise Tukey's *post hoc* testing revealed all groups are significantly different.

6.2.5.3 2D versus 3D culture conditions of primary cortical neurones

Cortical neurones were cultured within 3D scaffolds made from these materials to provide a preliminary assessment of neuronal survival and differentiation. Images of the cortical neurones cultured in 3D within the xyloglucan are shown in Figure 10. More cells were found near the bottom of the culture than near the surface and this was attributed to cells sinking during gelation. The gel was ~5000 μm thick, and the culture medium was placed on top of the material once it had gelled. Therefore, the pores size supported cell viability at depths of 4900 μm below the material surface and allowed nutrients, oxygen and metabolites to be transported throughout the scaffold. The

interconnected structure of the 3D scaffolds is shown in Figure 6, confirming that diffusion of oxygen and nutrients could readily occur.

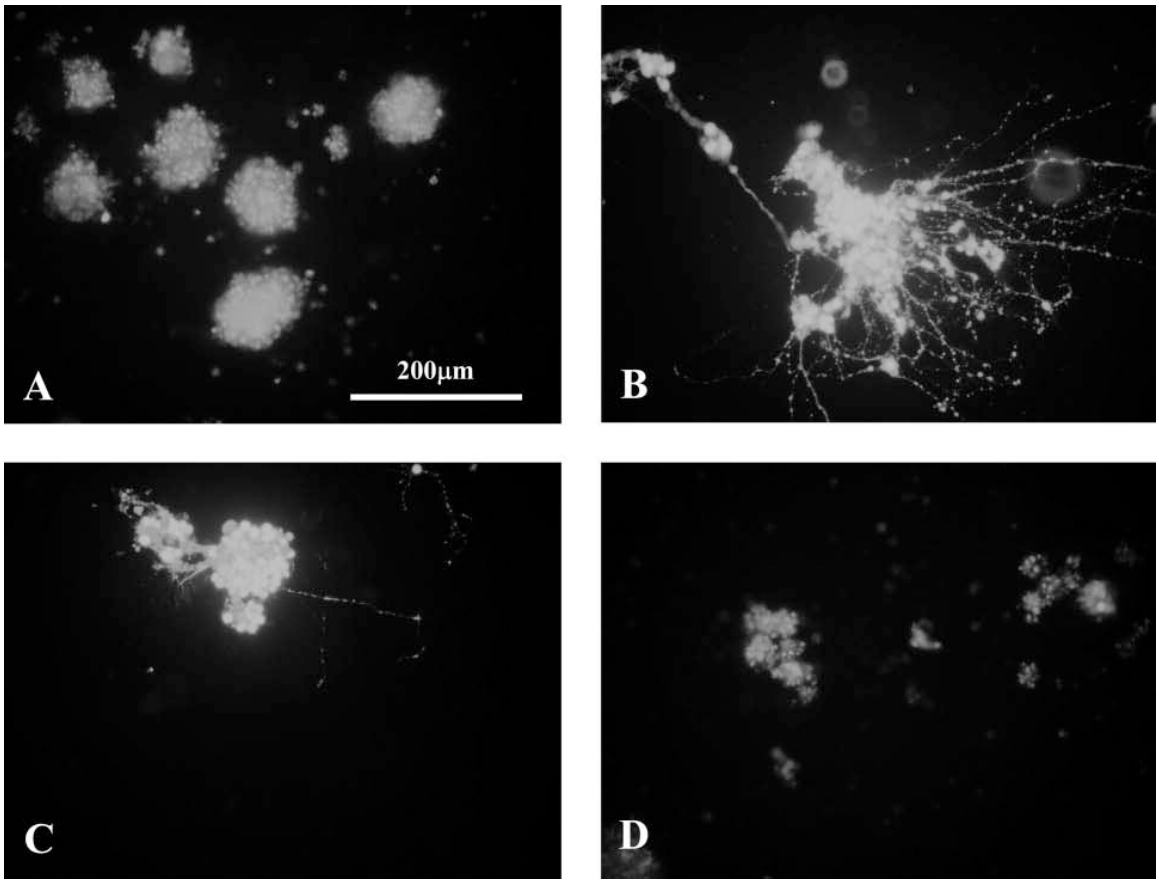

Figure 10. Epifluorescence images of cortical neurons cultured within different 3D samples, (A) 100% xyloglucan, (B) 90:10 xyloglucan-graft-PDL, (C) 50:50 xyloglucan-graft-PDL, (D) 100% xyloglucan-graft-PDL.

All cells formed processes when grown on 2D surfaces. However, when cultured on the same material in a 3D environment, cells growing on blends of xyloglucan and xyloglucan-PDL were the only ones to send out processes, with some process growing three-dimensionally throughout the scaffold and other being restricted to two-dimensions. This is most likely because the hydrogel (shown in Fig. 6) consists of very large flat sheets; therefore, the outgrowth of neurites in some instances is restricted to two

dimensions. However, most neurites were "unrestricted" and capable of 3D growth. The average neurite lengths and density was much greater on the 90:10 xyloglucan to xyloglucan-PDL sample (200 ± 20 μm and 0.020 ± 0.008 neurites/μm, respectively) than on the 50:50 xyloglucan to xyloglucan-PDL (80 ± 15 μm and 0.008 ± 0.001 neurites/μm). The 100% xyloglucan and 100% xyloglucan-PDL samples formed large colonies of cells, which survived but did not change shape or form neurites.

6.2.5.4 2D neurosphere study

Neurospheres were plated onto 2D gels at a density of 5×10^4 cells/mL, and their responses to the scaffolds were assessed using fluorescent immunocytochemistry. The proportion of β-tubulin-III-positive cells per sphere were similar when cultured on PLL (data shown after references), 50:50 xyloglucan-graft-PDL and 100% xyloglucan-graft-PDL. However, very few neurospheres cultured on 100% xyloglucan and the 90:10 xyloglucan-graft-PDL surfaces attached and those that did showed no signs of migration (data not shown). Surface coating with 50:50 xyloglucan-graft-PDL and the 100% xyloglucan-graft-PDL distinctly improved adherence so that almost 60% of spheres attached (this was assessed 2 h after plating) (Fig. 11). As with primary cultures, the increased adherence and neurite extension may be due to interactions between the cationic PDL attached to the xyloglucan.

Neurite length and cell body area of β-tubulin-III-positive cells was also assessed when cultured in the absence of serum. Neurite length on the 50:50 xyloglucan-graft-PDL [32 μm ± 4 (n = 52)] was less than on PLL controls (88 μm ± 7; n = 67; $p < 0.01$ by ANOVA (Fig. 12). However, on the 100% xyloglucan-graft-PDL surface the neurite length was considerably greater than that of the positive control [141 μm ± 3 (n = 70)]. The length of the neurites on the functionalized xyloglucan scaffold was much greater than has been shown for neurospheres cultured on other polysaccharide systems such as chitosan (82 μm ± 3 μm),[40] and the lengths can readily be optimized (i.e. the neurite length controlled).

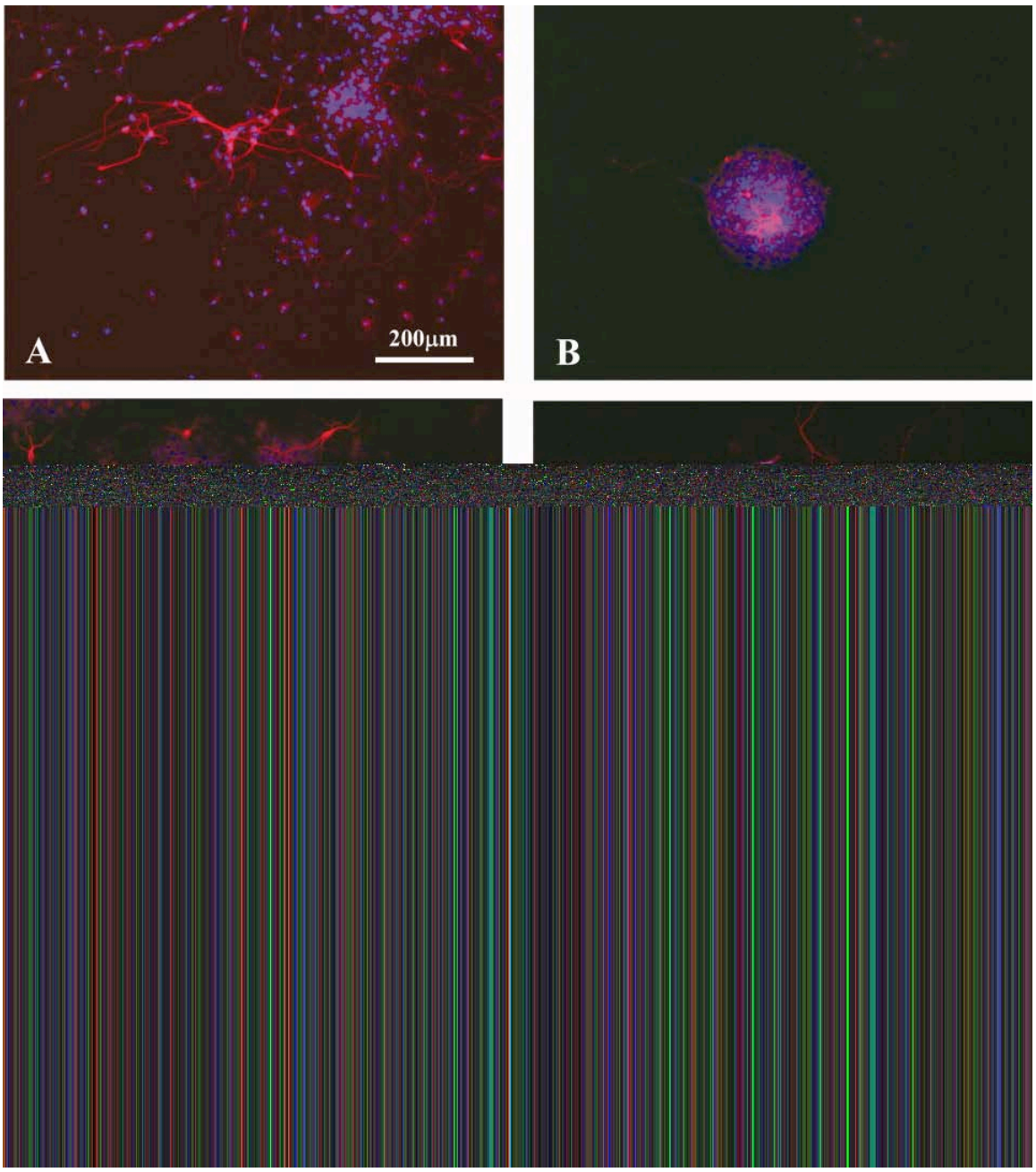

Figure 11. Epi-fluorescence images of neurospheres cultured on 2D samples of (A) polylysine positive control, (B) 50:50 xyloglucan-graft-PDL, (C) 50:50 xyloglucan-graft-PDL, (D) 100% xyloglucan-graft-PDL, (E) 100% xyloglucan-graft-PDL, (F) 100% xyloglucan-graft-PDL. Several images of the same samples (A and B) and (D-F) are shown to highlight the differing morphologies of the neurospheres within the same sample. The red is monoclonal anti-β-tubulin-III and the blue is nuclei Hoescht-33258.

The cell body area of β-tubulin-III-positive neurones grown on 100% xyloglucan-graft-PDL samples (Figs. 11 and 12) was substantially greater than those grown on PLL controls. This effect of the scaffold on the neuronal cell body is consistent with enhanced trophic support. Undifferentiated neurospheres synthesize an array of different trophic molecules that may be secreted in autocrine/paracrine fashion.[41] It is speculated that the scaffolds are capable of stabilizing certain crucial trophic factors in solution, which may amplify their biological effect. Further investigation of the molecular nature of this phenomenon is warranted. Similar synergistic interactions of trophic molecules and extracellular matrix molecules have already been described with different FGFs, for example.[42] However, the direct trophic effect of the scaffold on neuronal cells can also not be ruled out.

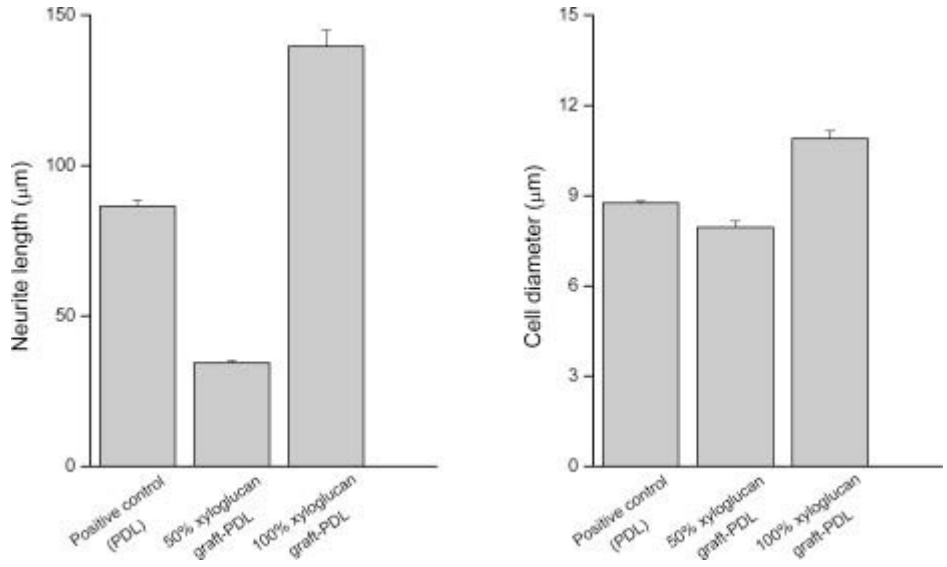

Figure 12. Neurite lengths and cell body areas for the neurospheres cultured on modified 2D xyloglucan. The results are reported as mean ± standard deviation. For both the neurite density and cell diameter data an ANOVA with pair wise Tukey's *post hoc* testing revealed all groups are significantly different.

These results provide *in vitro* evidence of a robust effect of 100% xyloglucan-graft-PDL on neurite extension and on maintenance of trophic milieu. This is closely related to the results obtained from cultures of primary cortical neurones and warrants further *in vitro* experiments. Optimal percentage of PDL attachment seems to depend on cell type and culture conditions.

6.2.6 CONCLUSIONS

In this study, xyloglucan was functionalized successfully by immobilizing ~1.44 molecule of PDL per xyloglucan repeat unit. Xyloglucan under 2D and 3D culture conditions were non-toxic and supported neuronal differentiation. Furthermore, functionalization controlled the cell number, diameter, migration and the neurite density of primary cortical neurones and could be used to optimize these parameters *in vitro*. This capacity of the xyloglucan-based scaffold is unique and further experiments will be required to investigate the interaction between neurones and glia within the cultures to establish whether the scaffolds can be used for *in vivo* spinal cord repair.

This study also investigated the interaction of xyloglucan-based scaffolds with NSC cultures and confirmed the versatile function of xyloglucan functionalization in the controlled development of NSCs *in vitro*. Functionalized scaffolds not only supported the growth of mature neurones but also the differentiation of precursors into neurones. Functionalization of xyloglucan yielded biological scaffolds that had superior capacity to support *in vitro* neuronal survival, differentiation, and neurite extension under 2D and 3D culture conditions, which is encouraging for future *in vivo* experiments addressing the transected spinal cord.

6.2.7 ACKNOWLEDGEMENTS

The authors thank S. Shirakawa from the Dainippon Sumitomo Pharma, Japan, for kindly supplying the galactose-modified xyloglucan. David Nisbet was supported by an Australian Postgraduate Award and the CRC for Polymers.

6.2.8 REFERENCES

1 Iwata A,Browne KD,Pfister BJ,Gruner JA,Smith DH. Long-term survival and outgrowth of mechanically engineered nervous tissue constructs implanted into spinal cord lesions. *Tissue Eng* 2006; **12**: 101-110.

2 Yu TT,Shoichet MS. Guided cell adhesion and outgrowth in peptide-modified channels for neural tissue engineering. *Biomaterials* 2005; **26**: 1507-1514.

3 Stabenfeldt SE,Garcia AJ,LaPlaca MC. Thermoreversible laminin-functionalized hydrogel for neural tissue engineering. *J Biomed Mater Res (Appl Biomater)* 2006; **77**: 718-725.

4 Chen S,Pickard JD,Harris NG. Time course of cellular pathology after controlled cortical impact injury. *Exp Neurol* 2003; **182**: 87-102.

5 Schwab ME. Regenerative nerve fiber growth in the adult central nervous system. *News Physiol Sci* 1998; **13**: 294-298.

6 Tian WM,Hou SP,Ma J,Zhang CL,Zu QY,Lee IS,Li HD,Spector M,Cui FZ. Hyaluronic acid-poly-**D**-lysine-based three dimensional hydrogel for traumatic brain injury. *Tissue Eng* 2005; **11**: 513-525.

7 Mahoney MJ,Anseth KS. Three-dimensional growth and function of neural tissue in degradable polyethylene glycol hydrogels. *Biomaterials* 2006; **27**: 2265-2274.

8 Rosiak JM,Yoshii F. Hydrogels and their medical applications. *Nucl Instrum Methods Phys Res Sect B* 1999; **151**: 56-64.

9 Hoffman AS. Hydrogels for biomedical applications. *Adv Drug Delivery Rev* 2002; **43**: 3-12.

10 Crompton KE,Prankerd RJ,Paganin DM,Scott TF,Horne MK,Finkelstein DI,Gross KA,Forsythe JS. Morphology and gelation of thermosensitive chitosan hydrogels. *Biophys Chem* 2005; **117**: 43-49.

11 Lee KY,Alsberg E,Mooney DJ. Degradable and injectable poly(aldehyde guluronate) hydrogels for bone tissue engineering. *J Biomed Mater Res* 2001; **56**: 288.

12 Ratner BD,Hoffman AS. Synthetic hydrogels for biomedical applications. *Hydrogels Med Related Appl* 1976; 1-36.

13 Sieminski AL,Gooch KJ. Biomaterial-microvasculature interactions. *Biomaterials* 2000; **21**: 2233-2241.

14 Goraltchouk A,Scanga V,Morshead CM,Shoichet MS. Incorporation of protein-eluting microspheres into biodegradable nerve guidance channels for controlled release. *J Controlled Release* 2006; **110**: 400-407.

15 Tsai EC,Dalton PD,Shoichet MS,Tator CH. Synthetic hydrogel guidance channels facilitate regeneration of adult rat brainstem motor axons after complete spinal cord transection. *J Neurotrauma* 2004; **21**: 789-804.

16 Stokols S,Sakamoto J,Breckon C,Holt T,Weiss J,Tuszynski MH. Templated agarose scaffolds support linear axonal regeneration. *Tissue Eng* 2006; **12**: 2777-2787.

17 Bunge MB. Bridging areas of injury in the spinal cord. *Neuroscientist* 2001; **7**: 325-339.

18 Dillon GP,Yu Z,Sridharan A,Ranieri JP,Bellamkonda RV. The influence of physical structure and charge on neurite extension in a 3D hydrogel scaffold. *J Biomaterials Sci Polym Ed* 1998; **9**: 1049-1069.

19 Varon S. The culture of chick embryo dorsal root ganglionic cells on polylysine-coated plastic. *Neurochem Res* 1979; **4**: 155-173.

20 Crompton KE,Goud JD,Bellamkonda RV,Gengenbach TR,Finkelstein DI,Horne MK,Forsythe JS. Polylysine-functionalised thermoresponsive chitosan hydrogel for neural tissue engineering. *Biomaterials* 2007; **28**: 441-449.

21 Willits RK,Skornia SL. Effect of collagen gel stiffness on neurite extension. *J Biomater Sci Polym Ed* 2004; **15**: 1521-1531.

22 Balgude AP,Yu X,Szymanski A,Bellamkonda R. Agarose gel stiffness determines rate of DRG neurite extension in 3D cultures. *Biomaterials* 2001; **22**: 1077-1084.

23 Leach JB,Brown XQ,Jacot JG,DiMilla PA,Wong JY. Neurite outgrowth and branching of PC12 cells on very soft substrates sharply decreases below a

threshold of substrate rigidity. *J Neural Eng* 2007; **4**: 26-34.

24 Even-ram S,Artym V,Yamada KM. Matrix control of stem cell fate. *Cell* 2006; **126**: 645-647.

25 Seo SJ,Park IK,Yoo MK,Shirakawa M,Akaike T,Cho CS. Xyloglucan as a synthetic extracellular matrix for hepatocyte attachment. *J Biomater Sci Polym Ed* 2004; **15**: 1375-1387.

26 Strickland FM,Sun Y,Darvill A,Eberhard S,Pauly M,Albersheim P. Preservation of the delayed-type hypersensitivity response to alloanitigen by xyloglucans or oligogalacturonide does not correlate with the capacity to reject ultraviolet-induced shin tumors in mice. *J Invest Dermatol* 2001; **116**: 62-68.

27 Miyazaki S,Suisha F,Kawasaki M,Shirakawa M,Yamatoya K,Attwood D. Thermally reversible xyloglucan gels as vehicles for rectal drug delivery. *J Controlled Release* 1998; **56**: 75-83.

28 Suisha F,Kawasaki M,Miyazaki S,Shirakawa M,Yamatoya K,Sasaki M,Attwood D. Xyloglucan gels as sustained release vehicles for the intraperitoneal administration of mitomycin C. *Int J Pharm* 1998; **172**: 27-32.

29 Shirakawa M,Yamotoya K,Nishinari K. Tailoring of xyloglucan properties using an enzyme. *Food Hydrocolloids* 1998; **12**: 25-28.

30 Nisbet DR,Crompton KE,Hamilton SD,Shirwakawa S,Prankerd RJ,Finkelstein DI,Horne MK,Forsythe JS. Morphology and gelation of thermosensitive xyloglucan hydrogels. *Biophys Chem* 2005; **121**: 14-20.

31 Burgalassi S,Raimondi L,Pirisino R,Banchelli G,Boldrini E,Saettone MF. Effect of xyloglucan (tamarind seed polysaccharide) on conjunctival cell adhesion to laminin and on corneal epithelium wound healing. *Eur J Ophthal* 2000; **10**: 71-76.

32 Teng YD,Lavik EB,Qu X,Park KI,Ourednik J,Zurakowski D,Langer R,Snyder EY. Functional recovery following traumatic spinal cord injury mediated by a unique polymer scaffold seeded with neural stem cells. *PNAS* 2002; **99**: 3024-3029.

33 Chen G,Ito Y,Imanishi Y,Magnani A,Lamponi S,Barbucci R. Photoimmobilization of sulfated hyaluronic acid for antithrombogenitcity. *Bioconjugate Chem* 1997; **8**: 730-734.

34 Nisbet DR,Pattanawong S,Nunan J,Shen W,Horne MK,Finkelstein DI,Forsythe JS. The effect of surface hydrophilicity on the behaviour of embryonic cortical neurons. *J Colloid Interface Sci* 2006; **299**: 647-655.

35 Nisbet DR,Pattanawong S,Ritchie NE,Shen W,Finkelstein DI,Horne MK,Forsythe JS. Interaction of embryonic cortical neurones on nanofibrous scaffolds for neural tissue engineering. *J Neural Eng* 2007; **4**: 1-7.

36 Moses D,Teper Y,Gantois I,Finkelstein DI,Horne MK,Drago J. Murine embryonic EGF-responsive ventral mesencephalic neurospheres display distinct regional specification and promote survival of dopaminergic neurons. *Exp Neurol* 2006; **199**: 209-221.

37 Draberova E,Lukas Z,Ivanyi D,Viklicky V,Draber P. Expression of class III beta-tubulin in normal and neoplastic human tissues. *Histochem Cell Biol* 1998; **109**: 231-239.

38 Bilston LE,Thibault LE. The mechanical properties of the human cervical spinal cord in vitro. *Ann Biomed Eng* 1996; **24**: 67-74.

39 Coughlan DC,Corrigan OI. Drug-polymer interactions and their effect on thermoresponsive poly(*N*-isopropylacrylamide) drug delivery systems. *Int J Pharm* 2006; **313**: 163-174.

40 Hung CH,Lin YL,Young TH. The effect of chitosan and PVDF substrates on the behavior of embryonic rat cerebral cortical stem cells. *Biomaterials* 2006; **27**: 4461-4469.

41 Benoit BO,Savarese T,Joly M,Engstrom CM,Pang L,Reilly J,Recht LD,Ross AH,Quesenberry PJ. Neurotrophin channeling of neural progenitor cell differentiation. *J Neurobiol* 2001; **46**: 265-280.

42 Dono R. Fibroblast growth factors as regulators of central nervous system development and function. Regulatory, integrative and comparative physiology.

Am J Physiol 2003; **284**: 867-881.

Appendix 1

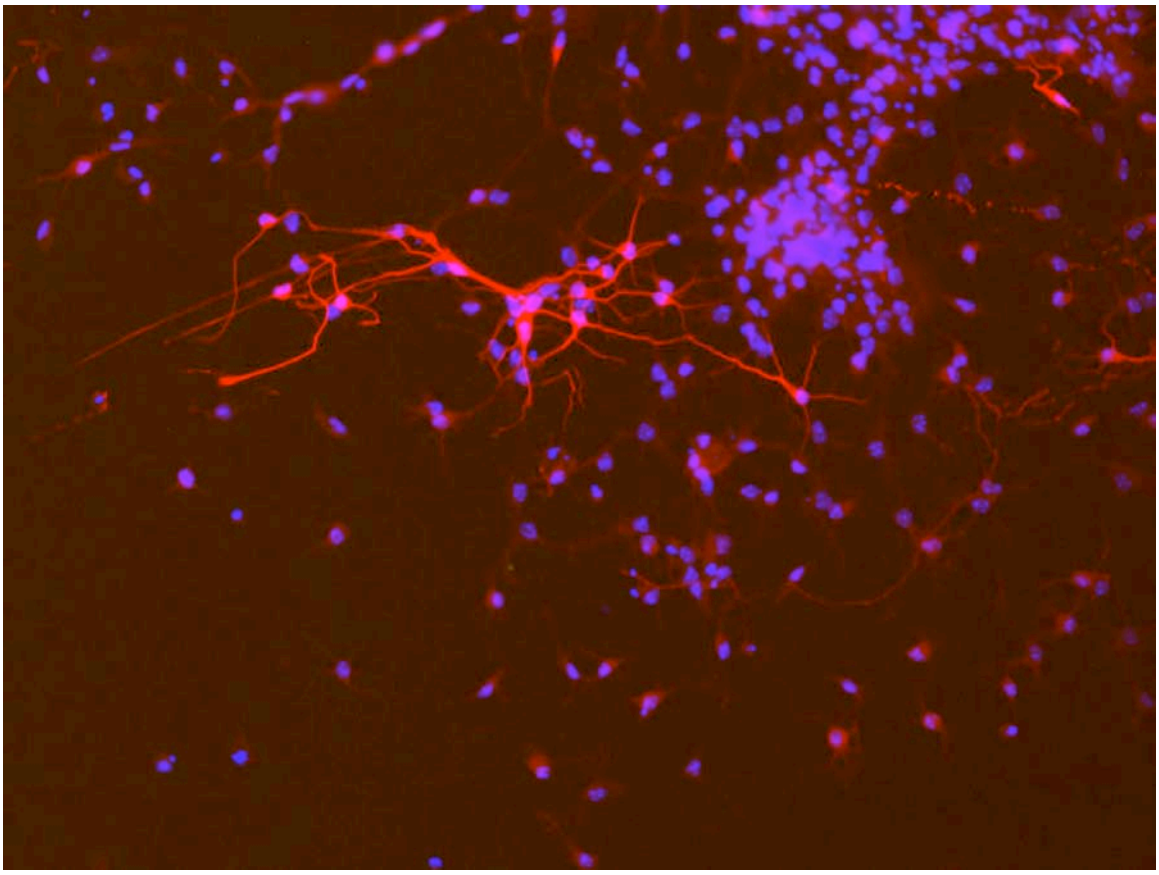

Appendix 1: Image of neural stem cell culture on PLL positive control surface. Here the red is a positive marker for neurons and the blue are the cell nuclei.

Chapter 7

Part II - Hydrogel

In vivo implantation

Contents

Declaration

One publication has been inserted into chapter 7. Below the reference information and publication status for this publication is provided.

Chapter 7.1

1. **D. R. Nisbet**, A. Rodda, M. K. Horne, J. S. Forsythe, D. I. Finkelstein, “Characterisation of the cellular response to the implantation of functionalised xyloglucan hydrogel within the brain”, *Biomaterials.*, prepared for submission, February 2008.

Declaration for Thesis Chapter 7.1

Monash University

Declaration by candidate

In the case of Chapter 7.1 the nature and extent of my contribution to the work was the following:

Nature of contribution	Extent of contribution (%)
Experimental design and conduct and article writing	85

The following co-authors contributed to the work. Co-authors who are students at Monash University must also indicate the extent of their contribution in percentage terms:

Name	Nature of contribution	Extent of contribution (%) for students
A.E. Rodda	Assisted in experimentation & corrected manuscript	5
M.K. Horne	Experimental design and corrected manuscript	N/A
J.S. Forsythe	Experimental design and corrected manuscript	N/A
D.I. Finkelstein	Experimental design and corrected manuscript	N/A

Candidate's Signature	[redacted]	**Date** 14/10/2008

Declaration by co-authors

The undersigned hereby certify that:

(1) the above declaration correctly reflects the nature and extent of the candidate's contribution to this work, and the nature of the contribution of each of the co-authors.
(2) they meet the criteria for authorship in that they have participated in the conception, execution, or interpretation, of at least that part of the publication in their field of expertise;
(3) they take public responsibility for their part of the publication, except for the responsible author who accepts overall responsibility for the publication;
(4) there are no other authors of the publication according to these criteria;

(5) potential conflicts of interest have been disclosed to (a) granting bodies, (b) the editor or publisher of journals or other publications, and (c) the head of the responsible academic unit; and
(6) the original data are stored at the following location(s) and will be held for at least five years from the date indicated below:

Name	Location
A.E. Rodda	Monash University - Department of Materials Engineering
M.K. Horne	Melbourne University - Howard Florey Institute
J.S. Forsythe	Monash University - Department of Materials Engineering
D.I. Finkelstein	The Mental Health Research Institute of Victoria

Name	Signature	Date
A.E. Rodda		14/10/2008
M.K. Horne	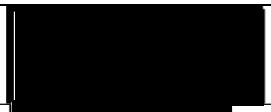	14/10/2008
J.S. Forsythe	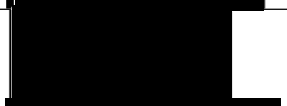	14/10/2008
D.I. Finkelstein		14/10/2008

7.0 *In vivo* implantation

7.1 Evaluation of the inflammatory response of thermally gelling xyloglucan hydrogels

In-order to ascertain the biocompatibility of neural tissue engineering scaffolds *in vivo*, it is essential to appropriately characterise the scaffold, including an assessment of the inflammatory response upon implantation. Thus far in Part II of this thesis all of the experiments ultilised to evaluate the scaffolds have been conducted *in vitro*. Whilst *in vitro* studies and models have their place in the evaluation of new tissue engineering scaffolds, such studies simplify the interaction that a scaffold will experience in practice. For instance the complex cellular interactions that occur *in vivo*, in addition to the soluble growth factors that such cells excrete within this environment are difficult to simulate. For this reason, the next step was to implant these materials within the central nervous system. In this study, the inflammatory response and neurite infiltration was explored when the xyloglucan scaffolds were implanted into the caudate putamen of adult rats.

Characterisation of the cellular response to the implantation of functionalised thermally gelling xyloglucan hydrogel scaffolds within the brain

D.R. Nisbet[a], A.E. Rodda [a], M.K. Horne [b], J.S. Forsythe [a], D.I. Finkelstein [c] *

a *CRC for Polymers, Department of Materials Engineering, Division of Biological Engineering, Monash University, P.O. Box 69M, Victoria 3800, Australia*

b *Howard Florey Institute, Gate 11, Royal Parade, The University of Melbourne, Victoria 3010, Australia*

c *The Mental Health Research Institute of Victoria, Victoria 3010, Australia*

7.1.1 ABSTRACT:

In-order to develop neural tissue engineering strategy that is useful for repairing damaged neural pathways in the central nervous system (CNS) it is essential to control and optimize neuron and neurite interactions with scaffolds. In this study, the suitability of thermally gelling xyloglucan hydrogel scaffolds was assessed through its implantation within the caudate putamen of adult rats. The ability of the hydrogel to encourage the infiltration of axons within the scaffolds in a protected and controlled manner was investigated, as was the inflammatory response associated with the implantation. Unmodified xyloglucan and blends of xyloglucan-graft-poly-$_D$-lysine were assessed by studying the neurite infiltration in each of the scaffolds and the activation and interaction of astrocytes and microglia. The incorporation of immobilized poly-$_D$-lysine (PDL) within the hydrogel did not alter the inflammatory response within the endogenous brain tissue surrounding the implant, but did affect the amount of cell migration into the scaffold. There was a greater number of astrocytes and neurites present within the scaffolds when the level of immobilized PDL presented to the cells was the highest. .The findings of this study are likely to be useful for the future development of hydrogel scaffolds for neural tissue engineering applications.

7.1.2 Key words

hydrogel; xyloglucan; nerve regeneration; neural tissue engineering; central nervous system; neurite; astrocyte; microglia.

7.1.3 Introduction

Diseases and injury of the central nervous system (CNS) are the largest economic burden in western society, being even larger than that of cardiac disease. [1] This burden will continue, and perhaps become exacerbated in the future as populations continue to age. However, it is obviously not only the economic burden that is important; the burdens on the patients are extreme, and result in a loss of their independence and quality of life. [2] To achieve regeneration within the CNS and restore some of the functionality that is lost after damage, progress will most likely be made from the field of neural tissue engineering.[3, 4]

While axonal regeneration is essential for the treatment of CNS injury, glial cells (including astrocytes and microglia) in the adult CNS are heavily biased against axonal outgrowth. [5-7] Injury and disease are typically characterised by a severe inflammatory reaction from the body. Such a response is required to maintain tissue integrity and to remove tissue debris and foreign matter, but can also leads to astrocyte proliferation. Astrocytes can influence neurite regeneration considerably, and their influence can be either cytotrophic or cytotoxic. For instance, astrocytes provide physical and biochemical support for regenerating neurites, and are important to the maintenance of the blood brain barrier. They are also involved in the expression of membrane transports; [8] encouraging neurones to release ATP to stimulate oligodendrocytes to myelinate neurites; [2] and are essential in the regulation of neuronal blood flow. [9] However, their proliferation also produces scars which may physically and chemically impede axonal regrowth. [10] Furthermore, the scars may actively inhibit axonal outgrowth through the excretion of cytotoxic molecules whose job it is to kill off cells damaged by injury, but can inadvertently damage functional neurones as well. [11-15]

In-order to persuade endogenous axons to regenerate within an environment that is not normally permissible to this, attempts are being made to construct scaffolds that provide an artificial cellular microenvironment for neurones, [16, 17] while also allowing axons to extend through it in an uninterrupted manner. [18] The scaffold should offer protection for

the advancing growth cone, so that ultimately they can re-form chemical synapses within the neural circuity at a specific location, or on the other side of an injury. [10, 19] Thus far, attempts to achieve this have been largely unsuccessful, as it has proven difficult to engineer a scaffold that supports axonal extension, while controlling the inflammatory response and providing molecules to encourage directed regeneration. [20] Ideally such a scaffold should also actively exclude cytotoxic molecules that can be released from glia. [20]

Control and optimization of the interactions between neurones, activated glia and the scaffold will be required to achieve neural regeneration *in vivo*. This study evaluated the infiltration and migration of neurones and neurites with thermally sensitive xyloglucan scaffolds that were injected into the caudate putamen of adult rats, as well as the inflammatory response associated with the implantation. The xyloglucan used in this study was modified by the immobilisation of poly-$_D$-lysine at different concentrations in an attempt to influence cellular and neurite extension into the scaffold. The inflammation was assessed through analysis of the activated microglia and astrocytes, considering the number of cells and their morphology. Xyloglucan was selected for this study, as it has proven *in vitro* biocompatibility, being shown to maintain and support the differentiation of cortical neurones and neural stem cells (toward neurones) in 2 and 3D cultures. [21] It has also employed *in vivo* for the delivery of drugs in rabbits. [22] It was also selected because of its macroporous structure and high modulus post gelation that closely matches that of the human spinal cord (520,000 Pa). [23]

The gelation of xyloglucan at physiological temperature occurs in two distinct stages. The first stage consists of the formation of thin membranes within the gel, which occurs rapidly upon heating increasing the modulus of the gel to approximately 2000 Pa. [24] This may be a useful quality in tissue engineering if it was desirable to encapsulate cells within the gel and introduce them *in vivo*, as the gel would rapidly become robust during the first stage of gelation. The second stage of gelation consists of the formation of a three dimensional network, as the thin membranes join together. [25] In this stage the modulus increases dramatically (approximately between 250 550 kPa, depending on the gel

medium) so that the final modulus of the xyloglucan gel is similar to that of the native human spinal cord [21, 23], making the use of xyloglucan for the regeneration of spinal cord injuries attractive.

The end goal of this study is to address this application by employing xyloglucan hydrogels to assist in spinal cord regeneration to attempt to restore function. The current work represents a preliminary investigation where the infiltration of endogenous axons through the hydrogel scaffolds is assessed in the brain. The reason for this is that the brain is part of the CNS and consists of similar cell phenotypes, it is also an established technique for the evaluation of inflammation within this group.[11, 26-28] This preliminary work was designed to provide insight on how mature neurons interact with xyloglucan scaffolds and the inflammatory response that occurs upon implantation of this material within the CNS. This work provides some *in vivo* discernment for the development of a neural tissue engineering strategy that would be useful for the repair of damaged neural pathways within the CNS.

7.1.4 Experimental Method

7.1.4.1 Materials

The xyloglucan used in this study was kindly supplied by Dainippon Sumitomo Pharmaceutics Co. Ltd. and was prepared according to previous protocols.[29] Briefly, enzymatic modification of tamarind seed xyloglucan was utilized to remove 48% of the galactose side chains, so that the material gelled at physiological temperature. The material was purified by dissolving 1 wt% xyloglucan in deionised water at a temperature of 4 ºC. The materials were then precipitated at room temperature in 60% ethanol before being filtered through a sintered glass filter attached to a vacuum. The precipitate was then dried at room temperature in a vacuum oven for 3 days before being stored in a desiccator.

7.1.4.2 Immobilization of poly-D-lysine.

Poly-D-lysine was photocoupled to xyloglucan using a protocol described previously and shown graphically in Figure 1. [21] Briefly, this was achieved by mixing poly-D-lysine, *N*-(3-dimethylaminopropyl)-*N*-ethylcarbodiimide hydrochloride (EDAC) and 4-azidoaniline in ddH_2O (4 °C) at molar ratios of 40:1 (EDAC:PDL) and 4:1 4-azidoaniline:EDAC. The unreacted species were removed through a 500 Da MWCO cellulose ester membrane (Spectrum) before being lyophilised. The PDL-photoreactive species was then dissolved in PBS and added to the xyloglucan powder. The solution was then irradiated with UV light (Dymax® ultraviolet light source 2000- EC; wavelength ~ 360 nm) for 2 minutes, before being washed in deionised water and lyophilized. This procedure results in the immobilization of 1.44 molecules of PDL per xyloglucan repeat unit, determined by x-ray photoelectron spectroscopy, as described in a previous study. [21]

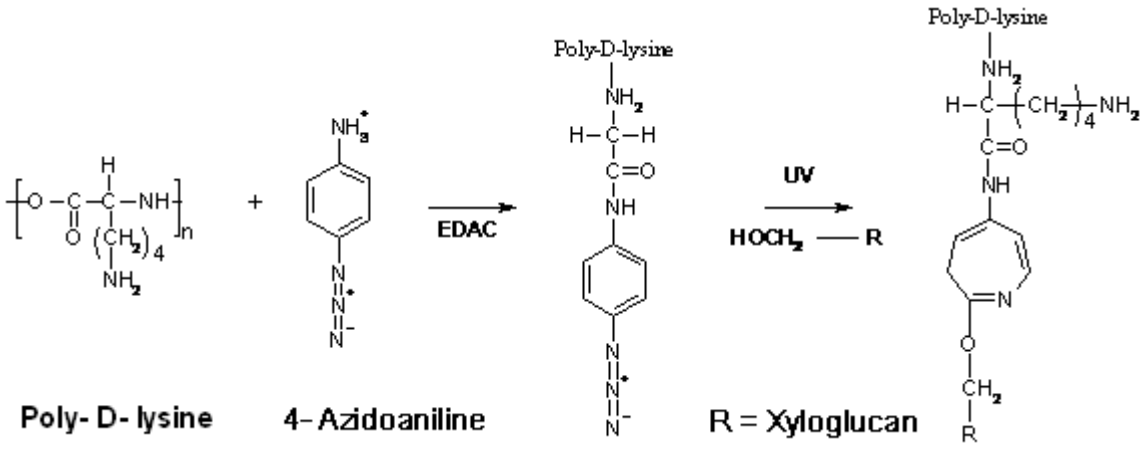

Figure 1 –Attachment of poly-$_D$-lysine to xyloglucan via 4-azidoaniline (the photoreactive species

7.1.4.3 Sample Preparation

Samples of unmodified xyloglucan and xyloglucan-graft-PDL (with 1.44 molecules of PDL per xyloglucan repeat structure) were prepared by sterilizing the powder in 70% ethanol followed by drying in a C2 laminar flow fume hood for 20 minutes and addition of sterilized PBS to produce 3 wt% solutions. Further samples were prepared for cell culture by blending xyloglucan powder with the xyloglucan-graft-PDL at ratios of 90/10 and 50/50 wt/wt %. The samples where then loaded into a 21 gauge sterile needle in preparation for surgery and stored at 4 ºC for no longer than 6 hrs.

7.1.4.4 Scaffold characterisation

The morphology of the macro-porous xyloglucan hydrogel was examined using scanning electron microscopy (SEM) The samples were gelled (at 37 ºC) on a glass microscope slide before being quenched in liquid nitrogen and freeze dried under vacuum for 72 hours. They were gold coated using a sputter coater (Balzers SCD-005, BAL-TEC) with a 25 mA current for a total coating time of 180 s before being imaged with SEM (15kV, S-570 Hitachi Toyko, Japan). Other properties, such as thermal and rheological characterisation, have been conducted by this group in the past and have not been repeated here. [21, 25]

7.1.4.5 Animals

84 Wistar rats (male) that weighed approximately 300 grams were utilised in this study, as well as 28 others used in previous studies as controls which were reused here. The experiments were conducted in triplicate over several different time points (1, 4, 7, 14, 21, 28 and 60 days). At each of these time points either 3 wt% unmodified xyloglucan or the xyloglucan-graft-PDL hydrogels were implanted within the brains of different rats. Blank needle controls or platinum wire controls were also implanted into further rats using similar methods. These experiments had prior approval from the Howard Florey Institute Animal Ethics Committee whilst also conforming to the Australian National Health and Medical Research Councils codes of conduct.

7.1.4.6 *In vivo* implantation of xyloglucan hydrogels

The animals were injected with a solution containing 0.25 ml of xylazine hydrochloride (20mg/ml, Toy Labs) and 0.1 ml of atropine in saline as a muscle relaxant. They were then anaesthetized using 4 % flurophan gas at a flow rate of 1.5 litres per minute for 15 minutes. Holes were then drilled in each side of the skull at a position anteroposterior 1.0 mm, lateral 2.5 mm from bregma, allowing for implantation into the caudate putamen.

The needles containing the sterilized xyloglucan or xyloglucan-graft-PDL gels were then fixed to a modified sterotaxic frame and the animals secured appropriately. The needle was then inserted to a depth of 7.5 mm before a specially designed plunger was inserted, so that upon withdrawal of the needle a xyloglucan tract of approximately 5 mm in length would be injected. For the control animals either a blank needle or platinum wire control was implanted under the same conditions and to the same depth.

At selected time points the animals were injected with a lethal overdose (0.5 mg/g) of sodium perntobarbitone (Letho-barb) before being prefused using 250 ml of 0.2 M PBS at 37 ºC followed by 4 % paraformaldehyde (Sigma-Aldrich, Australia) at 4 ºC. The brains were then removed and soaked in a 30 % sucrose/PBS mixture for 2 days. Liquid nitrogen was then employed to snap freeze the brains before they were stored at -80 ºC. Prior to sectioning the brains were mounted with frozen section medium (Stephens Scientific), then cut at -24 ºC into 40 μm thick sections using a cryostat (Leica).

7.1.4.7 *Fluorescent immunohistochemistry*

The immunohistochemistry procedures were adapted from previous protocols.[21, 30-32] The tissue was baked onto the gelatin coated glass slides at 37 °C for 1 hour to aid in attachment. The sections were again fixed with 4 % paraformaldehyde for 1 min before being washed 3 times in PBS for 5 min in a static environment. The sections were then permeablised and blocked for 1 hr at room temperature, using a solution of 3% normal goat serum (NGS) and 0.3 % Triton-X. They were then exposed to one of several antibodies; rabbit anti-SMI 32 (1:500; Sternberger Monoclonals) for neurites; mouse anti-GFAP Cy3 conjugate (1:1000; Sigma-Aldrich) for astrocytes and mouse anti-CD11b FITC conjugated (1:20; Chemicon) for microglia. Primary antibodies were diluted in a solution of PBS that also contained 3 % NGS, and reacted for 2 hrs at 37 ºC. The sections were again washed in PBS, and in the case of the SMI32 a secondary antibody AlexaFluor 488 (1:1000; Molecular Probes) applied for an additional hour at 37 ºC. The samples were washed and Vector Shield hard set mount with Dapi (VectorShield ©) applied before they were coverslipped. The samples were imaged using laser scanning confocal microscopy (Olympus FV1000) with a 20X air lens.

7.1.5 Results and Discussion

7.1.5.1 Materials Characterisation

The morphology of the macroporous xyloglucan hydrogel scaffolds are shown in Figure 2. Figure 2A shows a 3 wt% xyloglucan sample and Figure 2B is a 3 wt% xyloglucan-graft-PDL sample. SEM images of the hydrogel scaffolds show a highly porous 3D matrix that will adequately allow for the flow of nutrients and waste through the scaffold. The structure of the scaffold consists of ordered stacking of large laths, which is consistent with previous studies. [21, 25] It is known that the ionic strength of the solvent used when preparing the xyloglucan scaffold can influence the spacing between the laths [21] as well as speeding up the gelation process [33] resulting in the formation of holes within the laths. In this study, all samples were prepared in 0.2M PBS, which gave a spacing between membranes of 50 ± 10 μm (n=20). The holes were found to be approximately 6 ± 2 μm in diameter (n=20), which would most likely allow for increased fluid flow, an essential requirement for a tissue engineering scaffold. The ability of the xyloglucan to form laths during gelation was unaffected by the immobilization of PDL within the structure, as were the distance between the laths and the diameter of the micro-holes within the laths.

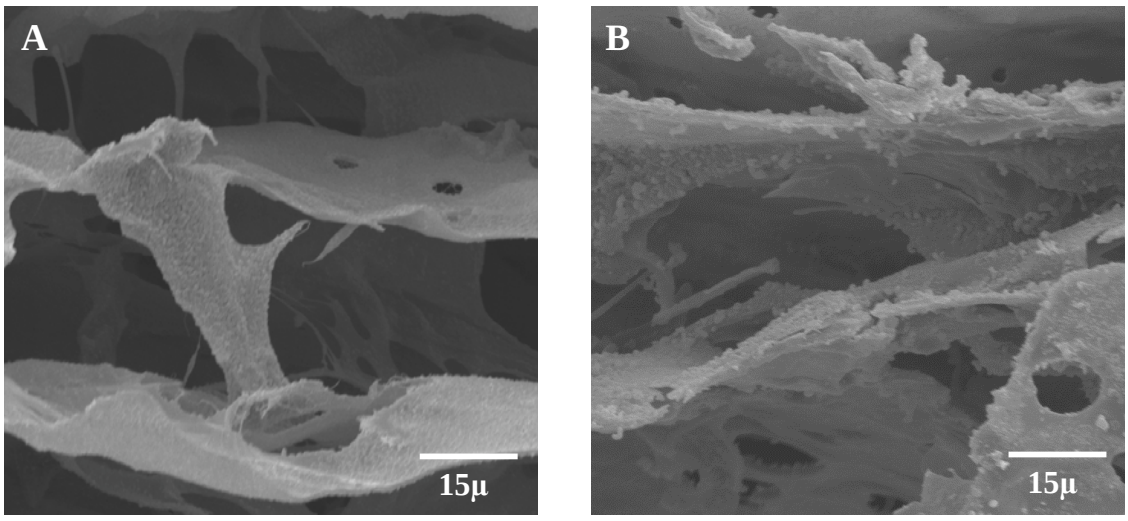

Figure 2 - SEM images of A) 3 wt% xyloglucan and B) xyloglucan-graft-PDL (1.44 molecules of PDL per xyloglucan repeat) produced in PBS and freeze dried.

7.1.5.2 Microglia Response

The unmodified xyloglucan, xyloglucan-graft-PDL and 90:10 and 50:50 blends of xyloglucan and xyloglucan-graft-PDL, were implanted into the caudate putamen and the inflammatory response within the first 500 µm from the surface of the scaffold into the surrounding tissue evaluated. The inflammation was assessed by comparing the number of microglia and astrocytes resulting from the implantation of the xyloglucan scaffolds, to that of a control stab wound, a sterilized platinum wire control and a normal rat brain.

Figure 3 represents the number of activated microglia upon implantation of A) unmodified xyloglucan and B) 100% xyloglucan-graft-PDL (1.44 molecules of PDL per xyloglucan residue) as a function of time as well as distance from the interface of the scaffold. No statistical difference in the number of activated microglia between the unmodified xyloglucan and the100% xyloglucan-graft PDL samples was evident. Results from the 90:10 and 50:50 xyloglucan-graft-PDL also showed no statistical difference upon analysis with posthoc variance testing.

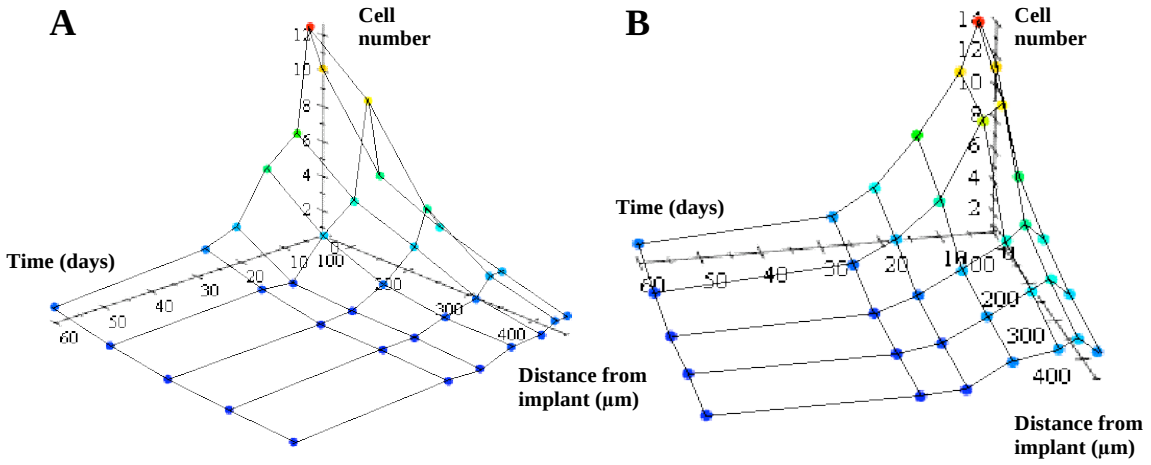

Figure 3 - 3D graphs representing the number of activated microglia activated (z axis), verses the time of implantation (x axis) and the distance (µm) from the surface of the scaffold (y axis). Errors were not included in this figure as their presence obscured the image, However, errors in the cell number for each data point was not greater than ± 2.0 (standard deviation)

The response of microglia to injury is the most rapid of any CNS cell phenotype, [34] and they migrate into an injury site within the CNS to metabolize tissue debris and foreign material. [27, 35] This study showed a typical inflammatory response from the microglia, with a large number of microglia (images not shown) migrating towards and accumulating close (within the first 100 µm) to the interface between the scaffold and the tissue. The microglia only migrated as far as the interface between the endogenous tissue and the scaffolds, accumulating there briefly for 3 days before their numbers exponentially subsided back to physiological levels by 21 days. These observations are shown in Figure 4 which compares the microglia levels after the implantation of the xyloglucan hydrogel scaffold to that of the 3 different controls; a platinum wire control;, a needle sham and a control animal that had undergone no surgery. It is clear that the implantation of the platinum wire results in extensive scarring as the number of microglia remains activated compared to all other samples even after 60 days. Here it is also

evident that number of microglia present post implantation of the xyloglucan gels rapidly subsides returning to physiological levels after 21 days. The interesting discovery from comparison with the controls, was that at all time points prior to 60 days the number of astrocytes present after the implantation of the needle sham was greater than that of the xyloglucan scaffolds. This indicates that the xyloglucan hydrogel may be suppressing the inflammation to some extent. Further discussion of this discovery is warranted and will be explored in greater detail later in this article, where the level of both microglia and astrocytes activated due to the implantation of xyloglucan can be compared to the needle sham. However, this finding may suggest that the microglia have not detected the xyloglucan hydrogel as a foreign material, as there was no evidence of an attempt to phagocytose the xyloglucan hydrogel. The implication of this for neural tissue engineering applications is positive, as unlike many other biomaterials that are encapsulated [36], or phagocytosed [26] by the body during the foreign body response, the xyloglucan and xyloglucan-graft-PDL scaffolds may have suitable residence time to allow for sufficient nerve regeneration to result.

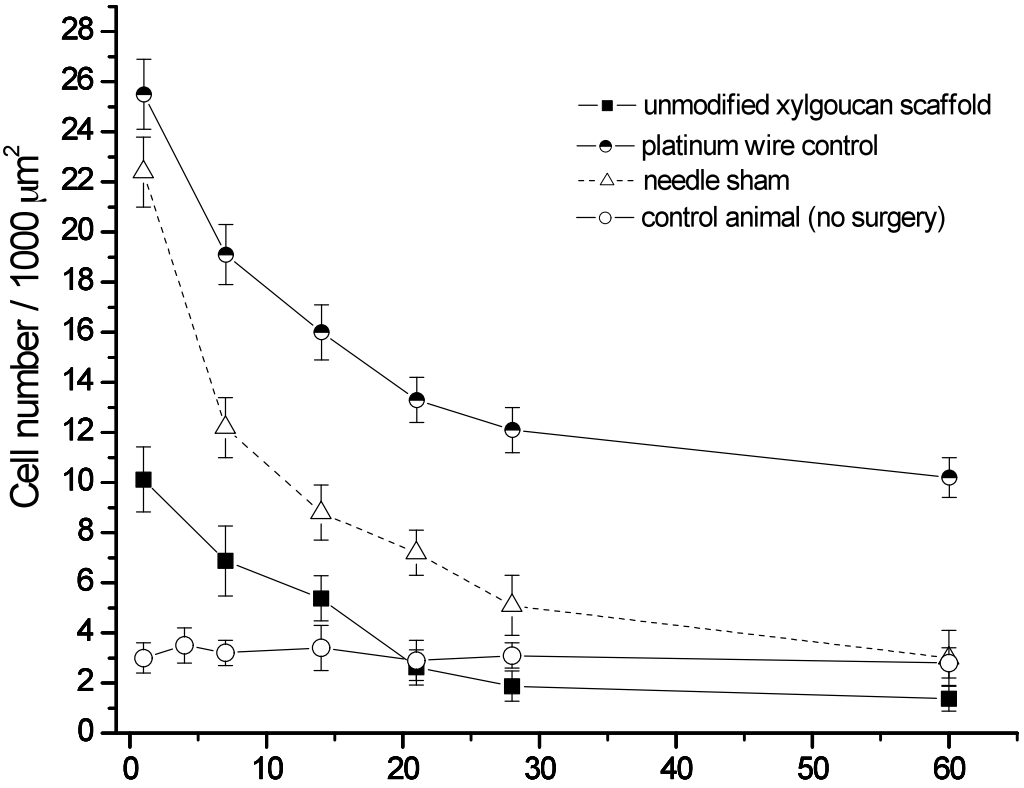

Figure 4 –Number of activated microglia plotted against time within a region of the caudate putamen that is less than 100 μm from the scaffold or the controls. The scaffold presented in this figure is unmodified xyloglucan, as the cellular response to this scaffold and that of the xyloglucan-graft-PDL scaffolds are statically the same at every distance and time point.

7.1.5.2.2 Astrocyte Response

The inflammatory response that accompanies injury to the CNS is essential for achieving neurite regeneration and maintaining tissue integrity, but ideally the response should subside over time towards physiological levels. Whilst this was seen with the microglia (Figure 3), they are not the only CNS cell phenotype that becomes activated as a result of injury.

Figure 5 shows the number of astrocytes activated upon injection of A) unmodified xyloglucan and B) 100% xyloglucan-graft-PDL into the caudate putamen. Results from both the 90/10 and 50/50 blends were almost identical to those from the xyloglucan-graft-PDL. The initial increase in astrocytes number occurs slower than that of the microglia, with the maximum first occurring at a time between 4-7 days. However, unlike that of the microglia (Figure 3) the astrocytes in the PDL-blended materials (Figure 4B) remain elevated until between 21 and 28 days, after which time their number begins to decrease, returning to physiological levels between 28 and 60 days. This prolonged accumulation of astrocytes was not seen in the unmodified xyloglucan scaffolds. The astrocytes also accumulate at the interface between the brain tissue and the xyloglucan scaffolds, however they did not form a fibrous capsule (or form a scar) around that scaffold. This is shown in Figure 6 taken 60 days after implantation.

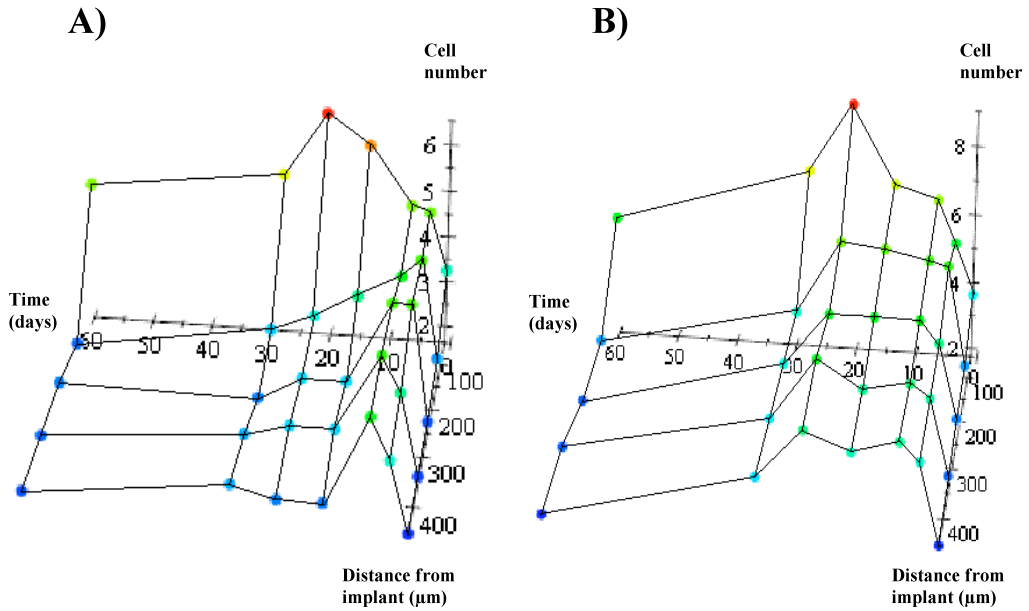

Figure 5 - 3D graphs showing the number of astrocytes activated (z axis), verses the time of implantation (x axis) and the distance (µm) from the implant (y axis). Errors were not included as their presence obscured the image. However, errors in the cell number for each data point was not greater than ± 1.7 (standard deviation).

Figure 6 shows no difference in the number of activated astrocytes within the endogenous tissue surrounding the scaffold, or in fact right at the interface between the endogenous brain tissue and the scaffolds for different implantation times. However, the amount of immobilized PDL does influence the number of astrocytes that infiltrate the scaffold. This is particularly obvious in Figure 6 C) and D), but was too difficult to characterise due to the heterogeneous nature of astrocytes and their processes within the scaffold. From inspection, the number of astrocytes that infiltrate the scaffold increase with increasing amounts of immobilized PDL on the scaffold. In the case of Figure 6 D) the astrocytes have actually grown through-out the entirety of the injected scaffold. This result was not surprising considering that poly-$_D$-lysine carries multiple positive charges, is known to mediate cellular adhesion to synthetic culture surfaces, and is also employed as a positive control in cell culture.[26, 31, 32, 37] In this instance the PDL is encouraging astrocytes to adhere to and migrate throughout the scaffold *in vivo*.

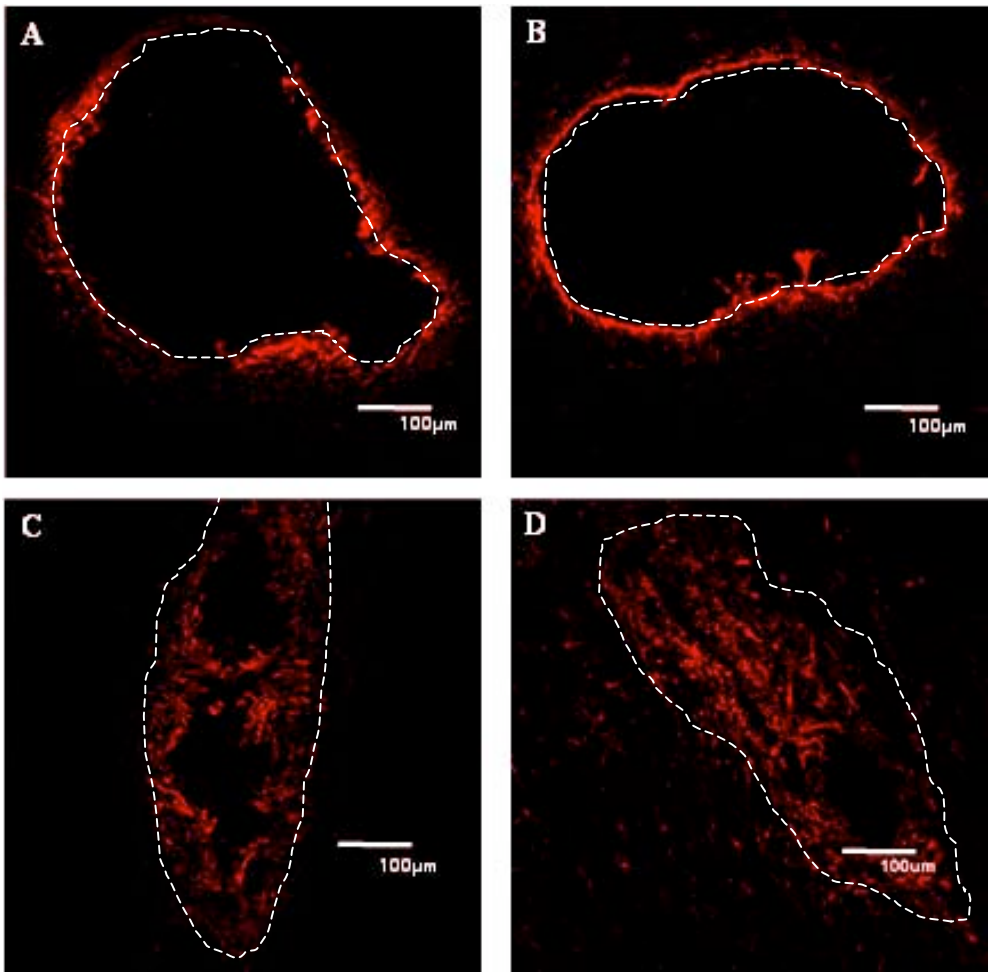

Figure 6 Fluorescence images (marked with GFAP) depicting the number of activated astrocytes surround the xyloglucan scaffold *in vivo* 60 days after implantation. In this instance the brains were sectioned perpendicular to the scaffold injection. A) unmodified xyloglucan; B) 90:10 blend of xyloglucan and xyloglucan-graft-PDL; C) 50:50 blend of xyloglucan and xyloglucan-graft-PDL and D) xyloglucan containing 1.44 molecules of PDL per repeat. White dotted lines represent the boundaries between the endogenous tissue and the xyloglucan scaffold.

Figure 7 compares the number of astrocyte (within the first 100 µm of tissue) after the implantation of un-modified xyloglucan hydrogel, to that of the platinum wire, needle sham controls and the animals that had undergone no surgery. It was clear, similar to Figure 4, that post implantation of the platinum wire the number of astrocytes remained

elevated compared to all other samples. The number of astrocytes present post implantation of the xyloglucan gel returned to resting physiological levels after 60 days. Consistent with the microglia response (Figure 4), the number of astrocytes for the first 21 days of implantation activated by the needle sham was much greater than the response to the xyloglucan scaffold. It is possible that the needle sham and the wire control (the wire surface and hole left by the sham) have acted as a physical barrier to cell migration, hence there was a pile up of astrocytes and microglia as they attempt to reach the implant. Alternatively, for the xyloglucan scaffold there was no obstacle to obscure cellular migration, as the cells were found to freely migrate into the scaffold (Figure 6) but were not measured using the counting method and may be difficult to quantify due to the heterogeneous nature of their migration. Another possibility that can not be ruled out was that the hole left by the sham interrupted tissue integrity and it collapsed in on itself. The role of astrocytes and microglia within the immune response in the CNS is to maintain tissue integrity, hence greater cellular proliferation and activation occurs when tissue is moved through collapse into the hole left from the needle sham. The platinum wire control also caused a considerable inflammatory response, as the large modulus (modulus mismatch with the endogenous tissue) may cause local trauma during movement due to tearing of surrounding tissue. Each of these hypotheses warrants further investigation, and are currently being investigated within the group.

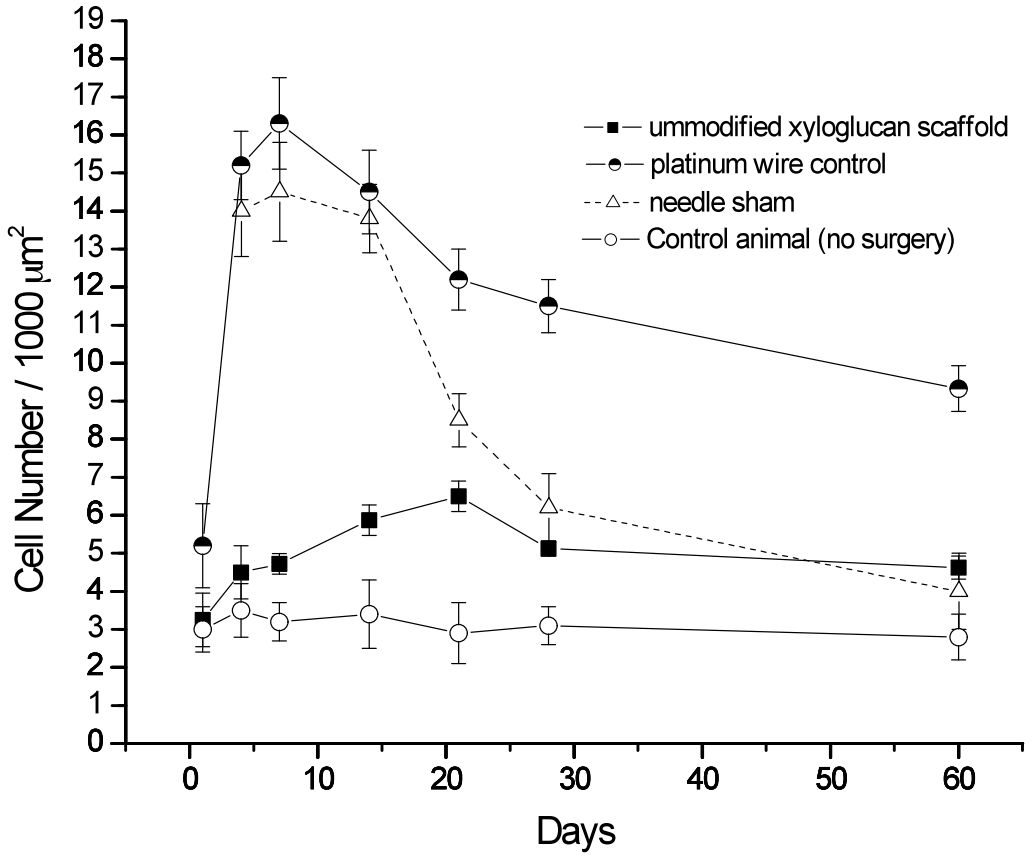

Figure 7 Number of activated astrocytes plotted against time within a region of the caudate putamen that is less than 100 μm from the scaffold or the controls. The scaffold presented in this figure is unmodified xyloglucan.

7.1.5.3 Interaction of Neurites with the Scaffold

It is well understood that the adhesion and migration of astrocytes into tissue engineering scaffolds can produce scarring that would physically inhibit neurite outgrowth, and/or may excrete cytotoxic molecules that actively inhibit axonal outgrowth. Therefore, once the inflammation for each of the different scaffolds had been characterised it was important to determine how neurones and their processes were interacting with the scaffold.

Figure 8 highlights the interaction of neurites within the implanted xyloglucan and xyloglucan-graft-PDL scaffolds of differing PDL concentrations. Neurites behaved very differently on the scaffolds depending on the level of immobilised PDL. No neurites extended into the unmodified sample (A), and the neurite density within the scaffold increased with higher concentrations of PDL presented to the cells (B-D). Interestingly the manner in which they interacted with the scaffolds that presented different levels of immobilised PDL was similar to what was seen for the astrocytes (Figure 6). This is highlighted in Figure 6 & 8 A) for the unmodified xyloglucan implant. For these scaffolds the astrocytes did not infiltrate them, instead accumulating at the interface between the xyloglucan and the endogenous tissue. In Figure 8 A) it is clear that the neurites interacted in a same manner, growing directionally around the scaffold on the interface between the brain and xyloglucan, hence they co-existed with the astrocytes. In fact the neurites also began to extend into the scaffold at a similar time point to that of the astrocyte infiltration, between 4-7 days. This indicated that through manipulation of amount of immobilised PDL that was presented to the cells, the level of inflammation, amount of astrocyte activation, and the neurite density inside the xyloglucan implant can be readily controlled and possibly optimised *in vivo.*

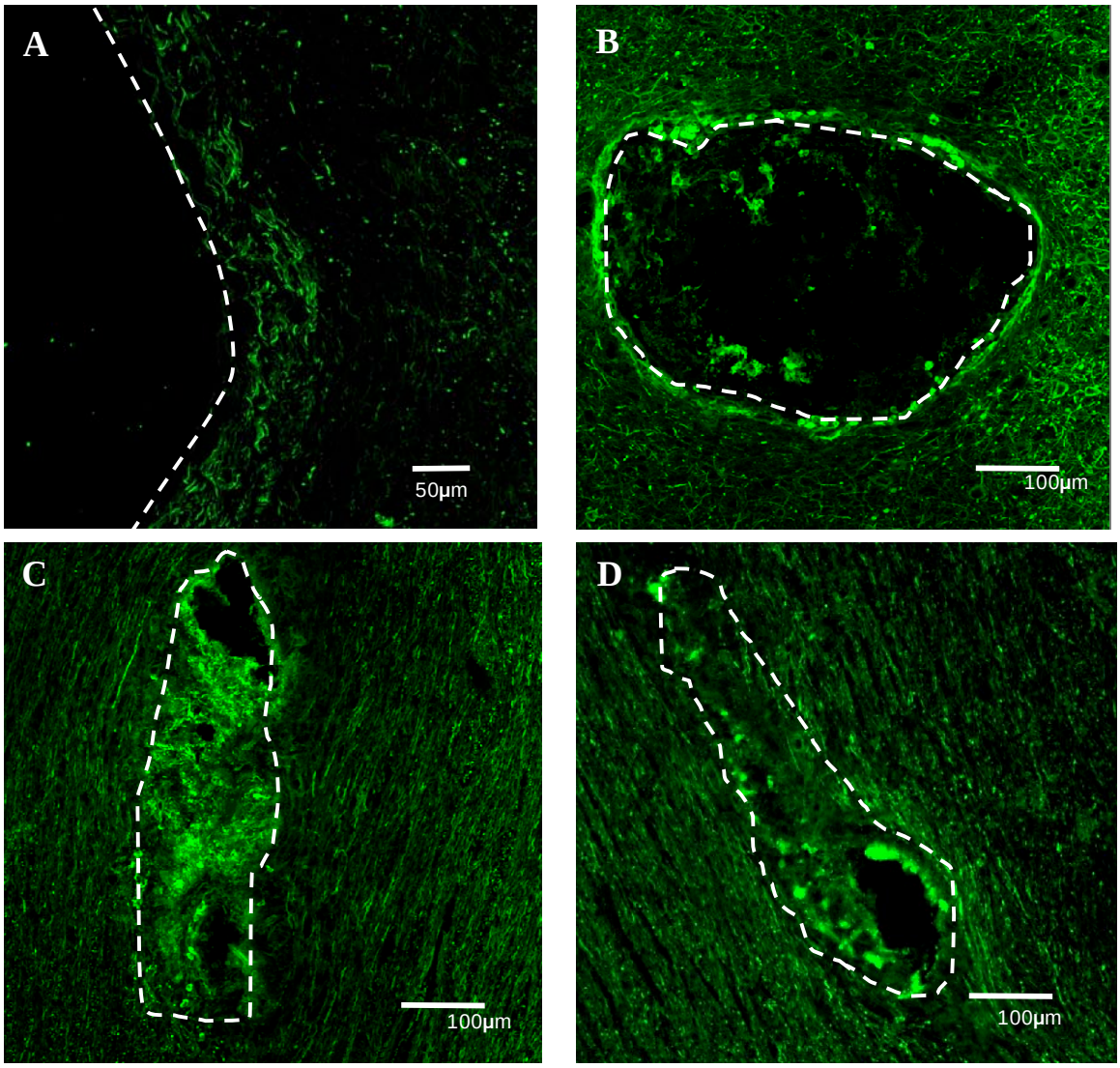

Figure 8 Fluorescence images showing neurites (marked with SMI 32) interacting within xyloglucan and xyloglucan-graft-PDL scaffolds implanted within the caudate putamen 60 days after implantation. A) unmodified xyloglucan; B) a blend of 90:10 xyloglucan and xyloglucan-graft-PDL; C) a blend of 50:50 xyloglucan and xyloglucan-graft-PDL; and D) 100 % xyloglucan-graft-PDL. The white dotted lines indicate the interface between the xyloglucan scaffolds and the brain tissue.

This result is consistent with our previous *in vitro* study that showed a strong correlation between the concentration of immobilised PDL within a xyloglucan scaffold and neurite density of cortical neurones. [21] This study suggests that astrocytes had a positive impact on the regrowth of neurones after injection of the scaffolds, as there was no scar tissue

present to impede neurite infiltration with astrocytes and neurites co-existing within the implanted xyloglucan-graft-PDL scaffold *in vivo*. Therefore it is possible that astrocytes have played a cytotrophic role and had facilitated neuronal sprouting [10, 38] by the excretion of guidance molecules. [39, 40] The next progression of this study is to attempt to establish the identity and release time of the molecules the astrocytes are expressing that metabolically support neuronal regeneration, and if those molecules are soluble or being bound to the surface of the xyloglucan.

7.1.6 Conclusion

In this study xyloglucan hydrogel scaffolds, with and without the incorporation of immobilised PDL, were assessed for their usefulness in regenerating neural pathways within the CNS. This was done by examining the reaction of microglia, astrocytes and neurites when xyloglucan hydrogels were injected into the caudate putamen of adult rats. The activation of microglia peaked after approximately 3 days at the tissue/scaffold intersection, and had decreased back to physiological levels in approximately 28 days. Penetration of microglia into the scaffold was not observed. Astrocytes reached a peak in activation after 4-7 days. In scaffolds composed of unmodified xyloglucan, this reaction subsided far more rapidly than in PDL functionalised scaffolds, which remained at this level until approximately 21-28 days, before subsiding back to normal levels by 60 days. In scaffolds functionalised with PDL, astrocytes and neurites were both found to penetrate the scaffold, with a higher concentration of PDL leading to better penetration in both cases. The timing of the influx of both these cell types also coincided, suggesting that astrocytes proliferation may be linked to the regrowth of neurons in these scaffolds. This did not occur in xyloglucan scaffolds that did not have PDL added.

7.1.7 Acknowledgements

We are grateful to the Australian postgraduate award and the Cooperative Research Centre (CRC) for Polymers (to DRN), and ARC Discovery (DP0663573) (to JSF) and the CRC (to AER) for funding.

7.1.8 References

[1] PMSEIC, Prime Minister's Science - Engineering and Innovation Council, Healthy Ageing in Australia Canberra, Australia (2003).

[2] T. Ishibashi, K. Dakin, B. Stevens, P. Lee, S. Kozlov, C. Steward, R. Fields, Astrocytes Promote Myelination in Response to Electrical Impulses, Neuron, 49 (2006) 823-832.

[3] L.G. Griffith, M.A. Swartz, Capturing Complex 3D Tissue Physiology *In Vitro*, Nature Reviews: Molecular Cell Biology, 7 (2006) 211-224.

[4] T.K. Borg, It's the Matrix!, The American Journal of Pathology, 164 (2004) 1141-1142.

[5] A.D. Buchli, M.E. Schwab, Inhibition of Nogo: A Key Strategy to Increase Regeneration, Plasticity and Functional Recovery of the Lesioned Central Nervous System, Annals of Medicine 37 (2005) 556-557.

[6] E.J. Fry, Central Nervous System Regeneration: Mission Impossible?, Clinical and Experimental Pharmacology and Physiology, 28 (2001) 253-258.

[7] O. Behar, K. Mizuno, S. Neumann, C.J. Woolf, Putting the Spinal Cord Together Again, Neuron, 26 (2000) 291-293.

[8] M. Santello, A. Vloterra, Synaptic Modulations by Astrocytes Via $Ca(^{2+})$ Dependent Glutamate Release, Neuroscience, Early View (2008) doi:10.1016/j.neruoscience.2008.

[9] R. Parri, V. Crunelli, An Astrocyte Bridge from Synapse to Blood Flow, Nature Neurosciece, 6 (2003) 5-6.

[10] D.R. Nisbet, K.E. Crompton, M.K. Horne, D.I. Finkelstein, J.S. Forsythe, Neural Tissue Engineering of the CNS Using Hydrogels – a Review, J Biomed Mater Res B Appl Biomater, 87 (2008) 251-263.

[11] G.T. Liberatore, D.I. Finkelstein, J.Y. Wong, M.K. Horne, M.J. Porritt, G.A. Donnan, D.W. Howell, Sprouting of Dopaminergic Axons after Striatal Injury: Confirmation by Markers Not Dependent on Dopamine Metabolism, Exp Neurol, 159 (1999) 565–573.

[12] R.B. Banati, J. Gehrmann, P. Schubert, G.W. Kreutzberg, Cytotoxicity of Microglia, Glia, 7 (1993) 111-118.

[13] P.E. Batchelor, D.W. Howells, CNS Regeneration: Clinical Possibility or Basic Science Fantasy, Journal of Clinical Neuroscience, 10 (2003) 523-534.

[14] X. Yu, R.V. Bellamkonda, Dorsal Root Ganglia Neurite Extension is Inhibited by Mechanical and Chondroitin Sulfate-Rich Interfaces., J Neurosci Res, 66 (2001) 303-310.

[15] S. Worely, Resorative Surgery of the Central Nervous System by Means of Tissue Engineering Using Neurogel Implants, Neurosurgical Review, 23 (2000) 125-136.

[16] H.M. Geller, J.W. Fawcett, Building a Bridge: Engineering Spinal Cord Repair, Experimental Neurology, 174 (2002) 125-136.

[17] L. Flynn, P.D. Dalton, M.S. Shoichet, Fiber Templating of Poly(2-Hydroxyethyl Methacrylate) for Neural Tissue Engineering, Biomaterials, 24 (2003) 4265-4272.

[18] D.R. Nisbet, W. Shen, D.I. Finkelstein, M.K. Horne, J.S. Forsythe, Electrospinning for Tissue Engineering Applications, Biomaterial Applications, (2008) Submitted.

[19] L.N. Novikova, L.N. Novikov, J.O. Kellerth, Biopolymers and Biodegradable Smart Implants for Tissue Regeneration after Spinal Cord Injury, Current Opinion in Neurology, 16 (2003) 711-715.

[20] P.J. Horner, F.H. Gage, Regenerating the Damaged Central Nervous System, Nature, 407 (2000) 963-970.

[21] D.R. Nisbet, D. Moses, J.S. Forsythe, D.I. Finkelstein, M.K. Horne, Enhancing Neurite Outgrowth from Primary Neurones and Neural Stem Cells Using Thermoresponsive Hydrogel Scaffolds for the Repair of Spinal Cord Injury, Journal of Biomedical Materials Research - Part A, In Press (2008).

[22] S. Miyazaki, Suisha, F., Kawasaki, N., Shirakawa, M., Yamatoya, K. and Attwood, D., Thermally Reversible Xyloglucan Gels as Vehicles for Rectal Drug Delivery, J Controlled Release, 56 (1998) 75-83.

[23] L.E. Bilston, L.E. Thibault, The Mechanical Properties of the Human Cervical Spinal Cord *In Vitro.*, Ann Biomed Eng 24 (1996) 67-74.

[24] D.R. Nisbet, K.E. Crompton, S.D. Hamilton, M. Shirakawa, R.J. Prankerd, D.I. Finkelstein, M. Horne, J.S. Forsythe, Morphology and Gelation of Thermosensitive Xyloglucan Hydrogels, Biophys Chem, 121 (2005) 14-20.

[25] D.R. Nisbet, K.E. Crompton, S.D. Hamilton, S. Shirwakawa, R.J. Prankerd, D.I. Finkelstein, M.K. Horne, J.S. Forsythe, Morphology and Gelation of Thermosensitive Xyloglucan Hydrogels, Biophysical Chemistry, 121 (2005) 14-20.

[26] K.E. Crompton, D. Tomas, D.I. Finkelstein, M. Marr, J.S. Forsythe, M. Horne, Inflammatory Response on Injection of Chitosan/GP to the Brain, J Mater Sci - Mater Med, 17 (2005) 633-639.

[27] D. Stanic, W. Tripanichkul, J. Drago, D.I. Finkelstein, M.K. Horne, Glial Responses Associated with Dopaminergic Striatal Reinnervation Following Lesions of the Rat Substantia Nigra Brain Research, 1023 (2004) 83-91.

[28] D. Stanic, C.L. Parish, W.M. Zhu, E.V. Krstew, A.J. Lawrence, J. Drago, D.I. Finkelstein, M.K. Horne, Changes in Function and Ultrastructure of Striatal Dopaminergic Terminals That Regenerate Following Partial Lesions of the Snpc, J Neurochem, 86 (2003) 329-343.

[29] M. Shirakawa, K. Yamotoya, K. Nishinari, Tailoring of Xyloglucan Properties Using an Enzyme, Food Hydrocolloids, 12 (1998) 25-28.

[30] D.R. Nisbet, L.M.Y. Yu, T. Zahir, J.S. Forsythe, M.S. Shoichet, Characterization of Brain-Derived Stem Cells on Electrospun Poly(ε-Caprolactone) Submicron Scaffolds: Evaluating Their Potential in Neural Tissue Engineering., Journal of Biomaterials Science Polymer Edition, (2007) Accepted 2007.

[31] D.R. Nisbet, S. Pattanawong, N.E. Ritchie, W. Shen, D.I. Finkelstein, M.K. Horne, J.S. Forsythe, Interaction of Embryonic Cortical Neurones on Nanofibrous Scaffolds for Neural Tissue Engineering, Journal of Neural Engineering, 4 (2007) 1-7.

[32] D.R. Nisbet, S. Pattanawong, J. Nunan, W. Shen, M.K. Horne, D.I. Finkelstein, J.S. Forsythe, The Effect of Surface Hydrophilicity on the Behaviour of Embryonic Cortical Neurons, J Colloid Interface Sci, 299 (2006) 647-655.

[33] D.C. Coughlan, O.I. Corrigan, Drug-Polymer Interactions and Their Effect on Thermoresponsive Poly(N-Isopropylacrylamide) Drug Delivery Systems., International journal of pharmaceutics, 313 (2006) 163-174.

[34] W.J. Streit, The Role of Microglia in Brain Injury, Neurotoxicology 17 (1996) 671–678.

[35] G.W. Kreutzberg, Microglia: A Sensor for Pathological Events in the CNS, Trends in neuroscience, 19 (1996) 312–318.

[36] B.D. Ratner, S.J. Bryant, Biomaterials: Where We Have Been and Where We Are Going, Annual Review of Biomedical Engineering, 6 (2004) 41-75.

[37] D.R. Nisbet, K.E. Crompton, M.K. Horne, D.I. Finkelstein, J.S. Forsythe, Neural Tissue Engineering of the CNS Using Hydrogels-a Review., Journal of Biomedical Materials Research, 87 (2008) 251-263.

[38] P.E. Batchelor, G.T. Liberatore, J.Y. Wong, M.J. Porritt, F. Frerichs, G.A. Donnan, D.W. Howells, Activated Macrophages and Microglia Induce Dopaminergic Sprouting in the Injured Striatum and Express Brain-Derived Neurotrophic Factor and Glial Cell Line-Derived Neurotrophic Factor., J Neurosci, 19 (1999) 1708-1716.

[39] P.E. Batchelor, G.T. Liberatore, M.J. Porritt, G.A. Donnan, D.W. Howells, Inhibition of Brain-Derived Neurotrophic Factor and Glial Cell Line-Derived Neurotrophic Factor Expression Reduces Dopaminergic Sprouting in the Injured Striatum, Eur J Neurosci, 12 (2000) 3462–3468.

[40] P.E. Batchelor, M.J. Porritt, P. Martinello, C.L. Parish, G.T. Liberatore, G.A. Donnan, D.W. Howells, Macrophages and Microglia Produce Local Trophic Gradients That Stimulate Axonal Sprouting toward but Not Beyond the Wound Edge, Mol Cell Neurosci, 21 (2002) 436–453.

Part III

Conclusion and Future Work

Chapter 8

Part III - Conclusion

Conclusion, Future Work, Perspectives

& Appendices

Table of contents

8.1 Conclusion

This thesis was concerned with the development of two unique neural tissue engineering scaffolds, designed to a) encourage guided neurite extension within the CNS and b) .provide a supportive, 3-dimensional cellular microenvironment to neural cells. For this reason, the thesis was structured into two, inter-related parts according to the scaffolds manufactured to meet their desired goals.

8.1.1 General conclusions for the electrospinning (Part I) of this thesis

8.1.1.1 *In vitro* studies

Cortical neurones were found to be biocompatible with 2D surfaces of P_LLA and PLGA and responded to small changes in surface hydrophilicity. Nerones formed colonies on the P_LLA and PLGA even when the surface hydrophilicity was altered. The PLGA surface, apart from the 0.1M KOH treated sample, supported more live cells than that for the P_LLA or the poly-$_D$-lysine positive control. This indicated that the formation of large colonies of cells on the surfaces (which was probably due to changes in the protein/cellular interactions due to surface energy) resulted in significantly improved cellular survival. In the case of the 0.1M KOH treated surfaces, whilst the cells still formed colonies, the size of the colonies were much smaller due to increase cellular spreading on the more hydrophilic surface. On such surfaces, it was clear that more cells existed individually, and they were larger and biopolar in morphology, appearing to more closely replicate those on the PDL control surface. There was considerably higher cellular death as a result of increased spreading. This preliminary study indicated that P_LLA and PLGA were biocompatible with cortical neurons, providing a surface for them to adhere and differentiate on. This study provided adequate grounds for attempting to electrospin 3D scaffolds from these materials.

Cortical neurons cultured within nanofibrous P_LLA and PLGA scaffolds adopted morphologies distinctly different from when they were cultured on the 2D surface and were similar in appearance to neurons *in vivo*. Changes in surface energy of the nanofibres did not influence the cell shape and size, or the number of primary and secondary branches, however, it did affect neurite extension. When the scaffolds were more hydrophobic there was a significantly greater overall neurite length of both the primary and secondary branches. Therefore polycaprolactone (PCL), which is more hydrophobic than P_LLA and PLGA was used for the remainder of the studies.

The interfibre distance of randomly aligned electrospun scaffolds was found to influence the way the neurites extended *in vitro*. When the interfibre distance was too large the neurites were forced to follow the fibres. On the other hand, neurites avoided regions of low interfibre distances and at all other distances, traversed perpendicular to the fibres. This meant that in the majority of cases, the neurites transversed perpendicularly to the electrospun polymer nanofibres. Therefore, it may be possible to control neurite extension though modifying the architecture of the electrospun scaffolds.

The interaction and differentiation of adult rat brain derived stem cells with randomly orientated electrospun nanofibrous scaffolds was investigated. Here, the PCL nanofibres were chemically modified with ED to insert amines on the surface for the later immobilization of growth factors. Such surface modification did not influence the differentiation of the stem cells, however it did have a profound effect on cellular adhesion. Interestingly PCL scaffolds influenced the differentiation of NSCs primarily into oligodendrocytes, demonstrating lineage specificity as a function of the scaffold's physical and not chemical properties. This research will be explored in the future within the laboratory, including investigation into the influence of immobilized growth factors (see future work – Chapter 8; section 8.2).

8.1.1.2 *In vivo* studies

Aligned and randomly orientation PCL nanofibrous scaffolds were fabricated using electrospinning and the inflammatory response upon the implantation of these scaffolds within the caudate putamen of adult rats was then assessed. It was discovered that the activation of microglia peaked after approximately 3 days, after which it immediately began to subside returning to physiological levels after 28 days. The activation of astrocytes was extended in comparison, with their maximum activation occurring after approximately 3 days and remaining elevated until 14 days, after which time the numbers began to subside. However, after 60 days the scaffold was not encapsulated by astrocytic scarring, hence the inflammatory response was able to be controlled. Furthermore, neurites were able to infiltrate the random electrospun scaffold, but could not penetrate the aligned scaffold. This most likely resulted because of smaller interfibre distance of the aligned nanofibres preventing neurite infiltration. However, the fact that neurites were observed to infiltrate the random electrospun scaffolds indicated that the scaffolds were integrated within the brain circuitry to some extent. Endogenous neurites also crossed the aligned PCL fibres perpendicular to the direction of fibre alignment *in vivo*, i.e. exhibiting perpendicular contact guidance.

Endogenous neurites entered the randomly orientation PCL scaffold after approximately 7 days, correlating to when the number of activated microglia began to decrease and astrocytes activation was at a maximum. Therefore, a tentative conclusion was drawn that microglia may not have a positive influence on neural regeneration, and it is probable that the astrocytes were delivering neurotropic signals to biochemically and physically support neurons, encouraging neurite infiltration.

8.1.2 General conclusions for the hydrogel (Part II) of this thesis

8.1.2.1 *In vitro* investigation

Galactose modified xyloglucan is a thermoreversible polysaccharide hydrogel that has a significantly higher modulus than many other physical hydrogels. Here, we investigated the microstructural and rheological properties of the gel, and discovered that gelation occurred via a 2 stage process. The first stage was not concentration dependant and involved the initial formation of large membrane structures in the pre gel. For this reason the pre-gel initially has a relative high modulus. The second stage of gelation involved the joining of membranes into a strong 3-dimensional network, and it was found that this process was independent on the ionic strength of the concentration media.

The xyloglucan was then functionalized through immobilising 1.44 mole equivalents of poly-$_D$-lysine (PDL) per xyloglucan repeat unit. The cellular response of cortical neurons to the scaffolds under 2D and 3D culture conditions showed that the hydrogels were non-toxic and supported neuronal differentiation. Furthermore, through changing the level of immobilised PDL being presented to the cell we were able to control the cell number, diameter, migration and the neurite density *in vitro*.

The interaction of xyloglucan-based scaffolds with embryo derived neural stem cell (NSC) cultures was also investigated and confirmed the versatile function of the PDL functionalised scaffolds in the controlled development of NSCs *in vitro*. Functionalisation also provided an ability to control the differentiation of precursor cells, encouraging them to differentiate towards the neuronal lineage. Functionalised xyloglucan produced tissue engineering scaffolds that had a superior capacity to support neuronal survival, differentiation and neurite extension. This result was encouraging and led to the next stage of this investigation which involved the *in vivo* evaluation of the scaffolds to assess their usefulness for neural tissue engineering.

8.1.2.2 *In vivo* investigation

This study evaluated the usefulness of xyloglucan scaffolds modified by the immobilisation of PDL for regenerating neurites within the central nervous system. Here, the materials were implanted within the caudate putamen of adult rats and the activation of microglia and astrocytes assessed. The microglial activation peaked after 3 days and had returned to physiological levels after 28 days, with minimal evidence of the migration of these cells within the scaffold. Alternatively the activation of astrocytes peaked after 4 days and remained at that level for 7 days before beginning to plateau off to physiological levels after approximately 60 days. Apart from the un-modified xyloglucan, all the samples containing immobilised PDL promoted the migration and differentiation of astrocytes within the implants. Furthermore it was discovered that this migration and differentiation increased with increasing concentration of PDL.

The xyloglucan-graft-PDL scaffolds also promoted the extension of neurites into the scaffold, with more neurites entering the scaffold with increasing concentration of PDL (similar to the response seen from the astrocytes). The timing of the influx of both the astrocytes and neurites coincided, suggesting that astrocytes proliferation may be responsible for physically and biochemically supporting neurite ingression. This response was not seen on the unmodified xyloglucan scaffold as there was no migration of either astrocytes or neurites within the scaffolds.

8.2 Future Work

Neurodegenerative diseases such as Parkinson's Disease (PD) result in the loss of neurones and associated neural tracks and therefore connectivity with other parts of the brain. The aim of this thesis was to develop a scaffold that had the potential to repair damaged neural pathways *in vivo*. Therefore, it was critical to develop materials that encourage directed neurite growth, so that ultimately such scaffolds could be employed to guide neurites and reconnect specific regions within the CNS, eg. the nigrostriatial tract for PD. This project has made considerable progress towards this goal, and was focused on the investigation of injectable scaffolds.

Throughout this thesis each scaffold material was investigated individually (with Part I concerning electrospun scaffolds and Part II exploring the xyloglucan hydrogel) to determine if they were suitable for use in the body for this particular application. Fundamentally, there are many different directions that the continuation of this project could take, which arise from the interpretation of the *in vivo* experiments (Chapter 4 and 7) and are discussed here.

8.2.1 Cellular studies on the materials, and controlled and directed differentiation of stem cells.

Such a study would involve continuing to investigate the materials independently. In this instance the evaluation of the materials would not only include cellular viability, assessed utilizing embryonic cortical neurons, but also employ mouse neural stem cells. Currently, this study is in progress for the electrospun PCL scaffolds and will soon be commenced on the xyloglucan and xyloglucan-graft-PDL scaffolds. In regard to the current study on the PCL scaffolds, the aim is to assess the cellular response and differentiation of stem cells cultured on PCL scaffolds with aligned and random fiber alignment. Furthermore, brain derived neurotrophic factor (BDNF) has been directly immobilised on the surface of the nanofibres, and the differentiation of the stem cells

being evaluated, again with both random and aligned fiber alignment. The next step in this study is to attempt to control the selective differentiation of neural progenitor cells by immobilizing different growth factors to the surfaces of the fibres, such as wnts (which is a signaling pathway of complex proteins that are involved in physiological processes in adult animals). Wnts are known to result in the rapid differentiation of cells into neurones, while discouraging the development of astrocytes. While the initial experiments are being conducted *in vitro*, these studies can be used to establish protocols for future *in vivo* work. Stem cells could be seeded onto the scaffolds and implanted into the brain, to evaluate if the differentiation of stem cells can also be controlled *in vivo*.

8.2.2 Incorporate both the xyloglucan and electrospun fibres into a "composite" scaffold to achieve superior neurite growth

Another exciting prospect will be to combine the electrospun scaffolds with the xyloglucan hydrogel, to offer contact guidance along the polymer fibres and protection and compliance matching of the scaffold to the endogenous tissue using the hydrogel properties. The implantation of xyloglucan is likely to result in the migration of astrocytes throughout the cell to where the polymer fibers are implanted. However, it has been shown *in vivo* (Chapter 7) that in these instances the astrocytes tend to biochemically and physically support the neurons and did not impede, but rather encouraged neurite outgrowth. A further extension to this work will be to employ the xyloglucan to deliver glial cell line-derived neurotrophic factor (GDNF) along with other similar growth factors, which have the ability to selectively nourish and regenerate neurones. Additionally the xyloglucan could also be used to deliver NGF and establish a chemotactic gradient, to encourage the neurones to grow through the electrospun scaffold.

This research will be useful for cell based therapies, where replacement cells are injected within the hydrogel scaffold and encouraged to grow along the aligned polymer nanofibres. However, there may even be no need to include cells within the scaffold prior to injection. If the scaffold extends between two locations where neurones are

present on both sides, and if it offers suitable protection from inhibiting molecules that limit neurite extension, it may be possible to restore the damaged tract without the addition of any replacement cells. Ultimately, this is a better approach as there are currently many unresolved issues surrounding the use of stem cells for therapeutic applications in humans.

8.2.3 Entirely in vivo studies

Another possibility is to conduct the research entirely *in vivo* after the biocompatibility of the materials have been assessed in the preliminary experiments (Chapter 4 & 7). In this instance the study could either be conducted on the composite materials (xyloglucan and PCL scaffolds combined), or the individual materials. This study is a combination of the two previous proposed studies. It would involve fabricating scaffolds and testing them within the CNS. This project is likely to employ chemical gradients to direct neurite extension along the scaffolds. If the two different materials are used together the xyloglucan would be injected with a growth factor incorporated, in such a way as to form a gradient. Then the neurite could have the electrospun fibres (aligned) to provide contact guidance, whilst also being directed by chemical gradients. This study may even provide preliminary results for the *in vivo* injection replacement cells and delivery of such cells within the CNS. However, it would be more focused on attempting to combine cell-cell interactions with contact guidance cues and growth factors to enhance neurite outgrowth.

Whilst the proposals have similarities they all answer different questions that are equally important. A selection of the most appropriate path to take after the submission of this thesis will need to be extensively considered, although some of the elements recommended in section 6.4.1 are currently being explored by the author.

8.3 Appendices

Two publications have been inserted into chapter 8 within the appendices section. These publications are ones that have not been inserted in the contents of this thesis, but provide some insight into the future directions of neural tissue engineering. Below the reference information and publication status for these publications is provided.

Chapter 8.3.1

D.R. Nisbet, J.S. Forsythe, "New stem cell stragies for nerve regeneration", Aus. Sci., 25, pp 23-25, 2008.

Chapter 8.3.2

D.R. Nisbet, J.S. Forsythe, "Feature Article – Monash researchers pioneers nano scaffolds to rebuild nerve damage", *Aust. Bio. Tech.*, 18, pp56-57, 2008.

8.3.1 New Nanotechnology Strategies for Nerve Regeneration

By David R Nisbet and John S Forysthe

CRC for Polymers, Department of Materials Engineering, Monash University, P.O. Box 69M, Victoria 3800, Australia

"Stem cells have created a lot of interest within the neural tissue engineering community because they could provide a therapeutic source of nerve cells for the treatment of spinal cord injuries."

Regeneration of nerves lost due to spinal cord injury may be possible if new research with stem cells is successful.

In Australia an estimated 12,000 people have spinal cord injuries, with 400 new reports annually. The majority of spinal cord injuries occur before the age of 30 and people can live for many years after the injury, resulting in significant financial and social costs. Spinal cord injuries have been estimated to cost the Australian public $1.2 billion per year, accounting for 2% of health expenditure, a significant percentage given that all cancers account for 5.8% of expenditure. More profound are costs to the affected individual as they struggle to maintain their independence after losing bowel, bladder, sexual and limb function. In many instances people with spinal injuries are dependent on carers and their families to maintain an acceptable quality of life.

The central nervous system (CNS) is the core control system of the body and consists of the brain and spinal cord. It is a pathway for motor and sensory information, allowing physiological responses requested by the brain to be carried out. Messages are carried in the form of electrical signals through axons, long fibres extending from nerve cells to other locations in the body. Anatomically, nerves are bundles of axons from different nerve cells that conduct electrical signals in the same direction. When nerves are

damaged, the electrical signals from the brain are interrupted, resulting in an inability of nerve cells to perform their functions, such as initiation of muscle movement. Nerves can be damaged in a variety of different ways, including trauma such as vehicle accidents and diving into shallow water, or as a result of diseases like multiple sclerosis and polio.

Most cells within the CNS are not nerve cells; they are glial cells, responsible for supporting nerve cells metabolically and physically. Injury to the CNS results in extensive inflammation, an important process that results in removal of tissue debris and maintains tissue integrity. However, it also results in proliferation of a particular type of glial cell, which can produce a scar that inhibits the axonal extension required for the regeneration of spinal cord injuries. Axons can also be impeded by molecules excreted by other types of such cells.

Why does CNS injury trigger a process that inhibits regeneration? CNS inhibition in adults provides a stable cellular scaffold that prevents nerve cells and axons contacting neighbouring locations within the nervous system, which would result in incorrect transmission of motor and sensory information, and functional loss. During foetal development, axons extend to new locations and once an axon has reached its target the outgrowth is shut down by inhibiting molecules, ultimately anchoring it to that location. This provides the highly complex CNS with a very limited ability to reorganise itself, ensuring that it fulfils and maintains its appropriate function.

There is no present cure for nerve damage in the CNS, with severe and permanent consequences for affected individuals. Stem cells have created a lot of interest within the neural tissue engineering community because they could provide a therapeutic source of nerve cells for the treatment of spinal cord injuries. Stem cells can be used to produce nerve cells, but production of nerve cells may not be necessary for treatment of spinal cord injuries – fundamentally, repair involves reconnection of existing axons, not necessarily growth of new nerve cells. For this reason our group is currently using so-

called “smart scaffolds” to help stem cells generate glial cells, providing existing nerves with physical and metabolic support to encourage axonal outgrowth. The synthetic and biodegradable cellular scaffold developed in our laboratories will allow axons to extend across an injury site.

Smart scaffolds provide permissible environments for cells, favouring nerve regeneration by circumventing physical and chemical barriers such as scarring and inhibitory molecular signals. Axons must be able to grow uninterrupted through an injured area, ultimately integrating with axons on the other side. A smart scaffold must:

- provide a supportive guidance channel along which axons can grow
- exclude inhibitory glial cells and bridging scar tissue
- provide molecular cues to enhance axonal growth, excluding inhibitors
- minimise the inflammatory response to itself.

Attempts to regrow axons have had limited success so far and scaffolds are still being engineered.

Our scaffolds consist of nanoscale polymer fibres approximately 100 times smaller than a human hair (Fig. 1). The fibres have been extensively modified to control stem cell behaviour and increase the ability of the CNS to regenerate. The scaffold is produced using a method known as electrospinning. This involves the application of a large positive voltage to a syringe of polymer dissolved in an appropriate solvent. At sufficiently high voltages the charge build-up on the drop surface results in elongation, and after the surface tension is broken, an extremely fine fibre breaks away. The polymer fibre continues to rapidly elongate as it is drawn towards a negatively charged collector plate and decreases dramatically in diameter into the nanometre scale (10^{-9} m). Processing conditions such as voltage and concentration can be easily adapted, allowing the fibre diameter to be varied.

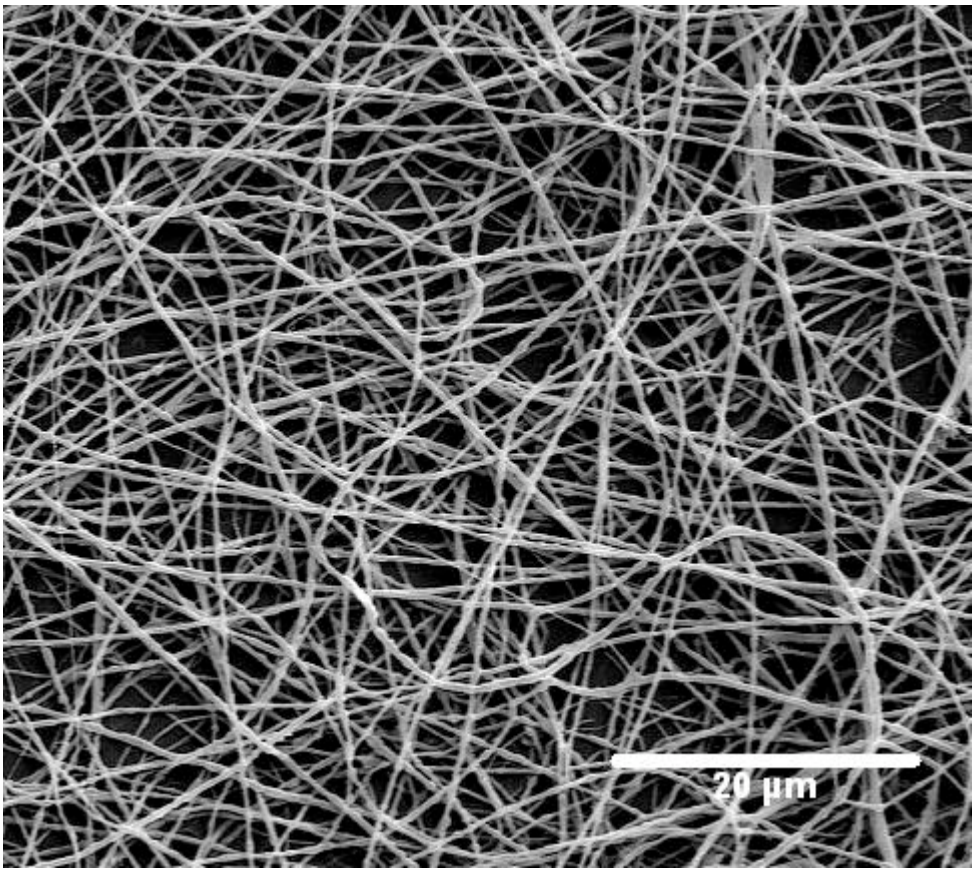

Figure 1. A typical structure of electrospun scaffolds generated for tissue engineering applications. In this figure the fibres are randomly orientated. However, the fibres can be aligned to direct axonal growth.

Recently we have investigated the interactions of nerve cells and stem cells within these nanofibrous scaffolds. By manipulating the surface chemistry and architecture of the nanofibres, we have achieved long and directed axonal extensions. We have also been investigating the proliferation of stem cells cultured on these scaffolds, helping them to produce glial cells. The migration of the stem cells can be readily controlled and optimised by altering the nanofibre properties (Fig. 2). More significantly, we have developed a means of driving stem cells to change primarily towards the preferred type of glial cell (to minimise inhibition of axonal extension; Fig. 3).

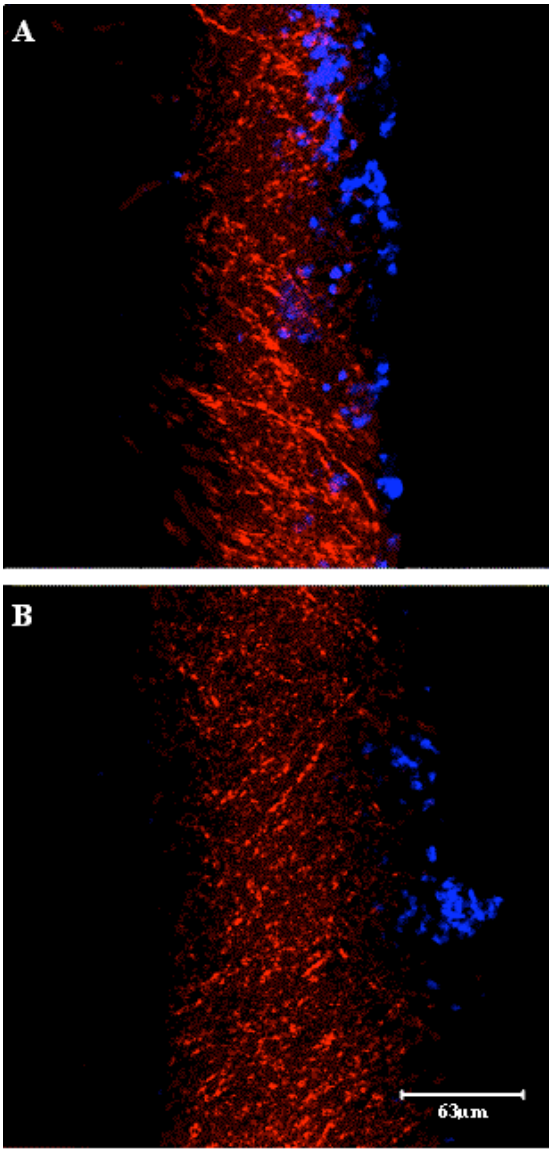

Figure 2. (A) Surface modified polymer fibres (red) where more nerve cells (nuclei shown in blue) have migrated into the scaffold over time. (B) Cellular response on the unmodified scaffold.

Prior to our work, the techniques used to introduce stem cells *in vivo* involved an injection into the spinal cord injury site. In these instances the cells do not immediately attach themselves to the nerve cells and there is considerably high cell death (of the introduced cells). Our studies have shown that stem cells can be anchored to a scaffold

and implanted *in vivo*, where they adapt to their environment and regenerate and proliferate more readily. This is due to a combination of the scaffold's architectural elements and the extensive changes to surface chemistry before the stem cells adhere.

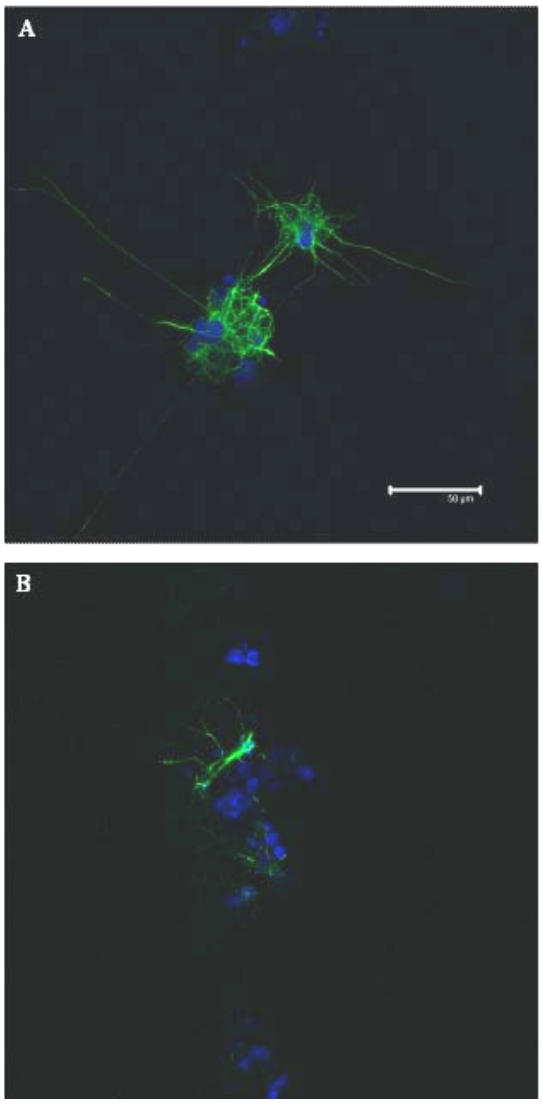

Figure 3. The similarities between the cells cultured on the control surface (A) and the electrospun scaffold (B) can be seen. (Nerve cell nuclei are blue; glial cells are green.)

We plan to introduce a scaffold pre-seeded with stem cells to an injury site, and use this as a means of targeted mass production of glial cells. Such cells will physically and

metabolically support nerve cells and encourage regeneration if we can control the sequence of events during the regeneration process. This is based on the knowledge of axonal outgrowth during foetal CNS development. We will use the nanofibrous scaffolds to physically isolate the glial cells from the nerve cells to avoid the inhibitory effects that arise from surface contact, while supporting the nerve cells to assist axonal growth and viability.

Most neural tissue engineers agree that regeneration of spinal cord injury requires a guidance channel for axon extension and integration. However, we support a fresh approach to axonal regeneration – one that uses stem cells to produce glial cells. Regeneration within the spinal cord requires a physically supportive scaffold for axonal extension, as well as minimisation of inflammation and provision of molecules that enhance axonal growth.

David Nisbet is a PhD candidate and Dr John Forsythe is a senior lecturer within the Department of Materials Engineering and Division of Biological Engineering at Monash University, Clayton, Victoria

<http://www.eng.monash.edu.au/materials/staff/forsythej.html>

8.3.2 Repairing Pathways – Feature Article

David R Nisbet

CRC for Polymers, Department of Materials Engineering, Monash University, P.O. Box 69M, Victoria 3800, Australia

Monash PhD student David Nisbet has used engineering principles and stem cells to develop a technique that can rebuild damaged nerves.

David Nisbet dreams of making a significant contribution towards a cure for injuries to the Central Nervous System, such as Parkinson's Disease and spinal cord injury. And he has moved one step closer, discovering a new technique that could revolutionize stem cell treatment for these conditions.

"Nerves lost due to degenerative diseases such as Parkinson's Disease or spinal cord injury are not regenerated and the consequences for the patient are severe." Mr Nisbet said.

"We aim to use engineering principles and stem cells to regenerate damaged nerves restoring function to the patient. This will be achieved by engineering next generation materials that assist stem cells in replacing damaged nerves".

Mr Nisbet, from Monash University's Department of Materials Engineering, has used existing polymer-based biodegradable fibres, 100 times smaller than a human hair, and re-engineered them to create a unique 3D cellular scaffold that encourages stem cells to attach and support nerves in the body more quickly and effectively. He said a combined process of electrospinning and chemical treatment was used to customize the fibre structure and surface, which can then be located within the body at the site requiring nerve regeneration.

“The scaffold can be injected into the body at the site requiring nerve regeneration. We can embed the stem cells into the scaffold outside the body or once the scaffold is implanted. The stem cells adhere to the scaffold and grow throughout it like ivy growing on the trellis. This effectively forms a bridge for the nerves to grow across and once achieved is the first step in restoring function. Over time, the scaffold breaks down and is naturally passed from the body, leaving the regenerated nerves intact.” Mr Nisbet said.

Figure 1 - David Nisbet in the lab

He said the existing processes release stem cells into the nervous system, but cells randomly “floated” around and did not immediately attaché themselves to the nerves and generally the majority of introduced cells would die.

“Our studies show that stem cells anchored to a scaffold not only attach more easily, but rapidly adapt to their environment and regenerate effectively. We are very excited about the therapeutic outcomes that could be obtained from our research,” Mr Nisbet said.

“We are at the verge of two once separate disciplines – nanotechnology and stem cell research – combining into a new exciting era of discovery which could be the first step towards a cure for conditions such as Parkinson’s Disease and spinal cord injury”.

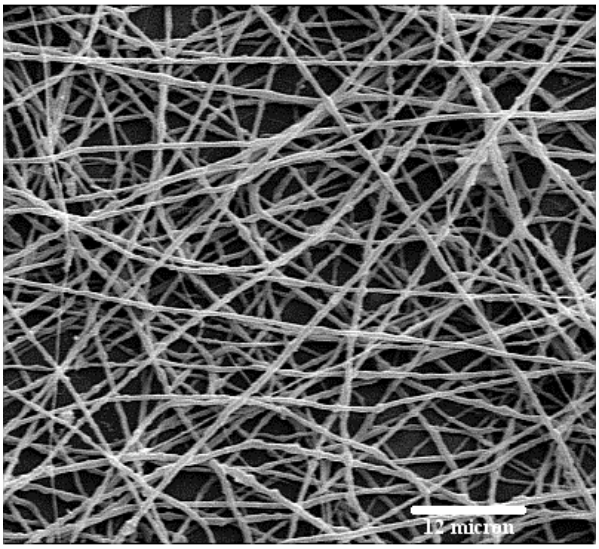

Figure 2 - Typical scaffold that has been produced by electrospinning. These polymer fibers have been imaged using a scanning electron microscope. In this case the fibers are randomly orientated, however, these can be readily aligned enabling the scaffold to be tailored to desired applications.

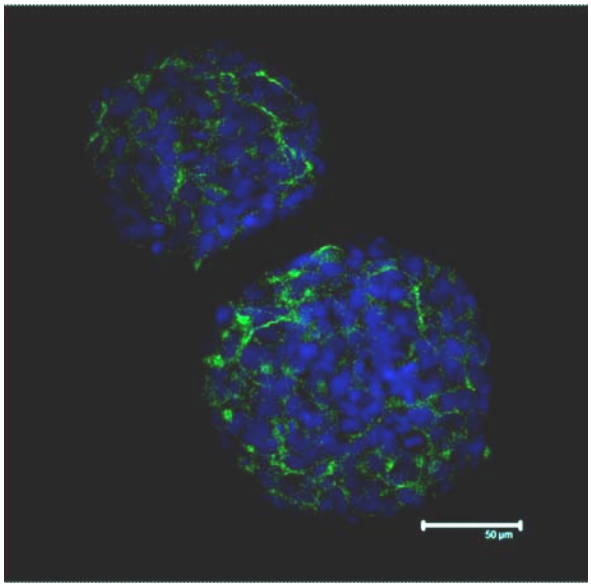

Figure 3 – Shows neurospheres (Neural Stem Cells) growing in cultures. The cell nuclei (center of the cells) is stain blue and the astrocytes (type of glia cell) is stained green.

“Repairing damaged neural pathways is the holy grail of many researchers. It is a very long road to success, which will require small steps from many people, but its wonderful to know we’re making such a significant contribution here at Monash University,” Mr Nisbet said.

The potential of Mr Nisbet’s findings has captured the interests of colleages. Professor Molly Shoichet at the University of Toronto in Canada and Proffessor Malcolm Horne at the Melbourne-based Howard Florey Institute are conduction further tests, with preliminary results showing strong potential.

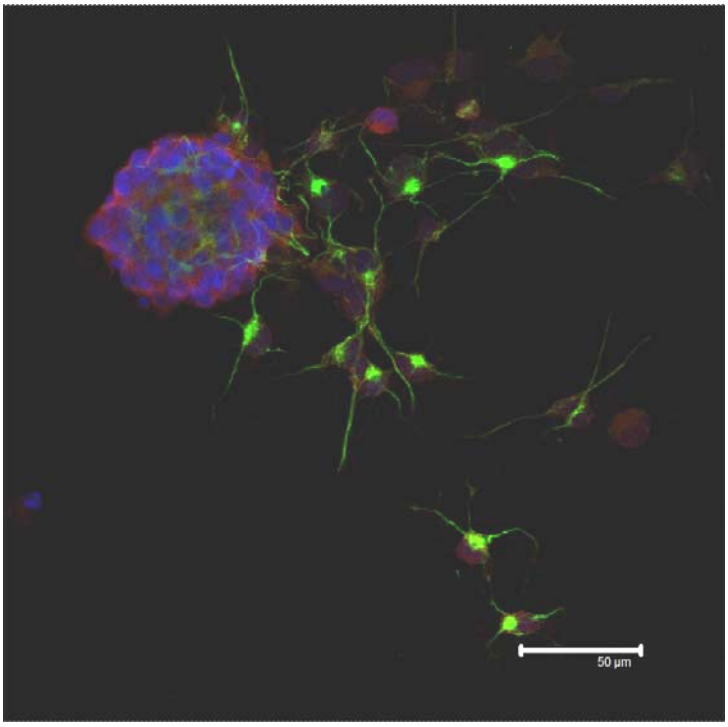

Figure 4 – Shows proliferating neural stem cells. Again the cell nuclei are stained blue. However, the green cells have been stained with nestin, meaning that they are undifferentiated neural stem cells. The red are immature neurones.

Another collaboration with Professor David Finkelstein at the Mental Health Research Institute of Victoria is investigating the potential of these scaffolds to treat damaged brain cells.

Mr Nisbet said the biodegradable fibers were commonly used in biomedical sciences and regenerative technologies, but his technique to design a 3-D cellular environment is a world first.

David Nisbet is a PhD candidate within the Department of Materials Engineering and Division of Biological Engineering at Monash University. He is supervised by Dr John Forsythe.

Email: david.nisbet@eng.monash.edu.au